UNIVERSITY OF CALIFORNIA
RIVERSIDE

Auditory Cortex Processing in Developmental and Adult Plasticity: Implications in Fragile X Syndrome

A Dissertation submitted in partial satisfaction
of the requirements for the degree of

Doctor of Philosophy

in

Psychology

by

Sarah Marie Reinhard

December 2018

Dissertation Committee:
Dr. Khaleel A. Razak, Chairperson
Dr. Iryna M. Ethell
Dr. Kelly Huffman

The Dissertation of Sarah Marie Reinhard is approved:

_____

_____

_____

Committee Chairperson

University of California, Riverside

Acknowledgements

Material in this dissertation, in part or in full, is a reprint of data as it appears in: 1) Reinhard, S.M., Razak, K., Ethell, I.M., 2015. A delicate balance: role of MMP-9 in brain development and pathophysiology of neurodevelopmental disorders. Frontiers in Cellular Neuroscience 9; 2) Wen, T.H., Afroz, S., Reinhard, S.M., Palacios, A.R., Tapia, K., Binder, D.K., Razak, K.A., Ethell, I.M., 2018. Genetic reduction of matrix metalloproteinase-9 promotes formation of perineuronal nets around parvalbumin-expressing interneurons and normalizes auditory cortex responses in developing fmr1 knock-out mice. Cerebral Cortex 28, 3951–3964; and 3) Lovelace, J.W., Wen, T.H., Reinhard, S., Hsu, M.S., Sidhu, H., Ethell, I.M., Binder, D.K., Razak, K.A., 2016. Matrix metalloproteinase-9 deletion rescues auditory evoked potential habituation deficit in a mouse model of Fragile X Syndrome. Neurobiology of Disease 89, 126–135.

The co-author(s) Khaleel A. Razak and Iryna M. Ethell listed in these publications directed and supervised the research which forms the basis for this dissertation.

Financial support for research presented here includes 1) National Science Foundation GRFP, 2) UC Riverside, Psychology dept., Chancellor's distinguished fellowship, 3) National Institute of Child Health and Human Development and the National Institute of Mental Health (1U54 HD082008- 01 to I.M.E., D.K.B., and K.A.R.); 4) U.S. Army Medical Research and Materiel Command (W81XWH-15-1-0436 and W81XWH-15-1-0434 to I.M.E., D.K.B., and K.A.R.), and 5) National Institute of Mental Health (MH67121 to I.M.E).

Dedication

This body of work is dedicated to all the people that helped along the way towards completion of my dissertation. First and foremost, to the two professors that took time to guide me, teach me, counsel me and endlessly edit my papers at every step along the way, Dr. Razak and Dr. Ethell, thank you. Your mentorship has taught me a lot about what effective leadership looks like, and I hope to model this in my future. To my lab mates, I would not have made it through graduate school without you, like, literally. From teaching me how to do the hands-on science, to supporting me through stressful times and breakdowns, to fulfilling my lifelong dream of painting rocks with Bob Ross, I have really been blessed to go through this process with such a great group of people. To my family, my parents, to the most awesome niece and nephew, and to my best little buddy Kody, thank you for your support and encouragement. Finally, without my faith I would have quit life a million times before I ever made it this far, thank you God for who you are, my friend and father, thank you.

ABSTRACT OF THE DISSERTATION

Auditory Cortex Processing in Developmental and Adult Plasticity: Implications in Fragile X Syndrome

by

Sarah Marie Reinhard

Doctor of Philosophy, Graduate Program in Psychology
University of California, Riverside, December 2018
Dr. Khaleel A. Razak, Chairperson

Neurodevelopmental disorders (NDD) are a large body of disorders that together affect 1 in 6 children in the U.S. (Center for Disease Control and Prevention). They are characterized by deficits in communication, cognition, attention, socialization and behavior. Abnormalities in sensory processing are also prevalent, and may underlie higher-order processing such as multisensory integration and perception. Determining a root cause in any one NDD is conflated by the multiplicity of brain regions affected, divergence of behavioral outcome measures in animal models and humans, and the multiple mechanistic underpinnings.

Targeting basic sensory processing in NDD is an approach that may address some of these problems. Sensory processing deficits, including auditory, somatosensory, motor and visual, are common in NDDs. While sensory processing may seem far removed from a concept like behavior or socialization, basic sensory processing does serve as the foundation for cognition. Sensory information is relayed to multisensory and emotion-

regulation regions of the brain which allow organisms to associate emotional states and salience to sensory information. Learning and memory events such as operant or appetitive conditioning induce stable modifications of processing in sensory regions of the brain, while loss of sensory function can affect working memory and attention. This indicates that disordered sensory processing in fact can affect an organism on multiple levels of function. Understanding the development of basic sensory processing and targeting specific developmental mechanisms may rescue processing deficits in NDD, with the potential for improvements in perception and 'higher-order' cognition.

In this series of studies, I focused on the auditory system and sought to increase our understanding of auditory cortex development, and its implications for adult behaviors in a fragile X Syndrome (FXS) mouse model. I discovered the developmental expression patterns of an array of proteins in both early and adult auditory cortices. I discovered differential regulation of proteins within sub-regions of auditory cortex in response to developmental plasticity. I further discovered that dysregulation of these same proteins in adult FXS mice impairs memory formation. Results point to a particular role for perineuronal nets in auditory cortex development and in adult plasticity.

Table of Contents

List of Figures/Tables

Chapter 5: Developmental noise exposure causes comparable plasticity in A1 and AAF in the mouse auditory cortex

Introduction

The study of sensory processing in the auditory cortex (AC) presents a unique challenge in the field of neuroscience. Compared to the visual and somatosensory systems, the auditory system is comprised of many more subcortical regions which perform computations on auditory input before cortical processing takes place. Extraction of meaningful sounds, such as comparison of contra- and ipsilateral input, localization of sounds, or fear responses to sounds, can be accomplished independently from auditory cortex. Subcortical “multisensory" or “affective” networks in the central nervous system (CNS) also process sounds independently of auditory cortex, including the amygdala (Antunes and Moita, 2010; Quirk et al., 1997), cerebellum (reviewed in Sens and Almeida, 2007) and superior colliculus (Drager and Hubel, 1975; Gordon, 1973). From this understanding a basic question arises, why is the auditory cortex necessary (reviewed in Shreiner and Polley, 2014)?

Importantly, current research on neurodevelopmental disorders, including autism spectrum disorder and fragile X syndrome (FXS; discussed in chapters 1, 2 and 3) have focused on sensory processing as an objective outcome measurement in humans and in mouse studies. However, in the auditory system behavioral and functional readouts on auditory tasks do not necessarily reflect cortical function, but can instead be inherited from these subcortical structures. Therefore, it is critical to understand basic auditory cortex processing, and the relative contribution of auditory cortex in the pathology of neurodevelopmental disorders, as well as in typical developmental and adult plasticity events.

In this series of experiments, I have taken a systems neuroscience approach to broaden our understanding of basic auditory cortex development (chapters 1 and 2), the regionalization of auditory cortex (chapters 4 and 5), and how auditory cortex is affected in adult learning and memory (chapter 3). This was accomplished using a combination of techniques, including *in vivo*

electrophysiology, immunohistochemistry, gelatin zymography, behavioral training and Western blotting. To study the potential cortical mechanisms underlying altered auditory processing in FXS, I used a mouse model of FXS and determined that the auditory cortex: 1) shows altered developmental protein expression in *fmr1* KO mice which is not apparent in the inferior colliculus, and 2) maintains impaired protein expression in adult *fmr1* KO mice which is associated with impaired sound-dependent memory formation. This indicates a potentially dissociable role for auditory cortex in FXS deficits, both at the cellular and behavioral levels.

To determine regional differences within the auditory cortex, I exposed mice to sounds during the auditory critical period and measured functional and cellular changes. Results indicate that multiple regions in auditory cortex respond to sound exposure by modifying cellular and functional properties, but that the primary auditory cortex (A1) seems to be particularly malleable to developmental sound exposure compared to the anterior auditory field (AAF). Altogether, the studies presented here suggest that targeting treatment specifically to A1 during auditory cortex development may provide a promising window for treatment of auditory processing deficits in FXS and other neurodevelopmental disorders.

References

Antunes, R., Moita, M.A., (2010). Discriminative auditory fear learning requires both tuned and nontuned auditory pathways to the amygdala. *Journal of Neuroscience,* **30**, 9782–9787. https://doi.org/10.1523/JNEUROSCI.1037-10.2010

Drager, U.C., Hubel, D.H., (1976). Topography of visual and somatosensory projections to mouse superior colliculus. *Journal of Neurophysiology,* **39**, 91–101.

Gordon, B., (1973). Receptive fields in deep layers of cat superior colliculus. *Journal of Neurophysiology*, **36**, 157–178.

Schreiner, C.E., Polley, D.B., (2014). Auditory map plasticity: diversity in causes and consequences. *Current Opinion in Neurobiology*, **24**, 143–156. https://doi.org/10.1016/j.conb.2013.11.009

Sens, P.M., Almeida, C.I.R., (2007). Participation of the cerebellum in auditory processing. *Brazilian Journal of Otorhinolaryngology*, **73**, 226-270.

Quirk, G.J., Armony, J.L., LeDoux, J.E., (1997). Fear conditioning enhances different temporal components of tone-evoked spike trains in auditory cortex and lateral amygdala. *Neuron*, **19**, 613–624.

Chapter 1:

A Delicate Balance: Role of MMP-9 in Brain Development and Pathophysiology of Neurodevelopmental Disorders

Reinhard, S.M., Razak, K., Ethell, I.M., 2015. A delicate balance: role of MMP-9 in brain development and pathophysiology of neurodevelopmental disorders. Frontiers in Cellular Neuroscience 9

Abstract

The extracellular matrix (ECM) is a critical regulator of neural network development and plasticity. As neuronal circuits develop, the extracellular matrix stabilizes synaptic contacts, while its cleavage has both permissive and active roles in the regulation of plasticity. Matrix Metalloproteinase 9 (MMP-9) is a member of a large family of zinc-dependent endopeptidases that can cleave ECM and several cell surface receptors allowing for synaptic and circuit level reorganization. It is becoming increasingly clear that the regulated activity of MMP-9 is critical for central nervous system development. In particular, MMP-9 has a role in the development of sensory circuits during early postnatal periods, called 'critical periods'. MMP-9 can regulate sensory-mediated, local circuit reorganization through its ability to control synaptogenesis, axonal pathfinding and myelination. Although activity-dependent activation of MMP-9 at specific synapses plays an important role in multiple plasticity mechanisms throughout the central nervous system, misregulated activation of the enzyme is implicated in a number of neurodegenerative disorders, including traumatic brain injury, multiple sclerosis, and Alzheimer's disease. Growing evidence also suggests a role for MMP-9 in the pathophysiology of neurodevelopmental disorders including Fragile X Syndrome. This review outlines the various actions of MMP-9 during postnatal brain development, critical for future studies exploring novel therapeutic strategies for neurodevelopmental disorders.

Abbreviations:

Arginine-glycine-aspartate (RGD); Central nervous system (CNS); Collapsin response mediator protein-2 (CRMP-2); Critical period plasticity (CPP); Dentate gyrus (DG); Extracellular matrix (ECM); Fragile X syndrome (FXS); Fragile X mental retardation gene 1 (*Fmr 1*); Fragile X mental retardation protein (FMRP); Intercellular adhesion molecule-5 (ICAM-5); Insulin growth factor – 1 (IGF-1); Insulin growth factor binding protein – 6 (IGFBP-6); Late-phase long term potentiation (l-LTP); Matrix metalloproteinase-9 (MMP-9); Mitogen-activated protein kinase (MAPK); Neurofascin (NF155); Neuroligin-1(NLG-1); Oligodendrocytes (OL); Perineuronal net (PNN); Protein kinase C (PKC); Superior colliculus (SC); Tissue inhibitor of metalloproteinase-1 (TIMP-1)

Outline

1. Introduction
2. MMP-9 activity, expression and regulation
3. Brain development and critical period plasticity
    - 3.1. Visual
    - 3.2. Somatosensory
    - 3.3. Auditory
    - 3.4. Cerebellum
    - 3.5. Hippocampus
4. Cellular mechanisms
    - 4.1. Synapse development and plasticity
    - 4.2. Axon regeneration and plasticity
    - 4.3. Myelination
5. MMP-9 in pathophysiology of neurologic disorders
    - 5.1. FXS and other developmental disorders
    - 5.2. MMP-9 in Epilepsy
    - 5.3. Therapeutic approaches
6. Conclusion

1. Introduction

The capacity of the central nervous system of an animal to adapt to changing internal and external environments must be offset by the capacity to maintain network stability following changes. This stability-plasticity balance is highly regulated and is necessary for adaptation and survival throughout the lifespan of an organism. An important challenge in neuroscience remains to identify the mechanisms that regulate the dynamics between stability and plasticity. With some 86-100 billion neurons and an approximately equal or larger number of glial cells, depending upon the brain region (Azevedo et al., 2009), the study of the brain has been likened to the quest for understanding the universe, with multiple cellular and molecular interactions that account for brain plasticity. Yet many key mechanisms underlying synaptic plasticity are found not in these brain cells themselves but in their interactions with molecules in the extracellular space surrounding them (reviewed by Dansie & Ethell, 2011; reviewed by Dityatev et al., 2010; reviewed by Nicholson & Sykova; reviewed by Ruoslahti, 1996 a, b; Shi, et al., 2006; Šišková et al., 2009). The extracellular matrix (ECM) can be thought of as a scaffold that surrounds neurons and glia within the extracellular space. It is rich with signaling cues that can guide plasticity while maintaining stable network connections over time, mediating synaptic and trans-synaptic interactions. These components can act as repulsive and/or attractive cues for cellular migration and can mediate cell-ECM or cell-cell interactions. While the role of ECM in the plasticity of neuronal circuits is not yet well understood, cleavage of the ECM through the actions of

matrix metalloproteinases (MMP) and other ECM-cleaving enzymes can drive plasticity in response to specific changes in neuronal activity.

Matrix metalloproteinase-9 (MMP-9) in particular stands out as an important molecule in central nervous system (CNS) development and plasticity. MMP-9 is a Zn^{2+}dependent endopeptidase expressed in both the central- and peripheral nervous systems and acts to cleave components of the ECM as well as cell adhesion molecules, cell surface receptors and other proteases. Research has focused on the role of MMP-9 in the progression of neurologic disorders such as epilepsy, multiple sclerosis, neuroinflammatory and autoimmune disorders. However, converging evidence suggests that MMP-9 plays an important role in both establishing synaptic connections during development and in the restructuring of synaptic networks in the adult brain. As improper maturation of sensory networks during development is implicated in many neurodevelopmental disorders and in cognitive deficits, understanding the mechanisms of MMP-9 mediated synaptic plasticity is essential for the development of therapeutic strategies. Such knowledge will guide future clinical studies on the possible role of MMP-9 in neurodevelopmental disorders. As it is possible to regain a state of plasticity and reverse cognitive deficits by manipulating the onset and closure of 'critical periods' (Bradbury et al., 2002; Pizzorusso et al., 2002; Pizzorusso et al., 2006), regulating MMP-9 activity during critical period plasticity may aid in further development of precise and targeted treatments for neurodevelopmental disorders.

2. MMP-9 activity, expression and regulation

MMP-9 is a Zn^{2+} dependent endopeptidase that is found in many cell types throughout the body, including neurons and glia, endothelial cells (Genersch et al., 2000), glandular epithelia, supportive connective tissue and muscle cells (Roomi et al., 2009). Among the 25 known MMPs (reviewed by Ethell & Ethell, 2007), MMP-9, MMP-2 and MMP-3 are widely expressed in the CNS. Furthermore, MMP-9 and MMP-2 share similar substrate specificity and are known as gelatinases. Their substrates include components of the ECM, as well as cell adhesion molecules and cell surface receptors, cytokines, growth factors, and other proteases (reviewed by Ethell & Ethell, 2007). Beside an active site containing Zn^{2+} that is necessary for its enzymatic activity, MMP-9 also contains three fibronectin type II repeats which can directly bind gelatin, laminin and collagens types I and IV (reviewed by Van den Steen et al., 2002).

MMP-9 expression is regulated during development, with high levels during early developmental time-points that decrease into adulthood (Aujla & Huntley, 2014; Bednarek et al., 2009; Oliveira-Silva et al., 2007; Vaillant et al., 1999). This pattern is consistent when measuring either the protein levels of MMP-9 with antibodies or the enzymatic activity levels of MMP-9 using gelatin zymography (Oliveira-Silva et al., 2007). Although MMP-9 levels remain low in the adult brain, MMP-9 activity increases in response to synaptic activity (Gawlak et al., 2009; Janusz et al., 2013). MMP-9 expression has been detected in several brain areas, including the hippocampus (Aujla & Huntley, 2014), the brainstem (Oliveira-Silva et al., 2007), the cerebellum (Vaillant et al., 1999), and the neocortex (Bednarek et al., 2009). MMP-9 proteolytic activity co-localizes

with excitatory synapses (Gawlak et al., 2009), while its mRNA is detected within the cell body, along the processes and in synaptoneurosome fractions of neurons (Janusz et al., 2013). MMP-9 is also expressed in astrocytes, microglia and along oligodendrocyte processes (reviewed by Dzwonek et al., 2004; Gawlak et al., 2009).

Importantly, the expression, translation and activity of MMP-9 are tightly regulated. Expression of MMP-9 can be regulated by growth factors, cytokines, oncogenes, metal ions and hormones through MAPK pathway signaling (reviewed by Van den Steen et al., 2002). MMP-9 translation is suppressed through its binding to Fragile X Mental Retardation Protein (FMRP), an mRNA binding protein, implicating MMP-9 in Fragile X Syndrome (FXS) (Janusz et al., 2013). MMP-9 mRNA is mainly localized in the cell body of hippocampal neurons and is translocated from the cell body to dendritic synapses in response to neuronal activity (Dziembowska et al., 2012) as a part of an FMRP containing granule (Janusz et al., 2013). mGluR activation causes the dissociation of FMRP from the MMP-9 mRNA (Janusz et al., 2013) followed by the association of MMP-9 mRNA with actively translating polyribosomes and *de novo* protein synthesis (Dziembowska et al., 2012). Once the MMP-9 protein is secreted from a cell by a yet to be discovered mechanism, it is in an inactive pro-from, also called a zymogen, where its enzymatic activity is inhibited by a pro-domain that masks the catalytic site through an interaction between Zn^{2+} and a cysteine residue in the pro-domain (reviewed by Ethell & Ethell, 2007). This pro-form cannot cleave its substrates until the pro-domain has been removed from the active site by proteolysis or protein unfolding, a process called a *cysteine switch*. This can be performed by other MMPs,

serine proteinases, by nitric oxide and by reactive oxygen species. The action of MMP-9 is further limited by degradation of the enzyme and by inhibition of its activity via thrombospondins or through tissue inhibitor of metalloproteinase-1 (TIMP-1) - which interestingly is secreted in response to synaptic activity at levels similar to MMP-9 (reviewed by Ethell & Ethell, 2007) and can form a complex with MMP-9 prior to secretion (Roderfeld et al., 2007). Thus, the tight regulation of MMP-9 activity is critical for its function in development and plasticity, and highlights a role for MMP-9 in cell-specific, activity-driven activation and remodeling of the pericellular environment, with spatially and temporally restrained effects.

A large body of research on MMP-9 has focused on its various roles in neurodegenerative disorders (reviewed by Yong, 2005). Nonetheless, it is becoming increasingly clear that MMP-9 has multiple functions in CNS development as well, and may contribute to neurodevelopmental disorders. MMP-9, through cleavage of surface- and cell-adhesion molecules, is implicated in active dendritic spine remodeling and stabilization (reviewed by Benson & Huntley, 2012; Bilousova et al., 2009), affecting the shape and function of dendritic synapses (Michaluk et al., 2011). MMP-9 also plays a role in pre- and postsynaptic receptor dynamics (Michaluk et al., 2009; Ning et al., 2013; Peixoto et al., 2012), in consolidation of long-term potentiation (Wang et al., 2008), myelination (Oh et al., 1999), and possibly in synaptic pruning (Wilczynski et al., 2008). It is further implicated in axonal elongation (Shubayev & Myers, 2004), pathfinding (Aujla & Huntley, 2014; Vaillant et al., 2003; Lin et al., 2008), regeneration (Ahmed et al., 2005) and degeneration (Costanzo et al., 2006). This review summarizes the various

roles of MMP-9 in diverse developmental processes within the central nervous system, with an emphasis on sensory development, and suggests a role for misregulated MMP-9 in neurodevelopmental disorders.

3. Brain development and critical period plasticity (CPP)

The critical period can be loosely defined as a time when experience-dependent activity can drive alterations in the structure, functional organization and physiological properties of brain regions. It occurs during postnatal development and is marked by increased plasticity and massive synaptic reorganization. The opening of the critical period is driven by the onset of sensory function, when peripheral sensory structures mature and begin to relay external sensory input into central structures. Reorganization takes place among thalamocortical projections, established prior to sensory input (reviewed by Feller & Scanziani, 2005), and among corticocortical connections, which together undergo increased synaptogenesis, axonal arborization, and pruning (Sanes et al., 2005) so that each sensory modality is able to respond optimally to behaviorally relevant stimuli (reviewed by Hensch, 2004). This increased plasticity during the critical period is time-limited, constrained by the development of stabilizing factors such as increased intracortical inhibition and the formation of perineuronal nets, a specialized ECM structure (reviewed by Hensch, 2005). The timing of this plasticity is different depending on species, sensory modality and even on the type of sensory manipulation used within a sensory modality (reviewed by Hensch, 2004). Non-sensory regions likewise have a window of postnatal synaptogenesis, reorganization, pruning and apoptosis (reviewed by Hashimoto and Kano, 2005; reviewed by Luo, 2005; Murase &

Table 1.1. MMP-9 expression in central nervous system development

	Developmental Window	Peak MMP-9 Expression	MMP-9 in Experience Dependent Plasticity	Reference
Visual System	Retinotectal map formation: P0-P21 (first 3 postnatal weeks) *r.*	Sup. Colliculus: P0-P10 *protein* P0-P14 *activity.*	Monocular enucleation increases MMP-9 enzymatic activity in SC	Oliveira-Silva et al., 2007
	Monocular deprivation: P21-P28 *r.*; Postnatal week 3-5 *r.;* P19-P32 *m.*	……..	Monocular deprivation increases MMP-9 mRNA in cortex	Spolidoro et al., 2012; Fagiolini et al. 1994; Gordon & Stryker, 1996
	Optic nerve myelination: P7-P9 *m.*	Optic Nerve: P7-P11 *activity.* P7 *mRNA*	……....	Oh et al., 1999; Larsen et al., 2006
Barrel Cortex	Thalamocortical input to Layer 4: P1-P4/5 *m., r.* Intracortical connections: Layer 4-2/3: P10-P14 *r.* Layer 2/3: thru adulthood *r.*		Whisker trimming in adolescent mice increases MMP-9 enzymatic activity; MMP-9 KO mice show reduced potentiation in L4 and L2/3 following trimming	Kaliszewska et al., 2011; Woolsey & Wann, 1976; Fox, 1992; Maravall, 2004; Kossut et al., 1988
Cerebellum	Granule cell proliferation, Climbing fibers refinement: Postnatal week 1 Granule cell migration; Parallel fiber innervation of Purkinje cells: Postnatal week 2-3 Purkinje cell arborization: Postnatal week 4	Granule precursors, Bergmann glia, Purkinje cells: P10 *protein* EGL, IGL and Purkinje cell layer: P11-P17 *protein*	MMP-9 KO mice at P12 exhibit: Decreased apoptosis of granule precursor cells; Delay in granule cell migration	*m*. Vaillant et al., 2003; *r.* Vaillant et al. 1999; *r.* Piccolini et al., 2012; *r.* Altman, 1972 a, b
Hippocampus	Spontaneous activity and apoptosis: P0-P7 *r. m.* Mossy fiber development: First postnatal month *r.* Synapse elaboration: First postnatal month *r.*	Axon tips:P4 *r. protein* DG, CA1, CA3: P4 r. *mRNA* Postsynaptic densities: P8 *r. protein*	MMP-9 mediates cell survival through interactions with laminin MMP-9 KO mice show accelerated synaptic maturation MMP-9 treatment exaggerates immature spine morphology	Murase & McKay, 2012; Ribak et al., 1985; Steward & Falk, 1991; Aujla & Huntley, 2014; Sidhu et al., 2014; Bilousova et al., 2009
Auditory	…….. Tonotopic reorganization: P11-P15 *m*. P11-P13 *r.* P9-P20 *m.* P11-P28 *r.*		Cochleotomy leads to increased MMP-9 levels in cochlear nucleus one day post-op	Illing et al., 2010 Barkat et al., 2011; de Villers-Sidani et al., 2007; Kim et al., 2013; Zhang et al., 2002

Key: *r*. rats; *m*. mouse,.*activity.* enzymatic activity measure by zymography.

McKay, 2012; Ribak et al., 1985; Steward & Falk, 1991). Periods of high MMP-9 activity correlate with synaptic reorganization during CPP and developmental windows across CNS regions (see Table 1.1), suggesting a role for MMP-9 in shaping CPP kinetics. Within this review we discuss CPP within rodent models due to the widespread use of these models for genetic manipulation of MMP-9 activity, and note that time-lines provided in this review for CPP windows are subject to variability between experimental procedures, protocols and outcome measures used, and are intended as a basic guideline.

3.1 Visual cortex

One of the first demonstrations of CPP came from studies by Hubel and Weisel (1964) in the kitten visual cortex, where they demonstrated that monocular deprivation alters both functional and anatomical organization in the cortex and, to a more limited extent, in the thalamus. Within the rodent visual cortex, the CPP window opens during the third postnatal week and closes into the fifth postnatal week, with adult-like functional properties by P45 (Fagiolini et al., 1994; Gordon & Stryker, 1996), though retinotectal reorganization occurs mostly in the first three postnatal weeks (Oliveira-Silva et al., 2007; Serfaty et al., 2005). Most neurons in the rodent visual cortex (Sawtell et al., 2003) and superior colliculus (SC) respond to contralateral eye stimulation and this contralateral preference can be manipulated during development by monocular deprivation. After eye closure (monocular deprivation), there is a reorganization of network connections contralateral to the deprived eye within the visual cortex (Spolidoro et al., 2012) and SC (Oliveira-Silva et al., 2007). Neuronal responses to stimulation of the deprived eye undergo depression and weakening of synaptic efficacy within 3 days (Sawtell et al., 2003), along with shrinkage of thalamocortical projections (reviewed by

Feller & Scanziani, 2005; Spolidoro et al., 2012). Between 4 to 7 days after monocular deprivation, responses to the non-deprived eye undergo potentiation, with a concomitant expansion in axonal arborization (reviewed by Feller & Scanziani, 2005; Sawtell et al., 2003; Spolidoro et al., 2012). The overall outcome is that more neurons will respond to visual stimulation of the non-deprived ipsilateral eye, termed an ocular dominance shift.

MMP-9 has been implicated in various aspects of visual CPP. In the SC, MMP-9 enzymatic activity and protein levels (both the proform and active forms) are high during the period of retinotectal map reorganization before and just after eye opening (from P0 to P14), and decrease during late (P21 to P42) postnatal development (Oliveira-Silva et al., 2007). Broad inhibition of MMPs from P0 to P7 alters the topographical organization of retinotectal terminals, while monocular enucleation at P10 increases MMP-9 enzymatic activity in the superior colliculus both contralateral and ipsilateral to the enucleated eye (Oliveira-Silva et al., 2007). Within the cortex, MMPs are involved in plasticity following monocular deprivation for either 3 or 7 days in adolescent rats (P21 to P45) (Spolidoro et al., 2012). Inhibition of MMP activity, using the broad spectrum MMP inhibitor GM6001 produces three main effects: 1) reduces the ocular dominance shift after monocular deprivation by selectively preventing the potentiation of open-eye responses without affecting the depression of deprived-eye responses, 2) blocks the deprivation-driven increase in spine density in layer 2/3 excitatory neurons contralateral to the deprived eye, and 3) blocks the potentiation of the deprived-eye responses after eye reopening. Though MMP-9 cannot be directly implicated in cortical ocular dominance plasticity based on these results, the authors noted that the only MMP to show mRNA

changes in response to monocular deprivation was MMP-9 (Spolidoro et al., 2012). MMP-2 is, however, expressed in the CNS at higher basal levels than MMP-9, and therefore may account for ocular dominance plasticity without mRNA up-regulation. To our knowledge there is no published work using MMP-9 KO mice to further test the role of MMP-9 in visual CPP, however MMP-3 KO mice, which have reduced activation of pro-MMP-9, do demonstrate altered visual CPP plasticity including reduced open-eye potentiation, suggesting a possible role for MMP-9 (Aerts et al., 2014).

3.2 Somatosensory cortex

MMP-9 has been more directly implicated in somatosensory barrel cortex plasticity. In rodent barrel cortex each whisker is represented in a one-to-one ratio by cortical cellular aggregate, termed a 'barrel'. Both the thalamocortical innervation of the barrels as well as the intracortical connections can be modified by removing the whiskers, with less dramatic reorganization after plucking or trimming of the whiskers. There are multiple windows of plasticity between cortical layers and across ages (reviewed by Fox, 2002), and the effect of experimental manipulation on barrel cortex plasticity depends both on the age, length and the type of manipulation used. Early postnatal CPP takes place largely in layer IV barrel cortex from P0 to P4/5 (Woolsey & Wann, 1976; Fox, 1992). It is characterized by receptive field plasticity, a conversion of silent synapses into active synapses, and changes in pre-synaptic thalamocortical arborization and barrel formation (reviewed by Erzurumlu & Gaspar, 2012 and Fox, 2002). Lesions within this window can induce structural reorganization of thalamocortical afferents (reviewed by Erzurumlu & Gaspar, 2012 and Fox, 2002). CPP in layer IV to II/III occurs from P10 to

P14 (reviewed by Erzurumlu & Gaspar, 2012; Maravall, 2004), whereas horizontal intracortical connections in layers II/III remain plastic through the third postnatal week and, to a lesser extent, throughout adolescence (reviewed by Fox, 2002). Adolescent plasticity is characterized as functional but not structural reorganization, including potentiation of spared input and depression of deprived input. More limited functional plasticity remains into adulthood (reviewed by Fox, 2002; Kossut et al., 1988).

One common manipulation to examine barrel CPP is to trim all but one row of whiskers. This can cause a topographic reorganization of functional sensory maps so that barrel columns in the cortex that have been deprived of peripheral sensory input will respond to deflections of the retained, intact whiskers. Such reorganization is possible in adolescent mice after one week of whisker trimming, and even more pronounced after 4 weeks. This manipulation causes an increase in the width of barrel activation when the spared-whiskers are deflected, an effect seen in all cortical layers of a vertical barrel column (Kaliszewska et al., 2011). When the spared-whisker is deflected there is also increased cellular activation in the barrel columns that directly border the spared row, as measured by c-fos density (Kaliszewska et al., 2011). After undergoing this deprivation-induced plasticity for 1 week, MMP-9 enzymatic activity levels are higher in the barrel cortex of mice when compared to the control non-deprived hemisphere, whereas there is no increase in MMP-2 (Kaliszewska et al., 2011). In MMP-9 KO mice, though 4 weeks of deprivation did increase the width of spared-row activation in all cortical layers when compared to the control non-deprived hemisphere, the width of layer IV activation was significantly smaller than in WT mice (Kaliszewska et al., 2011). Cellular activation of

the deprived rows was also significantly reduced in layer II/III of MMP-9 KO mice compared to WT mice, but was no different in any other layer (Kaliszewska et al., 2011). The fact that MMP-9 activity did not affect reorganization at all layers indicates a specific action of MMP-9, though the mechanism of the specificity is not known.

Understanding how MMP-9 is affecting plasticity at only certain levels of the circuit is difficult based on these results. The most likely site of functional reorganization in adult barrel cortex after deprivation or denervation may be through the unmasking of previously established silent or 'weak' synapses that project from the intact whisker onto neighboring columns (Kossut et al., 1988; Simons, 1978). It is possible that MMP-9 is necessary for integrating these weaker synapses into the circuit by maturation and stabilization of synaptic contacts (see the section on synapse development and plasticity below). Conversely, increased responses to the intact whisker column may be due to disinhibition from surrounding barrels (Kelly et al., 1999). The decreased potentiation in layer II/III observed in the deprived neighboring barrel columns in MMP-9 KO mice may be an effect of the reduced potentiation in layer IV of the intact barrel, as measurement of response latency suggests that information is transferred within a barrel column first, beginning in layer IV and transferring vertically between layers, before it is transferred outward to neighboring barrels (Armstrong-James et al., 1992; reviewed by Feldmeyer, 2012; reviewed by Fox, 2002). It is further possible that the increased functional activation in layer IV was reflective of changes in astrocytic activity instead of or in addition to neuronal activity. The method of 2-DG autoradiography used in Kaliszewska et al., 2011 measures metabolic activity including that of astrocytes which are located

within the somatosensory barrel cortex and which show an organizational pattern that parallels neuronal organization (Giaume et al., 2009; Logvinov et al., 2011). It is possible that loss of MMP-9 can affect astrocytic function, and that as-yet undetermined interactions exist between astrocytes, MMP-9 activity and synaptic plasticity in layer IV barrel cortex. More studies are needed to clarify the mechanisms that underlie changes in plasticity observed here.

3.3 Auditory cortex

To our knowledge, no studies have looked at the role of MMP-9 in auditory system CPP. MMP-9 does not influence the development of spiral ganglion cells, which relay information from cochlear hair cells to the CNS (Sung et al., 2014). On the other hand, after removal of the cochlea and spiral ganglion cells, MMP-9 protein in the cochlear nucleus peaks one day post-operation, with an increase in the neuropil and a decrease within cell bodies, suggestive of increased MMP-9 secretion from the cells and indicating that MMP-9 may be involved in degenerative and/or regenerative processes in early auditory pathways (Illing et al., 2010). Indirect evidence suggests MMP-9 may have a role in auditory CPP. In Fragile X mental retardation gene 1 (*Fmr1)* KO mice, a mouse model of FXS, auditory cortex CPP is deficient (Kim et al., 2013). MMP-9 enzymatic levels are elevated in the brain of *Fmr1* KO mice (Sidhu et al., 2014; Gkogkas et al., 2014) possibly due to a loss of FMRP transcriptional regulation of MMP-9 (Janusz et al., 2013). Genetic deletion of MMP-9 or pharmacological treatment that lowers MMP-9 levels during postnatal development rescues behavioral deficits in *Fmr1* KO mice in adulthood (Dansie et al., 2013; Sidhu et al., 2014). Therefore, it is possible that elevated

MMP-9 underlies deficient auditory cortex CPP in the *Fmr1* KO mice, which remains to be tested. This is an important avenue of research because CPP deficits may underlie later auditory processing deficits in FXS patients (Rotschafer & Razak, 2013).

3.4 Cerebellum

In the rodent cerebellum, a peak in MMP-9 expression also correlates with a window of synaptic and cellular reorganization. The cerebellum has a clear laminar distribution of cell types and function, with a deep layer called the granular layer or internal granular layer (IGL), a middle layer called the Purkinje cell layer, and a superficial layer called the molecular layer. During early postnatal development there is yet another layer which covers the surface of the cerebellum, the external granular layer (EGL). Cerebellar postnatal development is marked first by the proliferation of cerebellar granule neuron precursor cells in the EGL during the first postnatal week (Altman, 1972a; reviewed by Luo, 2005) and a refinement of climbing fiber excitatory input onto Purkinje cells (reviewed by Hashimoto & Kano, 2005). During the second postnatal week the EGL thins following the migration of granule precursor cells (Vaillant et al., 1999) and disappears by the end of the third postnatal week. During this same time frame the refinement of climbing fiber connections onto Purkinje cells is followed by the innervation of parallel fibers (granule cell axons) onto Purkinje cells as the Purkinje cells begin to form secondary and tertiary dendritic branches (Altman, 1972b; reviewed by Hashimoto & Kano, 2005). Finally Purkinje cells undergo an extensive arborization during the fourth postnatal week (reviewed by Luo, 2005). MMP-9 enzymatic activity peaks at P10 and decreases to adult levels by P15 (Vaillant et al., 1999). MMP-9 protein

at P10 is detectable in granule precursor cells, Bergmann glial cell bodies and processes, and in Purkinje cell dendrites, a pattern which is similar to MMP-9 mRNA expression (Vaillant et al., 1999). From P11 to P17, both MMP-9 and MMP-3 protein are expressed in the EGL, the IGL, and intensely in the molecular and Purkinje cell layers (Piccolini et al., 2012) where MMP-9 labels the soma of granular and Purkinje cells (Vaillant et al., 2003). At P12 MMP-9 expression in the EGL is concentrated in the premigratory pool of granule precursor cells and is present in migrating granular precursor cells dispersed in the molecular layer (Vaillant et al., 2003). Overlapping expression of MMP-9 and MMP-3 is important because MMP-3 can cleave and activate MMP-9. Indeed, MMP-9 plays an important role in cerebellar development as the application of an MMP-9 blocking antibody and genetic deletion of MMP-9 inhibit axonal outgrowth (parallel fibers) and the migration and apoptosis of granule cell precursors in the developing cerebellum (Vaillant et al., 2003).

3.5 Hippocampus

In the hippocampus, structural organization is largely established during embryogenesis, though in the germinal zone of the dentate gyrus (DG) active neurogenesis and granule cell migration continue into adulthood (Bayer, 1980). During the first postnatal week, there is spontaneous activity that drives reorganization and neuronal survival (Murase & McKay, 2012), while mossy fibers (Ribak et al., 1985) as well as synapses within the DG and CA1 (Steward & Falk, 1991) undergo elaboration and maturation throughout the first postnatal month. At P4, MMP-9 mRNA levels peak in the DG, CA1 and CA3, and MMP-9 and MMP-2 proteins are shown to co-

immunolabel with L1CAM (L1 cell adhesion molecule), a marker of growing axons (Aujla & Huntley, 2014). At a period of peak hippocampal synaptogenesis, MMP-9 and MMP-2 are localized near the postsynaptic densities immunolableled against PSD-95 (Aujla & Huntley, 2014). MMP-9 genetic deletion accelerates the maturation of dendritic spines showing an early increase in the number of mature mushroom-shaped spines at P8, which is normally observed later at P14-P21 (Sidhu et al., 2014). Conversely, an acute treatment of cultured hippocampal neurons with active MMP-9 leads to an increase in immature filopodia-like spines and a decrease in mature mushroom-shaped spines (Bilousova et al., 2009). While global genetic deletion of MMP-9 causes an increase in the number of mature spines during early postnatal hippocampal development and enhanced MMP-9 activity leads to the formation of immature spines in cultured hippocampal neurons, a transient release of MMP-9 at the level of a single synapse was shown to be associated with LTP-induced spine enlargement in adult hippocampus (Wang et al., 2008; see the section on synapse development and plasticity for more details). MMP-9 has been also implicated in spine head maturation during the development of visual cortex (Kelly et al., 2014). It is possible that genetic deletion of MMP-9 can lead to brain area specific compensatory effects of other MMPs (Esparza, 2004; Nagy et al., 2006), as MMP-3 is also expressed in the brain and is implicated in synaptic plasticity (Aerts et al., 2014).

Taken together, these studies suggest MMP-9 activity contributes to multiple aspects of neural network reorganization during early development, including regulation of CPP plasticity. This sensory-dependent, activity driven reorganization primes each

region to respond appropriately to external cues. The mechanisms underlying MMP-9-mediated CPP and synaptic reorganization though, are not well understood (see Table 1.2).

4. Cellular mechanisms

4.1 Synapse development and plasticity

The structural changes within the CNS thought to underlie neural plasticity, including learning and memory, can be traced to the level of the individual synapse and spine. Functional synaptic plasticity can be broadly classified into two underlying processes: one being depression, during which the post-synaptic potentials are reduced in amplitude relative to baseline, and the other being potentiation, characterized as an increase in synaptic strength. Additionally these changes in synaptic efficacy can be transient (short-term) or they can be maintained hours to days (long-term), where modification of receptors at synaptic sites through new protein synthesis is thought to underlie long-term changes. The mechanisms of both potentiation and depression can be localized to the presynaptic axon terminal, the postsynaptic dendrite, or both. Synaptic plasticity is a process that can incorporate new or changing input into a system, can form associative networks of connections and can respond to changes in the nervous system environment by scaling connections up or down over time to allow for fine-tuned network modification. As such, synaptic plasticity can be considered to be a fundamental cellular event underlying much of the brain ability to adapt and respond to changing environmental demands throughout a lifetime, from CPP sensory reorganization to learning and memory.

MMP-9 has been implicated in the maintenance of long-term potentiation (LTP). LTP can be classified into an early-phase LTP (e-LTP) that is independent of protein synthesis and a late-phase LTP (l-LTP) that requires new protein synthesis. l-LTP in particular may underlie the consolidation of memories by strengthening synapses for extended periods of time. A popular brain structure for the study of synaptic plasticity mechanisms is the hippocampus, due to its well-defined circuit organization and because of its role in learning and memory. Multiple hippocampal pathways have been used to study the role of MMP-9 in synaptic plasticity. In the mossy fiber-CA3 pathway, LTP induction in adolescent rats causes an increase in MMP-9 enzymatic activity, both the proform and the active form of the enzyme, and an increase in MMP-9 protein expression in CA3 neurons (Wiera et al., 2012). Both total genetic deletion of MMP-9 (mice) and a 15-fold overexpression of MMP-9 (rats) impair the maintenance of LTP in the mossy fiber-CA3 pathway in hippocampal adolescent slices (Wiera et al., 2013). In both MMP-9 KO and overexpressing models the initial potentiation after high frequency tetanic stimulation is comparable to wild types, but as early as 7 to 10 minutes post-stimulation, both models show a significantly reduced potentiation (Wiera et al., 2013). This indicates that too much or too little MMP-9 can lead to impaired LTP maintenance, including both early- and late-phase LTP. In a different hippocampal pathway, the Schaffer collateral-CA1 pathway, MMP-9 activity is also implicated in LTP. High frequency tetanic stimulation or chemically induced LTP (cLTP) increase the levels of active MMP-9 protein, peaking 30 minutes post-stimulation, but do not affect the levels of MMP-2 (Nagy et al., 2006). cLTP also increases the proteolytic activity of MMP-9

localized to the neuropil in CA1 stratum radiatum (Nagy et al., 2006). Inhibition of MMP-9 and MMP-2 in slices of both young and adult rats, or inhibition of MMP-9 alone in anesthetized rats *in vivo* (Bozdagi et al., 2007), does not affect initial potentiation and e-LTP but does impair l-LTP, with decreased potentiation by 60 minutes post-stimulation (Nagy et al., 2006). Total genetic deletion of MMP-9 in this same pathway impairs LTP overall, similar to the mossy fiber-CA3 pathway (Nagy et al., 2006). In the CA1 to prefrontal cortex pathway TIMP-1 overexpression, which reduces MMP activity, prevents l-LTP *in vivo* (Okulski et al., 2007). Similarly direct inhibition of MMP-9 *in vitro* blocks prefrontal l-LTP but not e-LTP (Okulski et al., 2007). The precise mechanisms by which MMP-9 affects synaptic plasticity are not fully understood. In the Schaffer collateral-CA1 pathway, increased MMP-9 levels after tetanic stimulation were dependent on N-methyl-D-aspartate (NMDA) receptor activation at postsynaptic sites (Nagy et al., 2006). Conversely in the mossy fiber-CA3 pathway, where LTP is also MMP-9 dependent, LTP occurs at presynaptic sites and is independent of NMDA receptors (Castillo et al., 1997; Harris & Cotman, 1986; Wiera et al., 2013). Moreover the experimental manipulations used to test MMP-9 necessity, by either genetic deletion or chemical inhibition, have differential effects on e-LTP induction, leaving in question the role of MMP-9 in e-LTP.

MMP-9 also affects the trafficking of both NMDA and α-amino-3-hydroxyl-5-methyl-4-isoxazole-propionate (AMPA) glutamate receptors. The modification and/or insertion of glutamate receptors to the postsynaptic site are thought to fundamentally relate to long-term synaptic plasticity. Bath application of auto activating MMP-9 in

cultured hippocampal neurons induces the lateral diffusion of NMDA receptors, but not GluA2-containing AMPA receptors, at synapses (Michaluk et al., 2009). On the other hand, after a chemical LTP induction (cLTP) in cultured hippocampal neurons, MMP activity is necessary for the immobilization and synaptic accumulation of GluA1- and GluA2-containing AMPA receptors (Szepesi et al., 2013; Szepesi et al., 2014) in dendritic spines. MMP-9 in particular was suggested to be involved in AMPA receptor trafficking because MMP-9 levels, but not MMP-2, were up-regulated following cLTP (Szepesi et al., 2013). The action of MMP-9 on lateral diffusion of NMDA receptors was shown to depend on integrin β1 signaling (Michaluk et al., 2009). Integrins are membrane-bound ECM receptors found on pre-and postsynaptic sites in many types of cells in the CNS. Activation of integrin receptors induces the elongation of dendritic spines in hippocampal culture (Shi, 2006). Longer, thinner spines are associated with immature synapses and are highly motile, whereas shorter spines with large spine heads are associated with mature, stable synaptic connections. MMP-9 transgenic overexpression or global bath application of active MMP-9 induces the elongation of dendritic spines, similar to integrin activation, while blocking integrin receptors prevents MMP-9-induced spine alterations (Michaluk et al., 2011; Bilousova et al., 2009). The effects of MMP-9 on integrin receptor signaling are not mediated through direct protein-protein interactions (Michaluk et al., 2009). Rather it is suggested that MMP-9 cleavage of ECM triggers a release of arginine-glycine-aspartate (RGD)-containing peptides that are potent activators of integrins (Ruoslahti, 1996). A direct application of RGD-containing peptide to cultured hippocampal neurons was also shown to induce spine

elongation and actin reorganization in dendritic spines in an NMDA-dependent manner (Shi, et al., 2006), possibly through integrin-mediated phosphorylation of NMDA receptors (Bernard-Trifilo et al., 2005).

Interestingly, local activation of MMP-9 at the level of individual synapses can induce the maturation of spine heads instead of spine elongation. After cLTP in culture, MMP-9 (and possibly MMP-2) enzymatic activity is localized around a small number of immature spines that preferentially undergo spine head enlargement (as opposed to already mature spines) (Szepesi et al., 2014). Additionally, experiments using theta burst stimulation to induce LTP in acute hippocampal slices demonstrated that MMP-9 activity is both necessary and sufficient to induce expansion of spine heads, including small and large spine (Wang et al., 2008). Blocking MMP activity produced a transient increase in head size that was quickly reduced to baseline, analogous to the MMP-9 dependent maintenance of LTP (Nagy et al., 2006; Okulski et al., 2007; Wang et al., 2008). Consistent with other reports, MMP-9-mediated spine head enlargement was also dependent on integrin signaling (Wang et al., 2008). In addition, both MMP-9 activation and cLTP were shown to induce the extension of filopodia-like protrusions from the heads of dendritic spines (Szepesi et al. 2013), which were also linked to a local change in connectivity in response to glutamate release (Richards et al., 2005). Taken together this indicates that MMP-9 can induce spine elongation or maturation depending on the level of MMP-9 activity, its localization and/or substrate. Why MMP-9 would have such differential effects is unclear. If endogenous MMP-9 does preferentially target immature spines to induce their maturation in response to neuronal activity (Szepesi et al. 2014),

Table 1.2. Role of MMP-9 in specific plastic events.

		References
Synaptic Plasticity	Late-phase LTP	Nagy et al., 2006 Okulski et al., 2007 Wang et al., 2008 Wiera et al., 2013
	NMDA receptor trafficking	Michaluk et al., 2009
	AMPA receptor trafficking	Szepesi et al., 2014
	Spine elongation	Bilousova et al., 2009 Michaluk et al., 2009; 2011
	Spine maturation	Wang et al., 2008 Kelly et al., 2014 Szepesi et al., 2014
	Integrin-dependent	Michaluk et al., 2009; 2011 Wang et al., 2008
	Involves ICAM-5	Tian et al., 2007 Ning et al., 2013 Kelly et al., 2014
Axonal plasticity	Pathfinding	Hehr, 2005 Vaillant et al., 2003 Aujla & Huntley, 2014
	Regeneration after injury	Ferguson, 2000 Shubayev & Myers, 2004 Ahmed et al., 2005
	Degeneration after injury	Costanzo et a., 2006
	EphB2 mediated growth cone collapse	Lin et al., 2008
Myelination	Oligodendrocyte process extension/formation	Uhm, et al., 1998 Oh et al., 1999 Šišková et al., 2009
	Oligodendrocyte/axon contact	Maier et al., 2006

exogenous application of MMP-9 could disrupt this selectivity, targeting mature synapses instead. It is likewise possible that MMP-9 cleavage of specific synaptic and perisynaptic targets at a specific time and place is necessary for spine head enlargement, but that if the action is not temporally restricted MMP-9 activity prevents these synaptic structures from maturing and stabilizing. Indeed, both genetic deletion and overexpression of MMP-9 impairs the maintenance of LTP in the mossy fiber-CA3 pathway in hippocampal slices (Wiera et al., 2013).

MMP-9 up-regulation in response to NMDA activity can also act on intercellular adhesion molecule-5 (ICAM-5) and neuroligin-1 to regulate dendritic spine morphology. ICAM-5 is a cell adhesion molecule found in excitatory cell bodies and in dendritic shafts and spines. In cultured hippocampal neurons, ICAM-5 is found in association with thin spines and filopodia more so than with mature mushroom-shaped spines (Ning et al., 2013; Tian et al., 2007). ICAM-5 within postsynaptic filopodia binds to presynaptic β1integrin receptors to mediate trans-synaptic signaling and this binding maintains immature spine morphology (Ning et al., 2013). Hippocampal neurons treated with NMDA show an increase in mushroom shaped spines with a concomitant increase in ICAM-5 cleavage, indicating that cleavage of ICAM-5 may induce spine maturation (Tian et al., 2007). Both MMP-9 and MMP-2 can cleave ICAM-5, and active levels of both enzymes are elevated after NMDA stimulation (Tian et al., 2007). Likewise, NMDA induced cleavage of ICAM-5 in dendritic shafts is rescued by inhibition of MMP-2 and MMP-9 (Tian et al., 2007). In the visual cortex during a period of active synaptogenesis, just prior to (P14) and during ocular dominance CPP (P28), there is a

developmental shift in ICAM-5 localization from dendritic protrusion at P14 to dendritic shafts by P28 (Kelly et al., 2014). However this shift does not occur in MMP-9 KO mice (Kelly et al., 2014). Instead there are increased ICAM-5 levels in dendritic protrusions at both P14 and P28 which do not change with age (Kelly et al., 2014). An increase in synaptic contacts between ICAM-5 labeled structures (presumably dendritic structures) and axon terminals is also observed in MMP-9 KO mice (Kelly et al., 2013). Together this may indicate that MMP-9 cleaves ICAM-5 in response to NMDA stimulation to induce spine maturation, while in the absence of MMP-9 ICAM-5 remains in dendritic protrusions and maintains immature synapses through its binding to presynaptic β1 integrin receptors. Neuroligin-1(NLG-1) is a postsynaptic adhesion molecule, specific to excitatory cells, which binds to presynaptic neurexins through trans-synaptic interactions (Peixoto et al., 2012). MMP-9 cleaves NLG-1 both *in vivo* and *in vitro*, and this cleavage induces a rapid destabilization of its presynaptic partner neurexin-1 (Peixoto et al., 2012). This destabilization is paralleled by a reduced frequency of mini excitatory postsynaptic potentials and an altered paired pulse ratio – indicative of reduced presynaptic release probability (Peixoto et al., 2012). MMP-9 cleavage of NLG-1 is dependent on NMDA activation and Ca^{2+}/calmodulin-dependent protein kinase signaling, and occurs locally at the excited spine (Peixoto et al., 2012). Interestingly, NLG-1 cleavage is also regulated by sensory experience associated with CPP in the visual cortex and is increased within 2 hours of light exposure after a 5 day light deprivation (dark rearing) in mice during a fourth postnatal week (Peixoto et al., 2012). Together these studies illustrate a role for MMP-9 in the active modification of postsynaptic sites to modulate synaptic efficacy, a

process important both during development and throughout adulthood. However the role of MMP-9 in presynaptic axon reorganization remains less clear.

4.2 Axon regeneration and plasticity

The basic pattern of axonal tract organization is largely established before birth. During embryonic development axonal processes migrate through the developing nervous system relying on chemical cues as well as cell-cell and matrix-cell interactions in order to find their target locations. They then undergo reorganization in response to sensory stimulation during the critical period, where there is an elaboration of axonal arborizations followed by pruning. The axon arbors are thought to remain relatively stable after CPP closure, but can undergo reorganization following injury or sensory deprivation. MMP-2 and MMP-9 have been implicated in embryonic axon path finding in the *Xenopus* (Hehr, 2005) and MMP-9 was more directly implicated in regeneration of axons after injury in the rat (Shubayev & Myers, 2004; Ahmed et al., 2005). MMP-9 protein is also expressed in growing axons during early postnatal synaptogenesis in the hippocampus (Aujla & Huntley, 2014) and is necessary for neurite outgrowth in cerebellar granular cells (Vaillant et al., 2003). Still, the role of MMP-9 in CPP axonal reorganization needs further investigation.

During axon outgrowth and regeneration, MMP-9 activity seems to have differential effects depending on the neuronal type. MMP-9 protein is localized to axon growth cones in regenerating nerve fibers 8 days after sciatic nerve injury in rats (Shubayev & Myers, 2004) and its active enzymatic activity can peak as soon as 21 hours

after sciatic nerve injury in the mouse (Ferguson, 2000), although this early increase may be associated with inflammatory processes at the injury site rather than with regeneration per se. MMP-9 in PC12 cell culture can increase the length of sprouting fibers without affecting the total number of sprouting fibers (Shubayev & Myers, 2004). Similarly, MMP-9 and MMP-2 treatment of dorsal root ganglion neurites grown in culture can increase the average length of the neurites (Ferguson, 2000). Conversely, MMP-9 treatment does not affect either the number or the length of neurites in neonatal spiral ganglion neurons cultured from 5 day old rats (Sung et al., 2014). After olfactory nerve injury, increases in MMP-9 protein levels overlap with degeneration of mature olfactory neurons, while MMP-9 decreases during the period of regeneration (Costanzo et al., 2006). In contrast, both MMP-9 and MMP-2 protein and enzymatic levels are increased in regenerating optic nerves compared to non-regenerating nerves, peaking 8 days after injury (Ahmed et al., 2005).

Mechanisms underlying MMP-9 activity in axon growth and repair are also diverse. MMP-9 and MMP-2 can cleave EphB2, a receptor tyrosine kinase that can differentially attract or repulse axonal fibers through interactions with the ephrin-B ligand (reviewed by Sloniowski & Ethell, 2012). MMP-9 cleavage of EphB2 triggers a cell repulsion and subsequent collapse of axon growth cones in cultured hippocampal neurons through Rho GTPase activation (Lin et al., 2008). Additionally, MMP-9 cleaves collapsin response mediator protein-2 (CRMP-2) (Bajor et al., 2012), a protein that is shown to induce neuronal polarization and the elongation of axons (Yoshimura et al., 2005) in part through its ability to bind with tubulin heterodimers and to thereby promote

microtubule formation (Fukata et al., 2002). How MMP-9 activity might affect the function of CRMP-2 is not yet clear, though the putative cleavage site for MMP-9 of CRMP-2 overlaps with its protein binding site (Bajor et al., 2012), indicating that MMP-9 cleavage might interfere with CRMP-2 binding to tubulin, thereby affecting axonal elongation. Furthermore, MMP-9 can create a permissive environment for nerve regrowth after injury by controlling the proliferation of Schwann cells through induction of the Ras/Raf/MEK–ERK pathway to suspend Schwann cell mitosis (Chattopadhyay & Shubayev, 2009). Together these studies indicate numerous roles for MMP-9 in axonal plasticity, including regeneration and degeneration after injury, polarization and growth of neurite fibers, axon repulsion and growth cone collapse, as well as interactions with glial cells. It remains to be seen whether similar mechanisms play a role in postnatal CNS development and CPP.

4.3 Myelination

MMP-9 is also expressed in oligodendrocytes (Oh et al., 1999) and MMP activity is implicated in the regulation of myelin formation in the CNS (Maier et al., 2006). Myelination is one of the last processes to occur in CNS development, a hallmark of mature, established axonal connections. In the CNS, myelination along axonal processes is performed by oligodendrocytes (OL), a type of glial cell. Each oligodendrocyte can myelinate as many as 40 internodes, a process that occurs in several steps. After oligodendrocytes migrate and proliferate during early postnatal development (reviewed by Pfeiffer et al., 1993) three further steps are involved in the process of myelination: 1) OLs begin a period of extensive outgrowth of processes radially from the cell body

toward the axons, 2) once contact with an axon has been made, the OL ensheaths the axon in myelin layers until 3) compaction of the myelin sheath occurs (Uhm et al., 1998). Neuronal signals are key in the maturation of OL, where for example adenosine acts as a neuron-glial signal to inhibit the proliferation of OL progenitor cells and promote differentiation and myelin formation (Stevens et al., 2002). Myelin formation peaks within the first four weeks after birth (Foran & Peterson, 1992), generally in a caudal to rostral organization (reviewed by Pfeiffer et al., 1993). Axons with larger diameters are myelinated first, followed by smaller-diameter axons (Matthews & Duncan, 1971; Ye et al., 1995b). However, there are specific periods of myelination within different brain regions, each with a specific onset/peak window as well as different organizational trajectories (Foran & Peterson, 1992).

In the mouse optic nerve, MMP-9 enzymatic activity levels gradually increase from P3 to P11, with elevated transcript levels in the optic nerve at P7 (Larsen et al., 2006) and strong gelatinolytic activity at P9 (Oh et al., 1999), a time period overlapping with the strong expression of myelin basic protein (MBP) (Oh et al., 1999). In contrast, in the rodent corpus callosum, MMP-9 protein expression increases from P7 to P28 (Uhm et al., 1998), a time that corresponds to developmental myelination. MMP protein and gelatinolytic activity are localized around the OL cell body, along OL processes and, notably, at the advancing tip of OL processes (Oh et al., 1999; Šišková et al., 2009), implicating MMP-9 in the first step of myelination, OL process outgrowth.

Indeed, in mouse, human and bovine cultures of OLs, (Oh et al., 1999) increased OL process formation following activation of protein kinase C (PKC) is accompanied by

MMP-9 secretion, likely the proform of the enzyme, and inhibition of MMP-9 activity reduces OL process outgrowth (Uhm et al., 1998). In MMP-9 KO mice, though the development of myelin formation in the optic nerve is comparable to WT mice, adult OLs in culture have impaired process outgrowth in response to PKC activation and reduced spontaneous process formation (Oh et al., 1999). In the corpus collosum of MMP-9 KO mice, however, there was a transient reduction in the amount of myelin basic protein from P7 to P10 and a decrease in the number of mature OL cells (Larsen et al., 2006). The reduction in the number of mature OL cells indicates a role for MMP-9 not only in process extension but also in OL maturation. Siskova and colleagues further demonstrated that the interaction of MMP-9 with ECM molecule fibronectin affects the distribution of MMP-9 enzymatic activity along OL processes, instead restricting its activity to OL cell bodies (2009). This change in MMP-9 localization from control conditions is associated with the inhibition of OL differentiation, characterized by fewer primary and secondary processes, implicating MMP-9 enzymatic activity in OL differentiation (Šišková et al., 2009).

MMP-9 may also be involved in the second stage of myelination, ensheathment, through indirect interactions with insulin-like growth factor-1 (IGF-1). IGF-1 promotes OL proliferation and/or survival, stimulates myelination production and increases myelin thickness, and can be inhibited by insulin growth factor binding protein–6 (IGFBP-6) (Ye et al., 1995a). MMP-9 and MMP-12 can both cleave IGFBP-6, while MMP-9 null mice show increased levels of IGFBP-6 (Larsen et al., 2006) and application of IGF-1 increases the number of mature OLs in MMP-12 null mice (Larsen et al., 2006). These

studies suggest a role for MMP-9 and MMP-12 in cleavage of IGFBP-6 that disinhibits IGF-1 and thereby promotes OL maturation and ensheathment. MMP activity is further implicated in mediating contact between OL cells and axons through a cleavage of the OL-specific 155-kDa isoform of neurofascin (NF155), a member of the L1-family of cell adhesion molecules (L1-CAM) (Maier et al., 2006). This function is important because the extracellular domain of NF155, localized on the oligodendrocyte, can interact directly with adhesion molecules located on the axonal membrane, such as contactin (Maier et al., 2006). This suggests a role for MMP-mediated cleavage of NF155 in establishing the interactions between myelin and axons. Thus, MMP-9 is involved in multiple steps of the myelination process including OL maturation, process outgrowth and ensheathment of axons through its association with ECM and neuronal receptors to 'guide' the myelination process.

5. MMP-9 in pathophysiology of neurologic disorders

While the regulation of MMP-9 is important for many aspects of normal CNS development and plasticity, misregulation of MMP-9 levels and activity is increasingly implicated in neurodevelopmental and psychiatric disorders that are associated with aberrant brain development.

5.1 Fragile X Syndrome (FXS) and other developmental disorders

Recently, MMP-9 has been implicated in several psychiatric disorders that are associated with abnormal development including FXS, autism spectrum disorder (ASD), bipolar disorder and schizophrenia. Increased levels of MMP-9 have been demonstrated in human subjects with FXS (Dziembowska et al., 2013; Sidhu et al., 2014), ASD

(Abdallah et al., 2012), bi-polar disorder (Rybakowski et al., 2013) and treatment-resistant schizophrenia (Yamamori et al., 2013). Still, there is limited literature on the precise function of MMP-9 in these disorders. Whether MMP-9 is responsible for the behavioral deficits associated with these disorders, or is a result of abnormal changes in the brain is still unclear and requires further investigation. However, recent research suggests that enhanced MMP-9 activity is a major factor contributing to the pathophysiology of Fragile X Syndrome and epilepsy.

FXS is a trinucleotide repeat disorder that leads to the transcriptional silencing of fragile X mental retardation gene 1 (*Fmr1*). The FMR protein encoded by the gene is involved in translation regulation, and genetic deletion of the *Fmr1* gene in mice mimics FXS-associated deficits, providing a useful model to study FXS. The loss of translational suppression of MMP-9 by FMRP may be driving some of the deficits associated with FXS, such as abnormal dendritic spine development and synaptic plasticity. MMP-9 protein and enzymatic activity levels are increased in the hippocampus of developing (P7), adolescent, and adult *Fmr1 KO* mice (Bilousova et al., 2009; Janusz et al., 2013; Sidhu et al., 2014; Gkogkas et al., 2014). This enhanced MMP-9 activity contributes to abnormal PI3K-Akt-mTOR signaling in the *Fmr1* KO mouse, a pathway implicated in FXS and other ASDs (Sidhu et al., 2014). Moreover, the ability of a tetracycline derivative, minocycline, to inhibit MMP-9 activity is suggested to underlie its beneficial effects in *Fmr1* KO mice. Minocycline treatment lowers MMP-9, but not MMP-2 levels, and restores normal dendritic spine development in young *Fmr1* KO mice (Bilousova et al., 2009), reduces audiogenic seizure severity and rescues abnormal behaviors in both

young and adult *Fmr1* KO mice (Dansie et al., 2013; Rotschafer et al., 2012). Genetic deletion of *MMP-9* also repairs abnormal dendritic spine development, normalizes mGluR5-dependent LTD and alleviates abnormal social behaviors and anxiety in *Fmr1* KO mice (Sidhu et al., 2014). In drosophila there are only two MMPs, the secreted form MMP-1 and the membrane-anchored form MMP-2. Inhibition of MMP-1 activity in *dfmr1* null flies, a drosophila model of FXS, rescues some or all of the defects associated with the deletion of *dfmr* (Siller & Broadie, 2011; reviewed by Siller & Broadie, 2012). This was demonstrated using three different approaches: either 1) the overexpression of tissue inhibitor of MMP (TIMP), 2) the generation of double null mutants *dfmr1;mmp1*, or 3) treatment with minocycline (Siller & Broadie, 2011; reviewed by Siller & Broadie, 2012).

In humans with FXS the levels of total MMP-9 enzymatic activity are elevated in the plasma, without changes in MMP-2 levels (Dziembowska et al., 2013). The analysis of postmortem FXS brain tissue samples also indicate elevated levels of MMP-9 protein in both the hippocampus and neocortex (Sidhu et al., 2014; Gkogkas et al., 2014). Minocycline treatment reduces plasma levels of MMP-9 in most but not all subjects, and is associated with improvements in behavior (Dziembowska et al., 2013; Leigh et al., 2013; Paribello et al., 2010; Utari et al., 2010) and a reversal of habituation deficits in auditory event related potentials (Schneider et al., 2013). This suggests that MMP-9 suppression may be a useful therapeutic approach. Together these studies indicate that increased MMP-9 levels in FXS may underlie molecular, cellular and behavioral deficits, many of which are associated with abnormal plasticity, learning and memory in FXS.

5.2 MMP-9 in Epilepsy

The role of MMP-9 in epilepsy has been seen in both humans (Konopka et al., 2013; Suenaga et al., 2008) and in animals, and is a useful model of MMP-9 in aberrant plasticity. Epilepsy is a disorder in which seizures become spontaneous and recurrent, with highly synchronized activity. Aberrant neuronal plasticity as a result of seizure activity or brain injury is thought to underlie the progression of epilepsy. In both animal models of epilepsy and human epilepsy subjects (Proper et al., 2000) this aberrant plasticity can include neuronal loss in hippocampal regions, astrogliosis, aberrant pruning of DG spines (Wilczynski et al., 2008), reorganization of interneuron terminals (Pollock et al., 2014), loss and/or disorganized perineuronal net structures (McRae et al., 2012; Pollock et al., 2014), and the sprouting of mossy fibers to create a recurrent network (Wilczynski et al., 2008).

In young and adult human epilepsy patients MMP-9 protein levels are higher compared to controls (Konopka et al., 2013). Though other MMPs are increased as well, including MMP-2, MMP-3 and TIMP-2 in adults, MMP-9 has the most prominent and consistent increase in protein levels across ages (Konopka et al., 2013). This protein expression is localized to neurons, astrocytic processes and synapses, and is more strongly expressed in dysmorphic neurons than healthy neurons (Konopka et al., 2013). One mechanism thought to underlie epilepsy progression may be through a change in the ratio of MMP-9 to TIMP-1, the endogenous inhibitor of MMP-9. Subjects with varying forms of epilepsy have an increase in the MMP-9/TIMP-1 ratio suggesting an increase in the extracellular levels of MMP-9 activity (Suenaga et al., 2008).

In rodent models of epilepsy, a kindling procedure can be used where animals are electrically or chemically stimulated at sub-threshold seizure levels over a period of weeks until spontaneous seizures take place. MMP-9 KO mice require a longer kindling period to develop epilepsy over controls (Mizoguchi et al., 2011; Wilczynski et al., 2008), and experience less severe seizures once fully kindled and an increased survival rate (Wilczynski et al., 2008). Conversely, transgenic MMP-9 overexpressing rats show increased susceptibility to epileptogenesis with kindling (Wilczynski et al., 2008). After epilepsy induction in mice, overall MMP-9 protein levels did not change in the dentate gyrus; however there was a marked increase in a number of spines expressing MMP-9 protein and gelatinolytic activity localized to dendrites (Wilczynski et al., 2008). Interestingly, DG spine density was significantly decreased in WT but not MMP-9 KO mice after kainite-induced seizure indicating MMP-9 may play a destructive role promoting kainate-evoked spine pruning (Wilczynski et al., 2008). The inhibition of MMP-9 in slices after kainate application produces a 90% decrease in the density of mossy fiber sprouting in the DG (Wilczynski et al., 2008). This indicates a functional role for MMP-9 both in synaptic pruning and in mossy fiber sprouting in rodent models of epilepsy.

It is likely that there are multiple targets of MMP-9 which contribute to the progression of epilepsy. It is possible that MMP-9 acts by creating a permissive state through cleavage of ECM molecules, in particular, through cleavage of aggrecan. After seizure induction there is a loss of perineuronal nets around parvalbumin positive interneurons (Pollock et al., 2014), including a specific reduction in aggrecan and an

increase in unbound hyaluronan (McRae et al., 2012). Doxycycline hyclate, an antibiotic that inhibits MMP-9, prevents the loss of perineuronal nets after kindling and delays epilepsy onset, possibly through the inhibition of MMP-9 (Pollock et al., 2014). MMP-9 mediated cleavage of ECM may also affect neuronal activity and potentiate NMDAR currents through the activation of integrins (see section on synapse development and plasticity for details). In addition, MMP-9 cleavage of pro-BDNF into mature BDNF may play a role in the development of epilepsy through mossy fiber sprouting. The BDNF to pro-BDNF ratio increases in kindled WT mice, but not in MMP-9 KO mice, during the progression of epilepsy (Mizoguchi et al., 2011) implicating MMP-9 in pro-BDNF cleavage. Because there is no difference in overall BDNF levels in fully kindled mice, this suggests that MMP-9 cleavage of pro-BDNF may accelerate the onset of epilepsy (Mizoguchi et al., 2011).

5.3 Therapeutic approaches

There are several drugs on the market that can directly or indirectly alter MMP-9 levels and activity, some of which are already in use in humans. For example, diazepam, a drug used to treat epilepsy in humans, is able to suppress the development of epilepsy in kindled mice and reduce MMP-9 levels (Mizoguchi et al., 2011). Likewise both doxycycline (Pollock et al., 2014) and minocycline (Beheshti Nasr et al., 2013; Dansie et al., 2013) treatment can reduce seizure severity or epilepsy onset in mice. Minocycline treatment also rescues behavioral, anatomical and social deficits in young and adult *Fmr1* KO mice (Bilousova et al., 2009; Dansie et al., 2013; Rotschafer et al., 2012). Clinical trials on the effects of minocycline in human subjects with FXS have demonstrated

improvement in language, social communication, anxiety and attention (Utari et al., 2010) stereotypy, irritability and hyperactivity (Paribello et al., 2010) as well as on behavioral-improvement scales based on caregiver reports in a randomized double-blind, placebo-controlled trial in children and adolescents with FXS (Leigh et al., 2013; Dziembowska et al., 2013). What's more, electrophysiological measures in the auditory cortex of human subjects with FXS indicate a reduction in auditory hyper-reactivity with minocycline treatment (Schneider et al., 2013).

Considering the widespread action of minocycline in the CNS, the effects of minocycline in FXS may not be limited to the inhibition of MMP-9. Minocycline can inhibit other MMPs and is shown to have anti-inflammatory and anti-apoptotic effects (reviewed by Elewa et al., 2006), can phosphorylate AMPA receptors (Imbesi et al., 2008), and affect MAPK signaling (Nikodemova et al., 2006). Doxycycline similarly has various effects on CNS functions. On the other hand, MMP-9 is itself expressed by many types of tissue throughout the body and, as in the CNS, it can have both detrimental and beneficial effects on biological systems (reviewed by Fingleton, 2008). The potential side effects of non-specific MMP-9 inhibition to treat neurodevelopmental disorders have not been thoroughly investigated, though MMP-9 KO mice have shown detrimental side effects as well as benefits in animal models of cancer (Coussens et al., 2000) and kidney disease (Zeisberg et al., 2006) and highlight the need for treatments specific to both the CNS and to key points in the progression of a disorder. Nonetheless recent studies discussed herein do demonstrate a relationship between the ability of minocycline to inhibit MMP-9 in FXS and a concomitant improvement on behavioral, morphologic and

physiological levels. Side effects of the treatment as reported in these studies are minor and are commonly associated with gastrointestinal discomfort (Dziembowska et al., 2013; Paribello et al., 2010; Utari et al., 2010). Altogether, this body of research points to the need for additional studies to understand the specific role of MMP-9 in the etiology of a disorder, including the time frame during which MMP-9 activity may have the largest deleterious effects, and to develop treatments targeted to MMP-9 in the progression of each disorder to further improve the lives of people with intellectual disabilities and autism.

6. Conclusions

Untangling the precise functions of MMP-9 is challenging. This is due to the fact that it is expressed by both neurons and glia; that its secretion and activation are regulated by a wide variety of factors; and that it can act on multiple targets, each of which can have differential and even opposing effects. In this review, we summarized the various roles of MMP-9 during early postnatal development within the central nervous system, with a focus on sensory development.

These developmental events, many of which recruit MMP-9 activity, occur in an organized and interactive fashion through specific cellular targets and in response to sensory experience that drives neuronal activity. MMP-9 recruited to specific extracellular sites can cleave ECM creating room within the extracellular space for cells to migrate and for neuronal processes to grow. Yet beyond being simply permissive, MMP-9, through cleavage and/or activation of cell surface and cell adhesion molecules, is implicated in active dendritic spine remodeling and stabilization; pre- and postsynaptic

receptor dynamics; consolidation of LTP; myelination and synaptic pruning. It is further implicated in axonal sprouting, path finding, regeneration and degeneration. MMP-9 is expressed just prior to and during CPP, a peak of reorganization in the sensory cortex, and its activity is down regulated in the adult brain. However, unregulated activity of MMP-9 can have detrimental effects on brain functions and may underlie deficits observed in several neurodevelopmental disorders. It is therefore important to better understand the mechanisms by which MMP-9 mediates early postnatal development and its role in neurodevelopmental disorders.

Several key questions remain unanswered. The role of MMP-9 in auditory CPP, for instance, is yet to be studied. Tonotopic maps in rodent primary auditory cortex do undergo reorganization during a 'sensitive window' after which the network is less plastic. Reorganization of the tonotopic frequency map can take place with as few as 3 days exposure to a single tone, from P11 to P13 (de Villers-Sidani et al., 2007), though time windows used to test auditory CPP vary (Barkat et al., 2011; Kim et al., 2013 ; Webster, 1983; Zhang et al., 2002). Recent studies have demonstrated an auditory CPP deficit in *Fmr1* KO mice (Kim et al., 2013) that may be related to enhanced levels of MMP-9 activity in the brain. The role of MMP-9 in these auditory deficits remains unclear. Because clarification may lead to new therapeutic strategies to treat auditory hypersensitivity and habituation deficits seen in FXS and ASD, understating this role is important.

Though MMP-9 seems to consistently be associated with early postnatal development across many sensory regions and is downregulated by adolescence and into

adulthood, mechanistic studies of MMP-9 have largely focused on l-LTP and synaptic plasticity in cultured hippocampal neurons. Furthermore, it is known that during development many receptors undergo changes in sub-receptor composition, localization and/or distribution within a network, as well as in their physiological properties. Similarly, intracellular signaling molecules, as well as cell surface and cell adhesion molecules and ECM components all have altered expression throughout development. Therefore it is uncertain whether the mechanisms underlying MMP-9 recruitment and activity in adolescent and adult hippocampal neurons are conserved across cortical regions throughout development.

In addition, given the overexpression of MMP-9 in multiple neurodevelopmental disorders, it is important to understand whether MMP-9 plays a regulatory and/or permissive role in critical period development, specifically through its interactions with ECM. The formation of perineuronal net (PNN) structures in the CNS, a specific sub-type of ECM, has been linked to the closure of visual CPP in rodents (reviewed by Hensch, 2005), associated with developmental song learning in the zebra finch (Balmer et al., 2009), and has been shown to be altered with sensory deprivation in rodent barrel cortex (McRae et al., 2007). MMP-9 can directly or indirectly induce cleavage of multiple components of perineuronal net structures, including laminin, brevican, tenascin-R and aggrecan (reviewed by Ethell & Ethell, 2007). Therefore elevated levels of MMP-9 during development may induce aberrant cleavage and alterations in perineuronal net structures. It remains to be seen whether PNNs are indeed altered in

neurodevelopmental disorders and whether MMP-9 inhibition can recover normal CPP through the stabilization of PNNs.

While MMP-9 activity is important for normal CNS development and for the consolidation of long-term memories from development through adulthood, misregulated expression and/or activity of MMP-9 is associated with many neurological disorders. Therefore, understanding the action of MMP-9 within specific cortical regions, developmental periods and in specific cellular processes is important for providing groundwork for new therapies that target MMP-9 in treatments for neurodevelopmental and other disorders.

References

Abdallah, M. W., Pearce, B. D., Larsen, N., Greaves-Lord, K., Norgaard-Pedersen, B., Hougaard, D. M., Mortensen, E. L., Grove, J. (2012). Amniotic fluid MMP-9 and neurotrophins in autism spectrum disorders: An exploratory study. *Autism Research*, **5**, 428–433.

Aerts, J., Nys, J., Moons, L., Hu, T.-T., & Arckens, L. (2014). Altered neuronal architecture and plasticity in the visual cortex of adult MMP-3-deficient mice. *Brain Structure and Function*, 1–15. doi.org/10.1007/s00429-014-0819-4

Ahmed, Z., Dent, R. G., Leadbeater, W. E., Smith, C., Berry, M., & Logan, A. (2005). Matrix metalloproteases: degradation of the inhibitory environment of the transected optic nerve and the scar by regenerating axons. *Molecular and Cellular Neuroscience*, **28**(1), 64–78. doi.org/10.1016/j.mcn.2004.08.013

Altman, J. (1972a). Postnatal development of the cerebellar cortex in the rat I. The external germinal layer and the transitional molecular layer. *Journal of Comparative Neurology*, **145**, 353–398.

Altman, J. (1972b). Postnatal development of the cerebellar cortex in the rat. II. Phases in the maturation of Purkinje cells and of the molecular layer. *Journal of Comparative Neurology*, **145**(4), 399–463.

Armstrong-James, M., Fox, K., & Das-Gupta, A. (1992). Flow of excitation within rat barrel cortex on striking a single vibrissa. *Journal of Neurophysiology*, **68**(4), 1345–1358.

Aujla, P. K., & Huntley, G. W. (2014). Early postnatal expression and localization of matrix metalloproteinases-2 and -9 during establishment of rat hippocampal synaptic circuitry: MMP proteolysis during hippocampal development. *Journal of Comparative Neurology*, **522**(6), 1249–1263. doi.org/10.1002/cne.23468

Azevedo, F. A. C., Carvalho, L. R. B., Grinberg, L. T., Farfel, J. M., Ferretti, R. E. L., Leite, R. E. P., … Herculano-Houzel, S. (2009). Equal numbers of neuronal and nonneuronal cells make the human brain an isometrically scaled-up primate brain. *The Journal of Comparative Neurology*, **513**(5), 532–541. doi.org/10.1002/cne.21974

Bajor, M., Michaluk, P., Gulyassy, P., Kekesi, A. K., Juhasz, G., & Kaczmarek, L. (2012). Synaptic cell adhesion molecule-2 and collapsin response mediator protein-2 are novel members of the matrix metalloproteinase-9 degradome: Proteomic discovery of MMP-9 substrates. *Journal of Neurochemistry*, **122**(4), 775–788. doi.org/10.1111/j.1471-4159.2012.07829.x

Balmer, T. S., Carels, V. M., Frisch, J. L., & Nick, T. A. (2009). Modulation of perineuronal nets and parvalbumin with developmental song learning. *Journal of Neuroscience*, **29**(41), 12878–12885. doi.org/10.1523/JNEUROSCI.2974-09.2009

Barkat, T. R., Polley, D. B., & Hensch, T. K. (2011). A critical period for auditory thalamocortical connectivity. *Nat Neurosci*, **14**(9), 1189–1194. doi.org/10.1038/nn.2882

Bayer, S. A. (1980). Development of the hippocampal region in the rat I. Neurogenesis examined with 3H-thymidine autoradiography. *Journal of Comparative Neurology*, **190**(1), 87–114.

Bednarek, N., Clément, Y., Lelièvre, V., Olivier, P., Loron, G., Garnotel, R., & Gressens, P. (2009). Ontogeny of MMPs and TIMPs in the murine neocortex. *Pediatric Research*, **65**(3), 296–300.

Beheshti Nasr, S. M., Moghimi, A., Mohammad-Zadeh, M., Shamsizadeh, A., & Noorbakhsh, S. M. (2013). The effect of minocycline on seizures induced by amygdala kindling in rats. *Seizure*, **22**(8), 670–674. doi.org/10.1016/j.seizure.2013.05.005

Benson, D. L., & Huntley, G. W. (2012). Building and remodeling synapses. *Hippocampus*, **22**(5), 954–968. doi.org/10.1002/hipo.20872

Bernard-Trifilo, J. A., Kramar, E. A., Torp, R., Lin, C.-Y., Pineda, E. A., Lynch, G., & Gall, C. M. (2005). Integrin signaling cascades are operational in adult hippocampal synapses and modulate NMDA receptor physiology. *Journal of Neurochemistry*, **93**(4), 834–849. doi.org/10.1111/j.1471-4159.2005.03062.x

Bilousova, T. V., Dansie, L., Ngo, M., Aye, J., Charles, J. R., Ethell, D. W., & Ethell, I. M. (2009). Minocycline promotes dendritic spine maturation and improves behavioural performance in the fragile X mouse model. *Journal of Medical Genetics*, **46**(2), 94–102. doi.org/10.1136/jmg.2008.061796

Bozdagi, O., Nagy, V., Kwei, K. T., & Huntley, G. W. (2007). In vivo roles for matrix metalloproteinase-9 in mature hippocampal synaptic physiology and plasticity. *Journal of Neurophysiology*, **98**(1), 334–344. doi:10.1152/jn.00202.2007

Bradbury, E., Moon, L. D. F., Popat, R. J., King, V. R., Bennett, G. S., Patel, P. N., … McMahon, S. B. (2002). Chondroitinase ABC promotes functional recovery after spinal cord injury. *Nature*, **416**(6881), 636–640.

Castillo, P., Janz, R., Sudhof, T. C., Tzounopoulos, T., Malenka, R. C., & Nicoll, R. A. (1997). Rab3A is essential for mossy fibre long-term potentiation in the hippocampus. *Nature*, **388**, 590–593.

Chattopadhyay, S., & Shubayev, V. I. (2009). MMP-9 controls Schwann cell proliferation and phenotypic remodeling via IGF-1 and ErbB receptor-mediated activation of MEK/ERK pathway. *Glia*, **57**(12), 1316–1325. doi.org/10.1002/glia.20851

Costanzo, R. M., Perrino, L. A., & Kobayashi, M. (2006). Response of matrix metalloproteinase-9 to olfactory nerve injury. *NeuroReport*, **17**(17), 1787–1791.

Coussens, L. M., Tinkle, C. L., Hanahan, D., & Werb, Z. (2000). MMP-9 supplied by bone marrow–derived cells contributes to skin carcinogenesis. *Cell*, **103**(3), 481–490.

Dansie, L. E., Phommahaxay, K., Okusanya, A. G., Uwadia, J., Huang, M., Rotschafer, S. E., … Ethell, I. M. (2013). Long-lasting effects of minocycline on behavior in young but not adult Fragile X mice. *Neuroscience*, **246**, 186–198. doi.org/10.1016/j.neuroscience.2013.04.058

Dansie, L. E., & Ethell, I. M. (2011). Casting a net on dendritic spines: The extracellular matrix and its receptors. *Developmental Neurobiology*, **71**(11), 956–981. doi.org/10.1002/dneu.20963

De Villers-Sidani, E., Chang, E. F., Bao, S., & Merzenich, M. M. (2007). Critical period window for spectral tuning defined in the primary auditory cortex (A1) in the rat. *Journal of Neuroscience*, **27**(1), 180–189. doi.org/10.1523/JNEUROSCI.3227-06.2007

Dityatev, A., Schachner, M., & Sonderegger, P. (2010). The dual role of the extracellular matrix in synaptic plasticity and homeostasis. *Nature Reviews Neuroscience*, **11**(11), 735–746. doi.org/10.1038/nrn2898

Dziembowska, M., Pretto, D. I., Janusz, A., Kaczmarek, L., Leigh, M. J., Gabriel, N., … Tassone, F. (2013). High MMP-9 activity levels in fragile X syndrome are lowered by minocycline. *American Journal of Medical Genetics Part A*, **161**(8), 1897–1903. doi.org/10.1002/ajmg.a.36023

Dziembowska, M., Milek, J., Janusz, A., Rejmak, E., Romanowska, E., Gorkiewicz, T., … Kaczmarek, L. (2012). Activity-dependent local translation of matrix metalloproteinase-9. *Journal of Neuroscience*, **32**(42), 14538–14547. doi.org/10.1523/JNEUROSCI.6028-11.2012

Dzwonek, J., Rylski, M., & Kaczmarek, L. (2004). Matrix metalloproteinases and their endogenous inhibitors in neuronal physiology of the adult brain. *FEBS Letters*, **567**(1), 129–135. doi.org/10.1016/j.febslet.2004.03.070

Elewa, H. F., Hilali, H., Hess, D. C., Machado, L. S., & Fagan, S. C. (2006). Minocycline for short-term neuroprotection. *Pharmacotherapy: The Journal of Human Pharmacology and Drug Therapy*, **26**(4), 515–521.

Erzurumlu, R. S., & Gaspar, P. (2012). Development and critical period plasticity of the barrel cortex: Barrel cortex plasticity. *European Journal of Neuroscience*, **35**(10), 1540–1553. doi.org/10.1111/j.1460-9568.2012.08075.x

Esparza, J. (2004). MMP-2 null mice exhibit an early onset and severe experimental autoimmune encephalomyelitis due to an increase in MMP-9 expression and activity. *The FASEB Journal*, **18**(14), 1682–1691. doi.org/10.1096/fj.04-2445com

Ethell, I. M., & Ethell, D. W. (2007). Matrix metalloproteinases in brain development and remodeling: Synaptic functions and targets. *Journal of Neuroscience Research*, **85**(13), 2813–2823. doi.org/10.1002/jnr.21273

Fagiolini, M., Pizzorusso, T., Berardi, N., Domenici, L., & Maffei, L. (1994). Functional postnatal development of the rat primary visual cortex and the role of visual experience: Dark rearing and monocular deprivation. *Vision Research*, **34**(6), 709–720.

Feldmeyer, D. (2012). Excitatory neuronal connectivity in the barrel cortex. *Frontiers in Neuroanatomy*, **6**. doi.org/10.3389/fnana.2012.00024

Feller, M. B., & Scanziani, M. (2005). A precritical period for plasticity in visual cortex. *Current Opinion in Neurobiology*, **15**(1), 94–100. doi.org/10.1016/j.conb.2005.01.012

Ferguson, T. (2000). MMP-2 and MMP-9 increase the neurite-promoting potential of Schwann cell basal laminae and are upregulated in degenerated nerve. *Molecular and Cellular Neuroscience*, **16**(2), 157–167. doi.org/10.1006/mcne.2000.0859

Fingleton, B. (2008). MMPs as therapeutic targets—Still a viable option? *Seminars in Cell & Developmental Biology*, **19**(1), 61–68. doi.org/10.1016/j.semcdb.2007.06.006

Foran, D. R., & Peterson, A. C. (1992). Myelin acquisition in the central nervous system of the mouse revealed by an MBP-Lac Z transgene. *The Journal of Neuroscience*, **12**(12), 4890–4897.

Fox, K. (2002). Anatomical pathways and molecular mechanisms for plasticity in the barrel cortex. *Neuroscience*, **111**(4), 799–814.

Fox, K. (1992). A critical period for experience-dependent synaptic plasticity in rat barrel cortex. *The Journal of Neuroscience*, **12**(5), 1826–1838.

Fukata, Y., Itoh, T. J., Kimura, T., Ménager, C., Nishimura, T., Shiromizu, T., … Kaibuchi, K. (2002). CRMP-2 binds to tubulin heterodimers to promote microtubule assembly. *Nature Cell Biology*, **4**, 583–591. doi.org/10.1038/ncb825

Gawlak, M., Górkiewicz, T., Gorlewicz, A., Konopacki, F. A., Kaczmarek, L., & Wilczynski, G. M. (2009). High resolution in situ zymography reveals matrix metalloproteinase activity at glutamatergic synapses. *Neuroscience*, ***158***(1), 167–176. doi.org/10.1016/j.neuroscience.2008.05.045

Generscb, E., Haye\s s, K., Neuenfeld, Y., & Haller, H. (2000). Sustained ERK phosphorylation is necessary but not sufficient for MMP-9 regulation in endothelial cells: Involvement of Ras-dependent and-independent pathways.

Journal of Cell Science, **113**(23), 4319–4330.

Giaume, C., Maravall, M., Welker, E., & Bonvento, G. (2009). The Barrel Cortex as a Model to Study Dynamic Neuroglial Interaction. *The Neuroscientist*, **15**(4), 351–366. doi.org/10.1177/1073858409336092

Gkogkas, C. G., Khoutorsky, A., Cao, R., Jafarnejad, S. M., Prager-Khoutorsky, M., Giannakas, N., … Sonenberg, N. (2014). Pharmacogenetic inhibition of eIF4E-dependent mmp9 mRNA translation reverses fragile X syndrome-like phenotypes. *Cell Reports*, **9**(5), 1742–1755. doi:10.1016/j.celrep.2014.10.064

Gordon, J. A., & Stryker, M. P. (1996). Experience-dependent plasticity of binocular responses in the primary visual cortex of the mouse. *The Journal of Neuroscience*, **16**(10), 3274–3286.

Harris, E. W., & Cotman, C. W. (1986). Long-term potentiation of guinea pig mossy fiber responses is not blocked by N-methyl D-aspartate antagonists. *Neuroscience Letters*, **70**, 132–137.

Hashimoto, K., & Kano, M. (2005). Postnatal development and synapse elimination of climbing fiber to Purkinje cell projection in the cerebellum. *Neuroscience Research*, **53**(3), 221–228. doi.org/10.1016/j.neures.2005.07.007

Hehr, C. L. (2005). Matrix metalloproteinases are required for retinal ganglion cell axon guidance at select decision points. *Development*, **132**(15), 3371–3379. doi.org/10.1242/dev.01908

Hensch, T. K. (2004). Critical Period Regulation. *Annual Review of Neuroscience*, **27**(1), 549–579. doi.org/10.1146/annurev.neuro.27.070203.144327

Hensch, T. K. (2005). Critical period plasticity in local cortical circuits. *Nature Reviews Neuroscience*, **6**(11), 877–888. doi.org/10.1038/nrn1787

Hubel, D. H., & Wiesel, T. N. (1964). Effects of monocular deprivation in kittens. *Naunyn-Schmiedeberg's Archives of Pharmacology*, **248**(6), 492–497.

Illing, R.-B., Rosskothen-Kuhl, N., Fredrich, M., Hildebrandt, H., & Zeber, A. C. (2010). Imaging the plasticity of the central auditory system on the cellular and molecular level. *Audiological Medicine*, **8**(2), 63–76. doi.org/10.3109/16513860903454583

Imbesi, M., Uz, T., Manev, R., Sharma, R. P., & Manev, H. (2008). Minocycline increases phosphorylation and membrane insertion of neuronal GluR1 receptors. *Neuroscience Letters*, **447**(2-3), 134–137. doi.org/10.1016/j.neulet.2008.10.006

Janusz, A., Milek, J., Perycz, M., Pacini, L., Bagni, C., Kaczmarek, L., & Dziembowska, M. (2013). The fragile X mental retardation protein regulates matrix metalloproteinase 9 mRNA at synapses. *Journal of Neuroscience*, **33**(46), 18234– 18241. doi.org/10.1523/JNEUROSCI.2207-13.2013

Kaliszewska, A., Bijata, M., Kaczmarek, L., & Kossut, M. (2012). Experience-dependent plasticity of the barrel cortex in mice observed with 2-DG brain mapping and c-Fos: Effects of MMP-9 KO. *Cerebral Cortex*, **22**(9), 2160–2170. doi.org/10.1093/cercor/bhr3

Kelly, E. A., Tremblay, M.-E., Gahmberg, C. G., Tian, L., & Majewska, A. K. (2014). Subcellular localization of intercellular adhesion molecule-5 (telencephalin) in the visual cortex is not developmentally regulated in the absence of matrix metalloproteinase-9: ICAM-5 ultrastructural localization. *Journal of Comparative Neurology*, **522**(3), 676–688. doi.org/10.1002/cne.23440

Kelly, E., Tremblay, M.-È., Gahmberg, carl, Tian, L., & Majewska, A. K. (2013). Interactions between intercellular adhesion molecule-5 positive elements and their surroundings in the rodent visual cortex. *Communicative & Integrative Biology*, **6**(6), e27315. doi.org/10.4161/cib.27315

Kelly, M. K., Carvell, G. E., Kodger, J. M., & Simons, D. J. (1999). Sensory loss by selected whisker removal produces immediate disinhibition in the somatosensory cortex of behaving rats. *The Journal of Neuroscience*, **19**(20), 9117–9125.

Kim, H., Gibboni, R., Kirkhart, C., & Bao, S. (2013). Impaired critical period plasticity in primary auditory cortex of fragile X model mice. *Journal of Neuroscience*, ***33***(40), 15686–15692. doi.org/10.1523/JNEUROSCI.3246-12.2013

Konopka, A., Grajkowska, W., Ziemiańska, K., Roszkowski, M., Daszkiewicz, P., Rysz, A., … Dzwonek, J. (2013). Matrix metalloproteinase-9 (MMP-9) in human intractable epilepsy caused by focal cortical dysplasia. *Epilepsy Research*, **104**(1-2), 45–58. doi.org/10.1016/j.eplepsyres.2012.09.018

Kossut, M., Hand, P. J., Greenberg, J., & Hand, C. L. (1988). Single vibrissal cortical column in SI cortex of rat and its alterations in neonatal and adult vibrissa-deafferented animals: a quantitative 2DG study. *Journal of Neurophysiology*, **60**(2), 829–852.

Larsen, P. H., Dasilva, A. G., Conant, K., & Yong, V. W. (2006). Myelin formation during development of the CNS is delayed in matrix metalloproteinase-9 and -12 null mice. *Journal of Neuroscience*, **26**(8), 2207–2214. doi.org/10.1523/JNEUROSCI.1880-05.2006

Leigh, M. J. S., Nguyen, D. V., Mu, Y., Winarni, T. I., Schneider, A., Chechi, T., … Hagerman, R. J. (2013). A randomized double-blind, placebo-controlled trial of minocycline in children and adolescents with fragile X syndrome. *Journal of Developmental & Behavioral Pediatrics*, **34**(3), 147–155. doi:10.1097/DBP.0b013e318287cd17

Lin, K.-T., Sloniowski, S., Ethell, D. W., & Ethell, I. M. (2008). Ephrin-B2-induced cleavage of EphB2 receptor is mediated by matrix metalloproteinases to trigger cell repulsion. *Journal of Biological Chemistry*, **283**(43), 28969–28979. doi.org/10.1074/jbc.M804401200.

Logvinov, A. K., Kirichenko, E. Y., Povilaitite, P. E., & Sukhov, A. G. (2011). Structural Organization of the Barrel Cortex in Rats (an immunohistochemical study). *Neuroscience and Behavioral Physiology*, **41**(1), 6–9.

Luo, J. (2005). The role of matrix metalloproteinases in the morphogenesis of the cerebellar cortex. *The Cerebellum*, **4**(4), 239–245. doi.org/10.1080/14734220500247646

Maier, O., van der Heide, T., Johnson, R., Vries, H. de, Baron, W., & Hoekstra, D. (2006). The function of neurofascin155 in oligodendrocytes is regulated by metalloprotease-mediated cleavage and ectodomain shedding. *Experimental Cell Research*, **312**(4), 500–511. doi.org/10.1016/j.yexcr.2005.11.014

Maravall, M. (2004). Development of intrinsic properties and excitability of layer 2/3 pyramidal neurons during a critical period for sensory maps in rat barrel cortex. *Journal of Neurophysiology*, **92**(1), 144–156. doi.org/10.1152/jn.00598.2003

Matthews, M. A., & Duncan, D. (1971). A quantitative study of morphological changes accompanying the initiation and progress of myelin production in the dorsal funiculus of the rat spinal cord. *Journal of Comparative Neurology*, **142**(1), 1–22.

McRae, P. A., Baranov, E., Rogers, S. L., & Porter, B. E. (2012). Persistent decrease in multiple components of the perineuronal net following status epilepticus: Perineuronal nets and status epilepticus. *European Journal of Neuroscience*, **36**(11), 3471–3482. doi.org/10.1111/j.1460-9568.2012.08268.x

McRae, P. A., Rocco, M. M., Kelly, G., Brumberg, J. C., & Matthews, R. T. (2007). Sensory deprivation alters aggrecan and perineuronal net expression in the mouse barrel cortex. *Journal of Neuroscience*, **27**(20), 5405–5413. doi.org/10.1523/JNEUROSCI.5425-06.2007

Michaluk, P., Mikasova, L., Groc, L., Frischknecht, R., Choquet, D., & Kaczmarek, L. (2009). Matrix metalloproteinase-9 controls NMDA receptor surface diffusion through integrin 1 signaling. *Journal of Neuroscience*, **29**(18), 6007–6012. doi.org/10.1523/JNEUROSCI.5346-08.2009

Michaluk, P., Wawrzyniak, M., Alot, P., Szczot, M., Wyrembek, P., Mercik, K., … Wlodarczyk, J. (2011). Influence of matrix metalloproteinase MMP-9 on dendritic spine morphology. *Journal of Cell Science*, **124**(19), 3369–3380. doi.org/10.1242/jcs.090852

Mizoguchi, H., Nakade, J., Tachibana, M., Ibi, D., Someya, E., Koike, H., … Yamada, K. (2011). Matrix metalloproteinase-9 contributes to kindled seizure development in pentylenetetrazole-treated mice by converting pro-BDNF to mature BDNF in the hippocampus. *Journal of Neuroscience*, **31**(36), 12963–12971. doi.org/10.1523/JNEUROSCI.3118-11.2011

Murase, S., & McKay, R. D. (2012). Matrix metalloproteinase-9 regulates survival of neurons in newborn hippocampus. *Journal of Biological Chemistry*, **287**(15), 12184–12194. doi.org/10.1074/jbc.M111.297671

Nagy, V., Bozdagi, O., Matynia, A., Balcerzyk, M., Okulski, P., Dzwonek, J., … Huntley, G. W. (2006). Matrix metalloproteinase-9 is required for hippocampal late-phase long-term potentiation and memory. *Journal of Neuroscience*, **26**(7), 1923–1934. doi.org/10.1523/JNEUROSCI.4359-05.2006

Nicholson, C., & Sykova, E. (1998). Extracellular space structure revealed by diffusion analysis. *Trends in Neurosciences*, **21**, 207–215.

Nikodemova, M., Duncan, I. D., & Watters, J. J. (2006). Minocycline exerts inhibitory effects on multiple mitogen-activated protein kinases and IκBα degradation in a stimulus-specific manner in microglia. *Journal of Neurochemistry*, **96**(2), 314– 323. doi.org/10.1111/j.1471-4159.2005.03520.x

Ning, L., Tian, L., Smirnov, S., Vihinen, H., Llano, O., Vick, K., … Gahmberg, C. G. (2013). Interactions between ICAM-5 and β1 integrins regulate neuronal synapse formation. *Journal of Cell Science*, **126**(1), 77–89. doi.org/10.1242/jcs.106674

Oh, L. Y. S., Larsen, P. H., Krekoski, C., Edwards, D., Donovan, F., Werb, Z., & Yong, V. W. (1999). Matrix metalloproteinase-9/Gelatinase B is required for process outgrowth by oligodendrocytes. *The Journal of Neuroscience*, **19**(19), 8464–8475.

Okulski, P., Jay, T. M., Jaworski, J., Duniec, K., Dzwonek, J., Konopacki, F. A., … Kaczmarek, L. (2007). TIMP-1 abolishes MMP-9-dependent long-lasting long-term potentiation in the prefrontal cortex. *Biological Psychiatry*, **62**(4), 359–362. doi.org/10.1016/j.biopsych.2006.09.012

Oliveira-Silva, P., Jurgilas, P. B., Trindade, P., Campello-Costa, P., Perales, J., Savino, W., & Serfaty, C. A. (2007). Matrix metalloproteinase-9 is involved in the development and plasticity of retinotectal projections in rats. *Neuroimmunomodulation*, **14**(3-4), 144–149. doi.org/10.1159/000110638

Paribello, C., Tao, L., Folino, A., Berry-Kravis, E., Tranfaglia, M., Ethell, I. M., & Ethell, D. W. (2010). Open-label add-on treatment trial of minocycline in fragile X syndrome. *BMC Neurology*, **10**(1), 91.

Peixoto, R. T., Kunz, P. A., Kwon, H., Mabb, A. M., Sabatini, B. L., Philpot, B. D., & Ehlers, M. D. (2012). Transsynaptic signaling by activity-dependent cleavage of neuroligin-1. *Neuron*, **76**(2), 396–409. doi.org/10.1016/j.neuron.2012.07.006

Pfeiffer, S., Warrington, A., & Bansal, R. (1993). The oligodendrocyte and its many cellular processes. *Trends in Cell Biology*, **3**, 191–197.

Piccolini, V. M., Avella, D., Bottone, M. G., Bottiroli, G., & Bernocchi, G. (2012). Cisplatin induces changes in the matrix metalloproteinases and their inhibitors in the developing rat cerebellum. *Brain Research*, **1484**, 15–28. doi.org/10.1016/j.brainres.2012.09.025

Pizzorusso, T., Medini, P., Landi, S., Baldini, S., Berardi, N., & Maffei, L. (2006). Structural and functional recovery from early monocular deprivation in adult rats. *Proceedings of the National Academy of Sciences*, **103**(22), 8517–8522.

Pizzorusso, T., Medini, P., Berardi, N., Chierzi, S., Fawcett, J. W., & Maffei, L. (2002). Reactivation of ocular dominance plasticity in the adult visual cortex. *Science*, **298**, 1248–1251.

Pollock, E., Everest, M., Brown, A., & Poulter, M. O. (2014). Metalloproteinase inhibition prevents inhibitory synapse reorganization and seizure genesis. *Neurobiology of Disease*, **70**, 21–31. doi.org/10.1016/j.nbd.2014.06.003

Proper, E. A., Oestreicher, A. B., Jansen, G. H., Veelen, C. W. M. v., van Rijen, P. C., Gispen, W. H., & de Graan, P. N. E. (2000). Immunohistochemical characterization of mossy fibre sprouting in the hippocampus of patients with pharmaco-resistant temporal lobe epilepsy. *Brain*, **123**, 19–30.

Ribak, C. E., Seress, L., & Amaral, D. G. (1985). The development, ultrastructure and synaptic connections of the mossy cells of the dentate gyrus. *Journal of Neurocytology*, **14**(5), 835–857.

Richards, D. A., Mateos, J. M., Hugel, S., de Paola, V., Caroni, P., Gähwiler, B. H., & McKinney, R. A. (2005). Glutamate induces the rapid formation of spine head protrusions in hippocampal slice cultures. *Proceedings of the National Academy of Sciences*, **102**(17), 6166–6171.

Roderfeld, M., Graf, J., Giese, B., Salguero-Palacios, R., Tschuschner, A., Müller- Newen, G., & Roeb, E. (2007). Latent MMP-9 is bound to TIMP-1 before secretion. *Biological Chemistry*, **388**(11). doi.org/10.1515/BC.2007.123

Roomi, M. W., Monterrey, J. C., Kalinovsky, T., Rath, M., & Niedzwiecki, A. (2009). Distinct patterns of matrix metalloproteinase-2 and -9 expression in normal human cell lines. *Oncology Reports*, **21**, 821–826. doi.org/10.3892/or_00000290

Rotschafer, S. E., Trujillo, M. S., Dansie, L. E., Ethell, I. M., & Razak, K. A. (2012). Minocycline treatment reverses ultrasonic vocalization production deficit in a mouse model of Fragile X Syndrome. *Brain Research*, **1439,** 7–14. doi.org/10.1016/j.brainres.2011.12.041

Rotschafer, S., & Razak, K. (2013). Altered auditory processing in a mouse model of fragile X syndrome. *Brain Research*, **1506**, 12–24. doi.org/10.1016/j.brainres.2013.02.038

Ruoslahti, E. (1996a). Brain extracellular matrix. *Glycobiology*, **6**(5), 489–492.

Ruoslahti, E. (1996b). RGD and other recognition sequences for integrins. *Annual Review of Cell and Developmental Biology*, **12**(1), 697–715.

Rybakowski, J. K., Remlinger-Molenda, A., Czech-Kucharska, A., Wojcicka, M., Michalak, M., & Losy, J. (2013). Increased serum matrix metalloproteinase-9 (MMP-9) levels in young patients during bipolar depression. *Journal of Affective Disorders*, **146**(2), 286–289. doi.org/10.1016/j.jad.2012.07.019

Sanes, D. H., Reh, T. A., & Harris, W. A. *Development of the Nervous System* (2nd ed.). Elsevier Science; Academic Press (2005). 392 p.

Sawtell, N. B., Frenkel, M. Y., Philpot, B. D., Nakazawa, K., Tonegawa, S., & Bear, M. F. (2003). NMDA receptor-dependent ocular dominance plasticity in adult visual cortex. *Neuron*, **38**(6), 977–985.

Schneider, A., Leigh, M. J., Adams, P., Nanakul, R., Chechi, T., Olichney, J., … Hessl, D. (2013). Electrocortical changes associated with minocycline treatment in fragile X syndrome. *Journal of Psychopharmacology*, **27**(10), 956–963. doi.org/10.1177/0269881113494105

Serfaty, C. A., Campello-Costa, P., & Linden, R. (2005). Rapid and long-term plasticity in the neonatal and adult retinotectal pathways following a retinal lesion. *Brain Research Bulletin*, **66**(2), 128–134. doi.org/10.1016/j.brainresbull.2005.04.005

Shi, Y. (2006). Integrins control dendritic spine plasticity in hippocampal neurons through NMDA receptor and Ca2+/calmodulin-dependent protein kinase II-mediated actin reorganization. *Journal of Neuroscience*, **26**(6), 1813–1822. doi.org/10.1523/JNEUROSCI.4091-05.2006

Shubayev, V. I., & Myers, R. R. (2004). Matrix metalloproteinase-9 promotes nerve growth factor-induced neurite elongation but not new sprout formation in vitro. *Journal of Neuroscience Research*, **77**(2), 229–239. doi.org/10.1002/jnr.20160

Sidhu, H., Dansie, L. E., Hickmott, P. W., Ethell, D. W., & Ethell, I. M. (2014). Genetic removal of matrix metalloproteinase 9 rescues the symptoms of Fragile X Syndrome in a mouse model. *Journal of Neuroscience*, **34**(30), 9867–9879. doi.org/10.1523/JNEUROSCI.1162-14.2014

Siller, S. S., & Broadie, K. (2012). Matrix metalloproteinases and minocycline: therapeutic avenues for fragile X syndrome. *Neural Plasticity*, Article ID 124548. doi.org/doi:10.1155/2012/124548

Siller, S. S., & Broadie, K. (2011). Neural circuit architecture defects in a Drosophila model of Fragile X syndrome are alleviated by minocycline treatment and genetic removal of matrix metalloproteinase. *Disease Models & Mechanisms*, **4**(5), 673–685. doi.org/10.1242/dmm.008045

Simons, D. J. (1978). Response properties of vibrissa units in rat SI somatosensory neocortex. *Journal of Neurophysiology*, **41**(3), 798–820.

Šišková, Z., Yong, V. W., Nomden, A., van Strien, M., Hoekstra, D., & Baron, W. (2009). Fibronectin attenuates process outgrowth in oligodendrocytes by mislocalizing MMP-9 activity. *Molecular and Cellular Neuroscience*, **42**(3), 234–242. doi.org/10.1016/j.mcn.2009.07.005

Sloniowski, S., & Ethell, I. M. (2012). Looking forward to EphB signaling in synapses. *Seminars in Cell & Developmental Biology*, **23**(1), 75–82. doi:10.1016/j.semcdb.2011.10.020

Spolidoro, M., Putignano, E., Munafo, C., Maffei, L., & Pizzorusso, T. (2012). Inhibition of matrix metalloproteinases prevents the potentiation of nondeprived-eye responses after monocular deprivation in juvenile rats. *Cerebral Cortex*, **22**(3), 725–734. doi.org/10.1093/cercor/bhr158

Stevens, B., Porta, S., Haak, L. L., Gallo, V., & Fields, R. D. (2002). Adenosine: a neuron-glial transmitter promoting myelination in the CNS in response to action potentials. *Neuron*, **36**(5), 855–868.

Steward, O., & Falk, P. M. (1991). Selective localization of polyribosomes beneath developing synapses: a quantitative analysis of the relationships between polyribosomes and developing synapses in the hippocampus and dentate gyrus. *Journal of Comparative Neurology*, **314**(3), 545–557.

Suenaga, N., Ichiyama, T., Kubota, M., Isumi, H., Tohyama, J., & Furukawa, S. (2008). Roles of matrix metalloproteinase-9 and tissue inhibitors of metalloproteinases 1 in acute encephalopathy following prolonged febrile seizures. *Journal of the Neurological Sciences*, **266**(1-2), 126–130. doi.org/10.1016/j.jns.2007.09.011

Sung, M., Wei, E., Chavez, E., Jain, N., Levano, S., Binkert, L., … Brand, Y. (2014). Inhibition of MMP-2 but not MMP-9 influences inner ear spiral ganglion neurons in vitro. *Cellular and Molecular Neurobiology*, **34**(7), 1011–1021. doi.org/10.1007/s10571-014-0077-2

Szepesi, Z., Bijata, M., Ruszczycki, B., Kaczmarek, L., & Wlodarczyk, J. (2013). Matrix metalloproteinases regulate the formation of dendritic spine head protrusions during chemically induced long-term potentiation. *PLoS ONE*, **8**(5), e63314. doi.org/10.1371/journal.pone.0063314

Szepesi, Z., Hosy, E., Ruszczycki, B., Bijata, M., Pyskaty, M., Bikbaev, A., … Wlodarczyk, J. (2014). Synaptically released matrix metalloproteinase activity in control of structural plasticity and the cell surface distribution of GluA1-AMPA receptors. *PLoS ONE*, **9**(5), e98274. doi.org/10.1371/journal.pone.0098274

Tian, L., Stefanidakis, M., Ning, L., Van Lint, P., Nyman-Huttunen, H., Libert, C., … Gahmberg, C. G. (2007). Activation of NMDA receptors promotes dendritic spine development through MMP-mediated ICAM-5 cleavage. *The Journal of Cell Biology*, **178**(4), 687–700. doi.org/10.1083/jcb.200612097

Uhm, J. H., Dooley, N. P., Oh, L., & Yong, V. W. (1998). Oligodendrocytes utilize a matrix metalloproteinase, MMP-9, to extend processes along an astrocyte extracellular matrix. *Glia*, **22**(1), 53–63.

Utari, A., Chonchaiya, W., Rivera, S. M., Schneider, A., Hagerman, R. J., Faradz, S. M. H., … Nguyen, D. V. (2010). Side effects of minocycline treatment in patients with fragile X syndrome and exploration of outcome measures. *American Journal on Intellectual and Developmental Disabilities*, **115**(5), 433–443. doi.org/10.1352/1944-7558-115.5.433

Vaillant, C., Didier-Bazès, M., Hutter, A., Belin, M.-F., & Thomasset, N. (1999). Spatiotemporal expression patterns of metalloproteinases and their inhibitors in

the postnatal developing rat cerebellum. *The Journal of Neuroscience*, **19**(12), 4994–5004.

Vaillant, C., Meissirel, C., Mutin, M., Belin, M.-F., Lund, L., & Thomasset, N. (2003). MMP-9 deficiency affects axonal outgrowth, migration, and apoptosis in the developing cerebellum. *Molecular and Cellular Neuroscience*, **24**(2), 395–408. doi.org/10.1016/S1044-7431(03)00196-9

Van den Steen, P., Dubois, B., Nelissen, I., Dwek, R., & Opdenakker, G. (2002). Biochemistry and molecular biology of gelatinase B or matrix metalloproteinase- 9 (MMP-9). *Critical Reviews in Biochemistry and Molecular Biology*, **37**(6), 375–536.

Wang, X., Bozdagi, O., Nikitczuk, J. S., Zhai, Z. W., Zhou, Q., & Huntley, G. W. (2008). Extracellular proteolysis by matrix metalloproteinase-9 drives dendritic spine enlargement and long-term potentiation coordinately. *Proceedings of the National Academy of Sciences*, **105**(49), 19520–19525.

Webster, D. B. (1983). A critical period during postnatal auditory development of mice. *International Journal of Pediatric Otorhinolaryngology*, **6**, 107–118.

Wiera, G., Wozniak, G., Bajor, M., Kaczmarek, L., & Mozrzymas, J. W. (2013). Maintenance of long-term potentiation in hippocampal mossy fiber-CA3 pathway requires fine-tuned MMP-9 proteolytic activity. *Hippocampus*, **23**(6), 529–543. doi.org/10.1002/hipo.22112

Wiera, G., Wójtowicz, T., Lebida, K., Piotrowska, A., Drulis-Fajdasz, D., Gomułkiewicz, A., … Mozrzymas, J. W. (2012). Long term potentiation affects intracellular metalloproteinases activity in the mossy fiber — CA3 pathway.

Molecular and Cellular Neuroscience, **50**(2), 147–159. doi.org/10.1016/j.mcn.2012.04.005

Wilczynski, G. M., Konopacki, F. A., Wilczek, E., Lasiecka, Z., Gorlewicz, A., Michaluk, P., … Kaczmarek, L. (2008). Important role of matrix metalloproteinase 9 in epileptogenesis. *The Journal of Cell Biology*, **180**(5), 1021–1035. doi.org/10.1083/jcb.200708213

Woolsey, T. A., & Wann, J. R. (1976). Areal changes in mouse cortical barrels following vibrissal damage at different postnatal ages. *Journal of Comparative Neurology*, **170**(1), 53–66.

Yamamori, H., Hashimoto, R., Ishima, T., Kishi, F., Yasuda, Y., Ohi, K., … Takeda, M. (2013). Plasma levels of mature brain-derived neurotrophic factor (BDNF) and matrix metalloproteinase-9 (MMP-9) in treatment-resistant schizophrenia treated with clozapine. *Neuroscience Letters*, **556**, 37–41. doi.org/10.1016/j.neulet.2013.09.059

Ye, P., Carson, J., & D'Ercole, A. J. (1995a). In vivo actions of insulin-like growth factor-I (IGF-I) on brain myelination: studies of IGF-I and IGF binding protein-1 (IGFBP-1) transgenic mice. *The Journal of Neuroscience*, **15**(11), 7344–7356.

Ye, P., Carson, J., & D'Ercole, A. J. (1995b). Insulin-like growth factor-I influences the initiation of myelination: studies of the anterior commissure of transgenic mice. *Neuroscience Letters*, **201**(3), 235–238.

Yong, V. W. (2005). Metalloproteinases: Mediators of pathology and regeneration in the CNS. *Nature Reviews Neuroscience*, **6**(12), 931–944. doi.org/10.1038/nrn1807

Yoshimura, T., Kawano, Y., Arimura, N., Kawabata, S., Kikuchi, A., & Kaibuchi, K. (2005). GSK-3β regulates phosphorylation of CRMP-2 and neuronal polarity. *Cell*, **120**(1), 137–149. doi.org/10.1016/j.cell.2004.11.012Zhang, L. I., Bao, S., & Merzenich, M. M. (2002). Disruption of primary auditory cortex by synchronous auditory inputs during a critical period. *Proceedings of the National Academy of Sciences*, **99**(4), 2309–2314.

Zeisberg, M., Khurana, M., Rao, V. H., Cosgrove, D., Rougier, J.-P., Werner, M. C., … Kalluri, R. (2006). Stage-specific action of matrix metalloproteinases influences progressive hereditary kidney disease. *PLoS Medicine*, **3**(4), e100. doi.org/10.1371/journal.pmed.0030100

Zhang, L. I., Bao, S., & Merzenich, M. M. (2002). Disruption of primary auditory cortex by synchronous auditory inputs during a critical period. *Proceedings of the National Academy of Sciences*, **99**(4), 2309–2314.

Chapter 2:

The effects of Minocycline treatment on matrix metalloproteinase-9 expression in the developing auditory cortex of *fmr1* KO mice

Abstract

Fragile X syndrome (FXS), an autism spectrum disorder, is characterized by disruptions in sensory processing and cognitive impairment. Auditory processing is, in particular, profoundly affected, with hyperacusis, inability to habituate to sounds, and deficits in speech. Delays in cortical development during the critical period may lead to these later disruptions in auditory processing and higher cognitive functions. Fragile X mental retardation protein (FMRP), which is hypermethylated in people with FXS, typically is enriched in early postnatal developmental, where it has a role in regulation of Matrix Metaloproteinase-9 (MMP-9), an enzyme important in synaptic maturation. Here we first characterize the normal expression of FMRP in the auditory cortex during post-natal development using western blot. Levels of MMP-9 were characterized in both WT and *fmr1* knockout mice using gel zymography, and the effect of Minocycline treatment on MMP-9 levels was measured. Finally, we tested if administration of Minocycline, either alone or with Acamprosate, was able to rescue audiogenic seizures in *fmr1* KO mice. We found that FMRP levels peak during the second postnatal week in the auditory cortex of WT mice and decrease into adulthood; MMP-9 levels mirrored the same pattern. In *fmr1* KO mice, increased levels of MMP-9 were sustained at all time-points tested. Treatment with Minocycline caused a moderate reduction in MMP-9 levels, however Minocycline either with or without Acamprosate could fully rescue seizure activity in *fmr1* KO mice. Results suggest key developmental time points for future studies of auditory critical period plasticity mechanisms.

Abbreviations:

α-Amino-3-hydroxy-5-methyl-4-isoxazolepropionic acid (AMPA receptors), Extracellular matrix (ECM), Fragile X mental retardation protein (FMRP), Fragile X syndrome (FXS), γ-aminobutyric acid type A receptor (GABA-A), Long-term depression (LTD), Group 1 metabotropic glutamate receptor (mGluR1/5), Matrix metalloproteinase - 9 (MMP-9), *N*-Methyl-D-aspartate (NMDA), Perineuronal nets (PNN), Parvalbumin positive interneuron (PV), Tonic seizure (TS), Wild running and jumping (WRJ)

1. Introduction

Fragile X Syndrome (FXS) is one of the most common genetic causes of autism and the leading cause of heritable mental retardation in males (Brown, 1990), accounting for two to five percent of all autism cases (Bagni et al., 2012; Wassink et al., 2001). The root cause of FXS is a trinucleotide repeat in the noncoding CGG region of the gene (Verkeck, 1991). This non-coding region, which would normally be cut out of the DNA strand during translation, is instead integrated into the genome leading to variation in repeat length (5 to 50 in normal individuals, 50 to >200 in people with FXS) and a strong tendency for larger expansions with each new generation of mutation carriers (Fernandez-Carvajal et al., 2009). A full *fmr1* mutation becomes likely at repeats greater than 200, when the gene becomes hyper-methylated and transcriptionally silenced (Fu, 1991).

Throughout the body, fragile X mental retardation protein (FMRP) is expressed in many types of tissue, mostly concentrated in the central nervous system and in reproductive tissues. Within the central nervous system, it is expressed in both excitatory and inhibitory neurons (Till et al., 2012) as well as glial cells (Higashimori et al., 2013), and it binds to up to 4% of human fetal brain RNA (Ashley, et al., 1993), including 28 genes that overlap with candidate genes for autism (Darnell et al., 2011).

FXS symptoms include developmental delays, social and behavioral deficits, cognitive impairments and alterations in sensory processing. Auditory processing deficits are prominent in FXS (reviewed in Rotschafer and Razak, 2014). In humans with FXS, there is a decrease in the volume of the superior temporal gyrus, which is the locus of the

primary auditory cortex and an area involved in processing speech and complex sounds (Reiss et al., 1994). As well there is as an increase in the volume of temporal lobe white matter across the lifespan (Hazlett et al., 2012). Patients experience hyperacusis and an inability to habituate to sound (Castrén et al., 2003; Miller, 1999; Rojas et al., 2001; Schneider et al., 2013; St Clair et al., 1987; Van der Molen et al., 2012), with delays in word comprehension and speech production (Largo & Schinzel, 1985; Roberts et al., 2001). In addition, human subjects are prone to seizure activity in childhood (Berry-Kravis, 2002; Musumeci et al., 1999; Sabaratnam et al., 2001; Wisniewski et al., 1991).

A mouse model of FXS has been developed by replacing the wild type murine *fmr1* gene with a nonfunctional *fmr1* gene, creating a knockout mouse (KO) (Kooy, 1996; The Dutch-Belgian Fragile X Consortium et al., 1994). Multiple phenotypes of FXS have been reproduced in this mouse model that closely parallel symptoms found in human FXS patients, including macroordism, hyperactivity, and learning deficits (Kooy, 1996; The Dutch-Belgian Fragile X Consortium et al., 1994) as well as altered dendritic spine morphology (Galvez & Greenough, 2005). In the auditory cortex of *fmr1* KO mice there is an increased response magnitude to sounds, increased variability in first spike latency and abnormal spectrotemporal processing (Rotschafer & Razak, 2013). As well, *fmr1* KO mice are susceptible to audiogenic seizures (Musumeci et al., 2000). Furthermore, in the auditory cortex of a rat model of FXS there is impaired speech sound processing compared to wild type (WT) rats (Engineer et al., 2014).

These auditory processing deficits may arise due to abnormal changes in translational targets of FMRP during developmental critical periods. Indeed, auditory

cortex critical period plasticity is altered in the FXS mouse model (Kim et al., 2013; Wen et al., 2018a); however, the normal developmental expression pattern of FMRP in the auditory cortex has not been characterized. The first aim of this study was to determine the developmental levels of FMRP in auditory cortex of WT mice.

FMRP itself functions as a negative regulator of translation within a cell. Upon neuronal stimulation involving activation of Group I metabotropic glutamate receptors (mGluR1/5), FMRP has at least two demonstrated roles: it is recruited as part of a complex that traffics target proteins from the nucleus to dendritic cavities (Santoro et al., 2012), and also regulates the local translation of mRNAs already located at synapses (Janusz et al., 2013). Translation of FMRP itself has also been shown to be up-regulated near synapses in response to mGluR activity (Weiler et al., 1997). Of the various targets that FMRP binds to and regulates, many have been identified as dendritic mRNAs (as reviewed in Santoro et al., 2012).

The impact of FMRP silencing on cortical networks seems to be most pronounced during critical period development. The critical period is a time when primary sensory regions in the cortex undergo a period of synaptogenesis, refinement, and reorganization in response to external sensory stimuli, in order to respond best to salient environmental cues (reviewed in Hensch, 2004). During this critical period many network changes take place. Dendritic spines normally undergo a process of maturation with a profusion of elongated filopodia which then shrink as long, thin spines develop and eventually grow into mushroom shaped, stubby spines with short necks into adulthood (as reviewed in Harris, 1999; Majewska & Sur, 2003). Changes in both pre- and postsynaptic terminals

take place during this maturational period, including changes in the number and type of receptors and sub-receptor components (Nase et al., 1999) as well as the amount of neurotransmitter released (as reviewed in Craig, 1998). The overall result is an alteration in synaptic kinetics, with reduced neurotransmitter release, shortened action potential duration, reduced pre- and postsynaptic membrane thresholds and a more limited window for temporal summation of synaptic inputs (Nase et al., 1999).

Many of these developmental benchmarks are delayed or malfunctioning in FXS (Deng et al., 2011; Deng et al., 2013; He et al., 2014; Pacey et al., 2013). In particular, in FXS there is abnormal spine morphology, characterized by an increase in the percentage of long, thin, and immature dendritic spines. This abnormality is among the few consistent cortical abnormalities found across studies and ages in human FXS patients (Hinton et al., 1991; Irwin et al., 2001; Rudelli et al., 1985) and is most pronounced during the critical period of development in mice (Sidhu et al., 2014), normalizing to control levels by one month of age (Nimchinsky et al., 2001; Till et al., 2012) and becoming exaggerated again at older ages (Comery et al., 1997; Galvez & Greenough, 2005; Irwin et al., 2002). The elongated, immature spines that persist in FXS remain more motile, highly excitable and with more non-specific activity in response to environmental input (as reviewed in Bourne & Harris, 2007).

FMRP expression level is higher during developmental time points in both somatosensory cortex (Harlow et al., 2010; Till et al., 2012) and hippocampus (Aujla & Huntley, 2014), while manipulation of critical period onset in visual cortex of rats by dark rearing showed an increase in FMRP expression immediately after light exposure

(Gabel, 2004), indicating that FMRP levels are responsive to early sensory events. Deficits in critical period plasticity have been demonstrated in FXS both at the structural (Till et al., 2012; Wen et al., 2017) and physiological levels (Kim et al., 2013).

Furthermore, changes in the inhibitory network also take place during the normal critical period. Among other changes, there is an increase in the number of parvalbumin positive (PV) interneurons (Huang et al., 1999), the development of which correlates with the opening of the critical period. Furthermore, increasing inhibition has been shown to induce critical period plasticity (Fagiolini & Hensch, 2000; Iwai et al., 2003), and this appears to be mediated through PV specific receptors (Fagiolini, 2004). The development of the characteristic fast-spiking inhibition of PV cells is also correlated with the closure of the critical period (Hensch, 2004; Hensch, 2005; Huang et al., 1999). PV-cells establish contacts with postsynaptic terminals through GABA-A (γ-aminobutyric acid type A) alpha-subunits expressed at somatic locations (Fagiolini, 2004) where their fast spiking activity, shaped by kV3.1 potassium channels (Lien & Jonas, 2003) and supported by perineuronal nets surrounding the cell body (Saghatelyan, 2001), acts to shorten the duration of action potentials in excitatory neurons and allows for a higher frequency of action potentials within a given period of time. Disruption of this fast-spiking inhibition leads to an increase in excitability (Saghatelyan, 2001).

Again, many of these benchmarks of development are disrupted in FXS, including a reduction in PV-cells, altered perineuronal net structure and a decrease in kV3.1 channels (Selby et al., 2007; Strumbos et al., 2010; Wen et al., 2018a), resulting in increased network excitability. In addition, there is a decrease in GABA-A receptors

throughout the cortex, brainstem and hippocampus in FXS – indicating a reduction of inhibition in FXS (El Idrissi et al., 2005). This altogether suggests that loss of FMRP during early development leads to altered circuits maturation, possibly underlying hyper-responsive sensory systems in adulthood and the cognitive impairments seen in FXS.

It has been hypothesized that the increase in α-Amino-3-hydroxy-5-methyl-4-isoxazolepropionic acid (AMPA) receptor internalization, due to exaggerated long-term depression (LTD) in FXS, may lead to the structural changes found in FXS dendritic spines (Bear et al., 2004), yet this accounts for only a fraction of the developmental deficits characterized in FXS. While LTD likely plays a part, other mechanisms downstream of FMRP have been shown to play a role as well.

In particular, FMRP regulates the translation of Matrix Metalloproteinase-9 (MMP-9) (Janusz et al., 2013). MMP-9 is a zinc-dependent protease, an enzyme which functions to cleave certain substrates of the Extracellular Matrix (ECM) - the scaffolding that surrounds neurons and glia within the extracellular space and which comprises perineuronal nets – as well as surface and cell adhesion molecules (reviewed in Benson & Huntley, 2012). Although MMP-9 has an important role in the establishment and remodeling of the early pericellular microenvironment (Aujla & Huntley, 2014; reviewed in Dziembowska & Wlodarczyk, 2012; reviewed in Reinhard et al., 2015; Spolidoro et al., 2012; Tian et al., 2007; Wang et al., 2008) without FMRP in the system to regulate MMP-9 translation, it becomes globally overexpressed and may be responsible for observed phenotypes in FXS (Bilousova et al., 2008; Michaluk et al., 2011; Sidhu et al., 2014). Reducing MMP-9 levels in *fmr1* KO mice through Minocycline treatment, a

tetracycline analogue which inhibits MMP-9 activity (Dziembowska et al., 2013), rescues altered dendritic spines, behavioral deficits (Bilousova et al., 2008), and impaired ultrasonic vocalizations (Rotschafer et al., 2012). Minocycline treatment also reduces the severity of audiogenic seizures in *fmr1* KO mice (Dansie et al., 2013). *MMP-9/FMR1* double KO mice also show rescue of hippocampal deficits (Sidhu et al., 2014), while genetically reducing MMP-9 using *fmr1* KO mice heterozygous for MMP-9 rescues impaired auditory development (Wen et al., 2017). Taken together it seems that many FXS phenotypes can be improved by reduction of MMP-9 in *fmr1* KO mice, therefore it is important to establish key windows in which reduction of MMP-9 might be most effective. Here we will characterize the normal expression of MMP-9 during auditory cortex development, and directly test whether Minocycline administration during this time can reduce MMP-9 levels in WT and *fmr1* KO mice.

A useful biomarker for FXS is seizure activity, a phenotype present in 11- 40% of FXS patients and in *fmr1* KO mice (Berry Kravis, 2002; Chen & Toth, 2001; Musumeci et al., 2000; Musumeci et al., 2007). Global hyper-excitability in FXS likely leads to the seizures, and application of GABA-B receptor agonists has been shown to decrease audiogenic seizure activity in *fmr1* KO mice (Pacey et al., 2009). MMP-9, with its role in the elongation of dendritic spines and possibly in the cleavage of PNNs, may also play a role in the increased excitability leading to seizure activity. MMP-9 overexpression has been shown to increase the severity of induced seizure activity and to possibly lead to epileptogenesis (Wilczynski et al., 2008), while the inhibition of MMP-9 (with Minocycline) has been shown to reduce the severity of audiogenic seizures (Dansie et al.,

2013). But while both the application of GABA-B agonists and the inhibition of MMP-9 were able to *reduce* the severity of seizures, neither method alone has been able to prevent seizure activity in mice. Acamprosate is an FDA approved drug which is thought to antagonize NMDA and mGluR5 receptors while activating GABA-A receptors, allowing increased network inhibition (Williams, 2005) and has been tested for treatment of FXS in human patients (Erickson et al., 2010; Erickson et al., 2013; Erickson et al., 2014). It may be that a combination of Minocycline and Acamprosate treatment together may completely prevent seizures.

In this study therefore focuses on the development of the auditory cortex, using audiogenic seizure activity as an outcome measure for the role of MMP-9 in cortical hyper-excitability. FMRP expression will be characterized throughout development, from before hearing onset into adulthood. As an important player in early development and spine morphology, we will also characterize the expression of MMP-9 in WT and *fmr1* KO mice during the same developmental time points. The effect of Minocycline administration on MMP-9 levels in the auditory cortex and inferior colliculus will be determined, and audiogenic seizures used to measure the behavior outcome of Minocycline and/or Acamprosate treatment.

2. Methods and Materials

2.1 Ethics statement

All animal care protocols and procedures were approved by the UC Riverside Animal Care & Use Program, which is accredited by AAALAC International, and animal

welfare assurance number A3439-01 is on file with the Office of Laboratory Animal Welfare (OLAW).

2.2 Animal Use

FVB.129P2-Fmr1tm4Cgr (*fmr1* KO) and their control strain FVB.129P2-Pde6b+Tyrc-ch/AntJ (wild-type, WT) were obtained from Jackson Laboratories and housed in an accredited vivarium with 12 h light/dark cycle. These mice do not suffer from retinal degeneration due to restoration of the pde6b allele and do not develop blindness. The FVB strain shows no indication of deafness at least up to 8 months of age (Zheng et al., 1999). Food and water were *ad libitum*, with standard mouse chow. All studies were performed in accordance with the National Institutes of Health and with Institutional Animal Care and Use Committee guidelines. Ages of mice used for gel zymography were perinatal days P3, P7/8, P12/13, P18 and P40/41. Ages P3 - P7/8 reflect a period before hearing onset, which occurs around P10-P11 (McKay & Oleskevich, 2007). The earliest auditory critical period ranges from P11 - P14, followed by a series of developmental 'windows' that extend to ~P39 (Barkat et al., 2011; Carrasco et al., 2013; de Villers-Sidani et al., 2007; Insanally et al., 2009; Kim et al., 2013). At P40, response properties of neurons in auditory cortex (A1) have mostly matured.

2.3 Gel Zymography

Mice were euthanized with isoflurane (all mice P12 and older) or cervical dislocation (mice from P3 - P7/8), the auditory cortex was dissected and flash-frozen in dry ice. Because there are no clear anatomical indicators of auditory cortical boundaries

in the mouse, in all cases dissections were centered 2/3rds caudal from the frontal lobe and 2/3rds lateral from the midline, dorsal to the rhinal fissure. This includes the auditory cortex per the mouse brain atlas and is also the region of skull exposure that reliably gives auditory responses in *in vivo* electrophysiology experiments (Rotschafer and Razak, 2013). Nissl staining on post-dissection brains was performed to verify the specificity of the dissected region. Brains were post-fixed in paraformaldehyde for 24 hours and then cryoprotected in a 30% sucrose solution, cut in 100μm coronal slices with a cryostat, and stained with Cresyl violet.

Tissue was homogenized in 100 µL of buffer-1 (500mM CaCl2, 10% Triton X-100, 100 mM Tris-HCL pH to 7.6, 1.5 M NaCl, 30% Brij 35, 2% NaN3, 100 mM PMSF, 50 µL PIC, milli-Q H20), rotated for one hour at 4° C followed by centrifugation for 15 minutes at 4° C. The triton-soluble supernatant fraction was collected, enriched with gelatin sepharose beads and rotated overnight at 4° C. Samples were spun down at 2-5 rpm for two minutes at 4° C, the supernatant was collected and frozen, and 30 µL of 2x Sample buffer (Invitrogen) was added to the beads. Samples were vortexed slightly, incubated for 30 minutes at room temperature with shaking, then loaded (20 µL each) and run on 10% zymogram (gelatin) gel (Novex) at 125 volts for two hours or until each sample ran to the bottom of the gel. Gels were incubated two times for 30 minutes in 1x renaturing buffer (Novex) and then incubated in 1x in developing buffer (Novex) for 96 hours at 37° C. Gels were incubated in staining buffer overnight (40mL Methanol, 50mL H2O, 10 mL Acidic Acid, and 2g Coomassie), then washed in de-staining buffer (400 mL Methanol, 100mL Acidic Acid, and 500 mL H2O) until the desired contrast between

bands and background was reached. Bands for MMP-9 and MMP-2 activity levels were quantified using Image J (AC development) or CS3 Adobe Photoshop (Minocycline treatment).

2.4 Western Blot

The Triton-soluble supernatants remaining from gel zymography were used to quantify the levels of FMRP in the mouse auditory cortex during development. BCA protein assay was performed on the samples. Aliquots of equal parts supernatant and 2x Laemmli buffer were boiled at 100ºC for 10 minutes, and then run on 8-16% Tris-Glycine gel (Novex). The proteins were transferred to Nitrocellulose (GE Healthcare; Protran BA 85) and blocked for 1 h at room temperature in 5% skim milk. Primary antibody incubations were done overnight at 4°C using appropriate antibodies diluted in TBS/0.1% Tween-20. Primary antibodies and dilutions were as follows: Mouse α-FMRP - 1:500 (Chemicon Industries, Millipore), and Mouse α-GAP-DH – 1:1000 (Invitrogen). Blots were washed 3×10 min with TBS/0.1% Tween-20 and incubated with HRP-conjugated secondary antibodies for an hour at room temperature in a TBS/0.1% tween-20 and 5% skim milk buffer solution; secondary antibodies used were Donkey Anti-Mouse HRP - 1: 5,000 (Jackson Immuno Research). After secondary antibody incubations, blots were washed 3×10 min in TBS/0.1% Tween-20, and then developed with Peirce ECL 2 Western Blotting Substrate (Thermo Scientific). For GAP-DH re-probing, membrane blots were washed in stripping buffer (2% SDS, 100 mM β-mercaptoethanol, 50 mM Tris-HCl, pH 6.8) 2x15 min at 56°C, rinsed repeatedly with TBS/0.1% Tween-20, blocked with 5% skim milk, and then re-probed.

2.5 Drug Administration

Minocycline treatment. From P0 to ~P21 (weaning) lactating pups were administered 30mg/kg of Minocycline by dissolving Minocycline in the dam's drinking water in amber colored bottles. Calculations of 30mg/kg were based on the mother's weight, re-measured periodically throughout this time. Weaned mice were similarly administered Minocycline dissolved in the drinking water, with calculations of 30mg/kg based on the average weight and water consumption of co-habituating mice. All mice were treated until the day of experimentation. Water consumption was measured daily. Each week, both average daily water consumption and the weight of the dam/mice were used to confirm proper dosage and to readjust dosage if necessary. Control litters were given normal drinking water in amber drinking bottles, with the mother's weight and average water intake calculated as well. This method of minocycline administration has been previously shown to yield detectable concentrations of minocycline in the blood of adult mice (Lee et al., 2006) and in the breast milk of lactating dams (Lin et al., 2005; Luzi et al., 2009).

Acamprosate treatment. From these treated and control litters, mice were pseudo-randomly assigned to either saline or Acamprosate groups. Each mouse was administered two i.p. injections, 12 hours apart, of either 0.9% saline or 40mg/kg Acamprosate, diluted into 0.9% saline at 0.1 mL saline/10g of mouse (Gupta et al., 2008; Hinton et al., 2012). 30 minutes after the second injection, mice were tested using the audiogenic seizure protocol. A subset of mice was tested using a single i.p. injection of

either 200mg/kg Acamprosate, 400mg/kg Acamprosate, or 0.9% saline, diluted as above. Treatment conditions can be seen in Table 2.1.

Table 2.1. *Mice Used in Audiogenic Seizure Studies.*

Condition	Males	Females	Total
H2O, Acamprosate 400mg/kg chronic	6	1	7
H2O, Saline	5	3	8
Minocycline 30mg/kg, Acamprosate 400mg/kg	2	5	7
Minocycline 30mg/k, Saline	1	5	6
Acamprosate 200 mg/kg acute	4	0	4
Acamprosate 400 mg/kg acute	4	0	4
Saline acute	4	0	4
No Treatment Controls	10	11	21

2.6 Audiogenic seizures

Treated mice and no-treatment controls were placed in a transparent plastic cage with an open grid lid (28x17.5x19.5 cm) for testing of audiogenic seizures. After a five-minute baseline to assess normal behavior, all mice were exposed to a high intensity siren (105 dB SPL; alternating 500-ms upward frequency modulated (FM) sweeps and 495-ms downward FM sweeps; 8–2 kHz) for 15 min. The siren was generated using a custom program (Batlab, Dr. Don Gans, Kent State University, Kent, OH, USA), a Microstar digital signal processing board and Tucker Davis System programmable attenuators (PA5). The sounds were further amplified with a power amplifier (Parasound) and presented through a speaker (Fostex FT96H, Madisound, Middleton, WI, USA) that was

mounted on top of the open grid lid of the plastic cage. All testing took place in a sound-proof chamber lined with anechoic foam (Gretch-Ken Industries Inc., Lakeview, OR, USA). During each experiment a maximum of four mice were placed in the cage and seizure activity was digitally recorded for later scoring. A similar method has been previously shown to trigger seizures in *fmr1* KO mice of the same age (Yan et al., 2004, 2005). No WT mice were used, as it has previously been established that these WT mice are not prone to audiogenic seizures (Dansie et al., 2013).

2.7 Analysis of Results

Western blot and gel zymography band intensity values were each normalized to background levels. For the developmental characterization of MMP-9 and FMRP, each gel or blot was normalized to P7 WT values within the respective blot/gel due to differences of intensity between experiments; however, this was not necessary for the Minocycline study. Western blots were analyzed using a One-way ANOVA and gel zymography using two-way ANOVA, each with Bonferroni post hoc analysis. Gel zymography performed on minocycline treated mice were analyzed for each age group separately, using a two-way ANOVA between genotype and treatment.

Audiogenic seizure videos were scored and analyzed using three main outcomes measures: 1) wild running and jumping (WRJ), 2) tonic seizures (TS), and 3) death. Wild running and jumping is a form of seizure and is distinct from typical behavior, even under stressful conditions. Tonic seizures are also clearly identifiable, with the mice prostrate on their side as their limbs, tail, and ears extend outward. Clonic seizures, though present, were not measured due to subjectivity inherent in scoring them. A one-way

ANOVA was used to analyze the percentage of mice displaying a behavior. Additionally, a Kaplan-Meier survival curves for each of the 3 outcome measures was generated to analyze latency to a behavior, and the log-rank test was used to compare between the curves of each group.

3. Results

3.1 FMRP Levels in Development

Taking into account previous studies demonstrating an increase in FMRP expression correlated with the onset of critical period development, it was predicted that FMRP levels in the auditory cortex would peak at P12, a time point just after hearing onset and within the critical period of the primary auditory cortex (Barkat et al., 2011; McKay & Oleskevich, 2007). Indeed, an ANOVA showed that there was a difference between groups, $F(4, 13) = 36.42$, $p = 0.0001$, R^2 = 0.92. FMRP levels which were lower at P3 (n = 4, M = 0.41; P3 vs P7: $p < 0.001$) increased before hearing onset (P7: n = 10, $M = 1.01$) and remained high during the critical period (P12: n = 5, M = 0.93: P7 vs. P12: *ns*), with a steady decrease into adulthood (P18: n = 3, M = 0.51, P7 vs. P18: $p < 0.0001$; P40: n = 3, M = 0.31, P7 vs. P40: $p < 0.0001$; Fig. 2.1). To verify that this expression pattern reflects auditory cortex development specifically, brains collected after tissue dissection for WB and MMP-9 experiments were stained with Cresyl Violet and imaged, confirming that tissue samples did contain the primary and secondary auditory cortex, as well as the associative temporal cortex.

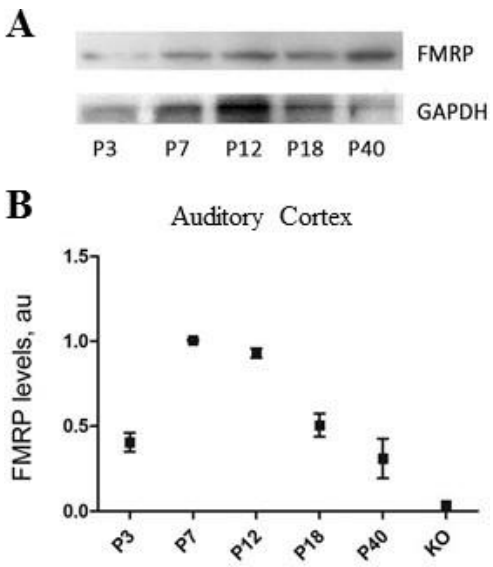

Figure 2.1. Expression of FMRP in the developing auditory cortex. A) Example western blot for FMRP and GAPDH in WT auditory cortex. B) FMRP levels peak at P7 and decrease into adulthood. Paired comparisons reveal that P7 and P12 are each significantly different from P3, P18 and P40, $p < 0.001$. N (WT): P3 4 mice; P7 10; P12 5; P18 3; P40 3.

3.2 MMP-9 Levels in Auditory Cortex Development

Given that MMP-9 is thought to have a role in early perisynaptic development, it was expected that MMP-9 activity levels in WT mice would peak throughout the critical period, at P12, and decrease into adulthood when there is reduced synaptic remodeling. Levels of MMP-9 activity in *fmr1* KO mice were expected to remain high at all ages because FMRP is a known translational repressor of MMP-9. We found that in WT mice, MMP-9 activity increased from P3 ($n = 4$, $M = 0.73$) to peak levels at P7 ($n = 8$, $M = 1$) at which point they declined by P12 ($n = 4$, $M = 0.42$) and remained low at P18 ($n = 4$, $M = 0.40$). In *fmr1* KO mice this same pattern was seen (Fig. 2.2), though at all time-

points the activity levels of MMP-9 were elevated compared to WT mice (P3: $n = 4$, $M = 1.35$; P7: $n = 8$, $M = 1.35$; P12: $n = 4$, $M = 1.01$; P18: $n = 4$, $M = 0.76$).

Statistical analysis confirmed that MMP-9 levels were overall elevated in *fmr1* KO mice across auditory development (effect of genotype: $F(1) = 13.07$, $p = 0.0017$). However, both genotypes showed a downregulation of MMP-9 across ages ($F(3) = 5.07$, $p = 0.009$; interaction: $F(3) = 0.29$, $p = 0.832$; Fig. 2.2B), with significantly less MMP-9 at P18 than at P7 ($p < 0.05$) in both WT and *fmr1* KO mice. MMP-2 levels also decreased in early postnatal AC (Means - WT: P3 = 1.8, P7 = 1.0, P12 = 0.6, P18 = 0.7; *fmr1* KO: P3 = 1.6, P7 = 1.3, P12 = 1.0, P18 = 0.8; effect of age: $F(3) = 5.28$, $p = 0.012$) but were not different between WT and *fmr1* KO mice (effect of genotype $F(1) = 0.78$, $p = 0.4$; Fig. 2.2C). Activated MMP-2 showed no difference across development and was expressed at similar levels in both WT and *fmr1* KO mice (effect of age: $F(3) = 1.31$, $p = 0.31$; effect of genotype: $F(1) = 1.56$, $p = 0.233$; Fig. 2.2D). Overall these data indicate that both WT and *fmr1* KO mice developmentally regulate MMP-9 and MMP-2 levels, which actually peak before hearing onset and decrease during the critical period. However, in *fmr1* KO cortex the levels of MMP-9 are elevated compared to WTs.

3.3 Minocycline moderately reduces MMP-9 levels in AC and Inferior Colliculus

Although Minocycline treatment rescues many FXS phenotypes in *fmr1* KO mice, it is not clear if this is due to its action on MMP-9 or another mechanism. Here the effects of Minocycline treatment on MMP-9 levels were directly tested in the developing AC and inferior colliculus (IC), a subcortical region important in auditory processing and audiogenic seizures.

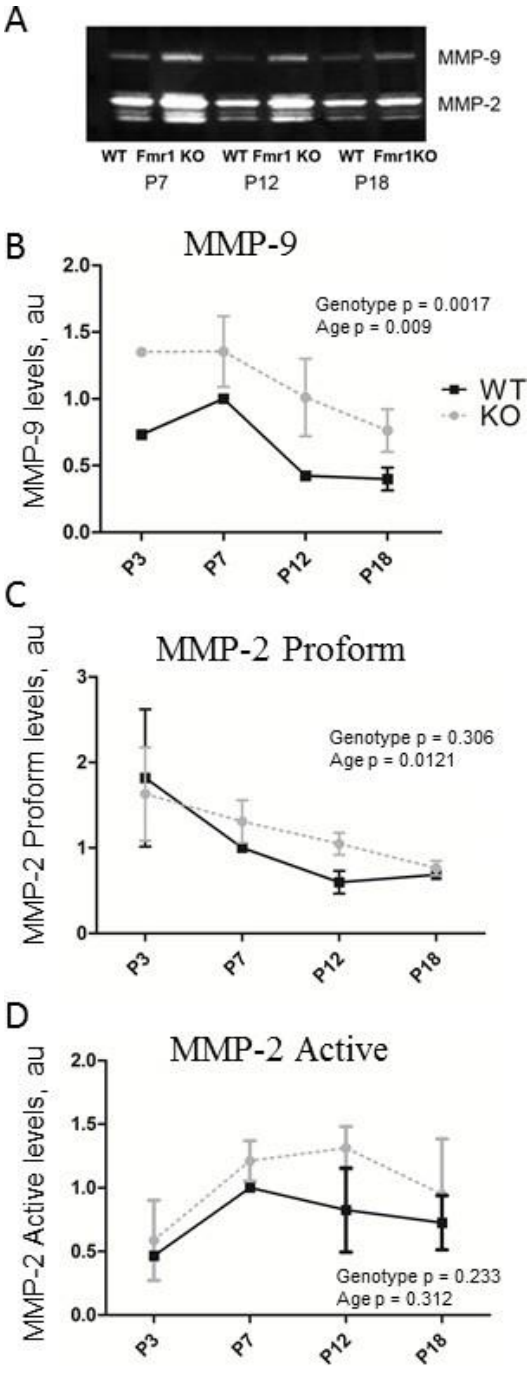

Figure 2.2. MMP-9 levels in auditory cortex development. A) Example Gelatin Zymography showing MMP-9 and MMP-2 regions of digestion. The proform (inactive) band of MMP-2 has a higher molecular weight than the activated MMP-2 band on the gel. Activated MMP-9 is not visible. B) MMP-9 levels peak at P7 and decrease during the critical period. However they remain elevated in f*mr1* KO mice. C) MMP-2 is also downregulated with age, but shows no difference between WT and *fmr1* KO mice. D) Activated MMP-2 levels show no age-related regulation or difference between genotypes. N for MMP-9: WT: P3 4, P7 8, P12 4, P18 4; *fmr1* KO: P3 4, P7 8, P12 4, P18 4. N for MMP-2 (both): WT: P3 6, P7 6, P12 3, P18 3; *fmr1* KO: P3 6, P7 6, P12 3, P18 3.

In the AC, MMP-9 levels were elevated in P7 *fmr1* KO mice (M = 104.7) compared to WTs (M = 57.17; effect of genotype: $F(1) = 15.93$, $p = 0.001$), consistent with the previous experiment. Although there was no overall effect of treatment ($F(1) = 0.035$, $p = 0.85$), paired comparisons revealed that untreated WT and *fmr1* KO mice were significantly different from each other ($p < 0.01$), but Minocycline treatment ameliorate this (Treated: WT = 66.06, *fmr1* KO = 92.24; *ns*). At P12 however, minocycline treatment had no effect on the elevated MMP-9 levels in *fmr1* KO mice (Untreated: WT = 17.98, *fmr1* KO = 37.86, $p < 0.001$; Treated: WT = 16.29, *fmr1* KO = 37.39, $p < 0.001$; effect of genotype: $F(1) = 48.07$, $p < 0.0001$; effect of treatment: $F(1) = 0.13$, $p = 0.718$). This was also true at P18 (Untreated: WT = 10.95, *fmr1* KO = 19.82; Treated: WT = 7.37, *fmr1* KO = 21.79; effect of genotype: $F(1) = 6.19$, $p = 0.026$; effect of treatment: $F(1) = 0.03$, $p = 0.866$). In P40 mice, MMP-9 levels remain elevated in *fmr1* KOs (effect of genotype: $F(1) = 19.98$, $p = 0.0004$). Although there was no overall effect of treatment ($F(1) = 0.372$, $p = 0.55$) the untreated WT and *fmr1* KO were significantly different from each other ($p < 0.001$; WT = 22.39, *fmr1* KO = 45.47) but Minocycline treatment ameliorated this (*ns*; WT = 27.47, *fmr1* KO = 36.07). Altogether this again shows that MMP-9 is elevated across auditory development in *fmr1* KO mice, which persists until P40. Although data did not demonstrate a strong reduction of MMP-9 in response to Minocycline treatment, at P7 and P40 partial recovery is suggested.

Unlike the auditory cortex, the IC did not show a large elevation of MMP-9 in *fmr1* KO mice. At P7 both WT and *fmr1* KO mice expressed similar levels of MMP-9, and this was not altered by Minocycline treatment (Untreated: WT = 84.53, *fmr1* KO =

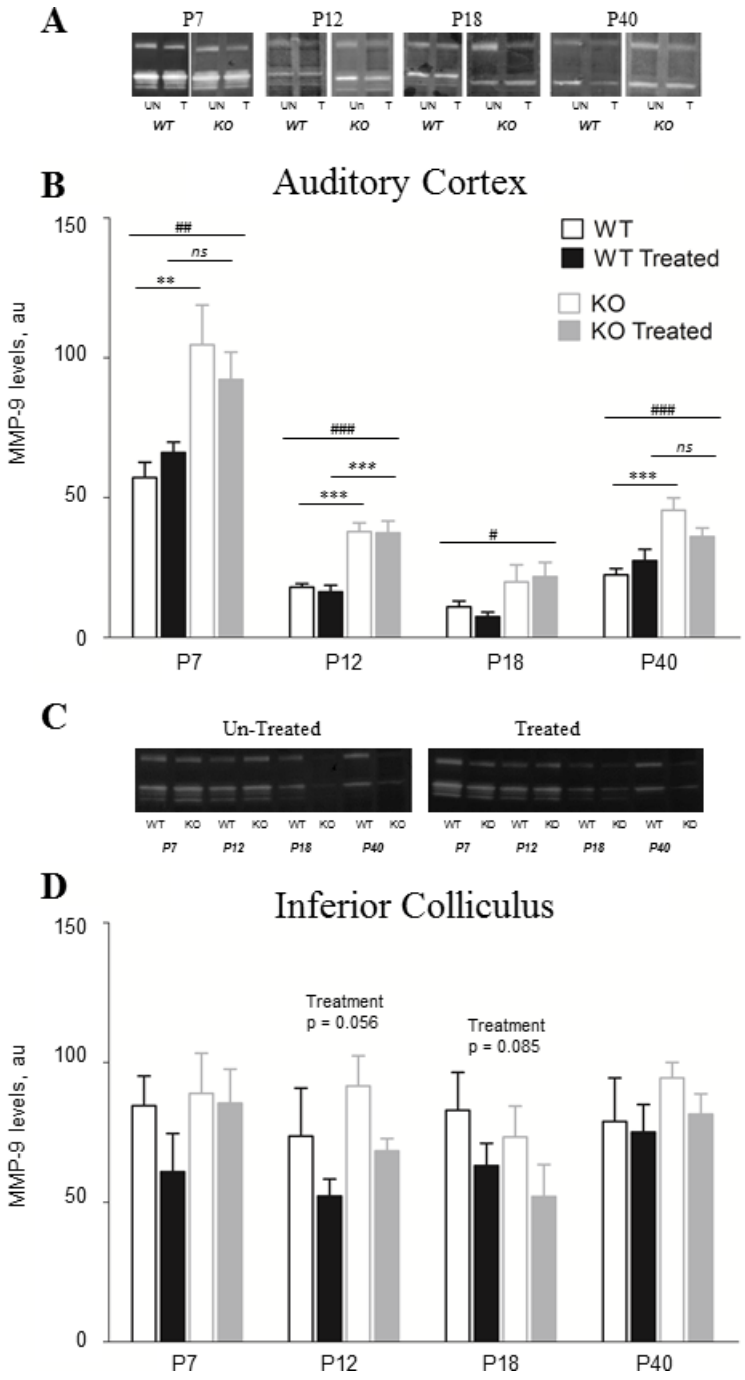

Figure 2.3. Minocycline treatment moderately reduces MMP-9 in the auditory system. A) Examples of gelatin zymography run on samples of auditory cortex and (C) inferior colliculus after Minocycline treatment. B) MMP-9 levels were elevated at all ages in the AC of *fmr1* KO mice, however after treatment, WT and *fmr1* KO mice were not different from each other (P7 and P40 only). D) In the IC, MMP-9 levels were similar in WT and *fmr1* KO mice. Minocycline treatment moderately reduced MMP-9 levels in P12 and P18 mice only. Significance values: * = paired comparison, # = main effect of genotype. * , **, *** correspond to p = 0.05, 0.01 and 0.001 respectively. N AC: WT: P7 5, P12 4, P18 4, P40 5; WT treated: P7 5, P12 5, P18 4, P40 5; *fmr1* KO: P7 5, P12 5, P18 5, P40 5; *fmr1* KO treated: P7 5, P12 5, P18 5, P40 5. N IC: WT: P7 6, P12 5, P18 5, P40 5; WT treated: P7 6, P12 5, P18 5, P40 5; *fmr1* KO: P7 5, P12 5, P18 5, P40 5; *fmr1* KO treated: P7 5, P12 5, P18 5, P40 6.

88.99; Treated: WT = 60.93, *fmr1* KO = 85.45; effect of genotype: F(1) = 1.26, p = 0.275; effect of treatment: F(1) = 1.11, p = 0.306). P12 mice also had similar levels of

MMP-9 between WT and *fmr1* KO mice (Untreated: WT = 73.63, *fmr1* KO = 91.58; effect of genotype: F(1) = 2.468, p = 0.135), however Minocycline treatment did reduce MMP-9 levels at this age (Treated: WT = 52.19, *fmr1* KO = 68.32; effect of treatment: F(1) = 4.248, p = 0.056). At P18 there was also a trend towards reduced MMP-9 after Minocycline treatment (Treated: WT = 63.12, *fmr1* KO = 52; effect of treatment: F(1) = 3.371, p = 0.085) but no genotype effect (Untreated: WT = 82.92, *fmr1* KO = 73.34; effect of genotype: F(1) = 0.853, p = 0.37). Minocycline treatment did not affect MMP-9 levels in P40 mice (Untreated: WT = 78.89, *fmr1* KO = 94.47; Treated: WT = 75.12, *fmr1* KO = 81.5; effect of genotype: F(1) = 1.19, p = 0.29; effect of treatment: F(1) = 0.69, p = 0.417). This data suggests that dysregulated MMP-9 in FXS may be particularly prevalent in cortical, but not subcortical regions. As in the auditory cortex, Minocycline treatment had a moderate effect on MMP-9 levels but this was not observed across all ages.

3.4 No significant effect of Minocycline and/or Acamprosate treatment on Audiogenic Seizures in *fmr1* KO mice

Because WT FVB mice are not susceptible to audiogenic seizures using methods in the current study (Dansie et al., 2013) all treatment and seizure experiments were performed on *fmr1* KO mice only. All mice were given either Minocycline or water in amber bottles during development (P0-P30), followed by an injection of either Acamprosate or saline 12 hours prior to testing. For each group (Table 2.1; Water w/

Saline, Minocycline w/ Saline, Minocycline with Acamprosate or Water with Acamprosate) three behaviors were measured – wild running/jumping (WRJ), tonic seizure (TS) and death.

3.4.1 Total Percent

Acamprosate is thought to reduce total cortical excitation through multiple mechanisms and might be expected to decrease audiogenic seizure activity in *fmr1* KO mice. Likewise, Minocycline treatment during the first postnatal month has been shown to attenuate seizure activity in *fmr1* KO mice (Dansie et al., 2013). Therefore, it is predicted that mice with Acamprosate or Minocycline treatment alone should display a reduction of the percent of mice that display WRJ and TS and death, while those mice that received a co-administration of both treatments should have a complete rescue of audiogenic seizure. Results are shown in Figure 2.4.

Tonic Seizures. 50% of control *fmr1* KO mice treated with water and saline, or saline alone, displayed tonic seizures. The percent decreased marginally in Minocycline treated mice (Minocycline/saline = 33%) but increased in Acamprosate treated mice (200 mg Acamprosate = 75%; 400 mg Acamprosate = 75%; Water/Acamprosate = 57%) as well as in mice with co-administration (Minocycline/Acamprosate = 71%) This resulted in no overall difference between groups *(*$F(6, 33) = 0.49$, $p = 0.8114$, $R^2 = 0.08$; Fig 2.4A).

Wild Running and Jumping. In control *fmr1* KO mice, treated with water and saline, 75% of mice displayed WRJ in response to the 105 dB siren. 100% of acute saline controls displayed WRJ. Treatment with Minocycline alone (Minocycline/Saline = 83%)

or Acamprosate alone (200 mg Acamprosate = 100%; 400 mg Acamprosate = 100%; Water/Acamprosate = 100%) or co-administrate of treatments (Minocycline/Acamprosate = 86%) did not reduce the percentage of mice displaying WRJ *(*$F(6, 33) = 0.71$, $p = 0.65$, $R^2 = 0.11$; Fig. 2.4B).

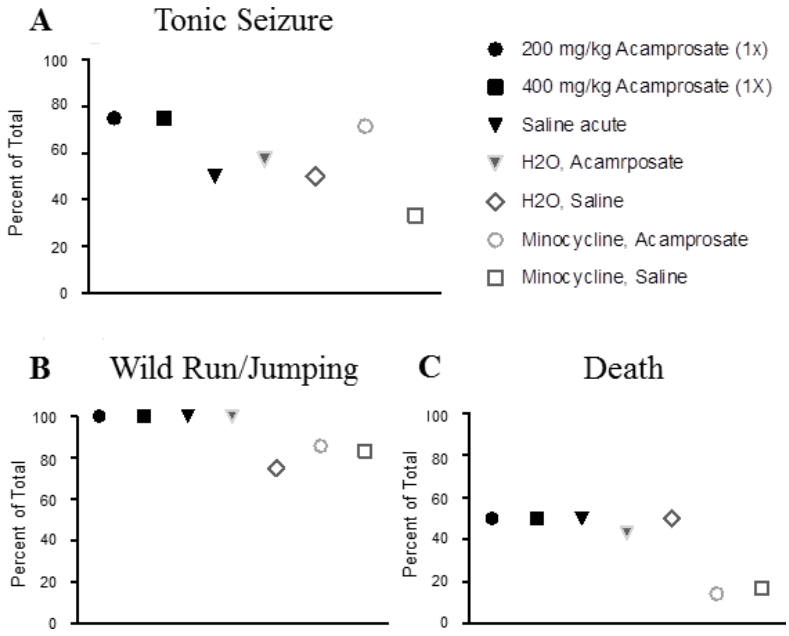

Figure 2.4. Treatment did not have a large impact on the seizure outcome by percent. No differences were found between groups in total percent of mice that displayed (A) tonic seizures, (B) wild running/jumping, or (C) death. Though not statistically significant, Minocycline treatment did reduce the total percent of dead from 50% to 17% and the percent of tonic seizures from 50% to 33%. Minocycline treatment with Acamprosate injection also reduced death from 50% to 14%.

Death following Seizures. In 50% of control *fmr1* KO mice, treated with water and saline or acute saline, death occurred as a result of the seizures. This was reduced in minocycline treated mice (Minocycline/saline = 17%) as well as in mice that received Minocycline and Acamprosate treatments (14%) however Acamprosate treatment alone did not prevent death (200 mg Acamprosate = 50%; 400 mg Acamprosate = 50%;

Water/Acamprosate = 43%). Even though the total percent is reduced in two treatment groups, overall the treatments were not different from each other ($F(6, 33) = 0.63$, $p = 0.7014$, $R^2 = 0.10$).

3.4.2 Latency

Though there was no difference in total percent of mice that seized or died between groups, it was hypothesized that in treated mice there would be an increased latency from sound onset to the start of WRJ, TS and death when compared to control mice. Increased latency might indicate that the increased network inhibition through drug administration is able to delay the onset of seizure activity.

Latency was measured using Kaplan-Meier survival curves. This method takes into account both the latency and percentage of mice within a group that display a given behavior throughout the time course of the experiment. A Kaplan-Meier curve was generated for each of the three outcome measures (WRJ, TS and death), to test the null hypothesis that there would be no difference between curves among each treatment group. Log-rank test found no differences between the curves of each treatment group for wild running and jumping ($x^2(6) = 6.68$, $p = 0.3512$) or for tonic seizures ($x^2(6) = 5.47$, $p = 0.4856$) or death ($x^2(6) = 3.66$, $p = 0.7233$). This is shown in Figure 2.5, where treatment groups are separated onto two graphs for clarity.

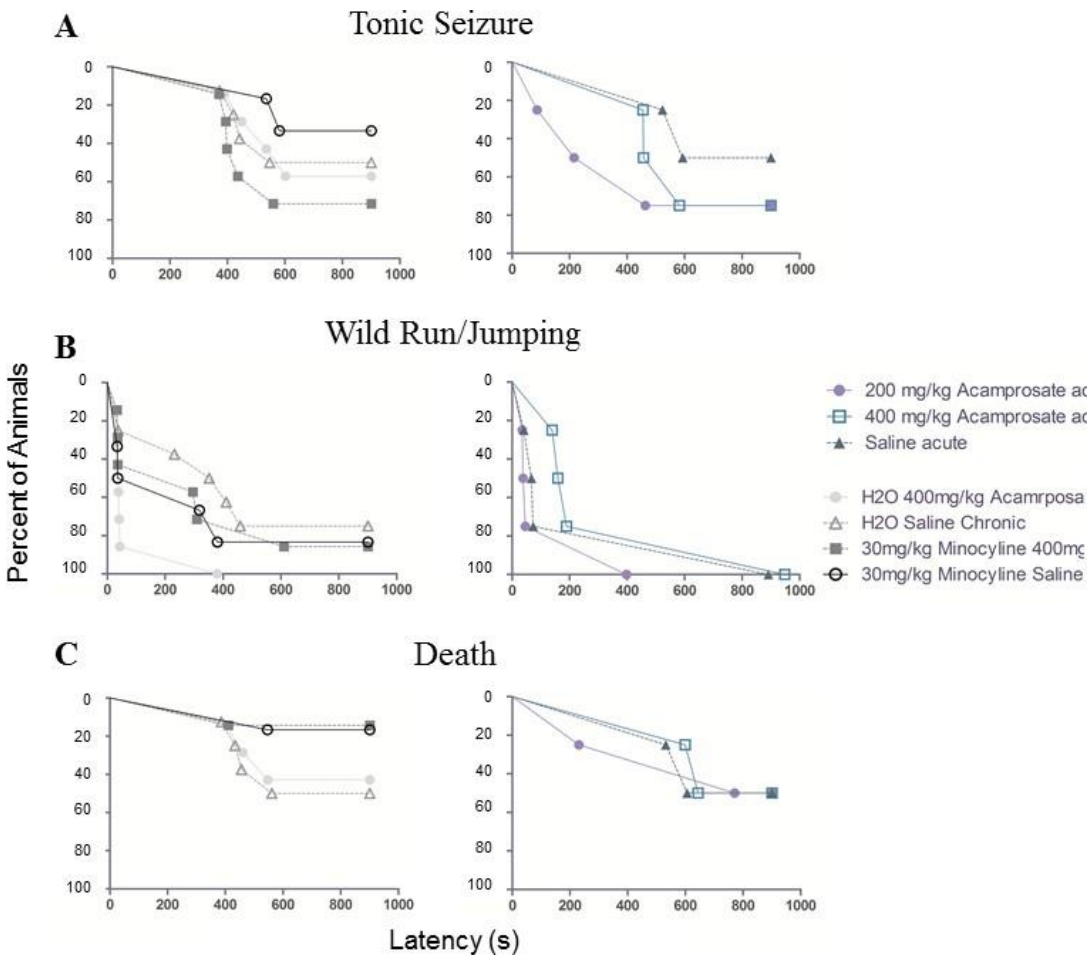

Figure 2.5. Treatment did not affect the latency to seizure activity. The x-axis shows the latency (s) of behavior onset for mice in each group. As more mice display the behavior, the percentage on the y-axis increases. Minocycline and/or Acamprosate treatment did not change the latency for (A) tonic seizures, (B) wild running and jumping, or (C) death.

Taken together the audiogenic seizure data indicate that neither Minocycline treatment or Acamprosate treatment alone, nor co-administration of both treatments was able to rescue audiogenic seizure phenotype in *fmr1* KO mice. However, in Minocycline treated mice, there was a trend toward a decreased percentage of mice that experience tonic seizure and death, consistent with previous studies.

4. Discussion

The main findings of this study are (1) FMRP levels are elevated during critical period development in the auditory cortex and (2) that at least one important target of FMRP regulation, MMP-9, also shows increased activity levels overlapping with FMRP. Interestingly, MMP-9 is not elevated in the inferior colliculus, implying it may have a particular role in cortical organization. These results point to an important window of focus when studying FXS. Minocycline treatment moderately decreases MMP-9 levels and moderately reduces tonic seizures and death, however these effects are not robust.

FMRP levels peaked during the auditory critical period. Levels were higher at postnatal days 7 and 12 than at other time points, decreasing into adulthood. This finding is consistent with previous findings in the somatosensory cortex of *fmr1* KO mice, where FMRP expression in layer IV barrel cortex was strongest during the critical period (P3 to P7; Harlow et al., 2010), and decreased to adult levels by P14. FMRP may therefore play an important role in sensory-activity driven, critical period plasticity.

This study is the first to look at development of MMP-9 levels in any cortical sensory system in the mouse. Similar to FMRP peak expression, MMP-9 activity levels also peaked at P7 in normal development but decreased during the critical period (P12) and remained low into adulthood. This suggests that the reduction and stabilization of MMP-9 activity, instead of its up-regulation, may be part of the molecular mechanisms involved in opening critical period plasticity. MMP-9 has been associated with early postnatal development in various brain regions in the rodent – peaking at P0 in the superior colliculus (Oliveira-Silva et al., 2007), at P4 in the hippocampus (Aujla &

Huntley, 2014), and at P10 in the cerebellum (Vaillant et al., 1999). Similarly, to FMRP peak expression patterns, the differences in peak MMP-9 expression across different brain regions at periods of respectively high plasticity and high cortical reorganization suggests that what is observed is not a global up-regulation in the central nervous system in the first two postnatal weeks, but more localized fluctuations in MMP-9 activity in conjunction with highly plastic network states.

In *fmr1* KO mice, MMP-9 activity levels were elevated at all time-points above WT mice, likely due to the lack of FMRP transcriptional regulation on MMP-9. Increases in MMP-9 activity have been shown to induce changes in dendritic spine morphology consistent with the immature FXS phenotype (Michaluk et al., 2009; Michaluk et al., 2011), and are thought to disrupt the structure of ECM, which itself is necessary for the stabilization synaptic contacts (reviewed in Wright et al., 2002). These effects of MMP-9, which would increase synaptic plasticity by delaying and/or disrupting synaptic maturation, are consistent with the "hyper-plasticity" model of FXS proposed by Dolen et al., 2007, in which *fmr1* KO mice actually show accelerated plasticity as demonstrated with measures such as ocular dominance and extinction of inhibitory avoidance. This model implicates disrupted mGluR group I signaling in the generation of hyper-plasticity. As MMP-9 is downstream of mGluR signaling, it is possible that excessive mGluR-mediated protein synthesis in FXS and lack of transcriptional regulation leads to the overexpression of MMP-9 seen here.

Interestingly, though MMP-9 (reviewed in Dziembowska & Wlodarczyk, 2012) and FMRP (Weiler et al., 1997) expression are both activity dependent, in WT mice they

both demonstrated peak expression at P7 – a time prior to hearing onset in the cortex. This high expression is likely due to spontaneous activity generated by inner hair cells in the cochlea (Tritsch et al., 2007; Tritsch et al., 2010) which stimulate the auditory nerve as early as P7 in rats. Moreover, during the critical period when environmentally evoked stimuli are driving cortical excitation (P12), FMRP levels were high but MMP-9 levels dropped off. This drop may reflect FMRP translational regulation on MMP-9, or it may be due to different mechanisms acting on MMP-9.

Minocycline treatment throughout the first month of development had a moderate effect on MMP-9 levels, and on seizure activity. However, treatment was not strong enough to reduce MMP-9 levels at all ages tested, or cause a significant reduction in seizures and death. Previous studies in humans have demonstrated that Minocycline administration can reduce MMP-9 levels in blood plasma of people with FXS (Dziembowska et al., 2013), however this was true in 6 out of 10 patients. In cultured hippocampal neurons, direct application of Minocycline to recombinant MMP-9 also reduced MMP-9levels (Bilousova et al., 2009). Here we demonstrate a similar finding with *in vivo* treatment, although the effect is not robust. Minocycline treatment has also previously been found to decrease the number and the total duration of tonic seizures and increase the percent of mice that survived (Dansie et al., 2013). Though our study did not find significance, a similar pattern was found. The total percent of dead decreased from 50% in control mice to 17% in Minocycline treated with saline injections, and 14% in Minocycline treated with Acamprosate injections. There was also a reduction in the percent of mice with tonic seizures, from 50% in controls to 33% in Minocycline treated

mice. It may be that this study did not include a large enough sample size to accurately reflect changes in the seizure phenotype. However, it does lend support to a moderate effect of Minocycline treatment in FXS.

This is the first study to test Acamprosate in *fmr1* KO mice, a drug previously tested and approved in the treatment of alcoholism and which is currently being tested as a treatment for FXS in human patients (Erickson et al., 2010; Erickson et al., 2013; Erickson et al., 2014). It is reported that the mechanism by which Acamprosate works is several fold - it acts directly on the inhibitory network by agonizing GABA-A receptors while also antagonizing both NMDA and mGluR receptors to decrease excitation. However, in FXS there is a reduction in GABA-A receptor subtypes in *fmr1* KO mice (El Idrissi et al., 2005), as well as impaired mGluR plasticity (Bear et al., 2004). Furthermore, as dendritic spines mature through the critical period there is a change in NMDA receptor subtypes, which alters the response property of the neuron (Moyner et al, 1994; Tovar & Westbrook, 1999) – however in FXS there is impaired maturation of spines which might imply an unusual NMDA composition. Altogether this suggests that the pathways through which Acamprosate works may themselves be altered in FXS, leading to unpredictable results.

In order to fully support any correlation observed between inhibition of MMP-9 and recovery of FXS phenotype, a better understanding of role of MMP-9 during critical period development will be essential. Because MMP-9 is involved in many diverse functions within the developing cortex (Larsen et al., 2006; Vaillant et al., 2003), a better understanding of the cell specific expression and localized effects of MMP-9

overexpression in FXS is needed. However, based on this study, a more specific inhibitor of MMP-9 activity will be useful to powerfully and specifically manipulate MMP-9 activity in auditory cortex.

References

Ashley, C. T., Wilkinson, K. D., Reines, D., & Warren, S. T. (1993). FMR1 protein: conserved RNP family domains and selective RNA binding. *Science*, **262**(5133), 563–566.

Aujla, P. K., & Huntley, G. W. (2014). Early postnatal expression and localization of matrix metalloproteinases-2 and -9 during establishment of rat hippocampal synaptic circuitry: MMP proteolysis during hippocampal development. *Journal of Comparative Neurology*, **522**(6), 1249–1263. doi:10.1002/cne.23468

Bagni, C., Tassone, F., Neri, G., & Hagerman, R. (2012). Fragile X syndrome: causes, diagnosis, mechanisms, and therapeutics. *Journal of Clinical Investigation*, **122**(12), 4314–4322. doi:10.1172/JCI63141

Barkat, T. R., Polley, D. B., & Hensch, T. K. (2011). A critical period for auditory thalamocortical connectivity. *Nat Neurosci*, **14**(9), 1189–1194. doi:10.1038/nn.2882

Bear, M. F., Huber, K. M., & Warren, S. T. (2004). The mGluR theory of fragile X mental retardation. *Trends in Neurosciences*, **27**(7), 370–377. doi:10.1016/j.tins.2004.04.009

Benson, D. L., & Huntley, G. W. (2012). Building and remodeling synapses. *Hippocampus*, **22**(5), 954–968. doi:10.1002/hipo.20872

Berry-Kravis, E. (2002). Epilepsy in fragile X syndrome. *Developmental Medicine & Child Neurology*, **44**(11), 724–728.

Bilousova, T. V., Dansie, L., Ngo, M., Aye, J., Charles, J. R., Ethell, D. W., & Ethell, I.M. (2008). Minocycline promotes dendritic spine maturation and improves behavioral performance in the fragile X mouse model. *Journal of Medical Genetics*, **46**(2), 94–102. doi:10.1136/jmg.2008.061796

Bourne, J., & Harris, K. M. (2007). Do thin spines learn to be mushroom spines that remember? *Current Opinion in Neurobiology*, **17**(3), 381–386. doi:10.1016/j.conb.2007.04.009

Brown, W. T. (1990). The fragile X: progress toward solving the puzzle. *American Journal of Human Genetics*, **47**(2), 175.

Carrasco, M. M., Trujillo, M., & Razak, K. (2013). Development of response selectivity in the mouse auditory cortex. *Hearing Research*, **296**, 107–120. doi:10.1016/j.heares.2012.11.020

Chen, L., & Toth, M. (2001). Fragile X mice develop sensory hyperreactivity to auditory stimuli. *Neuroscience*, **103**(4), 1043–1050.

Comery, T. A., Harris, J. B., Willems, P. J., Oostra, B. A., Irwin, S. A., Weiler, I. J., & Greenough, W. T. (1997). Abnormal dendritic spines in fragile X knockout mice: maturation and pruning deficits. *Proceedings of the National Academy of Sciences*, **94**(10), 5401–5404.

Craig, A. M. (1998). Activity and synaptic receptor targeting: the long view. *Neuron*, **21**(3), 459–462.

Dansie, L. E., Phommahaxay, K., Okusanya, A. G., Uwadia, J., Huang, M., Rotschafer, S. E., … Ethell, I. M. (2013). Long-lasting effects of minocycline on behavior in

young but not adult Fragile X mice. *Neuroscience*, **246**, 186–198. doi:10.1016/j.neuroscience.2013.04.058

Darnell, J. C., Van Driesche, S. J., Zhang, C., Hung, K. Y. S., Mele, A., Fraser, C. E., … Darnell, R. B. (2011). FMRP stalls ribosomal translocation on mRNAs linked to synaptic function and autism. *Cell*, **146**(2), 247–261. doi:10.1016/j.cell.2011.06.013

Deng, P.-Y., Rotman, Z., Blundon, J. A., Cho, Y., Cui, J., Cavalli, V., … Klyachko, V.A. (2013). FMRP regulates neurotransmitter release and synaptic information transmission by modulating action potential duration via BK channels. *Neuron*, **77**(4), 696–711. doi:10.1016/j.neuron.2012.12.018

Deng, P.-Y., Sojka, D., & Klyachko, V. A. (2011). Abnormal presynaptic short-term plasticity and information processing in a mouse model of fragile X syndrome. *Journal of Neuroscience*, **31**(30), 10971–10982. doi:10.1523/JNEUROSCI.2021-11.2011

De Villers-Sidani, E., Chang, E. F., Bao, S., & Merzenich, M. M. (2007). Critical period window for spectral tuning defined in the primary auditory cortex (A1) in the rat. *Journal of Neuroscience*, **27**(1), 180–189. doi:10.1523/JNEUROSCI.3227-06.2007

Bear, M. F. (2007). Correction of fragile X syndrome in mice. *Neuron*, **56**(6), 955– 962. doi:10.1016/j.neuron.2007.12.001

Dziembowska, M., Pretto, D. I., Janusz, A., Kaczmarek, L., Leigh, M. J., Gabriel, N., … Tassone, F. (2013). High MMP-9 activity levels in fragile X syndrome are lowered by minocycline. *American Journal of Medical Genetics Part A*, **161**(8), 1897–1903. doi:10.1002/ajmg.a.36023

Dziembowska, M., & Wlodarczyk, J. (2012). MMP9: A novel function in synaptic plasticity. *The International Journal of Biochemistry & Cell Biology*, **44**(5), 709–713. doi:10.1016/j.biocel.2012.01.023

El Idrissi, A., Ding, X.-H., Scalia, J., Trenkner, E., Brown, W. T., & Dobkin, C. (2005). Decreased GABAA receptor expression in the seizure-prone fragile X mouse. *Neuroscience Letters*, **377**(3), 141–146. doi:10.1016/j.neulet.2004.11.087

Engineer, C. T., Centanni, T. M., Im, K. W., Rahebi, K. C., Buell, E. P., & Kilgard, M. P. (2014). Degraded speech sound processing in a rat model of fragile X syndrome. *Brain Research*, **1564**, 72–84. doi:10.1016/j.brainres.2014.03.049

Erickson, C. A., Mullett, J. E., & McDougle, C. J. (2010). Brief report: acamprosate in fragile X syndrome. *Journal of Autism and Developmental Disorders*, **40**(11), 1412– 1416. doi:10.1007/s10803-010-0988-9

Erickson, C. A., Ray, B., Maloney, B., Wink, L. K., Bowers, K., Schaefer, T. L., … Lahiri, D. K. (2014). Impact of acamprosate on plasma amyloid-β precursor protein in youth: A pilot analysis in fragile X syndrome-associated and idiopathic autism spectrum disorder suggests a pharmacodynamic protein marker. *Journal of Psychiatric Research*, **59**, 220–228. doi:10.1016/j.jpsychires.2014.07.011

Erickson, C. A., Wink, L. K., Ray, B., Early, M. C., Stiegelmeyer, E., Mathieu-Frasier, L., … McDougle, C. J. (2013). Impact of acamprosate on behavior and brain-derived neurotrophic factor: an open-label study in youth with fragile X syndrome. *Psychopharmacology*, **228**(1), 75–84. doi:10.1007/s00213-013-3022-z

Fagiolini, M. (2004). Specific GABAA circuits for visual cortical plasticity. *Science*, **303**(5664), 1681–1683. doi:10.1126/science.1091032

Fagiolini, M., & Hensch, T. (2000). Inhibitory threshold for critical-period activation in primary visual cortex. *Nature*, **404**(6774), 180–183.

Fernandez-Carvajal, I., Lopez Posadas, B., Pan, R., Raske, C., Hagerman, P. J., & Tassone, F. (2009). Expansion of an FMR1 grey-zone allele to a full mutation in two generations. *The Journal of Molecular Diagnostics*, **11**(4), 306–310. doi:10.2353/jmoldx.2009.080174

Fu, Y.-H., Kuhl, D. P. A., Pizzuti, A., Pieretti, M., Sutcliffe, J. S., Richards, S., … Caskey, C. T. (1991). Variation of the CGG repeat at the fragile X site results in genetic instability: Resolution of the Sherman paradox. *Cell*, **67**(6), 1047–1058. doi:10.1016/0092-8674(91)90283-5

Gabel, L. A. (2004). Visual experience regulates transient expression and dendritic localization of fragile X mental retardation protein. *Journal of Neuroscience*, **24**(47), 10579–10583. doi:10.1523/JNEUROSCI.2185-04.2004

Galvez, R., & Greenough, W. T. (2005). Sequence of abnormal dendritic spine development in primary somatosensory cortex of a mouse model of the fragile X mental retardation syndrome. *American Journal of Medical Genetics Part A*, **135A**(2), 155–160. doi:10.1002/ajmg.a.30709

Gupta, T., Syed, Y. M., Revis, A. A., Miller, S. A., Martinez, M., Cohn, K. A., … Rhodes, J. S. (2008). Acute effects of acamprosate and MPEP on ethanol drinking-

in-the-dark in male C57BL/6J Mice. *Alcoholism: Clinical and Experimental Research*. doi:10.1111/j.1530-0277.2008.00787.x

Harlow, E. G., Till, S. M., Russell, T. A., Wijetunge, L. S., Kind, P., & Contractor, A. (2010). Critical period plasticity is disrupted in the barrel cortex of Fmr1 knockout mice. *Neuron*, **65**(3), 385–398. doi:10.1016/j.neuron.2010.01.024

Harris, K. M. (1999). Structure, development, and plasticity of dendritic spines. *Current Opinion in Neurobiology*, **9**, 343–348.

Hazlett, H. C., Poe, M. D., Lightbody, A. A., Styner, M., MacFall, J. R., Reiss, A. L., & Piven, J. (2012). Trajectories of early brain volume development in fragile X syndrome and autism. *Journal of the American Academy of Child & Adolescent Psychiatry*, **51**(9), 921–933. doi:10.1016/j.jaac.2012.07.003

Hensch, T. K. (2004). Critical period regulation. *Annual Review of Neuroscience*, **27**(1), 549–579. doi:10.1146/annurev.neuro.27.070203.144327

Hensch, T. K. (2005). Critical period plasticity in local cortical circuits. *Nature Reviews Neuroscience*, **6**(11), 877–888. doi:10.1038/nrn1787

He, Q., Nomura, T., Xu, J., & Contractor, A. (2014). The developmental switch in GABA polarity is delayed in fragile X mice. *Journal of Neuroscience*, **34**(2), 446–450. doi:10.1523/JNEUROSCI.4447-13.2014

Higashimori, H., Morel, L., Huth, J., Lindemann, L., Dulla, C., Taylor, A., … Yang, Y. (2013). Astroglial FMRP-dependent translational down-regulation of mGluR5 underlies glutamate transporter GLT1 dysregulation in the fragile X mouse. *Human Molecular Genetics*, **22**(10), 2041–2054. doi:10.1093/hmg/ddt055

Hinton, D. J., Lee, M. R., Jacobson, T. L., Mishra, P. K., Frye, M. A., Mrazek, D. A., … Choi, D.-S. (2012). Ethanol withdrawal-induced brain metabolites and the pharmacological effects of acamprosate in mice lacking ENT1. *Neuropharmacology*, **62**(8), 2480–2488. doi:10.1016/j.neuropharm.2012.02.022

Hinton, V. J., Brown, W. T., Wisniewski, K., & Rudelli, R. D. (1991). Analysis of neocortex in three males with the fragile X syndrome. *American Journal of Medical Genetics*, **41**(3), 289–294. doi:10.1002/ajmg.1320410306

Huang, Z. J., Kirkwood, A., Pizzorusso, T., Porciatti, V., Morales, B., Bear, M. F., … Tonegawa, S. (1999). BDNF regulates the maturation of inhibition and the critical period of plasticity in mouse visual cortex. *Cell*, **98**(6), 739–755.

Insanally, M. N., Kover, H., Kim, H., & Bao, S. (2009). Feature-dependent sensitive periods in the development of complex sound representation. *Journal of Neuroscience*, **29**(17), 5456–5462. doi:10.1523/JNEUROSCI.5311-08.2009

Irwin, S. A., Idupulapati, M., Gilbert, M. E., Harris, J. B., Chakravarti, A. B., Rogers, E. J., … Greenough, W. T. (2002). Dendritic spine and dendritic field characteristics of layer V pyramidal neurons in the visual cortex of fragile-X knockout mice. *American Journal of Medical Genetics*, **111**(2), 140–146. doi:10.1002/ajmg.10500

Greenough, W. T. (2001). Abnormal dendritic spine characteristics in the temporal and visual cortices of patients with fragile-X syndrome: A quantitative examination. *American Journal of Medical Genetics*, **98**(2), 161–167. doi:10.1002/1096-8628(20010115)98:2<161::AID-AJMG1025>3.0.CO;2-B

Iwai, Y., Fagiolini, M., Obata, K., & Hensch, T. K. (2003). Rapid critical period induction by tonic inhibition in visual cortex. *The Journal of Neuroscience*, **23**(17), 6695–6702.

Janusz, A., Milek, J., Perycz, M., Pacini, L., Bagni, C., Kaczmarek, L., & Dziembowska, M. (2013). The fragile X mental retardation protein regulates matrix metalloproteinase 9 mRNA at synapses. *Journal of Neuroscience*, **33**(46), 18234–18241. doi:10.1523/JNEUROSCI.2207-13.2013

Kim, H., Gibboni, R., Kirkhart, C., & Bao, S. (2013). Impaired critical period plasticity in primary auditory cortex of fragile X model mice. *Journal of Neuroscience*, **33**(40), 15686–15692. doi:10.1523/JNEUROSCI.3246-12.2013

Kooy, F. R. (1996). Transgenic mouse model for the fragile X syndrome. *American Journal of Medical Genetics*, **64**, 241–245. doi:10.1002/(SICI)1096-8628(19960809)64:2<241::AID-AJMG1>3.0.CO;2-X

Largo, R. H., & Schinzel, A. (1985). Developmental and behavioural disturbances in 13 boys with fragile X syndrome. *European Journal of Pediatrics*, **143**(4), 269–275.

Larsen, P. H., Dasilva, A. G., Conant, K., & Yong, V. W. (2006). Myelin formation during development of the CNS is delayed in matrix metalloproteinase-9 and -12 null mice. *Journal of Neuroscience*, **26**(8), 2207–2214. doi:10.1523/JNEUROSCI.1880-05.2006

Lee, C. Z., Yao, J. S., Huang, Y., Zhai, W., Liu, W., Guglielmo, B. J., … Young, W. L. (2006). Dose–response effect of tetracyclines on cerebral matrix metalloproteinase-9 after vascular endothelial growth factor hyperstimulation. *Journal of Cerebral Blood Flow & Metabolism*, **26**(9), 1157–1164.

Lien, C.-C., & Jonas, P. (2003). Kv3 potassium conductance is necessary and kinetically optimized for high-frequency action potential generation in hippocampal interneurons. *The Journal of Neuroscience*, **23**(6), 2058–2068.

Lin, S., Wei, X., Bales, K. R., Paul, A. B. C., Ma, Z., Yan, G., … Du, Y. (2005). Minocycline blocks bilirubin neurotoxicity and prevents hyperbilirubinemia-induced cerebellar hypoplasia in the Gunn rat. *European Journal of Neuroscience*, **22**(1), 21– 27. doi:10.1111/j.1460-9568.2005.04182.x

Luzi, P., Abraham, R. M., Rafi, M. A., Curtis, M., Hooper, D. C., & Wenger, D. A. (2009). Effects of treatments on inflammatory and apoptotic markers in the CNS of mice with globoid cell leukodystrophy. *Brain Research*, **1300**, 146–158. doi:10.1016/j.brainres.2009.09.017

Majewska, A., & Sur, M. (2003). Motility of dendritic spines in visual cortex in vivo: changes during the critical period and effects of visual deprivation. *Proceedings of the National Academy of Sciences*, **100**(26), 16024–16029.

McKay, S. M., & Oleskevich, S. (2007). The role of spontaneous activity in development of the endbulb of Held synapse. *Hearing Research*, **230**(1-2), 53–63. doi:10.1016/j.heares.2007.05.006

Michaluk, P., Mikasova, L., Groc, L., Frischknecht, R., Choquet, D., & Kaczmarek, L. (2009). Matrix metalloproteinase-9 controls NMDA receptor surface diffusion through integrin 1 signaling. *Journal of Neuroscience*, **29**(18), 6007–6012. doi:10.1523/JNEUROSCI.5346-08.2009

Michaluk, P., Wawrzyniak, M., Alot, P., Szczot, M., Wyrembek, P., Mercik, K., … Wlodarczyk, J. (2011). Influence of matrix metalloproteinase MMP-9 on dendritic spine morphology. *Journal of Cell Science*, **124**(19), 3369–3380. doi:10.1242/jcs.090852

Miller, L. J., McIntosh, D. N., McGrath, J., Shyu, V., Lampe, M., Taylor, A. K., … others. (1999). Electrodermal responses to sensory stimuli in individuals with fragile X syndrome: a preliminary report. *American Journal of Medical Genetics*, **83**(4), 268–279.

Morell, P., Greenfield, S., Costantino-Ceccarini, E., & Wisniewski, H. (1972). Changes in the protein composition of mouse brain myelin during development. *Journal of Neurochemistry*, **19**(11), 2545–2554.

Moyner, H., Burnashev, N., Laurie, D., Sakmann, B., & Seeburg, P. (1994). Developmental and regional expression in the rat brain and functional properties of four NMDA receptors. *Neuron*, **12**, 529–540.

Musumeci, S. A., Calabrese, G., Bonaccorso, C. M., D'Antoni, S., Brouwer, J. R., Bakker, C. E., … Catania, M. V. (2007). Audiogenic seizure susceptibility is reduced in fragile X knockout mice after introduction of FMR1 transgenes. *Experimental Neurology*, **203**(1), 233–240. doi:10.1016/j.expneurol.2006.08.007

Musumeci, S. A., Hagerman, R. J., Ferri, R., Bosco, P., Bernardina, B. D., Tassinari, C. A., … Elia, M. (1999). Epilepsy and EEG findings in males with fragile X syndrome. *Epilepsia*, **40**(8), 1092–1099.

Musumeci, S. A., Bosco, P., Calabrese, G., Bakker, C. E., De Sarro, G., Ferri, R., & Oostra, B. A. (2000). Audiogenic seizures susceptibility in transgenic mice with fragile X syndrome. *Epilepsia*, **41**(1), 19–23.

Nase, G., Weishaupt, J., Stern, P., Singer, W., & Monyer, H. (1999). Genetic and epigenetic regulation of NMDA receptor expression in the rat visual cortex. *European Journal of Neuroscience*, **11**(12), 4320–4326.

Nimchinsky, E. A., Oberlander, A. M., & Svoboda, K. (2001). Abnormal development of dendritic spines inFMR1 knock-out mice. *The Journal of Neuroscience*, **21**(14), 5139–5146.

Oliveira-Silva, P., Jurgilas, P. B., Trindade, P., Campello-Costa, P., Perales, J., Savino, W., & Serfaty, C. A. (2007). Matrix metalloproteinase-9 is involved in the development and plasticity of retinotectal projections in rats. *Neuroimmunomodulation*, **14**(3-4), 144–149. doi:10.1159/000110638

Pacey, L. K. K., Heximer, S. P., & Hampson, D. R. (2009). Increased GABAB receptor-mediated signaling reduces the susceptibility of fragile X knockout mice to audiogenic seizures. *Molecular Pharmacology*, **76**(1), 18–24. doi:10.1124/mol.109.056127

Pacey, L. K. K., Xuan, I. C. Y., Guan, S., Sussman, D., Henkelman, R. M., Chen, Y., … Hampson, D. R. (2013). Delayed myelination in a mouse model of fragile X syndrome. *Human Molecular Genetics*, **22**(19), 3920–3930. doi:10.1093/hmg/ddt246

Reinhard, S. M., Razak, K., & Ethell, I. M. (2015). A delicate balance: role of MMP-9 in brain development and pathophysiology of neurodevelopmental disorders. *Frontiers in Cellular Neuroscience,* **9**. https://doi.org/10.3389/fncel.2015.00280

Reiss, A. L., Lee, J., & Freund, L. (1994). Neuroanatomy of fragile X syndrome The temporal lobe. *Neurology*, **44**(7), 1317–1317.

Roberts, J. E., Mirrett, P., & Burchinal, M. (2001). Receptive and expressive communication development of young males with fragile X syndrome. *Journal Information*, **106**(3).

Rojas, D. C., Benkers, T. L., Rogers, S. J., Teale, P. D., Reite, M. L., & Hagerman, R. J. (2001). Auditory evoked magnetic fields in adults with fragile X syndrome. *NeuroReport*, **12**(11).

Rossetti, F., Rodrigues, M. C. A., Oliveira, J. A. C. de, & Garcia-Cairasco, N. (2006). EEG wavelet analyses of the striatum–substantia nigra pars reticulata–superior colliculus circuitry: Audiogenic seizures and anticonvulsant drug administration in Wistar audiogenic rats (War strain). *Epilepsy Research*, **72**(2-3), 192–208. doi:10.1016/j.eplepsyres.2006.08.001

Rotschafer, S. E., & Razak, K. A. (2014). Auditory processing in fragile X syndrome. *Frontiers in Cellular Neuroscience*, **8**. doi:10.3389/fncel.2014.00019

Rotschafer, S. E., Trujillo, M. S., Dansie, L. E., Ethell, I. M., & Razak, K. A. (2012). Minocycline treatment reverses ultrasonic vocalization production deficit in a mouse model of fragile X syndrome. *Brain Research*, **1439**, 7–14. doi:10.1016/j.brainres.2011.12.041

Rotschafer, S., & Razak, K. (2013). Altered auditory processing in a mouse model of fragile X syndrome. *Brain Research*, **1506,** 12–24. doi:10.1016/j.brainres.2013.02.038

Rudelli, R. D., Brown, W. T., Wisniewski, K., Jenkins, E. C., Laure-Kamionowska, M., Connell, F., & Wisniewski, H. M. (1985). Adult fragile X syndrome. *Acta Neuropathologica*, **67**(3-4), 289–295.

Sabaratnam, M., Vroegop, P. ., & Gangadharan, S. . (2001). Epilepsy and EEG findings in 18 males with fragile X syndrome. *Seizure*, **10**(1), 60–63. doi:10.1053/seiz.2000.0492

Saghatelyan, A. (2001). Reduced perisomatic inhibition, increased excitatory transmission, and impaired long-term potentiation in mice deficient for the extracellular matrix glycoprotein tenascin-R. *Molecular and Cellular Neuroscience*, **17**(1), 226–240. doi:10.1006/mcne.2000.0922

Santoro, M. R., Bray, S. M., & Warren, S. T. (2012). Molecular mechanisms of fragile X syndrome: A twenty-year perspective. *Annual Review of Pathology: Mechanisms of Disease*, **7**(1), 219–245. doi:10.1146/annurev-pathol-011811-132457

Schneider, A., Leigh, M. J., Adams, P., Nanakul, R., Chechi, T., Olichney, J., … Hessl, D. (2013). Electrocortical changes associated with minocycline treatment in fragile X syndrome. *Journal of Psychopharmacology*, **27**(10), 956–963. doi:10.1177/0269881113494105

Selby, L., Zhang, C., & Sun, Q.-Q. (2007). Major defects in neocortical GABAergic inhibitory circuits in mice lacking the fragile X mental retardation protein. *Neuroscience Letters*, **412**(3), 227–232. doi:10.1016/j.neulet.2006.11.062

Sidhu, H., Dansie, L. E., Hickmott, P. W., Ethell, D. W., & Ethell, I. M. (2014). Genetic removal of matrix metalloproteinase 9 Rescues the symptoms of fragile X Syndrome in a Mouse Model. *Journal of Neuroscience*, **34**(30), 9867–9879. doi:10.1523/JNEUROSCI.1162-14.2014

Spolidoro, M., Putignano, E., Munafo, C., Maffei, L., & Pizzorusso, T. (2012). Inhibition of matrix metalloproteinases prevents the potentiation of nondeprived-eye responses after monocular deprivation in juvenile rats. *Cerebral Cortex*, **22(**3), 725–734. doi:10.1093/cercor/bhr158

St Clair, D., Blackwood, D.H.R., Oliver, C., & Dickens, P. (1987). P3 abnormality in fragile X syndrome. *Biological Psychiatry*, **22**, 303–312.

Strumbos, J. G., Brown, M. R., Kronengold, J., Polley, D. B., & Kaczmarek, L. K. (2010). Fragile X mental retardation protein is required for rapid experience-dependent regulation of the potassium channel Kv3.1b. *Journal of Neuroscience*, **30**(31), 10263–10271. doi:10.1523/JNEUROSCI.1125-10.2010

The Dutch-Belgian Fragile X Consorthium, Bakker, C. E., Verheij, C., Willemsen, R., van der Helm, R., Oerlemans, F., … Willems, P. J. (1994). Fmr1 knockout mice: A model to study fragile X mental retardation. *Cell*, **78**(1), 23–33. doi:10.1016/0092-8674(94)90569-X

Tian, L., Stefanidakis, M., Ning, L., Van Lint, P., Nyman-Huttunen, H., Libert, C., … Gahmberg, C. G. (2007). Activation of NMDA receptors promotes dendritic spine development through MMP-mediated ICAM-5 cleavage. *The Journal of Cell Biology*, **178**(4), 687–700. doi:10.1083/jcb.200612097

Till, S. M., Wijetunge, L. S., Seidel, V. G., Harlow, E., Wright, A. K., Bagni, C., … Kind, P. C. (2012). Altered maturation of the primary somatosensory cortex in a mouse model of fragile X syndrome. *Human Molecular Genetics*, **21**(10), 2143–2156. doi:10.1093/hmg/dds030

Tovar, K., & Westbrook, G. (1999). The incorporation of NMDA receptors with a distinct subunit composition at nascent hippocampal synapses in vitro. *The Journal of Neuroscience*, **19**(10), 4180–4188.

Tritsch, N. X., Rodríguez-Contreras, A., Crins, T. T. H., Wang, H. C., Borst, J. G. G., & Bergles, D. E. (2010). Calcium action potentials in hair cells pattern auditory neuron activity before hearing onset. *Nature Neuroscience*, **13**(9), 1050–1052. doi:10.1038/nn.2604

Tritsch, N. X., Yi, E., Gale, J. E., Glowatzki, E., & Bergles, D. E. (2007). The origin of spontaneous activity in the developing auditory system. *Nature*, **450**(7166), 50–55. doi:10.1038/nature06233

Vaillant, C., Didier-Bazès, M., Hutter, A., Belin, M.-F., & Thomasset, N. (1999). Spatiotemporal expression patterns of metalloproteinases and their inhibitors in the postnatal developing rat cerebellum. *The Journal of Neuroscience*, **19**(12), 4994–5004.

Vaillant, C., Meissirel, C., Mutin, M., Belin, M.-F., Lund, L., & Thomasset, N. (2003). MMP-9 deficiency affects axonal outgrowth, migration, and apoptosis in the developing cerebellum. *Molecular and Cellular Neuroscience*, **24**(2), 395–408. doi:10.1016/S1044-7431(03)00196-9

Van der Molen, M. J. W., Van der Molen, M. W., Ridderinkhof, K. R., Hamel, B. C. J., Curfs, L. M. G., & Ramakers, G. J. A. (2012). Auditory change detection in fragile X syndrome males: A brain potential study. *Clinical Neurophysiology*, **123**(7), 1309–1318. doi:10.1016/j.clinph.2011.11.039

Verkerk, A. J. M. H., Pieretti, M., Sutcliffe, J. S., Fu, Y.-H., Kuhl, D. P. A., Pizzuti, A., … Warren, S. T. (1991). Identification of a gene (FMR-1) containing a CGG repeat coincident with a breakpoint cluster region exhibiting length variation in fragile X syndrome. *Cell*, **65**(5), 905–914. doi:10.1016/0092-8674(91)90397-H

Wang, X., Bozdagi, O., Nikitczuk, J. S., Zhai, Z. W., Zhou, Q., & Huntley, G. W. (2008). Extracellular proteolysis by matrix metalloproteinase-9 drives dendritic spine enlargement and long-term potentiation coordinately. *Proceedings of the National Academy of Sciences*, **105**(49), 19520–19525.

Wassink, T. H., Piven, J., & Patil, S. R. (2001). Chromosomal abnormalities in a clinic sample of individuals with autistic disorder. *Psychiatric Genetics*, **11**(2), 57–63.

Weiler, I. J., Irwin, S. A., Klintsova, A. Y., Spencer, C. M., Brazelton, A. D., Miyashiro, K., … Greenough, W. T. (1997). Fragile X mental retardation protein is translated near synapses in response to neurotransmitter activation. *Proceedings of the National Academy of Sciences*, **94**(10), 5395–5400.

Wen, T. H., Afroz, S., Reinhard, S. M., Palacios, A. R., Tapia, K., Binder, D. K., … Ethell, I. M. (2018). Genetic Reduction of Matrix Metalloproteinase-9 Promotes Formation of Perineuronal Nets Around Parvalbumin-Expressing Interneurons and Normalizes Auditory Cortex Responses in Developing Fmr1 Knock-Out Mice. *Cerebral Cortex*, **28**(11), 3951–3964. https://doi.org/10.1093/cercor/bhx258

Wilczynski, G. M., Konopacki, F. A., Wilczek, E., Lasiecka, Z., Gorlewicz, A., Michaluk, P., … Kaczmarek, L. (2008). Important role of matrix metalloproteinase 9 in epileptogenesis. *The Journal of Cell Biology*, **180**(5), 1021–1035. doi:10.1083/jcb.200708213

Williams, S. H. (2005). Medications for treating alcohol dependence. *Am Fam Physician*,**72**(9), 1775–80.

Wisniewski, K. E., Segan, S. M., Miezejeski, C. M., Sersen, E. A., & Rudelli, R. D. (1991). The Fra (X) syndrome: neurological, electrophysiological, and neuropathological abnormalities. *American Journal of Medical Genetics*, **38**(2-3), 476–480.

Wright, J. W., Kramár, E. A., Meighan, S. E., & Harding, J. W. (2002). Extracellular matrix molecules, long-term potentiation, memory consolidation and the brain angiotensin system. *Peptides*, **23**(1), 221–246.

Yan, Q. J., Asafo-Adjei, P. K., Arnold, H. M., Brown, R. E., & Bauchwitz, R. P. (2004). A phenotypic and molecular characterization of the fmr1-tm1Cgr fragile X mouse. *Genes, Brain and Behavior*, **3**(6), 337–359. doi:10.1111/j.1601-183X.2004.00087.x

Zheng, Q. Y., Johnson, K. R., & Erway, L. C. (1999). Assessment of hearing in 80 inbred strains of mice by ABR threshold analyses. *Hearing Research*, **130**(1), 94–107.

Chapter 3:

Reduced Perineuronal Net Expression in *Fmr1* KO mice is linked to Impaired Fear-Associated Memory

Abstract

Fragile X syndrome (FXS) is a leading cause of heritable intellectual disability and monogenic autism. Among many symptoms, humans with FXS show debilitating anxiety, sensory hypersensitivity and impaired learning. The sensory deficits and increased anxiety may underlie impaired learning, in particular emotion-related memory formation that can be studied using auditory fear conditioning protocol in the *fmr1* KO mice, an animal model of FXS. Our previous study reported that auditory hypersensitivity in *fmr1* KO mice was linked to impaired development of parvalbumin (PV) positive interneurons and perineuronal nets (PNN) in the auditory cortex. It is not clear if these deficits continue into adulthood and whether they have implications for learning and memory in *fmr1* KO mice. In this study, we examined if learning-induced changes in PV and PNN expression are impaired in the fear conditioning circuit of *fmr1* KO mice, focusing on the amygdala, hippocampus and auditory cortex. We found impaired tone-associated memory formation in *fmr1* KO mice after fear conditioning. This was paralleled by reduced PNN density in the amygdala and auditory cortex of *fmr1* KO mice in all conditions, as well as reduced PNN intensity in CA2 hippocampus. There was also a positive correlation between tone-associated memory and PNN density in the amygdala and auditory cortex but not in CA2, consistent with a tone-association deficit. We further found impaired learning-associated regulation of PNNs but not PV expression in the superficial layers of auditory cortex in *fmr1* KO mice. PV positive cell density decreased in the auditory cortex in response to fear conditioning in both WT and *fmr1* KO mice. However, learning-induced increase of PV expression in the CA3 hippocampus

was only observed in WT mice. Altogether our studies suggest a possible link between impaired PV and PNN expression within the fear conditioning circuit and impaired tone memory formation in *fmr1* KO mice after fear conditioning.

Abbreviations:

Auditory cortex (AC), Basolateral amygdala (BLA), Fear conditioning (FC), Fragile X syndrome (FXS), Lateral amygdala (LA), Matrix metalloproteinase-9 (MMP-9), Parvalbumin (PV), Perineuronal nets (PNN)

1. Introduction

While fear-associative memory formation is important for survival, the inappropriate activation of fear-associative circuits in humans can become an impediment to daily function, causing arousal, anxiety and aversion to stimuli that are not threatening. Behavioral tools that include fear conditioning paradigms have long been useful in studying anxiety disorders. Indeed, people with anxiety show heightened fear responses (Duits et al., 2015; Lissek et al., 2005), and regions of the central nervous system (CNS) that are known to be active during fear conditioning paradigms (Andreatta et al., 2015; LaBar et al., 1998) show abnormal activation in people with anxiety disorders (reviewed in Shin and Liberzon, 2010). Many neurodevelopmental disorders share heightened anxiety as a core feature, including fragile X syndrome (FXS). FXS is the leading cause of heritable intellectual disability in males and one of the most prevalent monogenic causes of autism (reviewed in Hagerman and Hagerman, 2002; reviewed in Santoro, et al., 2012; reviewed in Yoo, 2015). It is caused by an increase in the number of CGG repeats that lead to hypermethylation of fragile X mental retardation gene-1 (*fmr1*) and a reduction of the protein product, FMRP. Symptoms of FXS include intellectual disabilities, attention deficits (Cornish et al., 2001), stereotyped behaviors and sensory processing deficits (Miller et al., 1999). In addition, individuals with FXS demonstrate anxiety-associated behaviors, which can manifest as aggression, social withdrawal and gaze aversion (Sullivan et al., 2007). High anxiety in FXS correlates with decreased activation of the amygdala, an important fear/emotion processing region of the CNS in FXS individuals (Kim et al., 2014; Hessl et al., 2007; Hessl et al., 2011).

Given the widespread reports of heightened anxiety in individuals with FXS (Bailey et al., 2008; Cordiero et al., 2011; Kim et al., 2014), it might be expected that altered anxiety related behaviors would be a consistent phenotype in FXS animal models. One commonly studied mouse model of FXS is generated by deletion of the *fmr1* gene (*fmr1* KO mouse; Bakker and Oostra, 2003; Kooy et al., 1996; Paradee et al., 1999) and recapitulates many phenotypes of FXS (Castren et al., 2003; reviewed in Dahlhaus, 2018; Dzeimbowska et al., 2013; Sidhu et al., 2014; Lovelace 2016) but behavioral reports on anxiety measures are mixed. In terms of classical fear conditioning, some groups have shown reduced fear memory in *fmr1* KO mice while others have shown no deficit (de Diego-Otero et al., 2009; Dobkin et al., 2000; Eadie et al., 2012; Oddi et al., 2015; Olmos-Serrano et al., 2011; Paradee et al., 1999; Peier et al., 2000; Romero-Zerbo et al., 2009; Spencer et al., 2006; Thomas et al., 2011; Van Dam et al., 2000). If we are to study the contribution of anxiety in FXS and whether treatment of anxiety alone may ameliorate additional FXS symptoms, consensus is needed on behavioral measures of anxiety-regulation in animal models, and on the nature of changes to CNS circuits involved in anxiety-related memory formation. Circuits involved in fear conditioning have discernable roles in acquisition and consolidation of specific components of a fear-associated memory and, as such, understanding potential deficits in fear-memory acquisition may elucidate key mechanisms underlying pathophysiology in FXS.

Major regions of the CNS involved in fear memory formation and consolidation include the amygdala (Raybuck and Lattal, 2011; Phillips and LeDoux, 1992; Quirk et al., 1997), hippocampus (Esclasasn et al. 2009; Lee and Kesner, 2004; Roy et al., 2017;

Daumas et al. 2005) and the sensory cortices, including the auditory cortex (Letzkus et al., 2011; Froemke et al. 2007; Antunes and Moita, 2010). Inhibitory neurons across these regions, particularly parvalbumin (PV) expressing cells, play a pivotal role in shaping the memory engram. Either through direct perisomal inhibition of excitatory neurons (Trouche et al., 2013) or through local disinhibitory microcircuits (Lettzkus et al. 2011; Wolff et al., 2014; Courtin et al., 2014), PV cells control the activation of specific populations of excitatory cells during the acquisition or consolidation of a fear memory. Perturbing the function of PV cells can alter the formation of a fear memory (Ognjanovski et al., 2017; Morrison et al. 2016). Conversely increasing PV cell activity can increase the persistence of a fear memory (Caliskan et. al, 2016).

Similarly, perineuronal nets (PNN), which are specialized assemblies of extracellular matrix, play an important role in learning and memory circuits. PNNs form around the cell bodies and proximal dendrites of both excitatory and inhibitory cells. In particular, PNNs ensheath a large percentage of PV cells (Dityatev et al., 2006; McRae et al., 2007; Lee et al., 2012; Ueno et al., 2018) and may shape the firing properties of these cells (Balmer, 2016; Dityatev et al., 2006; Favuzzi et al., 2017). These structures are thought to act as a "brake" on formation of new synaptic contacts (Carstens et al., 2016; Gogolla et al., 2009) or stabilization of existing synapses. While reorganization of PNNs is necessary for new long-term memory formation (Xue et al., 2014; Happel et al. 2014) and/or consolidation after fear conditioning (Banerjee et al., 2017; Hylin et al., 2013),

PNNs also preserve fear-associated memories over time (Gogolla et al., 2009) and disruption of PNNs impairs fear memory acquisition (Hylin et al. 2014; Banerjee et al., 2017).

Multiple studies have shown altered inhibitory cell function in the *fmr1* KO mice, particularly PV cells (Selby et al., 2007; Patel et al., 2013; Gibson et al., 2008; Olmos-Serrano et al., 2010; Martin et al., 2014; Wen et al., 2018a). Abnormal PNN development is also associated with several neurological conditions, including FXS (reviewed in Wen et al., 2018b). But, the extent to which PNN is abnormal in fear-associated circuitry in FXS, or how fear conditioning changes PV and PNN expression in these circuits in FXS remains unknown. Any abnormal changes in PV and PNN expression in regions important for fear memory formation may underlie impaired fear conditioning in *fmr1* KO mice. Therefore, in this study we examined changes in the expression of PV and PNN in WT and *fmr1* KO mouse auditory cortex, amygdala and hippocampus in response to fear conditioning.

2. Methods

2.1 Mice

Breeding pairs of FVB.129P2-Pde6b^{+}Tyr$^{c\text{-}ch}$ Fmr1^{tm1Cgr}/J (Jax 004624; *Fmr1* KO) and their congenic controls FVB.129P2-Pde6b^{+}Tyr$^{c\text{-}ch}$/AntJ controls (Jax 002848; WT) were obtained from the Jackson Laboratory and housed in an accredited vivarium on a 12-hlight/dark cycle. Food and water were provided *ad libitum* and confirmation of genotypes was conducted using PCR analysis of genomic DNA isolated from tail clippings. University of California, Riverside's Institutional Animal Care and Use

Committee approved all procedures used. Experiments were conducted in accordance with NIH *Guide for the Care and Use of Laboratory Animals.* The total number of mice used for behavior tests was: WT Naïve = 24, WT Fear Conditioned = 32; *fmr1* KO Naïve =22, *fmr1* KO Fear Conditioned = 26. From these, 10-11 mice per group were used for immunohistochemistry. Naïve conditioned mice (N) underwent all handling/habituation/training and recall but without the shock (tone was still played). Fear conditioned mice (FC) underwent all procedures including the tone/shock pairing during training. An additional 7 WT mice and 6 *fmr1* KO mice, which we reference as control mice (C), were those raised in the vivarium and tested without any exposure to the fear conditioning arena. All mice used were 2-4 month old males.

2.2 Fear Conditioning

Mice were handled in the training room for 5 days prior to training, with ~2 minutes of handling per day for each mouse. Mice were acclimated to the training room for at least 30min daily before any testing/handling took place.

Day 1: One day prior to training, mice were habituated to the training and recall contexts (context A and context B) for 10min each. Context A is the training context, where mice receive a shock (unconditioned stimulus; US) paired with a tone (conditioned stimulus; CS), and are retested 24 h later for context recall. Context A is a square arena with metal walls and metal grid bars on the floors; it has white lighting and is scented with Quatricide. Context B is where mice undergo tone recall; this is a square arena with checker-patterned walls, inside of which is placed a circular glass arena that has bedding on the floors; it has yellow lighting and is scented with Windex. The combination of

different tactile, visual and olfactory information was to ensure that mice do not generalize from training in context A to tone recall testing in context B. The arena was cleaned after each mouse, using: (context A) 70% ethanol, Quatircide, and DiI water followed by a further spray of Quatricide; or (context B) 70% ethanol, Windex and DiI water, followed by a further spray of Windex.

Day 2: Training in context A occurred 24 h after habituation. Mice had a period of 3min of silence after being placed in context A, followed by 5 CS-US pairings (30 s tone, 9 kHz, 78-80 dB; co-terminating with a scrambled footshock, 2 s, 0.6 mA). The interval between tone-shock pairings was pseudo-random (60-120 s) to avoid an association with the delay interval between tones.

Day 3: 24 h after fear conditioning, mice were tested for their recall of the context- and tone- associated fear memories. This included, in context B, a baseline measurement of normal activity levels and then tone recall (baseline: 3 min of silence; tone recall: 3 min with tone), and in context A, context recall as well as context + tone recall (context recall: 3 min of silence; context + tone: 3 min with tone). The order that recall was tested (context then tone recall vs. tone then context recall) was counterbalanced between mice, with at least 1 h between each recall test. Mice used for further tissue processing had 3h and 30min between the first and second contexts and were perfused 30 min after the last recall. Modification of PNNs can occur within 4 h of a training event, so this timing was planned to control for any modification of the circuit after re-exposure to fear-associated cues without the shock reinforcement (Banerjee et al., 2017). Two control groups were included, 1) control mice taken directly from their home cage in the vivarium and

immediately perfused; 2) naïve mice that underwent an identical protocol as conditioned mice except without the footshock at the end of the tone. The experimenter was blinded to the genotype of mice throughout training, and blind to the condition (naïve or FC) except on training day. Mice were trained and tested in a pseudo random order when possible to avoid order effects.

Statistics. Freezing was measured using Freezeframe software (Colbourn Instruments, Holliston, MA, USA), with a threshold of 1s for determining "freezing" behavior. Videos were further manually checked to determine whether the software measurement of "freezing" behavior was consistent with observed freezing behavior. Three-way or two-way ANOVA was used as appropriate with Bonferroni-corrected paired comparisons. An unpaired t-test was used to compare freezing during habituation. Statistical analysis was performed using Graphpad Prism 6 or SPSS.

2.3 Analysis of Additional Behaviors in Fear Conditioned Mice

To further understand the behavioral response characteristics of *fmr1* KO mice after fear conditioning, videos from a subset of mice were manually scored, using six categories of mouse behaviors which were based on studies of elevated plus maze and adapted for our purposes (Table 3.1). Videos were scored at 10 second intervals during: 1) baseline (context B; 3 min; silence), 2) tone recall (context B; 3 min; tone), 3) context recall (context A; 3 min; silence) and 4) context + tone recall (context A; 3 min; tone) using 9-11 mice per group (WT, *fmr1* KO; N, FC). Definitions for visual scoring are provided in Table 3.1 and are based on previous studies (Coimbra et al., 2017; Cruz et al., 1994; Rodgers & Johnson, 1995). At every interval, the recording was paused and the

observer noted which behavior was in progress according to the parameters established (Table 3.1). The percentage of total observations was calculated (18 observations for each 3 min recall session) of a behavior and analyzed with a two-way RM ANOVA for each recall session separately.

Table 3.1. Definitions of Ethnologic Mouse Behavior for Scoring

Behavior	Definition	References
Immobility	Complete stillness without head and body movement	[Shin & Liberzon, 2010]
Scanning	Head orienting, sniffing, air sampling, without body movement	[Coimbra et al., 2017]
Stretch Attend Posture (SAP)	Forward elongation of the body followed by retreat to the original position or pivoting within a circle	[Coimbra et al., 2017]
Self-Grooming	Species-typical sequence that begins with grooming of the snout, progressing to the ears, and ending with whole body	[Kalueff et al., 2016]
Digging	Use of the paws to dig through bedding	[Silverman et al., 2010]
Rearing	Bipedal posture is supported with the hind paws	[Coimbra et al., 2017]
In Motion	Any action that incorporates both front and hind paws and allows for full-body movement within the chamber	[Bailey, 2009]

2.4 Immunocytochemistry and Image Analysis

Naïve and FC mice were sacrificed 30 minutes after the last recall test with isoflurane and perfused transcardially with cold phosphate-buffered saline (PBS, 0.1 M) and 4% paraformaldehyde (PFA). Control mice were perfused immediately after removal from their home cages. Brains were removed and post-fixed for 2-4 h in 4% PFA. 100 µm coronal sections were obtained using a vibratome (Campden Instruments 5100mz Ci). For each mouse, 3-5 slices containing auditory cortex (from bregma: -2.03mm to -2.53mm), dorsal hippocampus (-1.91 mm to -2.53mm) and amygdala (-1.91mm to -2.15mm; Allen Mouse Brain Atlas) were taken and processed for immunohistochemistry. Approximately the same rostral-caudal range of slices was used for each mouse. To determine whether the order of recall testing leads to differential PV and PNN modifications the order of recall testing was treated as two separate experiments (context-tone *or* tone-context)

5-6 mice per condition (2 treatments (N, FC) x 2 genotypes (WT, *fmr1* KO) were tested in each experiment (context-tone *or* tone-context). In order to control for differences in staining between rounds of IHC, one slice from each mouse within an experiment (20-22 mice, 1 slice each) was included in the 24 well plate, with additional 1-3 slices from control mice. This was repeated until 3-5 slices per mouse were stained and imaged. Control mouse data was combined from both experiments and presented with figures in text. For staining, slices were post-fixed for an additional 2 h in 4% PFA and then washed (3x, 10 min) in 0.1M PBS. Slices were then quenched with 50 mM ammonium chloride for 15 minutes and washed with PBS (3x, 10m). Next, brain tissue

was permeabilized with 0.1% triton-X in PBS. Afterwards non-specific staining was blocked with a 5% Normal Goat Serum (NGS) (Vector Laboratories) and 1% Bovine Serum Albumin (BSA) (Fisher Scientific) in 0.1M PBS solution. Slices were incubated overnight with primary antibody rabbit-anti parvalbumin (1:1000; SWANT PV25) and Wisteria floribunda agglutinin (WFA) in a 1% NGS, 0.5% BSA, and 0.1% tween solution. WFA (1:500; Vector Laboratories; Green Florescein Wisteria Floribunda Lectin FL 1351) is a lectin that binds to chondroitin sulfate proteoglycan glycosaminoglycan side chains, which make up perineuronal nets (Pizzorusso et al 2002). After overnight incubation with primary antibody and WFA at 4° C, slices were washed in 0.5% tween (3x, 10m) and incubated at room temperature with secondary antibodies in 0.1M PBS for 1 h. Secondary antibodies used were Alexa donkey-anti-rabbit 594 (1:500; Invitrogen). Finally, slices were washed with 0.5% tween (2x, 10m) and 0.1M PBS (1x, 10m), mounted in Vectashield with DAPI (Vector Labs), and cover-slipped with Cytoseal (ThermoScientific).

Slices were imaged using Leica SP5 confocal microscope (10x objective). Microscope settings were consistent across all images. Imaged Z-stacks covering 10 μm (1 μm step size) were acquired and then summed projections were created in ImageJ. ImageJ was used to count number of PNN positive cells, number of PV positive cells, and number of cells co-localized with PNN and PV by a blinded observer.

In hippocampus and auditory cortex, a fixed area was used for analysis across all images (see photomicrographs of Figures 3.1 - 2.4). For CA1, a 381x1000 μm^2 box was used for analysis, aligned with the superficial edge of dentate gyrus granule cell layer. In

CA2 a triangle radiating at a 45^{o} angle from the superficial edge of dentate gyrus (dimensions: 768 x 538 x 1015 μm) was used for analysis. CA3 analysis was within a freehand polygon shape (357,617 μm^2 area) beginning from the inferior edge of dentate gyrus taking care that CA2 and CA3 area did not overlap. For the dentate gyrus, a 520x1537 μm^2 box was used for analysis and cells from the tail end of CA3 within the box were excluded. A box of 500μm width and spanning from pia to white matter was used to analyze auditory cortex (AC). The layer specific counts in AC were determined based on a previously published study (Anderson et al., 2009), where 50% of the length between pia and white matter was used as the boundary between deep and superficial layers. A fixed area of analysis could not be used in the amygdala because the size of the structure varies from rostral to caudal slices. Therefore, a freehand tool was used to select amygdala. Lateral and basolateral amygdala were determined from the Allen Mouse Brain Atlas, visible landmarks and PV/PNN expression patterns. Two-way ANOVA was used to compare between genotype and condition for each brain region. Bonferroni correction was used for post-hoc analysis. When the initial ANOVA indicated an overall effect of conditioning, because there were 3 conditions (C, N and SE) it could not be determined which groups were different using our statistical package. Therefore, additional two-way ANOVAs were used to determine if the difference was between N and C, N and SE *or* C and SE mice. This was necessary for understanding the effects of fear conditioning independent of naïve conditioning, and will be noted as "2-Cond Test" in text. These values were only reported if they met the Bonferroni corrected significance value of (0.05/3 tests) $p = 0.0166$.

2.5 Correlation of freezing levels and cell counts

To better understand the relationship between the cell counts and the freezing behavior of mice, correlations were calculated between the freezing levels of each mouse (for context, tone and context + tone recall) and the observed density of PV cells, PNN cells and co-localized PV/PNN in different brain regions examined. All mice used for tissue processing were included in this analysis. WT and *fmr1* KO mice were first combined to assess overall correlation among all mice. Additionally, a regression curve and R-value for WT and *fmr1* KO groups was calculated separately, and the slopes and the R-values of each genotype were compared.

To test the null hypothesis that R-values are from the same population the following was used, where r is the R-value taken from the regression analysis:

1) Convert r values to r' : $r' = (0.5)\ln[\frac{1+r}{1-r}]$

2) Compute test statistic: $z = \frac{r'1 - r'2}{\sqrt{\frac{1}{n1-3}+\frac{1}{n2-3}}}$

To test the null hypothesis that the curve is the same for both WT and *fmr1* KO mice, the following statistic was used, where *b* is the slope (from regression analysis) and *S* is the error of the slope:

1) $Z = \frac{b1-b2}{S_{b1-b2}}$

2) To compute the error: $S_{b1-b2} = \sqrt{S_{b1}^2 + S_{b2}^2}$

2.6 Meta-Analysis of Fear Conditioning in *fmr1* KO Mice

Many studies have been conducted on fear conditioning in *Fmr1* KO mice, with varying results. As a way of testing for an overall consensus from these studies, a meta-analysis was conducted on contextual and tone fear memory in *fmr1* KO mice. To compile the data set, we searched published articles using PubMed and Google Scholar. Of note, in the FXS literature both null and significant results are often reported, as studies often test multiple behaviors to understand the effect of a treatment on an array of behaviors. The following criteria were used: 1) only mouse models of FXS were included; 2) studies using trace fear conditioning were excluded because this involves potentially different memory pathways; 3) studies using eye-blink or olfactory conditioning were excluded. Finally, studies that induced contextual fear without any auditory cue were included as well as studies with a tone-shock pairing, as in our own design.

Some features of these studies were similar due to standardized procedures (see Table 3.2). For instance, all studies used male mice only, and all mice were 2-4 months of age at testing. Other features vary among studies including the background strain (C57 and FVB), the intensity of shock (0.2 – 0.75 milliamps), and the number of shocks the mice received (ranging from 1-5 shocks). To address a possible effect of strain differences, a separate meta-analysis for each strain was conducted (included in supplemental), as well as all studies combined. Two of the published articles included in this analysis tested WT and *fmr1* KO mice using two separate strains of mice, and these were treated as independent studies because the same mice were not used twice.

Table 3.2. Summary of Studies in Meta Analysis

Authors	Protocol	Age	Sex	Strain	n	r effect size: Tone	r effect size: Context
Thomas et al., 2011	2x CS_US	2-4 m	Male	C57	46	0.15	0.09
				C57	38	0.16	0.16
Paradee et all, 1999	2x CS_US	70-100 d	Male	C57	36	0.35*	0.36*
Dobkin et al., 2000	3x CS_US	4m	Male	FVB	17	-0.23	0.21
				C57	19	-0.08	0.03
Van Dam et al., 2000	2x CS_US	2-3 m	Male	C57	34	0.30	0.18
Peier et al., 2000	2x CS_US	3-4 m	Male	C57	52	0.10	0.04
Olmos-Serrano et al., 2011	3x CS_US	3 m	Male	FVB	16	0.62*	0.06
Spencer et al., 2006	2x CS_US	8 w	Male	C57	20	-0.15	0.14
Diego-Otero t al., 2009	2x CS_US	60-120 d	Male	FVB	20	0.55*	0.43*
Romero-zerbo et al., 2008	1 CS_US	90-120 d	Male	FVB	22	0.42*	0.37
Oddi et al., 2015	5x US CTX	3 m	Male	FVB	13	n/a	0.60*
Eadie et al., 2010	1 US / 4 d	2–4 m	Male	C57	28	n/a	0.32

We calculated the correlation coefficient r as the effect size for each study (Hiller et al., 1999; Ambady and Rosenthal, 1993). The distribution of r as sampled from the population can become skewed, therefore to compare/combine effect sizes, the r was converted to the Fisher's z for all computations, which have a more normal distribution.

For each Fisher's z, results in opposite directions were noted with a positive/negative sign. For ease of interpretation, these values were converted back and reported as r effect size (Table 3.2). The average effect sizes of all studies was reported, using both an unweighted mean as well as a mean weighted based on the size of each study. We tested for heterogeneity of the effect sizes which yields a χ^2distribution. A 95% confidence interval was included for the r-effect size of the combined studies.

Statistical tests on the data were performed using the Stouffer's Z, which yield values distributed on a Z-scale (Rosenthal, 1991). To run these tests, the t-value and one-tailed p-value for each study were compiled, which values can be found based on the relationship, between t and F (t^2 = F). From the p-value, the corresponding Z-value was calculated making sure to denote results in opposite directions with a positive/negative sign. For studies that employed an omnibus F test with multiple degrees of freedom in the numerator, these first had to be converted to a 1 degree of freedom value. To do this, a set of contrast weights was designed testing the hypothesis of reduced freezing in *fmr1* KO mice. Using these weights an r-alerting was conducted (Rosnow et al., 2000). If the data in a given study are consistent with the hypothesized contrast weights it will yield a high r-alerting correlation value, and if it is not consistent it will yield a low r-alerting value. This value is transformed back into an F-test with 1 degree of freedom, and from this the corresponding one-tailed p-value was calculated. In addition to the Stouffer's Z, a t-test was also performed on the Z scores derived from the p-values.

3 Results

3.1 Mouse Behavior

3.1.1 Tone fear memory is impaired in *fmr1* KO mice

Mice were first habituated to each context. During habituation, WT and *fmr1* KO mice showed no difference in baseline activity levels (overall low freezing) in context A (WT: 6.912 ± 0.8020 %; *fmr1* KO: 5.665 ± 0.665%; $p = 0.250$). There was a difference in context B (WT: 1.884 ± 0.368%; *fmr1* KO: 0.6862 ± 0.156%; $p = 0.0046$) driven by almost no freezing in the majority of *fmr1* KO mice (Fig. 3.1B). During training, both groups showed an increase in freezing from the first CS-US pairing (WT: 4.672%; *fmr1* KO: 4.6725%) to the last CS-US pairing (WT: 74.21%; *fmr1* KO: 50.52%) indicating both WT and *fmr1* KO mice responded with increased freezing to the CS-US pairing ($p < 0.0001$). However, *fmr1* KO mice did not freeze to the level of WT mice (effect of genotype: $p < 0.0001$; Fig 3.1C). Though *fmr1* KO mice freeze less than the WT, they did significantly increase their freezing levels compared to naïve *fmr1* KOs by tone 4 and 5 (tone 4: FC *fmr1* KO: 42.10%; N *fmr1* KO: 13.52%; tone 5: FC *fmr1* KO: 50.52%: N *fmr1* KO: 13.98%; effect of conditioning: $p < 0.0001$) indicating they did respond to the training.

Mice were tested 24 h later for tone recall, context recall and context recall with the tone playing (context + tone), including a baseline freezing measurement. Significant differences in freezing levels were found between the different recall tests ($p < 0.0001$) as well as between genotypes ($p < 0.0001$) reflecting overall lower levels of freezing in *fmr1*

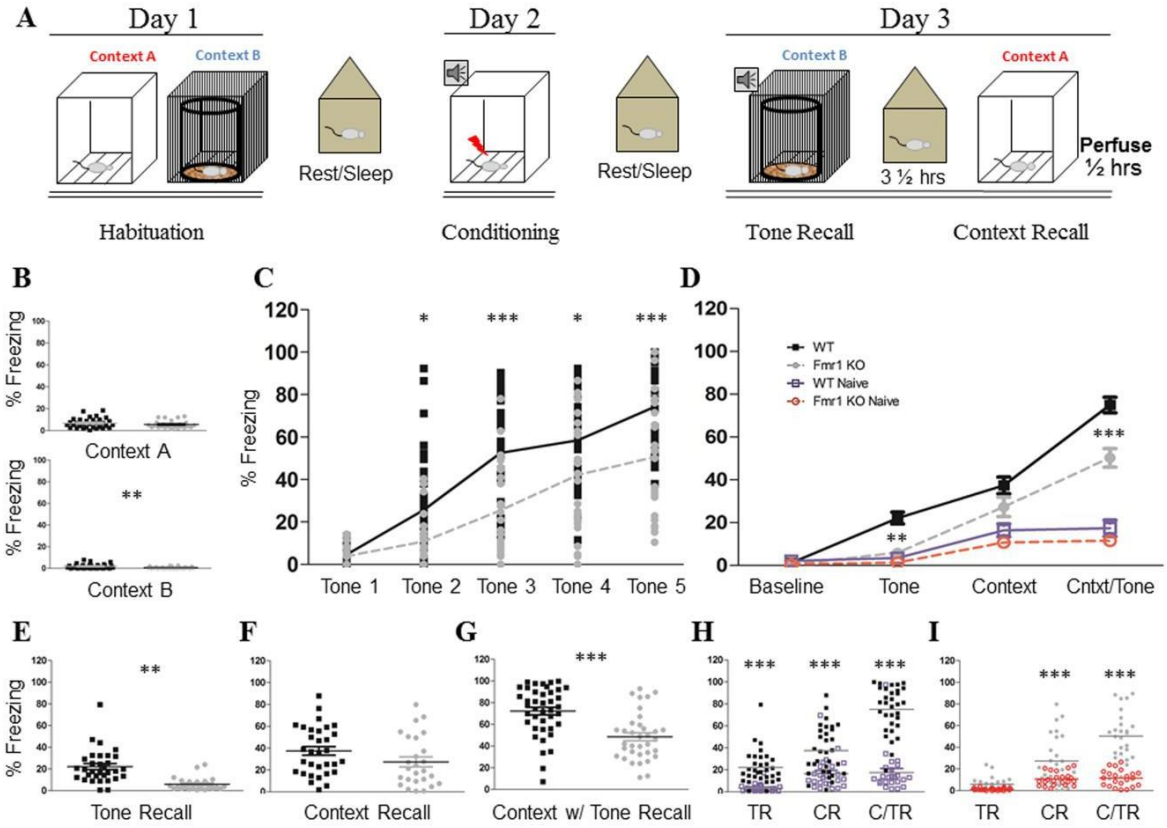

Figure 3.1. Impaired tone recall in *Fmr1* KO mice after fear conditioning. A) Schematic of training protocol: On day 1, mice were habituated to Context A and Context B for 10 min each. 24 hours later mice were trained with 5 tone-shock parings in Context A and returned to their home cage. Recall of the tone and context memories were tested 24 hours later with 3½ hours between tests. 30 min after the final recall session brain tissue was harvested. B) Habituation: All animals had low levels of freezing during habituation. C) During training both genotypes increased their freezing significantly across the training session when compared to naïve controls; however FC *fmr1* KO mice consistently froze at a lower level than FC WT mice. D) 24-hour Recall: *fmr1* KO mice had impaired freezing during tone recall and contextual +tone. (Individual data for each test is shown in E, F and G). H) FC WT mice froze more than N WT on all three recall tests; I) but FC *fmr1* KO mice increased freezing to context and context + tone recall only. C, D, H and I: asterisks indicate paired comparison difference in two-way RM ANOVA all others indicate difference from t-test (*, **, *** / p = 0.05, .01, 0.001). N: WT N = 24; WT FC = 32*; fmr1* KO N = 22; *fmr1* KO FC 26.

KO mice across all tests. There was also an effect of the training condition ($p < 0.0001$) indicating that FC mice froze at higher levels than N mice (Fig. 3.1D). An interaction between recall tests, training condition and genotype was also found ($p = 0.027$). Paired comparison revealed that baseline freezing (context B without a tone; Fig. 3.1D) was not different between FC WT (1.211%) and *fmr1* KO mice (0.53%; $p > 0.05$). During recall testing, *fmr1* KO mice showed a deficit in tone recall (WT: 22.20± 2.71%; *fmr1* KO: 5.913 ± 1.155%; $p < 0.01$; Fig. 3.1E) and a deficit in context + tone recall (WT: 75.00 ± 3.647%; *fmr1* KO: 50.31 ± 4.371%; $p < 0.001$; Fig. 3.1G), but with no significant difference when context recall was tested (WT: 37.48 ± 3.884%; *fmr1* KO: 27.39 ± 4.530%; $p = 0.0947$; Fig. 3.1F).

The similar levels of activity and/or freezing during baseline measurement suggest similar locomotor activity in both genotypes. However, many studies have found increased locomotor activity in *fmr1* KO mice (de Diego-Otero et al., 2009; Kramvis et al., 2013; Oddi et al., 2015; Olmos-Serrano et al., 2011. Thomas et al., 2011) and it remains possible that the consistently low freezing observed in *fmr1* KO mice may be partially due to increased locomotor activity or hyperactivity that affects automated freezing measurements. To further clarify whether this is the case, each FC genotype was compared to its own N controls on the 3 recall tests. If increased freezing is observed in FC mice compared to N mice, this is evidence of formation of a fear-associated memory, independent of genotype differences. As might be expected, WT FC mice increased their freezing significantly compared to WT N mice on tests of tone recall (FC: 22.20%; N: 3.510%; $p < 0.001$), context recall (FC: 37.48%; N: 16.46%; $p < 0.001$) and context +

tone (FC: 75.00%; N: 17.40%; $p < 0.001$; Fig. 3.1H). In contrast, FC *fmr1* KO mice were not different from N *fmr1* KO mice on the tone recall test (FC: 5.913%; N: 1.304%; $p > 0.05$) but displayed higher freezing during context recall (FC: 27.39%; N: 10.75%; $p < 0.001$) and in the context + tone recall (FC: 50.31%; N: 11.60%; $p < 0.001$; Fig. 3.1I). Baseline between N and FC mice was not different in either genotype (data not shown). This confirms that reduced freezing during tone recall in *fmr1* KO mice is independent of possible genotype specific locomotion/activity differences and likely reflects a deficit in tone-associated fear memory.

To eliminate the possibility that deficits in fear memory recall were due to impaired training in the *fmr1* KO mice, we re-ran our analysis to exclude all *fmr1* KO mice that did not train at least to WT levels by tone 5 of the training session. The lowest level of freezing among WT mice during tone 5 was 38%. Therefore, any *fmr1* KO mice that froze less than 38% during tone 5 were excluded for this analysis. Analysis showed that 14 mice froze at least to 38% by tone 5, out of the 24 total *fmr1* KO mice (Fig 3.2A). In this analysis, both WT and *fmr1* KO groups froze to comparable levels by tones 4 and 5 (WT: tone 4: 58.4%, tone 5: 74.21%; *fmr1* KO: tone 4: 54.03%, tone 5: 71.64%; paired comparison: *ns*). Nevertheless, 24 h after training, *fmr1* KO mice froze significantly less during the tone recall (WT: 22.2%, *fmr1* KO: 8.5%; $p < 0.01$) and context + tone (WT: 75%, *fmr1* KO: 51.7%; $p < 0.001$) recall tests (Fig. 3.2B) but not during context recall (WT: 37.5%, *fmr1* KO: 28.5%; $p = 0.2056$). Taken together, these analyses confirm deficits in tone and context + tone recall in *fmr1* KO mice independent of training differences between the genotypes.

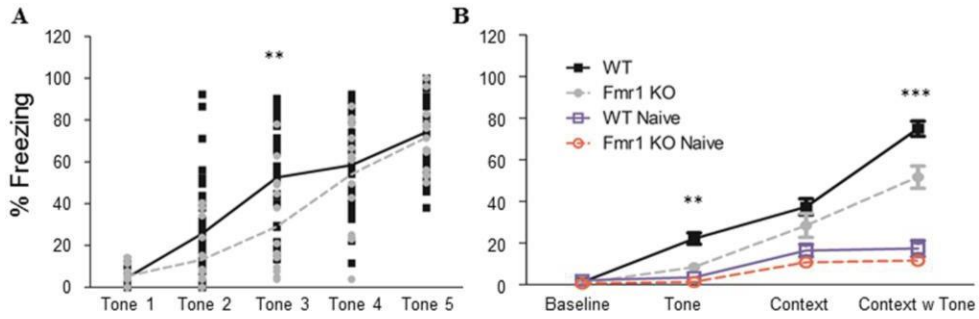

Figure 3.2: Deficit in *fmr1* KO mice remains even when low-freezers are excluded. A) In order to verify that *fmr1* KO deficit was not due to a deficit in training, all *fmr1* KO mice which froze below WT levels (below 38% during Tone 5) were excluded (N for mice included: WT FC: 32; *fmr1* KO FC: 14). By tones 4 and 5 all mice froze to comparable levels (WT: 58.4%, 74.21%, *fmr1* KO: 54.03%, 71.64%; *ns*). All mice increased their freezing across the training session (Training: $F(4) = 92.31$; $p < 0.0001$). There was a small genotype effect ($F(1)= 4.791$, $p = 0.034$) that was due to a difference in freezing during tone 3 (Tone 3: $p < 0.01$; Interaction $F(4)= 2.938$, $p = 0.022$). B) Although all mice included here trained to WT levels, still 24 hours after training *fmr1* KO mice froze significantly less during the tone recall ($p < 0.01$) and context-with-tone ($p < 0.001$) recall tests.

3.1.2 *Fmr1* KO mice show similar "exploratory" and "fear" behaviors as WT, but show impaired modification of behaviors after fear conditioning

In our previous analysis, we compared FC and N mice within each genotype to show that the *fmr1* KO mice do indeed freeze to a lower extent in the recall period. It remains possible that *fmr1* KO mice increase another type of "alerting" or "anxious-like" behavior in place of freezing. If this is the case, *fmr1* KO mice may actually consolidate fear-associated memories as well as WT mice but display this in a way that cannot be measured with standard software used to quantify freezing behavior. Therefore, a subset of videos, which were recorded during recall tests, was scored using 7 different observable and distinct behaviors (Table 3.1). Freezing, scanning and stretch-attend-posture (SAP) are behaviors associated with alerting or fear, whereas motion and rearing are associated with exploratory behavior (reviewed in: Blanchard et al., 2011; Coimbra et

al., 2017; Cruz et al., 1994; Rodgers & Johnson, 1995; reviewed in Roelofs, 2017). For context B, the mice had a layer of bedding on the bottom of the cage and so digging was included in the analysis. Grooming was also scored, but the levels of grooming were so low that these values were taken out of the final analysis. Because the "fear" behaviors and "exploratory" behaviors are potentially opposing types of behavior, they were analyzed separately (Fig. 3.3).

During the baseline period both WT and *fmr1* KO mice spend most of their time rearing or in motion (Rearing: WT N: 36.6%, *frm1* KO N: 38.8%, WT FC: 38.8%, *fmr1* KO FC: 31.3%; In motion: WT N: 28.3%, *fmr1* KO N: 37%, WT FC: 29.4%, *fmr1* KO FC: 32.2%; Fig. 3.3 row B) and very little time displaying "fear" behaviors. So in a context that has not been associated with shock, both genotypes show active exploration, even among those mice that underwent fear conditioning 24 h earlier.

During tone recall (Fig 3.3 row C), the WT mice significantly reduced their rearing (N: 31.1%, FC: 8.8%; $p < 0.001$) and motion (N: 33.3%, FC: 15%; $p < 0.001$) and increased scanning (N: 18.3%, FC: 35.5%; $p < 0.001$) and freezing behaviors (N: 5%, FC: 31.1%; $p < 0.001$). *Fmr1* KO mice behaved similarly, decreasing their rearing (N: 48.7%, 16.6%; $p < 0.001$) and increasing both freezing (N: 3%, FC: 16.1%, $p < 0.01$) and scanning (N: 11.7%, FC: 28.2%, $p < 0.001$), but their shifts in behavior were attenuated compared to WT mice. Consistent with the previous 'Freezeframe' analysis, *fmr1* KO mice froze significantly less than WT mice during tone recall (WT: 31.1%, *fmr1* KO: 16.1%, $p < 0.01$).

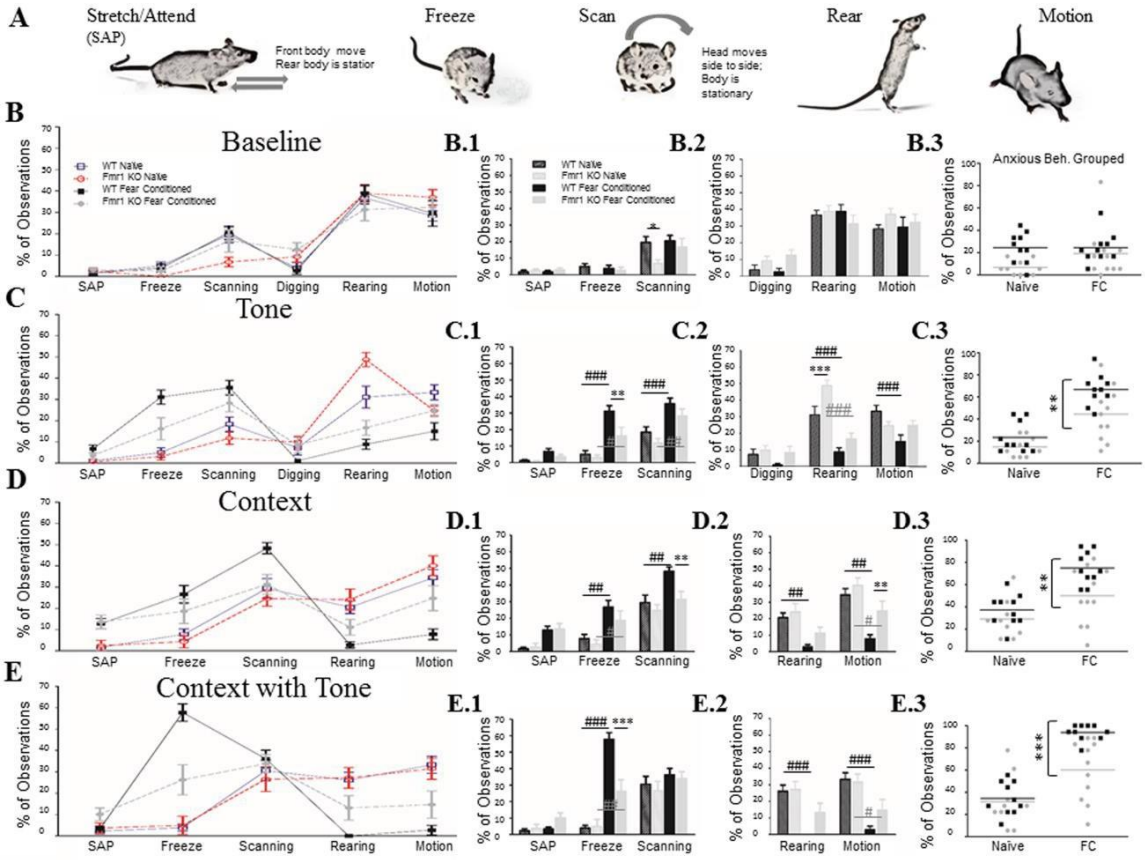

Figure 3.3: Manual analysis of characteristic mouse behaviors, confirms lower freezing and less alteration of baseline behaviors in *fmr1* KO mice. A) Characteristic mouse behaviors used for scoring recall tests. B) Baseline showed no overall difference in observed behaviors between WT and *fmr1* KO mice, either with "anxious-like" (B.1) or "non-anxious-like" (B.2) behaviors. C) During Tone recall, *fmr1* KO mice froze less than WT mice consistent with the computer-analyzed data. Both genotypes increased freezing after conditioning compared to control mice(C.1); both genotypes also increased their scanning after fear conditioning and decreased their rearing after fear conditioning (C.2). Only WT mice decreased their bouts of motion. D) During context recall both WT and *fmr1* KO mice increased their freezing after training, and decreased their motion; however only WT mice increased their scanning (D.1) and showed reduced rearing (D.2). Finally, during context + tone recall, both WT and *fmr1* KO increased their freezing after training, but *fmr*1 KOs froze significantly less than WTs (E.1). WT mice decreased their rearing and motion (E.2), whereas *fmr1* KO mice decreased their motion but not rearing. C.3/D.3/E.3) When both scanning and freezing are combined we see that *fmr1* KO mice show a deficit even in contextual recall. Within genotype effect of conditioning #, ##, ###; genotype effect *, **, *** (p = 0.05, 0.01, 0.001). N: WT Naïve = 10, WT FC = 10, *fmr1* KO Naïve = 9, *fmr1* KO FC = 11 .

During context recall (Fig 3.3, row D), WT mice again decreased their rearing (N: 20.5%, FC: 2.7%; $p < 0.01$) and motion (N: 34.4%, FC: 7.7%; $p < 0.001$) and increased freezing (N: 7.7%, FC: 26.6%; $p < 0.01$) and scanning (N: 29.4%, FC: 48.3%; $p < 0.01$). Again *fmr1* KO mice had a similar but attenuated shift, reducing their motion (N: 40.1%, FC: 24.7%; $p < 0.05$) and increasing freezing (N: 4.3%, FC: 18.6%; $p < 0.05$) with no change in rearing or scanning. In this recall session, *fmr1* KO mice scanned less than WT (WT: 48.3%; *fmr1* KO: 31.3%; $p < 0.01$) and displayed more motion (WT: 7.7%; *fmr1* KO: 24.7%; $p < 0.01$; Fig. 3.3 row D).

In context + tone test, (Fig. 3.3 row E), WT mice spend most of their time freezing (N: 3.8%, FC: 57.7%; $p < 0.001$), with no increase in scanning (N: 30.5%, FC: 36.1%; *ns*) and almost no time in motion or rearing. *Fmr1* KO mice did increase freezing (N: 4.9%, FC: 26.2%; $p < 0.01$) but froze significantly less than WT mice (WT: 57.7%, *fmr1* KO: 26.2%; $p < 0.001$; Fig. 3.3 row E), again supporting the previous analysis. There were very few observations of either SAP or digging in either genotype.

As mentioned above, *fmr1* KO mice showed appropriate behavioral shifts following conditioning, but their shifts in behavior were attenuated compared to WT mice. We quantified the attenuation by computing a difference score between baseline and recall scores for each mouse. The absolute value of the difference was used for further analysis, to account for the fact that freeze/scan/SAP behaviors typically have a positive difference while rearing/motion typically have a negative difference. When fear conditioned mice were analyzed in this way, it was confirmed that *fmr1* KO mice modify their behavior less during tone recall (effect of genotype: $F(1) = 6.58$, $p = 0.011$), during

context recall (effect of genotype: F(1) = 4.64, p = 0.033) and during context + tone (F(1) = 5.15, p = 0.025; Fig. 3.4).

Together, these data suggest that *fmr1* KO mice are not replacing immobility with another alerting or anxious-like behavior after fear conditioning. Instead both genotypes respond to fear conditioning with freezing and scanning behaviors during the recall tests, but the *fmr1* KO response is attenuated compared to WT mice. When the associative cues become more predictive of shock (context + tone), WT mice favor freezing behavior over all others. However, *fmr1* KO mice responded with a more distributed and attenuated set of behaviors.

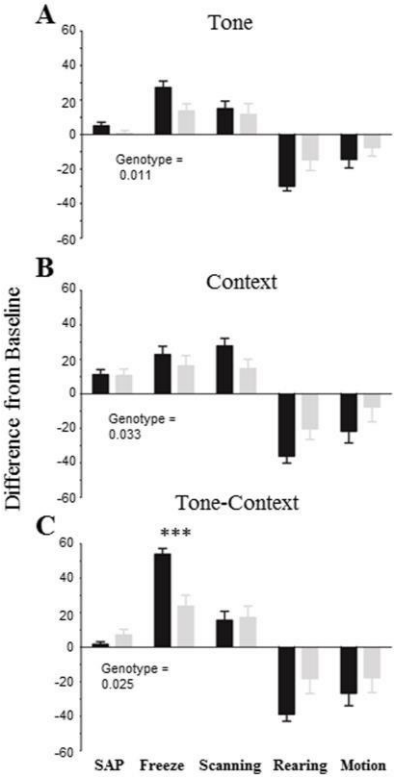

Figure 3.4. *Fmr1* KO mice have an attenuated shift their behavior during fear-recall tests. A difference score was computed between baseline measurements and recall tests. A) *Fmr1* KO mice had less of a shift in their behavior compared to baseline during tone recall F(1) = 6.58, (B) and during context recall F(1) = 4.64, (C) and during context with the tone F(1) = 5.15. Results are from a two-way ANOVA between behaviors and genotype, with Bonferroni corrected paired comparisons. Absolute values were used for statistical analysis. N: WT Naïve = 10, WT FC = 10, *fmr1* KO Naïve = 9, *fmr1* KO FC = 11 .

3.2 Meta analytic review of previous studies supports a deficit in fear memory association in *fmr1* KO mice

Using a meta-analysis, we next determined if the fear memory deficit found here is consistent with previous studies in *fmr1* KO mice. When considered independently, 4 of 11 studies on tone recall showed significant results and 3 out of 13 studies on context recall (indicated by a star next to the effect size in Table 3.2). Table 3.3 displays the effect size distribution, variability and tests for significance of contextual and tone fear memory. For contextual memory, 100% studies have a positive effect size indicating all results were in the same direction, where 50% would be expected under the null hypothesis. This means that across studies, *fmr1* KO mice freeze equal or less than WT mice during context recall. Tone memory tests showed that 73% were in the same direction, indicating that in some tone memory tests the *fmr1* KO mice froze more that WT's and in some they froze less.

3.2.1 Effect Sizes

The unweighted means for both tests were similar (0.23 contextual; 0.21 tone), and weighting the means by the sample size (N-3) to account for potential bias due to larger or smaller studies did not largely alter the means (0.20 contextual; 0.20 tone). The median for each variable was smaller than both the weighted and unweighted means (0.18 contextual; 0.16 tone), indicating that a larger proportion of studies have smaller effect sizes than the mean. However, the 95% confidence interval for the unweighted mean effect sizes was reasonably narrow (0.12 - 0.345 contextual; 0.00 - 0.40 tone), and the values of each study were not significantly different from each other

Table 3.3.
Meta Analysis of Tone and Contextual Recall in *fmr1* KO mice

Statistical Summary of Context Recall (n=13)			Statistical Summary of Tone Recall (n=11)		
Statistic	Value		Statistic	Value	
Central tendency (r)			Central tendency (r)		
Unweighted M	0.236		Unweighted M	0.21	
Weighted M	0.20		Weighted M	0.20	
Median	0.18		Median	0.16	
Proportion >0.00	100%		Proportion >0.00	73%	
Significance tests (Z from p)			Significance tests (Z from p)		
Combined Stouffer Z	4.18	***	Combined Stouffer Z	3.66	***
t-test	5.94	***	t-test	2.77	**
Variability (r)			Variability (r)		
X2 for heterogeneity	8.34	(0.75)	X2 for heterogeneity	15.67	(0.11)
Maximum	0.60		Maximum	0.62	
Quartile 3 (Q3)	0.37		Quartile 3 (Q3)	0.42	
Quartile 1 (Q1)	0.07		Quartile 1 (Q1)	-0.08	
Q3-Q1	0.30		Q3-Q1	0.50	
CI for r			CI for r		
95%	0.12 - 0.34		95%	0.00 - 0.40	

($\chi^2$for heterogeneity: χ^2 (12) = 8.34, p = 0.758, contextual; χ^2 (10) = 15.67, p = 0.11, tone). Of note, among tone recall tests there is a larger confidence interval and a larger

heterogeneity value than among contextual recall tests, indicating results for tone memory are more variable from study to study.

3.2.2 Significance Testing

Overall the results were significant for both contextual fear memory (Stouffer's Z = 4.18, $p = 0.0001$; $t(12) = 5.94$, $p = 0.000068$) and for tone fear memory (Stouffer's Z = 3.66, $p = 0.0003$; $t(10) = 2.77$, $p = 0.019787$).

3.3 PV and PNN Analysis

Parvalbumin protein and mRNA levels can be up- or down-regulated in response to altered neural activity (Filice et al., 2016; Donato et al., 2013; Favuzzi et al., 2017; Tropea et al., 2006; Cohen et al., 2016). PNNs are modified after learning events to allow for synaptic reorganization. Thus, changes in PV or PNN density may reflect synaptic or microcircuit reorganization among cells involved in new memory formation/consolidation (Banerjee et al., 2017; Favuzzi et al., 2017). To better understand circuit-level dynamics following fear conditioning, changes in PV and PNN expressing cell density were characterized in brain regions associated with context (hippocampus, amygdala) and tone-associated (amygdala, auditory cortex) fear memory.

To counterbalance the recall testing during behavior some mice underwent recall testing for the context prior to the tone, whereas others underwent testing of the tone recall prior to the context. Therefore, two separate groups of mice were analyzed based on the order of tone and context recall: 1) tone-context and 2) context-tone. The tone-context experiment is discussed in detail here, with context-tone experiments discussed in the figure legend, because the outcomes were largely similar between the two

experiments. The two exceptions to this were CA1 and DG areas that showed notable differences between the two experiments and are discussed here.

3.3.1 *Fmr1* deficiency affected fear conditioning-induced changes in PNNs, but not PV cell density in the auditory cortex

The most consistent deficit we found in *fmr1* KO mice after fear conditioning is reduced freezing during tone recall, which may indicate changes in auditory cortex processing of sounds and/or altered amygdala function. PV immunoreactivity and PNNs were analyzed in the auditory cortex of N and FC WT and *fmr1* KO mice. The auditory cortex was divided into superficial (layers 1-4) and deep cortical layers (5-6) for this analysis.

Both deep and superficial layers showed mostly similar trends in PV immunoreactivity. In superficial layers, PV cell density decreased (effect of conditioning: $p = 0.0056$) in both WT and *fmr1* KO mice after fear conditioning compared to naïve (2-Cond Test: $p = 0.012$; Fig. 3.5F) and to controls (2-Cond Test: $p = 0.0006$), indicating PV downregulation specifically in response to fear conditioning. In deep layers, PV cell density decreased moderately (effect of conditioning: $p = 0.06$) in FC mice compared to control mice (2-Cond Test: $p = 0.0068$; Fig. 3.5K), but did not change relative to N mice (2-Cond Test: $p = 0.2476$). Genotype had no effect on PV cell density (superficial layers: $p = 0.714$; deep layers: $p = 0.6041$). In both deep and superficial layers, the observed overall reduction in PV cell density was due to the loss of PV cells lacking PNNs (superficial layers: C v FC $p = 0.0002$; N v FC $p = 0.0086$; deep

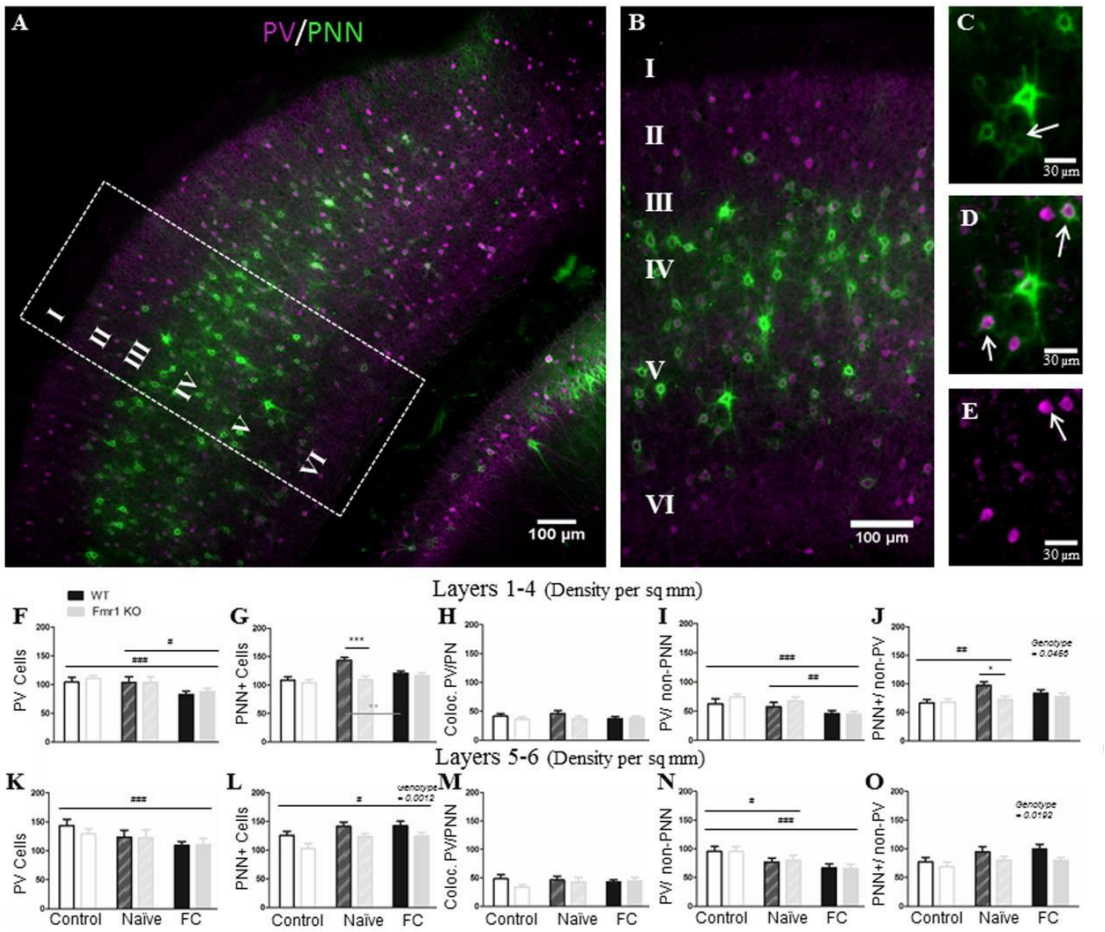

Figure 3.5. Fear conditioning causes reduced PV density across genotypes in auditory cortex, and dysregulation of PNNs in *fmr1* KO mice. A) Example image of WT naïve auditory cortex, with cropped image used for analysis (B). The far right panels identify examples of PNN surrounding non-PV cells (C; arrow), PV cells without PNN (E; arrow) and co-localized PV/PNN cells (D; arrow). F) Fear conditioning caused a decrease in PV density in both superficial (K) and deep layers, specifically in PV cells that were not surrounded by PNN (I; N). There was no genotype difference in PV cell density. L) There were overall fewer PNN cells in *fmr1* KO auditory cortex (deep layers), which were surrounding non-PV cells (O), but no difference was seen in PNNs which surround PV cells (H; M). In superficial layers WT mice upregulate PNNs after naïve conditioning, and downregulate them after fear conditioning, while *fmr1* KO mice show no change (G). Conditioning effect #, ##, ###; paired comparison *, **, *** (p = 0.05, 0.01, 0.001). N per group: WT N = 5; WT FC = 5; WT C = 3, *fmr1* KO N = 6, *fmr1* KO FC = 6, *fmr1* KO C = 5. Image # per group: WT N = 19, WT FC = 18, WT C = 15, *fmr1* KO N = 18, *fmr1* KO FC = 18, *fmr1* KO C = 18.

layers: C v FC p = 0.0003; Fig. 3.5I, 3.5N). There was no difference in density of PV cells with PNN either in superficial (effect of condition: $F(2) = 0.38$, $p = 0.684$; effect of genotype: $F(1) = 1.61$, $p = 0.207$) or in deep layers (effect of condition: $F(2) = 0.176$, $p = 0.838$; effect of genotype: $F(1) = 1.164$, $p = 0.283$).

Unlike PV density, PNN density was lower overall in *fmr1* KO mice compared to WTs (superficial layers: p = 0.0015; deep layers: p = 0.0012; Fig. 3.5G/ 3.5L), replicating previous findings in young mice (Wen et al., 2018a). Reduced PNNs were observed around non-PV cells (superficial layers: p = 0.0456; deep layers: 0.0193; Fig. 3.5J/ 3.5O), but no difference was seen in density of PNNs surrounding PV cells (superficial layers: p = 0.2074; deep layers: p = 0.2833; Fig. 3.5H/ 3.5M).

In deep layers, PNN density was increased (effect of conditioning: p = 0.0165) in FC mice compared to control mice (2-Cond Test: p = 0.0135). In contrast, fear conditioning specifically caused reduced PNN density (effect of conditioning: p = 0.0013) in superficial layers of WT mice (WT N: 143.2; WT FC: 120.8; $p < 0.01$), but not *fmr1* KO mice (*fmr1* KO N: 109.4; *fmr1* KO FC: 116.4) compared to N mice.

Together, the data show impaired PNN density in *fmr1* KO mice compared to WT mice in the auditory cortex. In contrast, PV cell density was similar across genotypes, and fear conditioning induced a decrease in PV cell density in both WT and *fmr1* KO mice, mainly among PV cells lacking PNNs. We also observed layer-specific differences in PNN regulation in WT mice and between genotypes, suggesting that (1) PNNs may be differentially regulated in different cortical layers and (2) PNN changes induced by tone fear conditioning in the superficial layers of WT mice were impaired in *fmr1* KO mice.

3.3.2 PNNs around PV and non-PV cells are reduced in the amygdala of *Fmr1* KO mice

The amygdala is comprised of multiple nuclei, which are associated with specific inputs, outputs and functions. In this study, we focused on the lateral and basolateral nuclei, which are readily identifiable and involved in fear-associative memory formation. Neither the lateral or basolateral amygdala showed genotype differences in overall PV cell density (Lateral: $p = 0.5193$; Basolateral: $p = 0.4382$; Fig 3.6J/ 3.6O) or showed an effect of fear conditioning (Lateral: $p = 0.6627$; Basolateral: $p = 0.1327$). However, a significant reduction in the density of PV cells lacking PNNs was observed in basolateral amygdala (effect of condition: $p = 0.046$; Fig. 3.6R).

In both lateral and basolateral amygdala, there were significantly fewer PNNs in *fmr1* KO mice than in WT mice (Lateral: $p < 0.0001$; Basolateral: $p = 0.0062$; Fig. 3.6K/ 3.6P), specifically fewer PNNs around non-PV cells (Lateral: $p = 0.0001$; Basolateral: $p < 0.0001$; Fig. 3.6N/ 3.6 S). There was no genotype difference in density of PV cells containing PNNs (Lateral: $p = 0.2352$; Basolateral: $p = 0.766$; Fig. 3.6L/ 3.6Q). These data show a heretofore-unknown baseline deficit in PNN formation in the amygdala of *fmr1* KO mice, compared to WT mice. In both genotypes PNN density was upregulated in N (2-Cond Test, N vs. C: $p < 0.0001$) and FC (2-Cond Test, FC vs. C: $p = 0.001$) mice compared to controls in the lateral amygdala (WT C: 68.82; WT N: 97.51; WT FC: 88.98; *fmr1* KO C: 36.16; *fmr1* KO N: 75.58; *fmr1* KO FC: 68.17; effect of conditioning: $p < 0.0001$) and in the basolateral amygdala (WT C: 33.96; WT N: 53.32; WT FC: 57.75; *fmr1* KO C: 24.4;

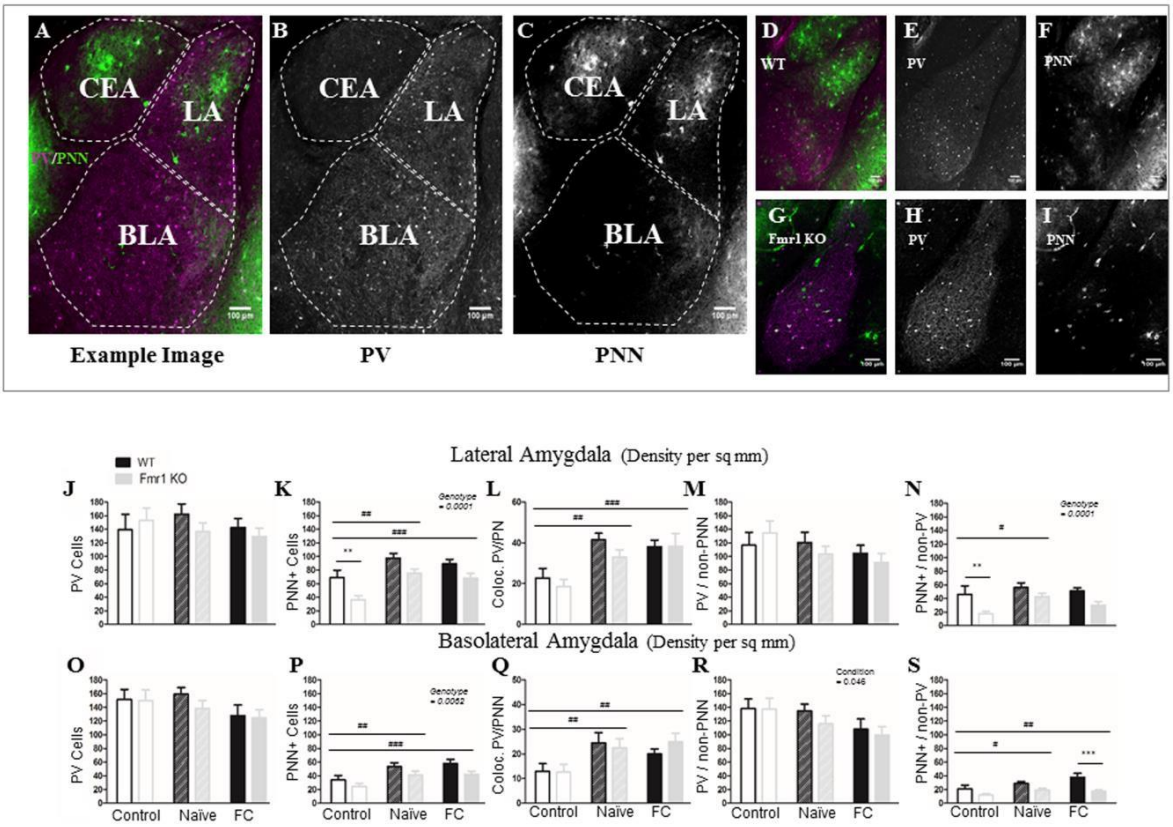

Figure 3.6: *Fmr1* KO mice have less PNN in the amygdala than WT mice, but can still upregulate PNNs after conditioning. A) Example image from a coronal section containing amygdala nuclei, including the lateral nucleus (LA), the basolateral nucleus (BLA) and the central nucleus (CEA). CEA was not identifiable in all slices and therefore was not counted. Area of each nucleus is determined using visible anatomic structures, gradation in cellular staining and the mouse Allan brain atlas. PV (B) and PNN (C) are shown to the right. D) Example image of a WT naïve slice and an (G) *fmr1* KO naïve slice, with PV (E; H) and PNN (F; I) to the right. Overall there are fewer PNNs in *fmr1* KO mice than WT in both LA (K) and BLA (P), specifically fewer PNNs surrounding non-PV cells (N; S). This genotype difference is not affected by conditioning. Both naïve and fear conditioned mice show an increase in PNNs across genotypes. J; O) While there was no difference in overall PV cell number either due to conditioning or to genotype, it seems that both the naïve exposure to the training protocol as well as full conditioning cause an increase in the number of PV cells that are surrounded by PNN (L; Q) probably due to increased overall PNN. At the same time there was a reduction in PV cells not surrounded with PNN after fear conditioning in the BLA (R) but not in the LA (M). Conditioning effect #, ##, ###; paired comparison *, **, *** (p = 0.05, 0.01, 0.001). N per group: WT N = 5; WT FC = 6; WT C = 3, *fmr1* KO N = 6, *fmr1* KO FC = 6, *fmr1* KO C = 4. Image # per group: WT N = 17, WT FC = 17, WT C = 13, *fmr1* KO N = 17, *fmr1* KO FC = 17, *fmr1* KO C = 17.

fmr1 KO N: 41.38; *fmr1* KO FC: 42.2; effect of conditioning: p = 0.0004; 2-Cond Test: C vs. N: p = 0.0014; C vs. FC: p = 0.0002). This upregulation of PNNs seemed to occur

around both PV cells (effect of conditioning: Lateral: p = 0.0001; Basolateral: p = 0.0043), and non-PV cells (effect of conditioning: Lateral: p = 0.0273; Basolateral: p = 0.0126). However, no difference was observed in PNN density between N and FC mice.

Thus in the amygdala similar to the AC, reduced PNN cell density, but not PV cell density, was observed in *fmr1*KO mice compared to WT mice. In contrast to AC, in the amygdala we saw no changes in PV cell density following fear conditioning, whereas PNN density increased in both N and FC mice, suggesting that these changes in PNNs may represent modifications due to context exposure instead of fear conditioning, potentially similar to environmental enrichment. Context-Tone results are in Figure 3.7.

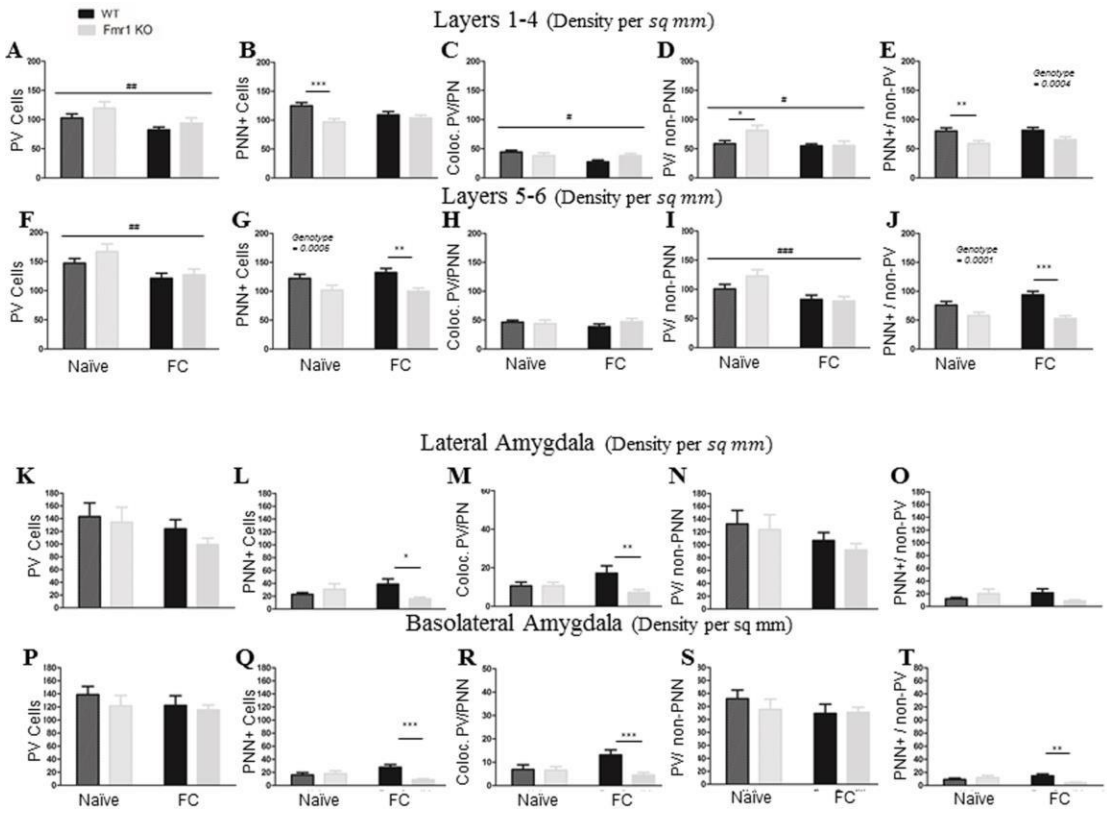

Figure 3.7:CONTEXT-TONE: PV cells in the auditory cortex are downregulated after fear conditioning but do not change in the amygdala; both regions show reduced PNN density in *fmr1* KO mice potentially due to dysregulation in *fmr1* KO mice.
Fear conditioning caused decreased PV cell density in both WT and *fmr1* KO mice, both in superficial (A; conditioning: F(1) = 7.8, p = 0.006; genotype: F(1) = 2.93, p = 0.089) and deep (F; conditioning: F(1) = 10.56, p 0.0015; genotype: F(1) = 1.64, p = 0.2) layers of auditory cortex. This took place largely in PV cells not surrounded by PNN (D; superficial: conditioning: F(1) = 5.14, p = 0.025; I: deep: conditioning F(1) = 12.53, p = 0.0006). PNNs are reduced in the deep layers of *frm1* KO mice (G; genotype: F(1) = 12.83, p = 0.0005), particularly PNNs surrounding non-PV cells (deep J; genotype: F(1) = 23.92, p < 0.0001; superficial E; F(1) = 13.6, p = 0.0004). However in superficial layers (B) the WT mice downregulate their PNN after fear conditioning (WT N vs. FC: p = 0.056; **Means:** WT N: 124.7; WT FC: 109) while *fmr1* KO mice do not (*fmr1* KO N vs FC: p = 0.36; **Means**: *fmr1* KO N: 96.89; *fmr1* KO FC: 103.8). C/H) Colocalized PV/PNN cells. Conditioning effect #, ##, ###; paired comparison *, **, *** (*p* = 0.05, 0.01, 0.001). N per group: WT N = 6; WT FC = 6; WT C = 3, *fmr1* KO N = 5, *fmr1* KO FC = 5, *fmr1* KO C = 5. Image # per group: WT N = 32, WT FC = 26, WT C = 15, *fmr1* KO N = 27, *fmr1* KO FC = 25, *fmr1* KO C = 18.
Amygdala. After fear conditioning there were fewer PNNs in *fmr1* KO mice than WT mice, both in the lateral (L) and the basolateral amygdala (Q). This seems to be due to both downregulation of PNNs in *fmr1* KO mice (lateral: *fmr1* KO N: 30.7, *fmr1* KO FC: 15.91; basolateral fmr1 N: 17.9, *fmr1* KO FC: 8.6) and upregulation in WT mice (lateral: WT N: 22.73, WT FC: 38.59; basolateral: WT N: 15.97, WT FC: 27.69) suggesting dysregulated PNNs in *fmr1* KO mice. These changes in PNN are largely occurring in PNN surrounding PV cells (M; R). PV cell density does not change either with conditioning or genotype (K; P). N;S) PV cells without PNN. O;T) PNN structures surrounding non-PV cells. Conditioning effect #, ##, ###; paired comparison *, **, *** (p = 0.05, 0.01, 0.001). N per group: WT N = 6; WT FC = 6; WT C = 3, *fmr1* KO N = 5*, fmr1* KO FC = 5, *fmr1* KO C = 4. Image # per group: WT N = 20, WT FC = 20, WT C = 13, *fmr1* KO N = 16*, fmr1* KO FC = 24, *fmr1* KO C = 17.

3.3.3 No genotype differences were observed in PV and PNN cell densities in CA1 hippocampus

The CA1 showed no genotype differences in PV density (p = 0.533) or differences due to conditioning (p = 0.077; Fig. 3.8O). PNN density was also not different between WT and *fmr1* KO mice (p = 0.3243). However, PNN density increased in both N (2-Cond Test: p < 0.0001) and FC mice (2-Cond Test: p = 0.0026) compared to controls (WT C: 42.58, N: 55.84, FC: 53.48; *fmr1* KO C: 41.34, N: 54.73, FC: 48.64; Fig. 3.8P; effect of conditioning: p < 0.0001). This increase in PNNs seemed to occur around both PV (effect of conditioning: p < 0.0001; Fig. 3.8Q) and non-PV cells (effect of

conditioning: p = 0.05; Fig.3.8S), and again indicates PNN modification more akin to an effect of environmental enrichment.

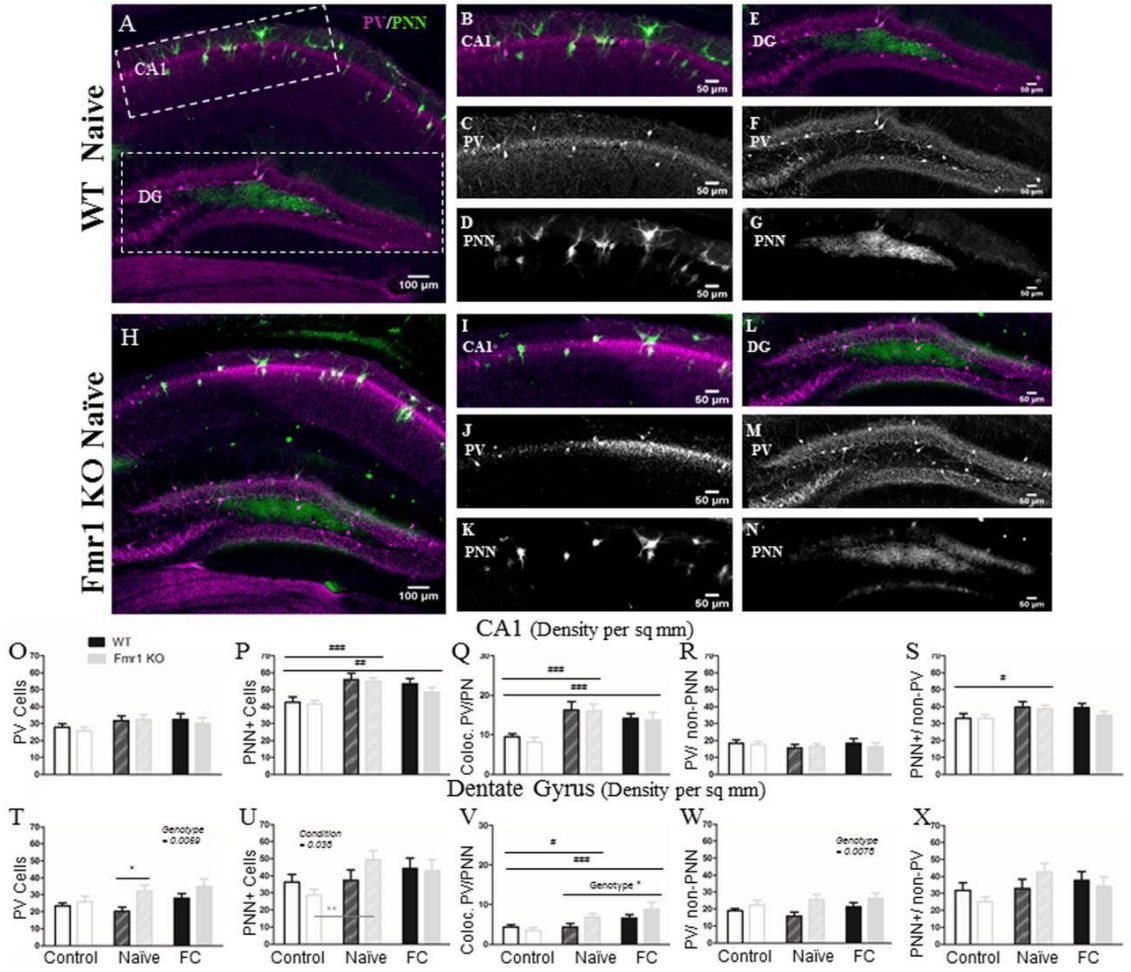

Figure 3.8: PV density is elevated in the dentate gyrus of *fmr1* KO mice but not in the CA1. A) Example images of coronal sections from a WT naïve and (H) an *fmr1* KO naïve mice. (B), with panels to the right depicting CA1 (B; I) and dentate gyrus (E; L). Panels below CA1 and DG show the PV (C; F; J; M) and PNN (D; G; K; N) channels separately. In CA1 both WT and *fmr1* KO mice have similar levels of PV (O; R) and PNN (P; S). Both genotypes had increased PNN denisty in naïve and fear conditioned mice (P). These PNNs were located both around PV cells (Q) and non-PV cells (S). In the DG, there were more PV cells in *fmr1* KO mice than WT mice (T), both PV cells surrounded by PNN (V) and PV cells without PNNs (W). Similar to CA1 there was increased PNN density in naïve and fear conditioned mice (U), but unlike CA1 the increased PNN seem to be around PV cells (V) and not around non-PV cells (X). Conditioning effect #, ##, ###; paired comparison *, **, *** (p = 0.05, 0.01, 0.001). N per group: WT N = 5; WT FC = 6; WT C = 6, *fmr1* KO N = 6, *fmr1* KO FC = 6, *fmr1* KO C = 5. Image # per group: WT N = 16, WT FC = 17, WT C = 28, *fmr1* KO N = 18, *fmr1* KO FC = 16, *fmr1* KO C = 27.

Although the tone-context experiment showed no modifications in PV or PNN cell density between N and FC mice (as discussed above), the context-tone experiment (data in supplemental material) showed a decrease in PV density (effect of conditioning: $p = 0.0033$) in FC compared to N mice in both genotypes (WT N: 33.44, FC: 27.04; *fmr1* KO N: 33.81, FC: 23.33; Fig. 3.9A), mainly in PV cells with PNNs (effect of conditioning: $p = 0.0058$; Fig. 3.9C). The context-tone experiment also showed opposing changes in PNN density between genotypes. WT mice showed no change in PNN density after FC (WT N: 39.93; FC: 45.38; *ns*) whereas FC *fmr1* KO mice had decreased PNN density compared to N mice (*fmr1* KO N: 55.27; FC: 38.93; $p < 0.01$; Fig. 3.9B). If we compare this to controls (shown in Fig. 3.8; WT C: 42.58; *fmr1* KO C: 41.34), it is apparent that WT mice had no changes in PNN density in N and FC mice as compared to controls, whereas *fmr1* KO mice showed an up-regulation in N mice compared to controls (N vs. C: $p < 0.01$) which was downregulated in FC mice.

Differences in PV and PNN between experiments in the CA1 may reflect modification of the contextual memory after re-exposure to the training contexts during recall tests. This is consistent with the role of the dorsal hippocampus in contextual memory formation. The differences in time between context recall and tissue collection in the two experiments, context-tone (4 h) versus tone-context (30 min), likely reflects modification of PV and PNN on different timescales post-recall. Four h after re-exposure to the context there is downregulation of PV expression in CA1 of all FC mice, and differential regulation of PNN density between WT and *fmr1* KO mice.

3.3.4 PV cell density is increased in the Dentate Gyrus of *fmr1* KO mice

The dentate gyrus (DG) is the main input region of the hippocampus. In contrast to the findings in the AC, amygdala and CA1, the dentate gyrus (DG) showed elevated density of PV cells in *fmr1* KO mice compared to WT mice (effect of genotype: p =0.0059; Fig. 3.8T), including PV cells with PNNs (p = 0.0478; Fig. 3.8V) and without PNNs (p = 0.0078; Fig. 3.8W).

Similar to amygdala, in the DG, PNN density changed after conditioning (effect of conditioning: p = 0.038; Fig. 3.8U). The means suggest this is due to increased PNN density in both naïve and FC mice when compared to control mice (WT: C: 36.21; N: 37.31; FC: 44.15; *fmr1* KO: C: 28.63; N: 49.33; FC: 42.93) but did not reach significance. However N *fmr1* KO mice did show increased PNNs compared to controls (C vs. N: $p < 0.01$) and this was not observed in WT mice (C vs. N: *ns*). There was no significant difference in PNN density between genotypes (p = 0.80). Conditioning-induced increase in PNNs was mainly observed around PV cells (effect of conditioning: p = 0.0003; Fig. 3.8V) whereas the density of non-PV cells with PNNs did not change following conditioning (effect of conditioning: p = 0.0958; Fig. 3.8X).

Similar to CA1, the DG showed differences between the tone-context experiment (discussed above) and the context-tone experiment (supplemental material). In the context-tone experiment there was an overall effect of conditioning (effect of conditioning: p = 0.022), with reduced PV cell density in FC mice compared to N mice, which was largely due to reduced PV density in *fmr1* KO mice but not in WT mice (WT: N: 40.85, FC: 41.92; *fmr1* KO: N: 50.58; FC: 35.49; Fig. 3.9Q). When this data is

compared to controls from Figure 3.8 (WT: C: 23.4*; fmr1* KO mice: C: 25.87), it is clear that both WT and *fmr1* KO mice upregulate PV density in N and FC mice compared to C mice (WT: C vs. N: $p < 0.001$, C vs. FC: $p < 0.001$; fmr1 KO: C vs. N: $p < 0.001$, C vs. FC: $p < 0.05$), but *fmr1* KO mice then decrease PV density after fear conditioning (N vs. FC: $p < 0.01$) whereas WT do not (N vs. FC: *ns*).

PNN density was also different between experiments and showed differential regulation in WT and *fmr1* KO mice, similar to observations in CA1. PNN density increased in WT mice after fear conditioning ($p < 0.05$), while PNN was slightly downregulated in *fmr1* KO mice (*ns*), leading to significantly fewer PNNs in FC *fmr1* KO mice ($p < 0.05$) compared to FC WT mice (WT: N: 20.22, FC: 32.53, *fmr1* KO: N:

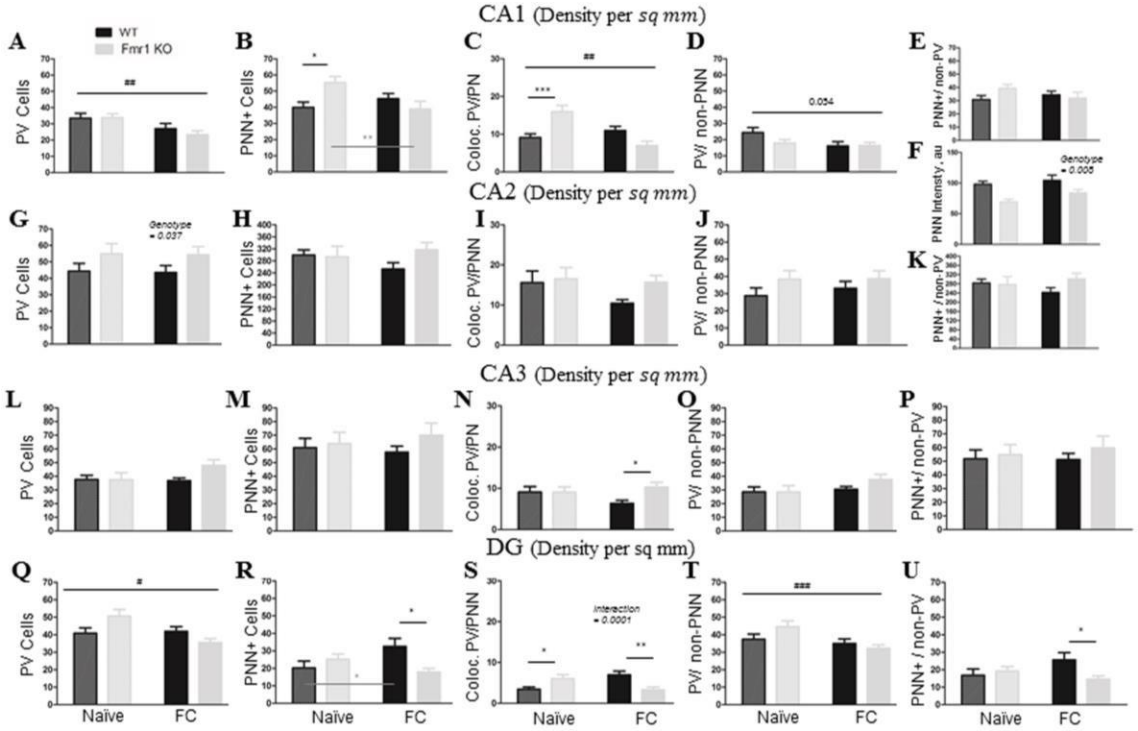

Figure 3.9: CA1 and DG show modification of PV and PNN expression after recall in CONTEXT-TONE experiment, indicating modification of the contextual memory engram.

CA1: A) PV density is reduced in conditioned mice in both genotypes (conditioning: $F(1) = 9.1$, $p = 0.0033$; WT N: 33.44, WT FC: 27; *fmr1* KO N: 33.8, *fmr1* KO FC: 23.33). C) Some of the reduced PV cells are those that are enwrapped with PNN (conditioning: $F(1) = 8$, $p = 0.0058$) carried by a large decrease in PV/PNNs in *fmr1* KO mice (N: 15.97, FC: 6.9) and not WT (N: 9, FC: 10.9). D) PV cells without PNN were also reduced (conditioning: $F(1) = 3.7$, $p = 0.054$) mainly in WT mice (N: 24.3, FC: 16) but not in *fmr1* KO mice (N: 17.8, FC: 16.3). B) There was no significant main effect for PNN density but there was an interaction ($F(1)= 8.2$, $p = 0.0052$) due to a large decrease in PNN density after fear conditioning in *fmr1* KO mice (N: 55.2, FC: 38.9) and instead a slight increase in WT mice (N: 39.9, FC: 45.3). E) PNNs around non-PV cells were not different.

CA2: G) There was an overall increase in PV cell density in *fmr1* KO mice compared to WTs (genotype: $F(1) = 4.4$, $p = 0.037$; WT N: 44.3, WT FC: 43.5; *fmr1* KO N: 54.34, *fmr1* KO FC: 54.34), but no significant difference in PV cells surrounded with PNN (I) or in PV cells without PNN (J). F) There was also decreased PNN intensity in *fmr1* KO mice (genotype: $F(1) = 15.9$, $p = 0.0002$; WT N: 98.13, WT FC: 104.4; *fmr1* KO N: 69.1, *fmr1* KO FC: 84.06) but no difference in overall PNN density (H), or in PNN density surrounding non-PV cells (K).

CA3: There was only a slight increase in co-localized PV/PNN in *fmr1* KO mice after fear conditioning (N) but no main effects were significant. There was no difference in PV cell density (L), PNN density (M), PV without PNN (O), or PNN without PV (P).

Dentate gyrus: Q) PV cell density was overall reduced after fear conditioning (conditioning: $F(1) = 5.4$, $p = 0.022$) but this difference seems to be carried by *fmr1* KO mice more than WT (WT N: 40.85, WT FC: 41.92; *fmr1* KO N: 50.58, *fmr1* KO FC: 35.49). T) This reduction is occurring among PV cells not surrounded by PNN (conditioning: $F(1) = 7$, $p = 0.0097$; WT N: 37.4, WT FC: 34.9; *fmr1* KO N: 44.5, *fmr1* KO FC: 32.2). R) PNN density was significantly reduced in *fmr1* KO mice compared to WT after fear conditioning ($p < 0.05$) due to an increase in PNN among WT mice (N: 20.2, FC: 32.5) and a decrease in *fmr1* KO mice (N: 25.1, FC: 17.8; Interaction $F(1) = 7.2$, $p = 0.0087$). U) Changes in PNN are occurring among PNNs surrounding non-PV cells (WT FC vs *fmr1* KO FC: $p < 0.05$; WT N: 16.7, WT FC: 25.5; *fmr1* KO N: 19.1, *fmr1* KO FC: 14.5). S) *Fmr1* KO and WT mice had opposite trends in regulation of co-localized PV/PNN population after fear conditioning (interaction: $F(1) = 16.1$, $p = 0.0001$; WT N: 3.4, WT FC: 6.9; *fmr1* KO N: 6, *fmr1* KO FC: 3.2).

Conditioning effect #, ##, ###; paired comparison *, **, *** (p = 0.05, 0.01, 0.001). N per group: WT N = 6; WT FC = 6; KO N = 5; KO FC = 5.
CA1/DG: Image # per group: WT N = 21, WT FC = 22, KO N = 21, KO FC = 21.
CA2/CA3 Image # per group: WT N = 22, WT FC = 21, KO N = 19, KO FC = 17.

25.18, FC: 17.81; Fig. 3.9R). Comparing these data to controls from Figure 3.8, (WT: C: 36.21; *fmr1* KO: C: 28.63), it becomes clear that N WT mice actually downregulate PNN compared to controls ($p < 0.0.1$), and then upregulate it after FC, whereas *fmr1* KO mice do not show PNN regulation. Together, these results suggest that PV and PNN are not being regulated in the same way in the DG of WT and *fmr1* KO mice. PV levels are higher and fluctuate more in *fmr1* KO mice than in WT mice. Comparison between tone-context and context-tone experiments suggest that regions of the hippocampus necessary for maintaining the contextual memory component of fear conditioning (CA1 and DG) undergo time-dependent changes in PV and PNN cell density that are different between genotypes.

3.3.5 PNN intensity in CA2 is reduced in *fmr1* KO mice

The CA2 has a region of high PNN expression. WFA labeling, which is a lectin that binds to proteoglycans present in PNNs and other extracellular matrix (ECM) structures, extends from the stratum pyramidal of CA2 to the dorsal granule cell layer of the dentate gyrus, potentially covering fibers from entorhinal cortex into CA2. As this labeling of fluorescently-tagged WFA is profuse and far outside the stratum pyramidal we measured PNN intensity in CA2 in addition to counting PNN positive cells. The WFA fluorescence intensity was reduced in *fmr1* KO mice compared to WT mice ($p = 0.0215$; Fig. 3.10S). Conditioning affected WFA fluorescence intensity (effect of conditioning: $p = 0.0084$) by decreasing fluorescence intensity in N mice compared to controls (2-Cond Test: $p = 0.0021$; WT C: 152.1, N: 107.1, FC: 127.5; *fmr1*

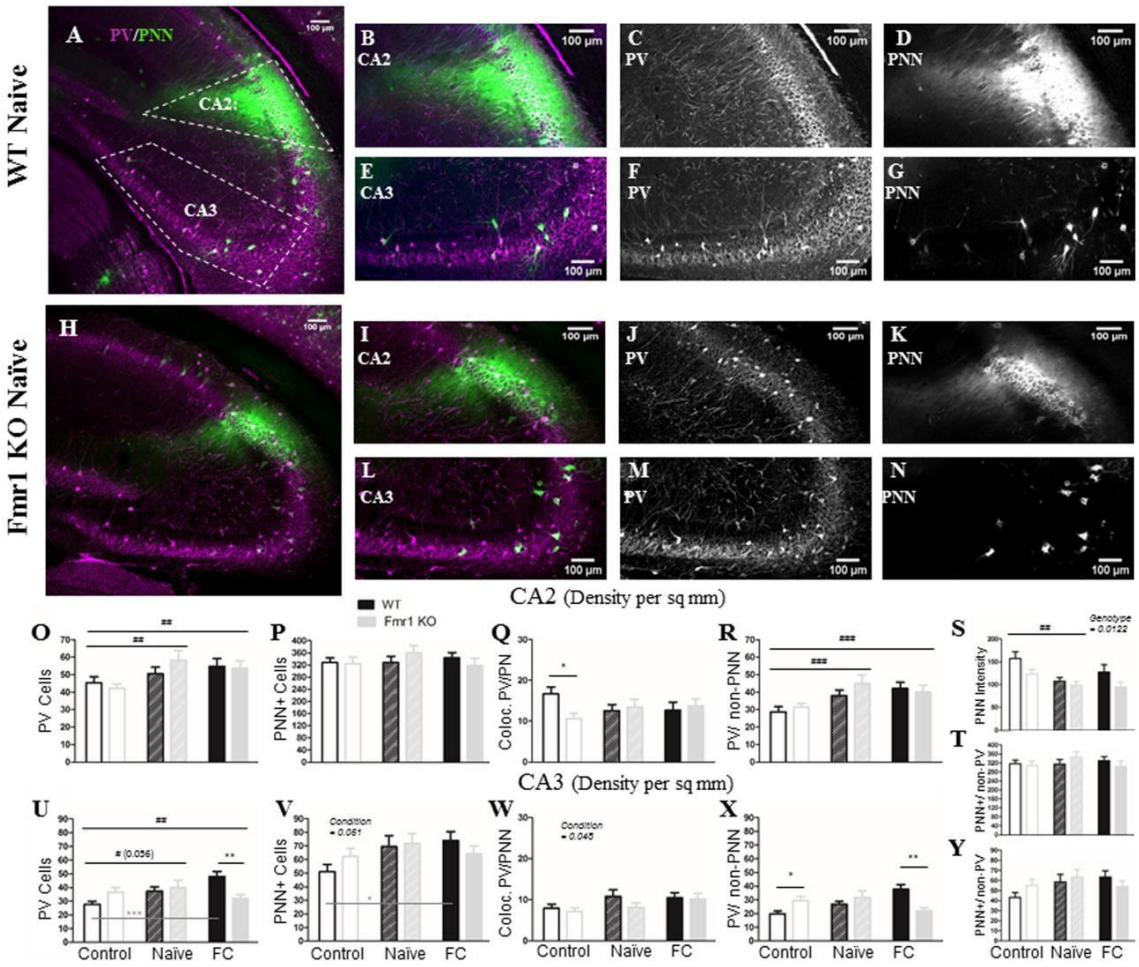

Figure 3.10: In CA2 both PV cell density and PNN intensity are modified after conditioning across genotypes; In CA3, PV cell modification is impaired in *fmr1* KO mice. A) Example image of a WT naïve coronal slice and (H) an *fmr1* KO naïve slice, with cropped images of CA2 (B; I) and CA3 (E; L). To the right of the cropped images are PV (C; F; J; M) and PNN (D; G; K; N) channels separated. In CA2 there was no genotype difference in PV density (O) or PNN density (P) between WT and *fmr1* KO animals. However PV cell density increased (O) in both naïve and fear conditioned mice across genotypes, among PV cells that are not surrounded by PNN (R). We measured WFA fluorescent intensity in CA2 across genotypes and conditioning. Using this metric we found *fmr1* KO mice have reduced WFA intensity compared to WT mice (S) and a decrease in WFA intensity after conditioning in both genotypes, but no change in PNN density (P; T) or in co-localized PV/PNN cells (Q). In CA3 there was an increase in PV cell density (U) and in PNN cell density (V) in both naïve and fear conditioned mice, which increased the number of co-localized PV/PNN cells (W; fear conditioned only). The increase in PV cells seems to be occurring only in WT mice (U) among PV cells that were not surrounded by PNNs (X). PNNs surrounding non-PV cells showed no change (Y). Conditioning effect #, ##, ###; paired comparison *, **, *** (p = 0.05, 0.01, 0.001). N per group: WT N = 5; WT FC = 6; WT C =7, *fmr1* KO N = 6, *fmr1* KO FC = 6, *fmr1* KO C = 5. Image # per group: WT N = 17, WT FC = 18, WT C = 32, *fmr1* KO N = 17, *fmr1* KO FC = 18, *fmr1* KO C = 25.

KO C: 124.5, N: 98.76, FC: 94.2). However, N and FC mice were not different from each other. ECM levels remained low in *fmr1* KO mice under all conditions. Although WFA fluorescence intensity decreased, PNN cell density was not different between genotypes ($p = 0.9682$) or in response to conditioning ($p = 0.69$; Fig. 3.10P).

PV density increased (effect of conditioning: $p = 0.0052$) after both naïve (2-Cond Test: $p = 0.0069$) and fear conditioning (2-Cond Test: $p = 0.005$) compared to controls (WT C: 45.39, N: 50.42, FC: 54.76; *fmr1* KO C: 42.1, N: 58.26, FC: 53.7; Fig. 3.10 O) with no genotype differences (effect of genotype: $p = 0.72$). Together these results suggest reduced ECM and an increase in PV expression after both naïve and fear conditioning, but no specific effect of fear conditioning alone in the CA2.

3.3.6 PV cell density in CA3 increases after conditioning in WT but not in *Fmr1* KO mice

PV cell density in the CA3 increases in FC mice when compared to control mice (2-Cond Test: $p = 0.0069$), but not compared to N mice (2-Cond Test: $p = 0.69$; effect of conditioning: $p = 0.026$). This increase seems to be carried by WT mice (WT C: 27.78, N: 37.42, FC: 48.15; C vs. N: *ns;* C vs. FC: $p < 0.0001$; N vs. FC: *ns*). Because *fmr1* KO levels do not change (*fmr1* KO C: 36.69, N: 40, FC: 32.25; paired comparisons: *ns*) but WT levels increase, this leads to significantly more PV in FC WT mice compared to FC *fmr1* KO mice ($p < 0.01$). However, the overall PV cell density is not different between genotypes ($p = 0.59$; Fig. 3.10U). We also observed a specific reduction in density of PV cells without PNNs in FC *fmr1* KO mice compared to FC WTs ($p < 0.01$; Fig. 3.10X).

PNN cell density is also altered in CA3 hippocampus after conditioning (effect of conditioning: $p = 0.051$), carried by an up-regulation of PNNs in WT FC compared to C mice ($p < 0.05$; WT C: 51.15, N: 69.44, FC: 73.92; *fmr1* KO C: 62.27, N: 71.57, FC: 64.2; Fig. 3.10V). We also observed an increase in the density of PV cells with PNNs after fear conditioning (effect of conditioning: $p = 0.048$; Fig. 3.10W) in both WT and *fmr1* KO mice, but no change in PNNs surrounding non-PV cells (effect of conditioning: $p = 0.1074$; Fig. 3.10Y).

Overall, CA3 shows an increase in PV and PNN cell density in WT mice after fear conditioning which is attenuated or absent in *fmr1* KO mice. However, density of PV cells with PNNs was upregulated in both WT and *fmr1* KO mice following FC. These effects cannot be attributed solely to fear conditioning, as FC and N mice were not different from each other.

3.4 Mouse behavior versus PV/PNN analysis

3.4.1 PNN levels in AC and amygdala correlate with the strength of the tone-associated memory.

To further understand the relationship between changes in molecular markers of plasticity and the mouse freezing behaviors during fear recall, we examined the correlation between the PV density, PNN density and PV/PNN co-localization with the three recall tests in FC WT and *fmr1* KO mice. This correlation could only be run on the subset of mice used for tissue collection (n = 11 WT, 11 *fmr1* KO; including context-tone and tone-context experiments). We combined both genotypes to assess the overall relationship between behavior and cellular changes, and also generated a regression curve

for each genotype separately to compare the curves and correlation values between WT and *fmr1* KO mice.

There is a positive correlation in auditory cortex (deep layers) between the density of PNNs and the strength of freezing during all recall tests when all mice are combined, where mice that freeze more tend to have higher PNN density (tone: r = 0.49, p = 0.024; context: r = 0.616, p = 0.0023; context+tone: r = 0.4524, p = 0.0345; Fig. 3.11 B4-6).

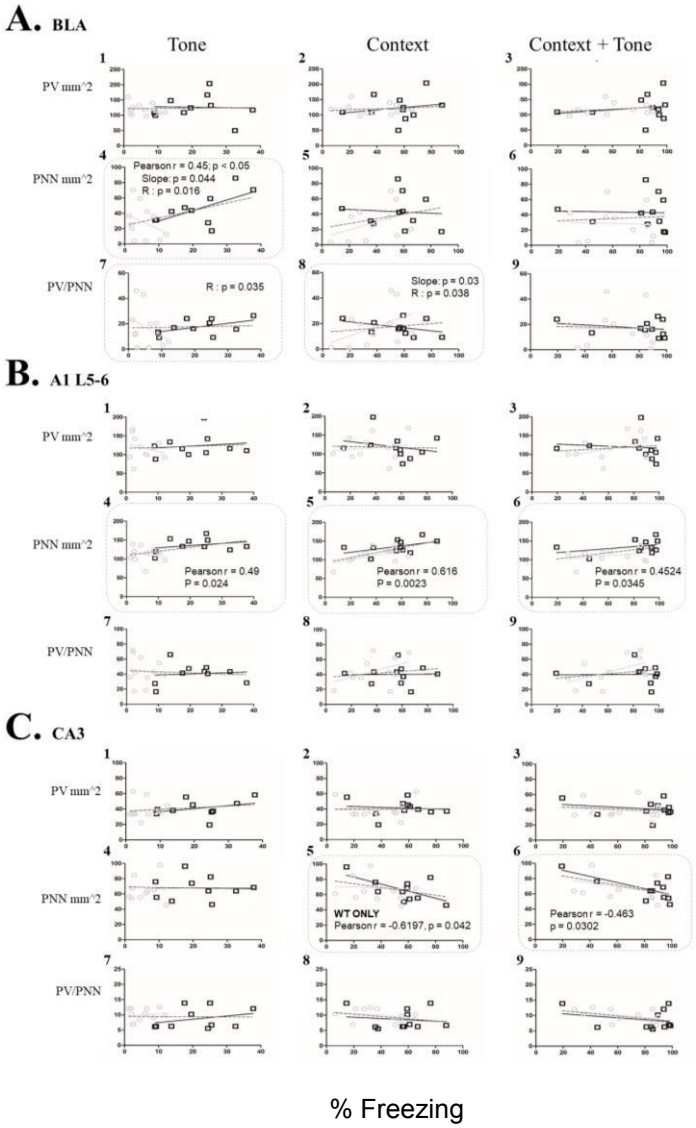

Figure 3.11: High PNN density is correlated with higher freezing behavior across multiple brain regions. Panel **A** shows basolateral amygdala, Panel **B** deep layers of auditory cortex and Panel **C** shows CA3. Each column shows the correlation between an animal's freezing during a recall test (Tone, Context or Context-with-Tone) and their levels of PV cell density (1-3), PNN density (4-6), or PV/PNN density (7-9). In both deep A1 and basolateral amygdala high freezing during tone recall was correlated with higher levels of PNN density. Additionally, in both deep A1 and CA3, high freezing during context or context-with-tone recall was correlated with high PNN levels. KEY: The grey line indicates *fmr1* KO regression curve, black line indicates WT regression curve, and the dotted line indicates the genotypes grouped. Pearson's r indicates correlation when both genotypes are grouped. "Slope" indicates the difference between the slopes of the regression curve for WT and *fmr1* KO mice on a Z-scale. R indicates the difference between the Pearson's r values for WT and *fmr1* KO mice on a Z-scale.

When WT and *fmr1* KO mice were separated and compared, the regression curves of each genotype were not different from each other. This same relationship with PNN density was found in the basolateral amygdala for tone recall (tone: $r = 0.45$, $p < 0.05$; Fig. 3.11 A4) when all mice were included. Mice that froze more tended to show higher PNN density. However, when WT and *fmr1* KO mouse data were separated, the curves and correlation coefficients between genotypes were different from each other (slope difference: $p = 0.044$, r difference: $p = 0.016$). Freezing in WT mice was positively correlated with PNN ($r = 0.6155$) but freezing in *fmr1* KO mice was negatively correlated ($r = -0.3387$). Taken together, it appears that in WT mice there is an increase in PNNs after fear conditioning in both basolateral amygdala and the deep layers of AC, and this increase is correlated with the strength of freezing during tone recall. *Fmr1* KO mice, which have consistently low freezing to the tone and reduced PNNs, do not show a relationship between PNN density in amygdala and freezing during tone recall.

3.4.2 PNN in CA3 is correlated with the strength of the contextual memory

When all mice were combined, the CA3 showed a negative correlation between PNN density and the amount of freezing during context-with-tone recall, where mice that tended to freeze more also showed less PNN (context + tone: $r = -0.463$, $p = 0.03$, genotype grouped; Fig. 3.12 C6). Freezing during context recall (without a tone) was negatively correlated with PNN density in WT mice only ($r = -0.6197$, $p = 0.042$; Fig. 3.12 C5) but not in *fmr1* KO mice ($r = -0.07$, ns) strengthening the idea that WT mice modify PNN density after fear conditioning.

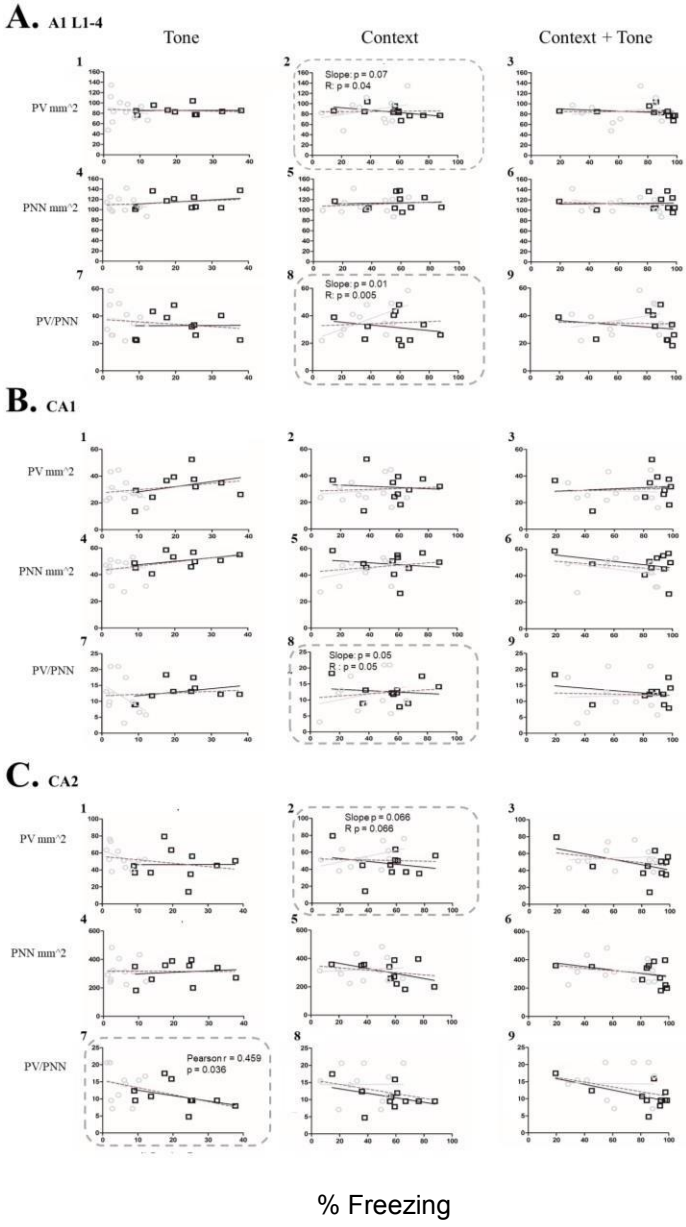

Figure 3.12: Differential relationship between co-localized PV/PNN and freezing in WT and *fmr1* KO mice. Panel **A** shows superficial A1, Panel **B** shows CA1, and Panel **C** shows CA2. Each column shows the correlation between an animal's freezing during a recall test (Tone, Context or Context + Tone) and their levels of PV cell density (1-3), PNN density (4-6), or PV/PNN density (7-9). During context recall both superficial A1, CA1 and basolateral amygdala (data not shown here) show a difference in the slope between *fmr1* KO and WT mice on correlations of context recall and co-localized PV/PNN density. Additionally, both superficial A1 and CA2 show a difference in the slope between genotypes when correlating context recall and PV density. In both cases, *fmr1* KO mice that freeze more often tend to have higher cell density, while WT mice that freeze more often have lower cell density. KEY: The grey line indicates *fmr1* KO regression curve, black line indicates WT regression curve, and the dotted line indicates the genotypes grouped. Pearson's r indicates correlation when both genotypes are grouped. "Slope" indicates the difference between the slopes of the regression curve for WT and *fmr1* KO mice on a Z-scale. R indicates the difference between the Pearson's r values for WT and *fmr1* KO mice on a Z-scale.

Context memory recall was also associated with differences in co-localized PV/PNN cells across brain regions. Interestingly, WT and *fmr1* KO mice showed opposite trends in PV/PNN expression and contextual recall. Specifically, *fmr1* KO mice showed a positive correlation between contextual memory and the density of co-localized cells (higher freezing mice had more co-localized cells), whereas the WT mice had a

negative correlation between these factors (higher freezing mice had fewer co-localized cells). This was true in CA1 (WT: r = -0.1325, *fmr1* KO: r = 0.2756; difference in slope: p = 0.05; difference in r: p = 0.05; Fig. 3.12 B8) and the basolateral amygdala (WT: r = -0.3945, *fmr1*KO: r = 0.4382; difference in slope: p =0.03; difference in r: p = 0.038; Fig. 3.12 B.2), but also true in the superficial layers of the auditory cortex (WT: r = -0.2048, *fmr1* KO: r = 0.6339; difference in slope: p = 0.01; difference in r: p = 0.005; Fig. 3.12 A8). This suggests not only PNN density, but the co-localization of PNN with PV cells may be particularly important for context memory formation.

4 Discussion

In this study we sought to determine whether CNS circuitry involved in fear-memory formation is altered in the *fmr1* KO mice, focusing on two important markers of plasticity, PV interneurons and PNNs. Our data show a consistent impairment in tone-associated fear memory in *fmr1* KO mice. A meta-analytic review of previous studies confirms that our results are in agreement with an overall impairment in fear memory association in *fmr1* KO mice. Baseline PNN expression is reduced in the amygdala, auditory cortex and CA2 of *fmr1* KO mice and PV expression is increased in the dentate gyrus. Fear conditioning causes a reduction in PV cell density in the auditory cortex across both genotypes and a differential regulation of PV in CA3 between WT and *fmr1* KO mice. The population of modified PV cells in AC primarily consisted of PV cells that were not surrounded by PNNs, suggesting these cells are more susceptible to learning induced plasticity. There was a positive correlation between overall density of PNNs and memory recall, in particular with tone recall, indicating that the lower levels of

PNN found in amygdala and auditory cortex may underlie impaired tone-associated fear memories in *fmr1* KO mice. These data provide a number of novel insights into memory deficits in FXS, suggesting in particular that PNNs may be the most pertinent cellular structure predictive of deficient fear-memory association. Summary of data in Fig.3.13.

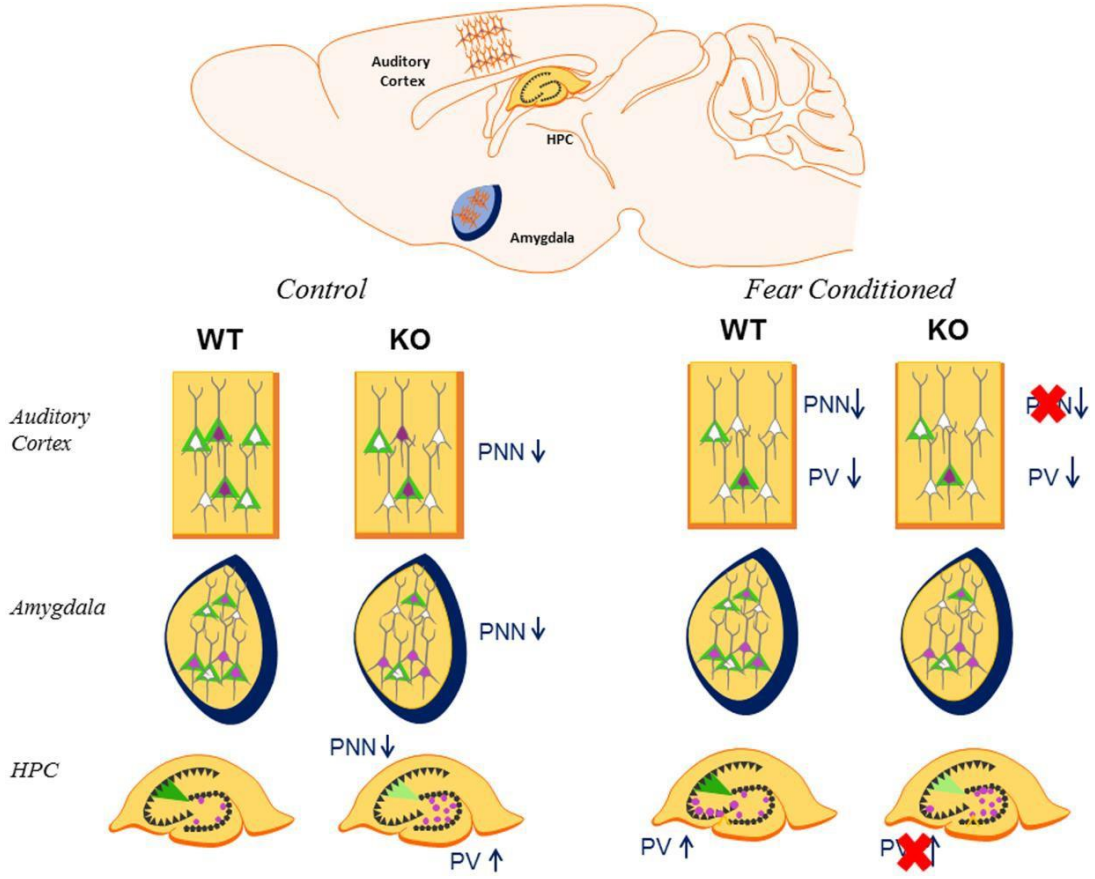

Figure 3.13: Summary of the effect of fear conditioning on PV and PNN in WT and FXS mice. In control conditions, *fmr1* KO mice have reduced PNN density in the auditory cortex and amygdala as well as reduced PNN intensity in CA2. Conversely, PV cell density is increased in DG of *fmr1* KO mice. After fear conditioning, WT mice had decreased PV cell density and decreased PNN density in the auditory cortex (superficial layers). *Fmr1* KO mice did not show PNN modulation in the AC. In the CA3 hippocampus, WT mice showed increased PV density in CA3 which was impaired in *fmr1* KO mice. Amygdala had no measurable changes in response to

We found impaired tone-associated fear memory in *fmr1* KO mice. As demonstrated by the meta-analysis, the overall lower freezing in *fmr1* KO mice is consistent with previous studies, although it might have been expected that both context and tone recall would be impaired. Reduced freezing after fear conditioning parallels human studies that found reduced activation of the amygdala in people with FXS in response to fearful stimuli (Kim et al., 2014; Hessl et al., 2007; Hessl et al., 2011). The reduced activation correlated with higher levels of anxiety (Kim et al., 2014) and with *FMR1* gene expression. Studies of anxiety disorders outside of the FXS population instead have found that people with anxiety disorders tend to have increased amygdala activation (reviewed in Shin and Liberzon, 2010), and potentiation of fear responses (Duits et al., 2015; Lissek et al., 2005). If it is generally true that people with anxiety have hyperactivation of amygdala while people with FXS tend to have hypo-activation, it's possible that mechanisms which drive anxiety are fundamentally different in FXS.

4.1 Behavioral performance in *fmr1* KO mice and relationship to FXS

In addition to freezing, we classified and scored other behaviors (Coimbra et al., 2017; Cruz et al., 1994; Rodgers & Johnson, 1995) to determine if *fmr1* KO mice displayed an alternate anxiety-related behavior in place of complete immobility. We found that *fmr1* KO mice display a similar range of behaviors as WT mice, but they do not modify them to the extent that WT mice do after fear conditioning. In *fmr1* KO mice, the observed changes were always attenuated compared to WT mice. Additionally, WT mice change their behavior profile when the tone is played in the training context, preferring freeing over all other behaviors when environmental cues are the most

predicative of shock. However, this was not observed in *fmr1* KO mice. The behavior "scanning" as defined here is consistent with the "orienting" or "risk assessment" (reviewed in: Blanchard et al., 2011; Roelfs, 2017). Risk assessment behaviors such as "scanning/ orienting" are thought to occur after a potential threat is detected. They help an animal choose the best defensive behavior for survival, including flight if there is an escape route, hiding if there is shelter, or freezing if neither flight nor hiding is possible. When both the tone and contextual cues were present WT mice switch from risk assessment behaviors to the defensive behavior of freezing, while the *fmr1* KO mice do not show this shift in behavior. This is consistent with reports of behavioral inflexibility in FXS and autism (Amodeo et al., 2012; Gross et al., 2015; Kramvis et al., 2013; reviewed in Santos et al., 2014).

4.2 PNN density in FXS

Both auditory cortex and amygdala play a role in the acquisition and/or consolidation of the tone-associated memory. Here we present novel data that both of these regions have reduced PNN density in adult *fmr1* KO mice compared to WT mice, consistent with their impaired tone-associated memory. In the auditory cortex, intact PNNs are necessary for the consolidation of auditory fear conditioning (Banerjee et al., 2017). In the visual cortex, PNNs are implicated in consolidation of remote fear conditioned memories using visual cues (Thompson et al., 2017). Likewise, PNNs in the amygdala have been shown to "protect" an established memory from erasure after the fear memory has undergone an extinction protocol (Gogolla et al., 2009). In our study, the reduced PNN density in both of these regions was correlated with impaired freezing

during the tone memory recall, whereas PV density showed no correlation with behavioral performance. This suggests that restoration of PNN density in *fmr1* KO mice may be a promising target for improving behavioral performance in FXS.

There is a growing body of work suggesting a role for matrix metalloproteinase-9 (MMP-9) in FXS symptoms (reviewed in Reinhard et al., 2015). MMP-9 is an enzyme which is elevated in FXS and which may break-down PNN structures by cleaving ECM components. Genetically reducing MMP-9 levels in *fmr1* KO mice using heterozygous MMP-9 KO mice crossed with *fmr1* KO mice rescues PNN formation in the developing auditory cortex of *fmr1* KO mice (Wen et al., 2018a). To confirm whether reduced PNN levels in adult *fmr1* KO mice have a causal role in impaired fear memory consolidation, future studies could pharmacologically inhibit MMP-9 in *fmr1* KO mice during a fear conditioning protocol using an MMP-9 inhibitor. As PNNs are implicated in stabilizing neuronal circuits involved in memory consolidation (Banerjee et al., 2017; Gogolla et al., 2009; Happel et al. 2014; Hylin et al., 2013; Xue et al., 2014), our data suggest that reduced number of cells containing PNNs observed in both auditory cortex and amygdala of *fmr1* KO mice may underlie impaired memory consolidation in *fmr1* KO mice.

4.3 Modification of AC in fear conditioning and FXS

PNN density, specifically in the superficial layers of AC, decreased in WT mice after fear conditioning. Such plasticity in PNN density was not seen in *fmr1* KO mice. Modification of superficial layers in WT mice is consistent with the known modification of circuitry in the auditory cortex in response to fear conditioning, where cholinergic input activates intracortical inhibition of layer 2/3 PV cells to disinhibit pyramidal cells

(Letzkus et al., 2011) causing a shift in their receptive fields for better representation of the conditioning tone (Froemke et al., 2007). Our data suggest that PNN plasticity in the superficial layers of AC may be involved in this circuit modification process after fear conditioning.

There is a large body of work that identifies impaired PV cell function and/or expression in *fmr1* KO mice across many brain regions (Selby et al., 2007; Patel et al., 2013; Gibson et al., 2008; Olmos-Serrano et al., 2010; Martin et al., 2014; Wen et al., 2018a). Therefore, we predicted impaired modification and/or impaired expression of PV in interneurons of *fmr1* KO mice associated with fear conditioning. Our data show the novel finding that fear conditioning was associated with reduced number of cells expressing PV in the auditory cortex, particularly PV cells without PNN, but this modification was observed in both WT and *fmr1* KO mice. The reduction in PV cell density in the auditory cortex is consistent with the previously mentioned cholinergic-induced disinhibitory microcircuit, wherein PV cells are inhibited in the auditory cortex after fear conditioning to allow for potentiation of responses to the conditioning tone stimulus (Letzkus et al., 2011). PV cells slowly regain perisomal inhibition onto excitatory cells within a 2hr time frame after stimulation (Froemke et al., 2007). The reduction in PV cell density observed in this study is likely a reflection of reduced PV protein within inhibitory cells (Filice et al., 2016) in response to their sustained inhibition, making them less detectable with fluorescence imaging after IHC. The parameters involved in regulating PV protein expression after a change in network excitation/inhibition have not been determined, but it is clear that PV cells and/or PV

protein expression are modulated in response to fear conditioning and environmental enrichment in the hippocampus (Donato et al., 2013) and after developmental manipulations in the auditory cortex (de Villers-Sidani et al., 2007) and the visual cortex (Tropea e al., 2006). Intracellular signaling pathways within PV cells are activated within only 20 min of sound stimulation (Cohen et al., 2016). In our study presented here we observed reduced PV levels in both WT and *fmr1* KO mice suggesting these changes are less likely to contribute to reduced tone-associated memory observed in *fmr1* KO mice.

4.4 The hippocampal circuit

4.4.1. PV changes in DG and CA3

The role of inhibition is important for the flow of information within the hippocampus. Information typically flows from the entorhinal cortex (EC) into the dentate gyrus granule cells, with some projections from EC also innervating CA3 and CA2 (reviewed in Jones and McHugh, 2011). The DG is thought to be involved in pattern separation, in part due to the small population of cells activated by EC input which form non-overlapping populations for memory encoding. If inhibition is either largely increased or decreased in DG there is impaired spatial learning, indicating that if too many or too few DG granule cells are active, there is improper encoding of discrete contexts. Strong inhibition within the DG is thought to limit the population of activated of granule cells, thereby controlling the memory trace (reviewed in Fournier and Duman, 2013). In support of this, there is indeed strong activation of inhibition during novel context exploration (Nitz and McNaughton, 2003). From the DG, mossy fiber terminals

innervate both excitatory and inhibitory cells in CA3, but contact a larger percentage of inhibitory cells (Acsady et al., 1998). This again suggests strong regional inhibition controls the population of cells coding for a memory in CA3.

In this study we observed an attenuated shift in behaviors in *fmr1* KO mice during contextual recall. Although it did not result in significantly impaired total freezing, *fmr1* KO mice showed reduced anxiety-like behaviors such as scanning during contextual recall. This reduction of response to the context was accompanied by modest changes in PV expression in DG and CA3 hippocampus in *fmr1* KO mice and differential regulation of PNNs between WT and *fmr1* KO mice.

Beginning with the region of input into the hippocampus, we found increased PV density in the DG of *fmr1* KO mice. This was particularly pronounced after naïve or fear conditioning. This adds to a body of work indicating impaired function and morphology in the DG of FXS mice (reviewed in Bostrom et al., 2016; Ivanco and Greenough, 2002; Scharkowski et al. 2018; Zhang et al., 2017). DG is known to respond to novel contexts (Davis, 2004; Moser, 1996; Straube et al., 2003) and also plays a role in pattern completion (reviewed in Knierim 2015), spatial learning and memory (Andrews-Zwilling et al., 2012). The enhanced PV expression in DG of *fmr1* KO mice may also explain impaired up-regulation of PV in CA3 of *fmr1* KO mice following contextual learning due to a lower excitatory input from DG to CA3 inhibitory neurons.

There were observable changes to PV density in response to fear conditioning in the CA3 region of the hippocampus in WT but not in *fmr1* KO mice. The increased PV density in WT mice is consistent with a previous report which demonstrated increased

intensity of PV expression after fear conditioning in CA3 (Donato et al., 2013). Activation of PV cells controlled performance on a hippocampal dependent memory task and demonstrated that levels of PV in the CA3 relate to behavioral performance (Donato et al., 2013). However, environmental enrichment reduced PV intensity (Donato et al., 2013), which might be at odds with the increase in PV density in our naïve conditioned mice.

4.4.2. CA2 and PNNs

Information flows next from CA3 through CA2 and into CA1. CA2 is beginning to be recognized as having an important role in hippocampal-dependent memory, and in our data we observed that both PNN intensity and PV density were modulated in response to naïve or fear conditioning. CA2 synapses do not show long-term potentiation in response to Schaffer's collateral (CA3) stimulation, but instead CA3 mediates long-term depression of CA2 inhibitory cells synapsing onto CA2 excitatory cells (Nasrallah et al., 2015). In contrast to this disinhibitory effect of CA3 input into CA2, stimulation of Schaffer's collateral terminals (CA3 axons) causes reliable long-term potentiation in CA1. This highlights the important but variable role that inhibition plays within each region of the hippocampus.

We also observed reduced ECM levels under basal conditions in the CA2 of *fmr1* KO mice. PNN structures within CA2 are thought to inhibit synaptic potentiation (Carstens et al., 2016), therefore reduced ECM intensity in *fmr1* KO mice may suggest increased excitability in CA2 which would also be an interesting avenue for future

studies. Neither CA2 nor DG showed modification of PV or PNNs specifically in response to fear conditioning.

4.4.3. PNN changes are dynamic

Although we did not observe modulation of PV or PNN in CA1 after fear conditioning in the tone-context experiment (30 min after contextual recall), significant changes were seen in the context-tone experiment 4 h after contextual recall. A similar phenomenon was observed in the DG of mice in the context-tone experiment. This differential modulation between experiments suggests that CA1 hippocampus is more dynamic in responding to alterations in the context, and possibly independent of the fear-associated component of the context. This is also consistent with a role for dorsal CA1 in context-specific memories and ventral CA1 in social and fear related memories (Fanselow and Dong, 2010). It has been noted that 'global remapping' of a context can take place in hippocampus after changes to an environment (reviewed in Knierim 2015) and observations presented here are consistent with CA1 and DG modifying their circuits in order to "update" the context memory after the animal has re-experienced the context without the shock. Strikingly changes in CA1 and DG 4 h after context re-exposure were quite similar: PV cell density was reduced in fear conditioned mice, while modification of PNN in WT and *fmr1* KO occurred in opposite directions (increased PNNs in WT and decreased PNNs in *fmr1* KO mice). This again confirms the idea that PNN regulation is disrupted in *fmr1* KO mice.

References

Acsady, L., Kamondi, A., Sık, A., Freund, T., Buzsáki, G., (1998). GABAergic cells are the major postsynaptic targets of mossy fibers in the rat hippocampus. *Journal of neuroscience,* **18**, 3386–3403.

Amodeo, D.A., Jones, J.H., Sweeney, J.A., Ragozzino, M.E., (2012). Differences in BTBR T+ tf/J and C57BL/6J mice on probabilistic reversal learning and stereotyped behaviors. *Behavioural Brain Research,* **227**, 64–72. https://doi.org/10.1016/j.bbr.2011.10.032

Anderson, L.A., Christianson, G.B., Linden, J.F., (2009). Mouse auditory cortex differs from visual and somatosensory cortices in the laminar distribution of cytochrome oxidase and acetylcholinesterase. *Brain Research,* **1252**, 130–142. https://doi.org/10.1016/j.brainres.2008.11.037

Andreatta, M., Glotzbach-Schoon, E., Mühlberger, A., Schulz, S.M., Wiemer, J., Pauli, P., (2015). Initial and sustained brain responses to contextual conditioned anxiety in humans. *Cortex,* **63**, 352–363. https://doi.org/10.1016/j.cortex.2014.09.014

Andrews-Zwilling, Y., Gillespie, A.K., Kravitz, A.V., Nelson, A.B., Devidze, N., Lo, I., Yoon, S.Y., Bien-Ly, N., Ring, K., Zwilling, D., Potter, G.B., Rubenstein, J.L.R., Kreitzer, A.C., Huang, Y., (2012). Hilar GABAergic Interneuron Activity Controls Spatial Learning and Memory Retrieval. *PLoS ONE*, **7**, e40555. https://doi.org/10.1371/journal.pone.0040555

Antunes, R., Moita, M.A., (2010). Discriminative auditory fear learning requires both tuned and nontuned auditory pathways to the amygdala. *Journal of Neuroscience,* **30**, 9782–9787. https://doi.org/10.1523/JNEUROSCI.1037-10.2010

Bailey, D.B., Raspa, M., Olmsted, M., Holiday, D.B., (2008) Co-occurring conditions associated with *FMR1* gene variations: Findings from a national parent survey. *American Journal of Medical Genetics Part A*, **146A**, 2060–2069. https://doi.org/10.1002/ajmg.a.32439

Bakker, C.E., Oostra, B.A., (2003). Understanding fragile X syndrome: insights from animal models. *Cytogenetic and Genome Research,* **100**, 111–123. https://doi.org/10.1159/000072845

Balmer, T.S., (2016). Perineuronal nets enhance the excitability of fast-spiking neurons. *eNeuro,* **3**. https://doi.org/10.1523/ENEURO.0112-16.2016

Banerjee, S.B., Gutzeit, V.A., Baman, J., Aoued, H.S., Doshi, N.K., Liu, R.C., Ressler, K.J., (2017). Perineuronal nets in the adult sensory cortex are necessary for fear learning. *Neuron*, **95**, 169-179.e3. https://doi.org/10.1016/j.neuron.2017.06.007

Blanchard, D.C., Griebel, G., Pobbe, R., Blanchard, R.J., (2011). Risk assessment as an evolved threat detection and analysis process. *Neuroscience & Biobehavioral Reviews,* **35**, 991–998. https://doi.org/10.1016/j.neubiorev.2010.10.016

Bostrom, C., Yau, S., Majaess, N., Vetrici, M., Gil-Mohapel, J., Christie, B.R., (2016). Hippocampal dysfunction and cognitive impairment in Fragile-X Syndrome. *Neuroscience & Biobehavioral Reviews,* **68**, 563–574. https://doi.org/10.1016/j.neubiorev.2016.06.033

Çalışkan, G., Müller, I., Semtner, M., Winkelmann, A., Raza, A.S., Hollnagel, J.O., Rösler, A., Heinemann, U., Stork, O., Meier, J.C., (2016). Identification of parvalbumin interneurons as cellular substrate of fear memory persistence. *Cerebral Cortex,* **26**, 2325–2340. https://doi.org/10.1093/cercor/bhw001

Carstens, K.E., Phillips, M.L., Pozzo-Miller, L., Weinberg, R.J., Dudek, S.M., (2016). Perineuronal nets suppress plasticity of excitatory synapses on CA2 pyramidal neurons. *The Journal of Neuroscience,* **36**, 6312–6320. https://doi.org/10.1523/JNEUROSCI.0245-16.2016

Castrén, M., Pääkkönen, A., Tarkka, I.M., Ryynänen, M., Partanen, J., (2003). Augmentation of auditory N1 in children with fragile X syndrome. *Brain topography,* **15**, 165–171.

Cohen, S.M., Ma, H., Kuchibhotla, K.V., Watson, B.O., Buzsáki, G., Froemke, R.C., Tsien, R.W., (2016). Excitation-transcription coupling in parvalbumin-positive interneurons employs a novel CaM Kinase-dependent pathway distinct from excitatory neurons. *Neuron,* **90**, 292–307. https://doi.org/10.1016/j.neuron.2016.03.001

Coimbra, N.C., Paschoalin-Maurin, T., Bassi, G.S., Kanashiro, A., Biagioni, A.F., Felippotti, T.T., Elias-Filho, D.H., Mendes-Gomes, J., Cysne-Coimbra, J.P., Almada, R.C., Lobão-Soares, B., (2017). Critical neuropsychobiological analysis of panic attack- and anticipatory anxiety-like behaviors in rodents confronted with snakes in polygonal arenas and complex labyrinths: a comparison to the elevated

plus- and T-maze behavioral tests. *Revista Brasileira de Psiquiatria,* **39**, 72–83. https://doi.org/10.1590/1516-4446-2015-1895

Cordeiro, L., Ballinger, E., Hagerman, R., Hessl, D., (2011). Clinical assessment of DSM-IV anxiety disorders in fragile X syndrome: prevalence and characterization. *Journal of Neurodevelopmental Disorders,* **3**, 57–67. https://doi.org/10.1007/s11689-010-9067-y

Cornish, K.M., Munir, F., Cross, G., (2001). Differential impact of the FMR-1 full mutation on memory and attention functioning: a neuropsychological perspective. *Journal of Cognitive Neuroscience,* **13**, 144–150.

Courtin, J., Chaudun, F., Rozeske, R.R., Karalis, N., Gonzalez-Campo, C., Wurtz, H., Abdi, A., Baufreton, J., Bienvenu, T.C.M., Herry, C., (2014). Prefrontal parvalbumin interneurons shape neuronal activity to drive fear expression. *Nature,* **505**, 92–96. https://doi.org/10.1038/nature12755

Cruz, A.P.M., Frei, F., Graeff, F.G., (1994). Ethnopharmacological analysis of rat behavior on the elevated plus-maze. *Pharmocology Biochemistry and Behavior,* **49**, 171–176.

Dahlhaus, R., (2018). Of Men and Mice: Modeling the Fragile X Syndrome. *Frontiers in Molecular Neuroscience,* **11**. https://doi.org/10.3389/fnmol.2018.00041

Daumas, S., (2005). Encoding, consolidation, and retrieval of contextual memory: Differential involvement of dorsal CA3 and CA1 hippocampal subregions. *Learning & Memory*, **12**, 375–382. https://doi.org/10.1101/lm.81905

Davis, C.D., (2004). Novel environments enhance the induction and maintenance of long-term potentiation in the dentate gyrus. *Journal of Neuroscience,* **24**, 6497–6506. https://doi.org/10.1523/JNEUROSCI.4970-03.2004

de Diego-Otero, Y., Romero-Zerbo, Y., el Bekay, R., Decara, J., Sanchez, L., Rodriguez-de Fonseca, F., del Arco-Herrera, I., (2009). α-tocopherol protects against oxidative stress in the fragile X knockout mouse: an experimental therapeutic approach for the Fmr1 deficiency. *Neuropsychopharmacology,* **34**, 1011.

Dityatev, A., Brückner, G., Dityateva, G., Grosche, J., Kleene, R., Schachner, M., (2007). Activity-dependent formation and functions of chondroitin sulfate-rich extracellular matrix of perineuronal nets. *Developmental Neurobiology,* **67**, 570– 588. https://doi.org/10.1002/dneu.20361

Dobkin, C., Rabe, A., Dumas, R., El Idrissi, A., Haubenstock, H., Brown, W.T., (2000). Fmr1 knockout mouse has a distinctive strain-specific learning impairment. *Neuroscience,* **100**, 423–429.

Donato, F., Rompani, S.B., Caroni, P., (2013). Parvalbumin-expressing basket-cell network plasticity induced by experience regulates adult learning. *Nature,* **504**, 272–276. https://doi.org/10.1038/nature12866

Duits, P., Cath, D.C., Lissek, S., Hox, J.J., Hamm, A.O., Engelhard, I.M., van den Hout, M.A., Baas, J.M.P., (2015). Updated meta-analysis of classical fear conditioning in the anxiety disorders. *Depression and Anxiety,* **32**, 239–253. https://doi.org/10.1002/da.22353

Dziembowska, M., Pretto, D.I., Janusz, A., Kaczmarek, L., Leigh, M.J., Gabriel, N., Durbin-Johnson, B., Hagerman, R.J., Tassone, F., (2013). High MMP-9 activity levels in fragile X syndrome are lowered by minocycline. *American Journal of Medical Genetics Part A*, **161**, 1897–1903. https://doi.org/10.1002/ajmg.a.36023

Eadie, B.D., Cushman, J., Kannangara, T.S., Fanselow, M.S., Christie, B.R., (2012). NMDA receptor hypofunction in the dentate gyrus and impaired context discrimination in adult Fmr1 knockout mice. *Hippocampus*, **22**, 241–254. https://doi.org/10.1002/hipo.20890

Esclassan, F., Coutureau, E., Di Scala, G., Marchand, A.R., (2009). Differential contribution of dorsal and ventral hippocampus to trace and delay fear conditioning. *Hippocampus,* **19**, 33–44. https://doi.org/10.1002/hipo.20473

Fanselow, M.S., Dong, H.-W., (2010). Are the dorsal and ventral hippocampus functionally distinct structures? *Neuron*, **65**, 7–19. https://doi.org/10.1016/j.neuron.2009.11.031

Favuzzi, E., Marques-Smith, A., Deogracias, R., Winterflood, C.M., Sánchez-Aguilera, A., Mantoan, L., Maeso, P., Fernandes, C., Ewers, H., Rico, B., (2017). Activity-dependent gating of parvalbumin interneuron function by the perineuronal net protein brevican. *Neuron*, **95**, 639-655.e10. https://doi.org/10.1016/j.neuron.2017.06.028

Filice, F., Vörckel, K.J., Sungur, A.Ö., Wöhr, M., Schwaller, B., (2016). Reduction in parvalbumin expression not loss of the parvalbumin-expressing GABA interneuron

subpopulation in genetic parvalbumin and shank mouse models of autism. *Molecular Brain*, **9**. https://doi.org/10.1186/s13041-016-0192-8

Fournier, N.M., Duman, R.S.,(2013). Illuminating hippocampal control of fear memory and anxiety. *Neuron*, **77**, 803–806. https://doi.org/10.1016/j.neuron.2013.02.017

Froemke, R.C., Merzenich, M.M., Schreiner, C.E., (2007). A synaptic memory trace for cortical receptive field plasticity. *Nature*, **450**, 425.

Gibson, J.R., Bartley, A.F., Hays, S.A., Huber, K.M., (2008). Imbalance of neocortical excitation and inhibition and altered UP states reflect network hyperexcitability in the mouse model of fragile X syndrome. *Journal of Neurophysiology,* **100**, 2615–2626. https://doi.org/10.1152/jn.90752.2008

Gogolla, N., Caroni, P., Lüthi, A., Herry, C., (2009). Perineuronal nets protect fear memories from erasure. *Science*, **325**, 1258–1261.

Hagerman, R.J., Hagerman, P.J., (2002). The fragile X premutation: into the phenotypic fold. *Current opinion in genetics & development,* **12**, 278–283.

Happel, M.F.K., Niekisch, H., Castiblanco Rivera, L.L., Ohl, F.W., Deliano, M., Frischknecht, R., (2014). Enhanced cognitive flexibility in reversal learning induced by removal of the extracellular matrix in auditory cortex. *Proceedings of the National Academy of Sciences,* **111**, 2800–2805. https://doi.org/10.1073/pnas.1310272111

Hessl, D., Rivera, S., Koldewyn, K., Cordeiro, L., Adams, J., Tassone, F., Hagerman, P.J., Hagerman, R.J., (2007). Amygdala dysfunction in men with the fragile X premutation. *Brain,* **130**, 404–416. https://doi.org/10.1093/brain/awl338

Hessl, D., Wang, J.M., Schneider, A., Koldewyn, K., Le, L., Iwahashi, C., Cheung, K., Tassone, F., Hagerman, P.J., Rivera, S.M., (2011). Decreased fragile X mental retardation protein expression underlies amygdala dysfunction in carriers of the fragile X premutation. *Biological Psychiatry*, **70**, 859–865. https://doi.org/10.1016/j.biopsych.2011.05.033

Hylin, M.J., Orsi, S.A., Moore, A.N., Dash, P.K., (2013). Disruption of the perineuronal net in the hippocampus or medial prefrontal cortex impairs fear conditioning. *Learning & Memory,* **20**, 267–273. https://doi.org/10.1101/lm.030197.112

Ivanco, T.L., Greenough, W.T., (2002). Altered mossy fiber distributions in adultFmr1 (FVB) knockout mice. *Hippocampus*, **12**, 47–54. https://doi.org/10.1002/hipo.10004

Jones, M.W., McHugh, T.J., (2011). Updating hippocampal representations: CA2 joins the circuit. *Trends in Neurosciences*, **34**, 526–535. https://doi.org/10.1016/j.tins.2011.07.007

Kim, S.-Y., Burris, J., Bassal, F., Koldewyn, K., Chattarji, S., Tassone, F., Hessl, D., Rivera, S.M., (2014). Fear-specific amygdala function in children and adolescents on the fragile X spectrum: A dosage response of the FMR1 gene. *Cerebral Cortex*, **24**, 600–613. https://doi.org/10.1093/cercor/bhs341

Knierim, J. J., (2015). The hippocampus. *Current Biology*, **25**, R1107–R1125.

Kooy, R.F., D'Hooge, R., Reyniers, E., Bakker, C.E., Nagels, G., De Boulle, K., Storm, K., Clincke, G., De Deyn, P.P., Oostra, B.A., (1996). Transgenic mouse model for the fragile X syndrome. *American journal of medical genetics*, **64**, 241–245.

LaBar, K.S., Gatenby, J.C., Gore, J.C., LeDoux, J.E., Phelps, E.A., (1998). Human amygdala activation during conditioned fear acquisition and extinction: a mixed-trial fMRI study. *Neuron*, **20**, 937–945.

Lee, I., Kesner, R.P., (2004). Differential contributions of dorsal hippocampal subregions to memory acquisition and retrieval in contextual fear-conditioning. *Hippocampus*, **14**, 301–310. https://doi.org/10.1002/hipo.10177

Lee, H., Leamey, C.A., Sawatari, A., (2012). Perineuronal nets play a role in regulating striatal function in the mouse. *PLoS One,* **7**, e32747.

Letzkus, J.J., Wolff, S.B.E., Meyer, E.M.M., Tovote, P., Courtin, J., Herry, C., Lüthi, A., (2011). A disinhibitory microcircuit for associative fear learning in the auditory cortex. *Nature*, **480**, 331–335. https://doi.org/10.1038/nature10674

Lissek, S., Powers, A.S., McClure, E.B., Phelps, E.A., Woldehawariat, G., Grillon, C., Pine, D.S., (2005). Classical fear conditioning in the anxiety disorders: a meta-analysis. *Behavior Research and Therapy,* **43**, 1391–1424.

Lovelace, J.W., Wen, T.H., Reinhard, S., Hsu, M.S., Sidhu, H., Ethell, I.M., Binder, D.K., Razak, K.A., (2016). Matrix metalloproteinase-9 deletion rescues auditory evoked potential habituation deficit in a mouse model of Fragile X Syndrome. *Neurobiology of Disease,* 89, 126–135. https://doi.org/10.1016/j.nbd.2016.02.002

Martin, B.S., Corbin, J.G., Huntsman, M.M., (2014). Deficient tonic GABAergic conductance and synaptic balance in the fragile X syndrome amygdala. *Journal of Neurophysiology*, **112**, 890–902. https://doi.org/10.1152/jn.00597.2013

McRae, P.A., Rocco, M.M., Kelly, G., Brumberg, J.C., Matthews, R.T.,(2007). Sensory deprivation alters aggrecan and perineuronal net expression in the mouse barrel cortex. *Journal of Neuroscience,* **27**, 5405–5413. https://doi.org/10.1523/JNEUROSCI.5425-06.2007

Miller, L.J., McIntosh, D.N., McGrath, J., Shyu, V., Lampe, M., Taylor, A.K., Tassone, F., Neitzel, K., Stackhouse, T., Hagerman, R.J., (1999). Electrodermal responses to sensory stimuli in individuals with fragile X syndrome: a preliminary report. *American journal of medical genetics,* **83**, 268–279.

Morrison, D.J., Rashid, A.J., Yiu, A.P., Yan, C., Frankland, P.W., Josselyn, S.A., (2016). Parvalbumin interneurons constrain the size of the lateral amygdala engram. *Neurobiology of Learning and Memory,* **135**, 91–99. https://doi.org/10.1016/j.nlm.2016.07.007

Moser, E.I., (1996). Altered inhibition of dentate granule cells during spatial learning in an exploration task. *Journal of Neuroscience,* **16**, 1247–1259.

Nasrallah, K., Piskorowski, R.A., Chevaleyre, V., (2015). Inhibitory plasticity permits the recruitment of CA2 pyramidal neurons by CA3. *eNeuro,* **2**. https://doi.org/10.1523/ENEURO.0049-15.2015

Nitz, D., McNaughton, B., (2004). Differential modulation of CA1 and dentate gyrus interneurons during exploration of novel environments. *Journal of Neurophysiology*, **91**, 863–872. https://doi.org/10.1152/jn.00614.2003

Oddi, D., Subashi, E., Middei, S., Bellocchio, L., Lemaire-Mayo, V., Guzmán, M., Crusio, W.E., D'amato, F.R., Pietropaolo, S., (2015). Early social enrichment

rescues adult behavioral and brain abnormalities in a mouse model of fragile X syndrome. *Neuropsychopharmacology*, **40**, 1113.

Ognjanovski, N., Schaeffer, S., Wu, J., Mofakham, S., Maruyama, D., Zochowski, M., Aton, S.J.,(2017). Parvalbumin-expressing interneurons coordinate hippocampal network dynamics required for memory consolidation. *Nature Communications,* **8**, 15039. https://doi.org/10.1038/ncomms15039

Olmos-Serrano, J.L., Corbin, J.G., Burns, M.P., (2011). The $GABA_A$ receptor agonist THIP ameliorates specific behavioral deficits in the mouse model of fragile X syndrome. *Developmental Neuroscience,* **33**, 395–403. https://doi.org/10.1159/000332884

Olmos-Serrano, J.L., Paluszkiewicz, S.M., Martin, B.S., Kaufmann, W.E., Corbin, J.G., Huntsman, M.M.,(2010). Defective GABAergic neurotransmission and pharmacological rescue of neuronal hyperexcitability in the amygdala in a mouse model of fragile X syndrome. *Journal of Neuroscience,* **30**, 9929–9938. https://doi.org/10.1523/JNEUROSCI.1714-10.2010

Paradee, W., Melikian, H.E., Rasmussen, D.L., Kenneson, A., Conn, P.J., Warren, S.T., (1999). Fragile X mouse: strain effects of knockout phenotype and evidence suggesting deficient amygdala function. *Neuroscience*, **94**, 185–192.

Patel, A.B., Hays, S.A., Bureau, I., Huber, K.M., Gibson, J.R., (2013). A target cell-specific role for presynaptic Fmr1 in regulating glutamate release onto neocortical fast-spiking inhibitory neurons. *Journal of Neuroscience,* **33**, 2593–2604. https://doi.org/10.1523/JNEUROSCI.2447-12.2013

Peier, A.M.,McIlwain, K.L., Kenneson, A., Warren, S.T., Paylor, R., Nelson, D. L., (2000). (Over)correction of FMR1 deficiency with YAC transgenics: behavioral and physical features. *Human Molecular Genetics,* **9**, 1145-59.

Phillips, R.G., LeDoux, J.E., (1992). Differential contribution of amygdala and hippocampus to cued and contextual fear conditioning. *Behavioral neuroscience,* **106**, 274.

Pizzorusso, T., Medini, P., Berardi, N., Chierzi, S., Fawcett, J.W., Maffei, L., (2002). Reactivation of ocular dominance plasticity in the adult visual cortex. *Science*, **298**, 1248–1251.

Quirk, G.J., Armony, J.L., LeDoux, J.E., (1997). Fear conditioning enhances different temporal components of tone-evoked spike trains in auditory cortex and lateral amygdala. *Neuron*, **19**, 613–624.

Raybuck, J.D., Lattal, K.M., (2011). Double dissociation of amygdala and hippocampal contributions to trace and delay fear conditioning. *PLoS ONE,* **6**, e15982. https://doi.org/10.1371/journal.pone.0015982

Reinhard, S.M., Razak, K., Ethell, I.M., (2015). A delicate balance: role of MMP-9 in brain development and pathophysiology of neurodevelopmental disorders. *Frontiers in Cellular Neuroscience,* **9**. https://doi.org/10.3389/fncel.2015.00280

Rodgers, R.J., Johnson, N.J.T.,(1995). Factor analysis of spatiotemporal and ethological measures in the murine elevated plus-maze test of anxiety. *Pharmocology Biochemistry and Behavior,* **52**, 297–303.

Roelofs, K., (2017). Freeze for action: neurobiological mechanisms in animal and human freezing. *Philosophical Transactions of the Royal Society B: Biological Sciences,* **372**, 20160206. https://doi.org/10.1098/rstb.2016.0206

Romero-Zerbo, Y., Decara, J., el Bekay, R., Sanchez-Salido, L., Del Arco-Herrera, I., de Fonseca, F.R., de Diego-Otero, Y., (2009). Protective effects of melatonin against oxidative stress in Fmr1 knockout mice: a therapeutic research model for the fragile X syndrome. *Journal of Pineal Research,* **46**, 224–234. https://doi.org/10.1111/j.1600-079X.2008.00653.x

Rosnow, R.L., Rosenthal, R., Rubin, D.B., (2000). Contrasts and correlations in effect-size estimation. *Psychological science,* **11**, 446–453.

Roy, D.S., Kitamura, T., Okuyama, T., Ogawa, S.K., Sun, C., Obata, Y., Yoshiki, A., Tonegawa, S., (2017). Distinct neural circuits for the formation and retrieval of episodic memories. *Cell*, **170**, 1000-1012.e19. https://doi.org/10.1016/j.cell.2017.07.013

Santoro, M.R., Bray, S.M., Warren, S.T., (2012). Molecular mechanisms of fragile X syndrome: A twenty-year perspective. *Annual Review of Pathology: Mechanisms of Disease*, **7**, 219–245. https://doi.org/10.1146/annurev-pathol-011811-132457

Scharkowski, F., Frotscher, M., Lutz, D., Korte, M., Michaelsen-Preusse, K., (2017). Altered connectivity and synapse maturation of the hippocampal mossy fiber pathway in a mouse model of the fragile X syndrome. *Cerebral Cortex*. https://doi.org/10.1093/cercor/bhw408

Selby, L., Zhang, C., Sun, Q.-Q., (2007). Major defects in neocortical GABAergic inhibitory circuits in mice lacking the fragile X mental retardation protein. *Neuroscience Letters,* **412**, 227–232. https://doi.org/10.1016/j.neulet.2006.11.062

Shin, L.M., Liberzon, I., (2010). The neurocircuitry of fear, stress, and anxiety disorders. *Neuropsychopharmacology,* **35**, 169–191.

Sidhu, H., Dansie, L.E., Hickmott, P.W., Ethell, D.W., Ethell, I.M., (2014). Genetic removal of matrix metalloproteinase 9 rescues the symptoms of fragile X syndrome in a mouse model. *Journal of Neuroscience,* **34**, 9867–9879. https://doi.org/10.1523/JNEUROSCI.1162-14.2014

Spencer, C.M., Serysheva, E., Yuva-Paylor, L.A., Oostra, B.A., Nelson, D.L., Paylor, R., (2006). Exaggerated behavioral phenotypes in Fmr1/Fxr2 double knockout mice reveal a functional genetic interaction between Fragile X-related proteins. *Human Molecular Genetics*, **15**, 1984–1994. https://doi.org/10.1093/hmg/ddl121

Straube, T., Korz, V., Frey, J.U., (2003). Bidirectional modulation of long-term potentiation by novelty-exploration in rat dentate gyrus. *Neuroscience Letters,* **344**, 5–8. https://doi.org/10.1016/S0304-3940(03)00349-5

Sullivan, K., Hooper, S., Hatton, D., (2007). Behavioral equivalents of anxiety in children with fragile X syndrome: parent and teacher report. *Journal of Intellectual Disability Research*, **51**, 54–65. https://doi.org/10.1111/j.1365-2788.2006.00899.x

Thomas, A.M., Bui, N., Graham, D., Perkins, J.R., Yuva-Paylor, L.A., Paylor, R., (2011). Genetic reduction of group 1 metabotropic glutamate receptors alters select

behaviors in a mouse model for fragile X syndrome. *Behavioural Brain Research,* **223**, 310–321. https://doi.org/10.1016/j.bbr.2011.04.049

Thompson, E.H., Lensjø, K.K., Wigestrand, M.B., Malthe-Sørenssen, A., Hafting, T., Fyhn, M., (2018). Removal of perineuronal nets disrupts recall of a remote fear memory. *Proceedings of the National Academy of Sciences,* **115**, 607–612. https://doi.org/10.1073/pnas.1713530115

Tropea, D., Kreiman, G., Lyckman, A., Mukherjee, S., Yu, H., Horng, S., Sur, M., (2006). Gene expression changes and molecular pathways mediating activity-dependent plasticity in visual cortex. *Nature Neuroscience,* **9**, 660–668. https://doi.org/10.1038/nn1689

Trouche, S., Sasaki, J.M., Tu, T., Reijmers, L.G., (2013). Fear extinction causes target-specific remodeling of perisomatic inhibitory synapses. *Neuron*, **80**, 1054–1065. https://doi.org/10.1016/j.neuron.2013.07.047

Ueno, H., Takao, K., Suemitsu, S., Murakami, S., Kitamura, N., Wani, K., Okamoto, M., Aoki, S., Ishihara, T., (2018). Age-dependent and region-specific alteration of parvalbumin neurons and perineuronal nets in the mouse cerebral cortex. *Neurochemistry International,* **112**, 59–70. https://doi.org/10.1016/j.neuint.2017.11.001

Van Dam, D., d'Hooge, R., Hauben, E., Reyniers, E., Gantois, I., Bakker, C.E., Oostra, B.A., Kooy, R.F., De Deyn, P.P., (2000). Spatial learning, contextual fear conditioning and conditioned emotional response in Fmr1 knockout mice. *Behavioural brain research,* **117**, 127–136.

Wen, T.H., Afroz, S., Reinhard, S.M., Palacios, A.R., Tapia, K., Binder, D.K., Razak, K.A., Ethell, I.M., (2018a). Genetic reduction of matrix metalloproteinase-9 promotes formation of perineuronal nets around parvalbumin-expressing interneurons and normalizes auditory cortex responses in developing Fmr1 knock-out mice. *Cerebral Cortex,* **28**, 3951–3964. https://doi.org/10.1093/cercor/bhx258

Wen, T.H., Binder, D.K., Ethell, I.M., Razak, K.A., (2018b). The perineuronal 'safety' net? Perineuronal net abnormalities in neurological disorders. *Frontiers in Molecular Neuroscience*, **11**. https://doi.org/10.3389/fnmol.2018.00270

Wolff, S.B.E., Gründemann, J., Tovote, P., Krabbe, S., Jacobson, G.A., Müller, C., Herry, C., Ehrlich, I., Friedrich, R.W., Letzkus, J.J., Lüthi, A., (2014). Amygdala interneuron subtypes control fear learning through disinhibition. *Nature*, **509**, 453–458. https://doi.org/10.1038/nature13258

Xue, Y.-X., Xue, L.-F., Liu, J.-F., He, J., Deng, J.-H., Sun, S.-C., Han, H.-B., Luo, Y.-X., Xu, L.-Z., Wu, P., Lu, L., (2014). Depletion of perineuronal nets in the amygdala to enhance the erasure of drug memories. *Journal of Neuroscience,* **34**, 6647–6658. https://doi.org/10.1523/JNEUROSCI.5390-13.2014

Yoo, H., (2015). Genetics of autism spectrum disorder: Current status and possible clinical applications. *Experimental Neurobiology,* **24**, 257. https://doi.org/10.5607/en.2015.24.4.257

Zhang, N., Peng, Z., Tong, X., Lindemeyer, A.K., Cetina, Y., Huang, C.S., Olsen, R.W., Otis, T.S., Houser, C.R., (2017). Decreased surface expression of the δ subunit of the GABA A receptor contributes to reduced tonic inhibition in dentate granule

cells in a mouse model of fragile X syndrome. *Experimental Neurology,* **297**, 168–178. https://doi.org/10.1016/j.expneurol.2017.08.008

Chapter 4:

Distinct effects of Developmental Noise Exposure on Inhibitory Cells and Perineuronal Nets in the Primary and Anterior Auditory Fields

Abstract

Within the auditory cortex, there are two primary-like regions considered to be 'core' cortical fields, the primary auditory cortex (A1) and the anterior auditory field (AAF). Both fields have sharp frequency tuning, tonotopic organization, and inputs from the ventral medial geniculate body of the thalamus. AAF seems to be more specialized for faster spectrotemporal processing than A1, but the underlying mechanisms are unclear. A1 has been studied extensively in developmental plasticity, but how AAF changes with developmental experience is less clear. To address potential cellular correlates of differences between the two fields we performed immunohistochemistry and quantified the density of GABA, parvalbumin (PV), and somatostatin (SOM) cells in A1 and AAF of mice. We also characterized differences between the density of perineuronal nets (PNN) in the two fields, a specialized assembly of extracellular matrix involved in network maturation and plasticity. Finally, we compared the effects of developmental noise exposure on inhibitory and PNN cell density in these two core regions. In adult mice there were more PNNs surrounding cell bodies in AAF than in A1, suggesting a potential cellular basis for fast spectrotemporal processing in mature AAF. Moderate level noise exposure during early development leads to 1) increased GABA and SOM cell density in both A1 and AAF, 2) modification of PV density in A1 that was attenuated in AAF, and 3) decreased PNN cell density in A1, but not AAF. Inhibitory cells without PNN appear to be more susceptible to changes following developmental noise exposure in both fields. Results are consistent with altered cortical gain control models and

impaired maturation of cortex in response to noisy environments, and suggest that PV cells and PNNs may be more prone to modification in A1 than AAF.

Abbreviations:

Anterior auditory field (AAF), Parvalbumin positive interneurons (PV), Perineuronal nets (PNN), Primary auditory cortex (A1), Somatostatin positive interneurons (SOM)

1. Introduction

The auditory cortex is composed of multiple fields that are delineated based on sources of inputs and outputs, tonotopy, and response selectivity. Of these, there are two 'core' auditory fields, the primary auditory cortex (A1) and the anterior auditory field (AAF), both of which receive inputs from the lemniscal auditory pathway. The response characteristics of A1 and AAF are well conserved across various species studied (Kaas, 2011). Both regions have short latency responses, peaked tuning curves and a tonotopic organization (Hackett et al., 2011; Polley et al., 2007; Stiebler et al., 1997). However, AAF appears to be better adapted for fast temporal processing than A1. This differentiation is based on shorter first spike latency and stronger selectivity for fast frequency and amplitude modulated sounds (Phillips and Irvine, 1982; Schreiner and Urbas, 1988; Tian and Rauschecker, 1994; Trujillo et al., 2011). The cellular bases for differential temporal properties between AAF and A1 are not known.

While a number of studies have addressed early auditory plasticity in A1 following developmental acoustic exposure (de Villers-Sidani et al., 2008; Insanally et al., 2009; Ranasinghe et al., 2012; reviewed in Sanes and Bao, 2009), relatively little is known about plasticity in AAF. Therefore, it is unclear if A1 and AAF show similar plasticity following developmental critical period manipulations. In early deaf cats, AAF becomes responsive to somatosensory and visual stimuli, while A1 does not (Meredith and Lomber, 2011), indicating the two regions respond differentially after a loss of peripheral input (Wong et al., 2015). On the other hand, administration of salicylate in adolescent mice causes modification of both A1 and AAF within 2 hours of

administration, including a shift in best frequency (BF) and decreased neural activation (Yanagawa et al., 2017). Exposing mice to tones also induces plasticity in both A1 and AAF, causing increased response amplitude and area of response to the exposure tone (Takahashi et al., 2006). However, AAF was altered only after early exposure (P0 – adolescence) while changes in A1 occurred after developmental or adult sound exposure (Takahashi et al., 2006).

Moderate level, continuous noise exposure in adults induces changes in the auditory cortex in a manner that suggests altered gain control to account for overstimulation (studies in cats; Pienkowski et al 2011; Pienkowski et al., 2013; Reviewed in Eggermont, 2017). When noise exposure takes place during the auditory critical period (CP), closure of developmental windows may be delayed until noise exposure ends (study in rats; de Villers-Sidani et al., 2008). Supporting the idea of a delayed CP closure, developmental noise exposure prevents the shift in GABA-A and NMDA receptor subunit composition (studies in rats; Xu et al., 2010, Sun et al., 2011). Band-limited noise reduced the density of cortical (A1) parvalbumin (PV) positive inhibitory neurons only within the exposed band frequency representation (de Villers-Sidani et al., 2008). Additionally, the balance of thalamocortical potentiation and depression at A1 synapses is altered to favor potentiation after developmental noise exposure (study in rats; Speechley et al., 2007). Though the balance of excitation and inhibition is clearly altered after noise exposure in A1, it is not clear what population of inhibitory cells may be particularly affected or whether AAF is susceptible to similar circuit modifications.

Inhibitory cells, particularly PV cells, are associated with perineuronal nets (PNNs). PNNs are specialized assemblies of an extracellular matrix. They typically form around cell bodies and proximal dendrites beginning in the second to third postnatal week in mouse cortex, a time window that coincides with critical periods (Nowicka et al., 2009; Wen et al., 2017; Ye and Miao, 2013; reviewed in Hensch, 2005) and maturation of cortical inhibitory properties (Oswald and Reyes, 2011). PNNs shape the fast spiking characteristics of PV+ interneurons (Balmer, 2016; Favuzzi et al., 2017) and protect PV neurons from oxidative stress (Cabungcal et al. 2013). They are implicated in plasticity as well as synaptic re-organization (Beurdeley et al., 2012, Happel et al., 2014, Favuzzi et al., 2017). In the visual cortex PNN development is delayed when mice are dark-reared (Ye and Miao, 2013), a manipulation which is thought to delay the onset of the critical period. Delayed PNN maturation also occurs after whisker trimming in somatosensory cortex (McRae et al., 2007). It remains unknown if PNN density is altered in the auditory cortex after moderate level continuous noise exposure, and if A1 and AAF are differently susceptible. Differences in PNNs between A1 and AAF may cause differences in firing properties of PV cells, which are involved in shaping the receptive field properties underlying fast spectrotemporal selectivity (Atencio and Schreiner, 2008).

To address these questions we compare the expression of somatostatin (SOM), PV and GABA in A1 and AAF of mouse auditory cortex. We characterize the density of PNNs surrounding SOM, PV and GABA inhibitory cells. Finally, we tested the effect of moderate noise exposure during auditory development (P9-P30) on the density of PNNs and inhibitory cells in A1 and AAF.

2. Methods

2.1 Mice

FVB.129P2-Pde6b^{+} Tyr$^{c\text{-}ch}$/AntJ mice ('sighted' FVB mice) were obtained from Jackson laboratories and housed in an accredited vivarium on a 12-hour light/dark cycle. Food and water were provided *ad libitum*. All procedures were approved by the Institutional Animal Care and Use Committee at the University of California, Riverside. The total number of mice used in this study was: 10 P60 controls, 10 P30 Controls, 11 P30 Naïve (sound attenuated chamber), and 11 P30 noise-exposed. 5-6 mice per condition were used for each inhibitory cell marker assessed, and PNNs were co-labeled with each. SOM and GABA experiments were performed on the same mouse tissue (consecutive slices; GABA, SOM, etc.), while PV experiments were performed with separate mice, making comparison of relative percentages of each inhibitory cell impractical.

2.2 Noise Exposure

Mice termed 'control' were raised under normal vivarium conditions. 'Naïve' and 'noise exposed' mice were raised in a sound-attenuating chamber (ambient noise ~35 dB SPL; dimensions 4'L x 4'W x 3'H) from P5 until the time of recording (P30). The room where the chamber was housed was accessed only for daily animal inspection and weekly cleaning, with a background room noise of ~55dB. Mice within the chamber were on a 12-hour light/dark cycle and were inspected daily for visible signs of health. Mice in the chamber were raised either with no additional sounds played (naïve) or were exposed to a ~70 dB continuous broadband noise from P9-P30. To minimize stress on

dams, the noise was stepped up to 70 dB over 2 days, from 50 dB when pups were P9, to 60 dB at P10, and finally 70 dB (P11). White noise stimulus was generated (Audacity software) and played using a speaker (UltraSoundGate Player BL Light; RECORDER USGH software; Avisoft Bioacoustics) mounted to the center of the chamber. Frequency spectrum of the white noise was from 40 Hz to 20 kHz. The intensity level of the noise was measured within a standard mouse cage placed inside the chamber (BK Precision 732A Sound Level Meter).

2.3 Mapping

The auditory cortex was mapped for tonotopy using multi-unit recordings to delineate A1 and AAF. For surgery and mapping of the auditory cortex, mice were anesthetized with a ketamine (10mg/mL) and xylazine mixture (1.35 mg/mL) with half dose supplements as needed. The right auditory cortex, identified based on coordinates from bregma and vascular landmarks, was exposed using a dental drill. Experiments were conducted in a sound-attenuating room (Gretch-Ken Industries Inc.) lined with anechoic foam. Acoustic stimulation and data acquisition were driven by custom software and Microstar digital signal processing system. Sounds were delivered with a calibrated free-field speaker (UltraSoundGate Player BL Light) located 6" and 45° from the left ear, contralateral to recording sites. Glass electrodes (1 M NaCl, 2-10 MΩ impedance) were advanced (Kopf 2660) to cortical depths between 300-500 μm from pia (layers III-IV) to record sound-driven responses. Multi-unit recordings were used to identify the characteristic frequency (CF; the frequency at which a neuron is excited at the lowest intensity tested) of a given neuron. The boundary between A1 and AAF was

determined based on the characteristic shift in tonotopy from A1 to AAF (A1: low to high CF; AAF: high to low CF; caudal to rostral). Once the mirror shift in tonotopy was determined, Fluoro-Ruby was iontophoretically injected (Stoelting Co.; 10 minutes at 4μA, 7s on/7s off) in the middle of the transition zone to mark the boundary between A1 and AAF. The mice were then sacrificed with a fatal injection of sodium pentobarbital for perfusion and tissue processing.

2.4 Immunohistochemistry

Mice were perfused transcardially with cold phosphate-buffered saline (PBS, 0.1 M) and 4% paraformaldehyde (PFA). Brains were removed and post-fixed for 24 hours in 4% PFA, followed by cryoprotection with 30% sucrose (in 0.1M PBS) for 48 hours. Brains were sectioned into 50 μm-thick coronal sections using a cryostat (Leica CM 1860). For each mouse, a full well plate (24 consecutive slices) was processed for free-floating immunohistochemistry. Slices were processed for IHC over a period of two days. On day 1, slices were washed in 0.1M PBS (2 x 5 min.). Slices were then quenched with 50 mM Ammonium Chloride (NH_4Cl; in 0.1M PBS) for 15 minutes, followed by washing (3 x 10 min 0.1M PBS) and permeabilization with 0.1% Triton X (10 min). The slices were incubated in a blocking solution with 5% Normal Goat Serum (NGS; Vector Laboratories) and 1% Bovine Serum Albumin (BSA; Fisher Scientific) in 0.1M PBS solution. For GABA and SOM staining, 0.1% Triton was added to the blocking buffer. Finally, the slices were incubated overnight on a shaker at 4°C with primary antibodies and Wisteria floribunda agglutinin (WFA) in a 1% NGS, 0.5% BSA, and 0.1% Tween solution. Antibodies used include rabbit-anti parvalbumin (1:1000; SWANT PV25),

rabbit-anti GABA (1:200; Sigma Life Sciences A2052) and rat-anti Somatostatin (1:150; Santa Cruz BiotechnologiesYC7). WFA (1:500; Vector Laboratories; Green Fluorescein Wisteria Floribunda Lectin FL 1351) is a lectin, which stains chondroitin sulfate proteoglycan glycosaminoglycan side chains in PNNs (Pizzorusso et al., 2002). Day 2 began with 3 washes (x10 min) in 0.5% Tween. Next, the slices were incubated in secondary antibody for 1 hour at room temperature. Secondary antibodies used were Alexa donkey-anti rabbit 594 (1:500; Invitrogen), Alexa donkey anti-rabbit 647 (1:1000; Invitrogen) and Alexa rabbit anti-rat 594 (1:500; Invitrogen). Slices were then washed with 0.5% Tween twice for 10 minutes, followed by a final wash in 0.1M PBS for 10 minutes, mounted in Vectashield with DAPI (Vector Labs), and cover-slipped with Cytoseal (ThermoScientific).

After slices were mounted, the boundary between A1 and AAF was identified as the slice(s) with the brightest Fluoro-Ruby staining. Slices used for analysis were taken 100-300 μm outside of the boundary region (1-3 slices on either side of the brightest slice(s) were not used), as this is likely the transition zone between A1 and AAF. 6-8 slices rostral to the border (AAF) and 6-8 slices caudal to the border (A1) were used for imaging and counting.

Slices were imaged using Leica SP5 confocal microscope (10x objective). Imaged Z-stacks covering 18 μm (1 μm step size) were acquired and summed projections were created in ImageJ. ImageJ was used to count the number of PNN positive cells, the number of PV/GABA/SOM positive cells, and the number of cells co-localized with PNN and an inhibitory marker by a blinded observer. A box of 500μm width and

spanning from pia to white matter was used as the window of analysis. The boundary between layer 4 and 5 of the auditory cortex was identified as in Anderson et al. (2009) to identify potential differences between superficial (1-4) and deep (5-6) layers.

2.5 Data Analysis

A two-way ANOVA with Bonferroni corrected post-hoc analysis was used to compare between brain regions (A1/AAF) vs. layers (deep/superficial) for Figures 4.1-4.3; brain region vs. exposure condition (control, naïve, noise-exposed) for Figures 4.4-4.5; and layers vs. exposure condition for Figures 4.6- 4.8.

3. Results

3.1 Adult mice have higher PNN cell density in AAF than in A1, but equivalent GABA cell density.

Figure 4.1 shows photomicrographs of coronal sections containing A1 (Fig. 4.1A, 1B) and AAF (Fig. 4.1C) stained for GABA and PNN from control mice at P60 age. GABA antibody labeled cells across all cortical layers while PNN was most dense in layers 4 and 5. Magnified image of PNN surrounding the cell body and proximal dendrites can be seen in Figure 4.1D. In P60 mice, no difference was observed in GABA cell density (all cell density values below is in cells/mm^2) between A1 (501.7 ± 31) and AAF (482.9 ± 22.3; $F(1) = 0.2239$, $p = 0.637$; Fig. 4.1E). There was also no difference between the superficial and deep layers ($F(1) = 0.3752$, $p = 0.542$) either in A1 (Layers 1-4 = 487.9 ± 37.6, Layers 5-6: = 515.5 ± 30.2) or AAF (Layers 1-4 = 511.2 ± 26.6, Layers 5-6 = 454.7 ± 25.7). However, PNN cell density was higher in AAF compared to A1 (A1 = 113.04 ± 0.7; AAF = 128.39 ± 4.1; $F(1) = 7.161$, $p = 0.0079$; Fig. 4.1F).

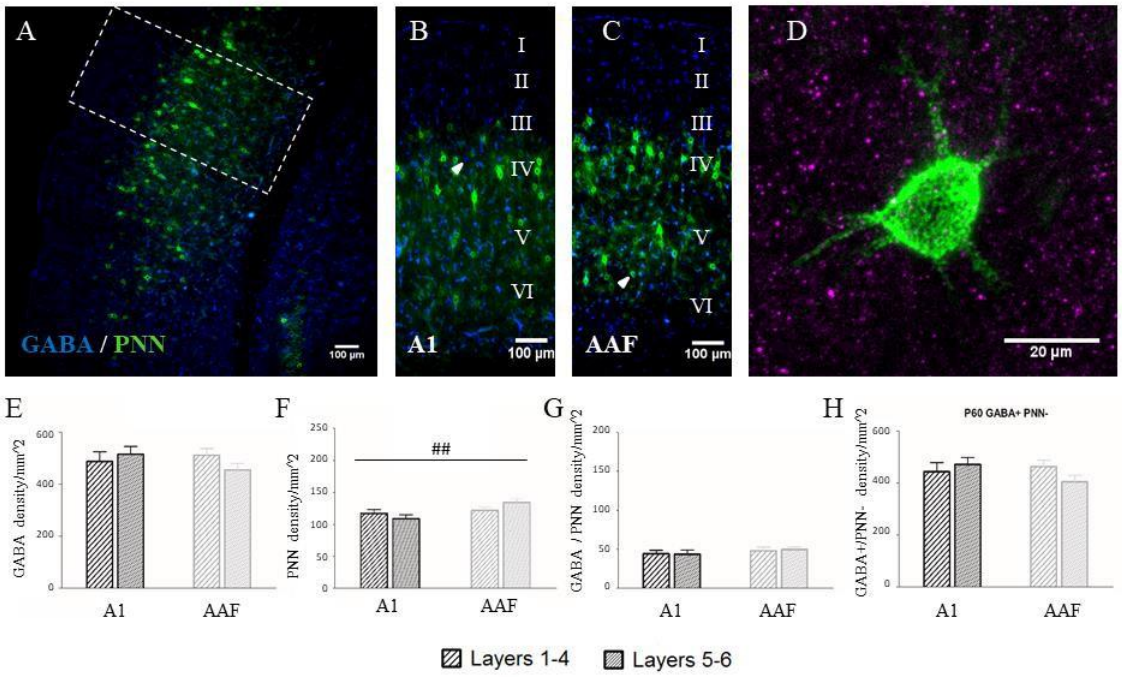

Figure 4.1. Adult mice have more PNN in the AAF than A1, but similar levels of GABA across both regions. A) Example image of a coronal A1 section taken from a P60 mouse stained with GABA (blue) and WFA (green). Box insert represents area used for analysis. B) Cropped example of A1 and (C) AAF taken from the same mouse. D) Example of a PNN structure stained with WFA. E) GABA density is similar across all layers, and is expressed in similar levels in both A1 and AAF. F) PNN density was higher in AAF than in A1, but was expressed at similar levels across the layers of cortex. G) Density of GABA cells surrounded with PNNs (white arrow in C). H) Density of GABA expressing cells without PNNs (white arrow in B). H) N: GABA = 5 mice, PNN = 10 mice; N # Images = **GABA** A1: 21, AAF: 20; **PNN** A1: 62, AAF: 72. Legend: #: between brain region, *: paired comparison between layers; * = 0.05, ** = 0.01, *** = 0.001.

PNNs were expressed in similar levels across superficial and deep layers in both A1 (Layers 1-4 = 117.3 ± 0.73, Layers 5-6 = 108.8 ± 0.8) and AAF (Layers 1-4 = 121.9 ± 4.8, Layers 5-6 = 134.4 ± 5.6; F(1) 0.128, p = 0.72). These data show that AAF contains a higher PNN cell density than A1.

Two subsets of GABA neurons were counted; those surrounded by PNNs (GABA/PNN+, Fig. 4.1G) and those without PNNs (GABA/PNN-, Fig. 4.1H). Neither

type of GABA cell showed a difference between A1 (GABA/PNN+ = 43.863 ± 4; GABA/PNN- = 457.882 ± 28.2) and AAF (GABA/PNN+ = 48.765 ± 3.2; GABA/PNN- = 434.126 ± 20.7; effect of brain region: GABA/PNN+: $F(1) = 0.011$, $p = 0.915$; GABA/PNN-: $F(1) = 0.279$, $p = 0.598$). There was also no difference in the expression of these cell types between layers (effect of layer: GABA/PNN+: $F(1) = 1.156$, $p = 0.285$; GABA+/PNN-: $F(1) = 0.697$, $p = 0.4$). Together, these results show that one major difference between A1 and AAF is in the density of PNN ensheathed cells.

3.2 PV cells are more abundant in deep versus superficial layers of both A1 and AAF

PV cells comprise the largest percentage of GABA expressing neurons. The characteristic fast-spiking properties of PV cells are implicated in maintaining the fast temporal dynamics necessary in auditory processing. As such, the density of PV cells was compared between A1 and AAF. Figure 4.2 shows coronal sections of A1 (Fig. 4.2B) and AAF (Fig. 4.2A, 4.2C) stained for PV and PNN. PV is not expressed in layer 1 and only sparsely labels layers 2 and 3. Statistical analysis revealed that PV-expressing cells were more abundant in the deep layers of auditory cortex compared to superficial layers (Fig. 4.2D). This was true both in A1 (Layer 1-4 = 83.47, ± 7.3, Layers 5-6 = 113.185 ± 8.8) and AAF (Layers 1-4 = 97.31 ± 4.6, Layers 5-6 = 119.1 ± 7.5; $F(1) = 12.79$, $p = 0.0005$). Across all layers, A1 and AAF had comparable levels of PV cell density (effect of brain region: $F(1) = 1.884$, $p = 0.172$; Fig. 4.2E). PV cells that were surrounded by PNNs were expressed in similar numbers across all layers (effect of layer:

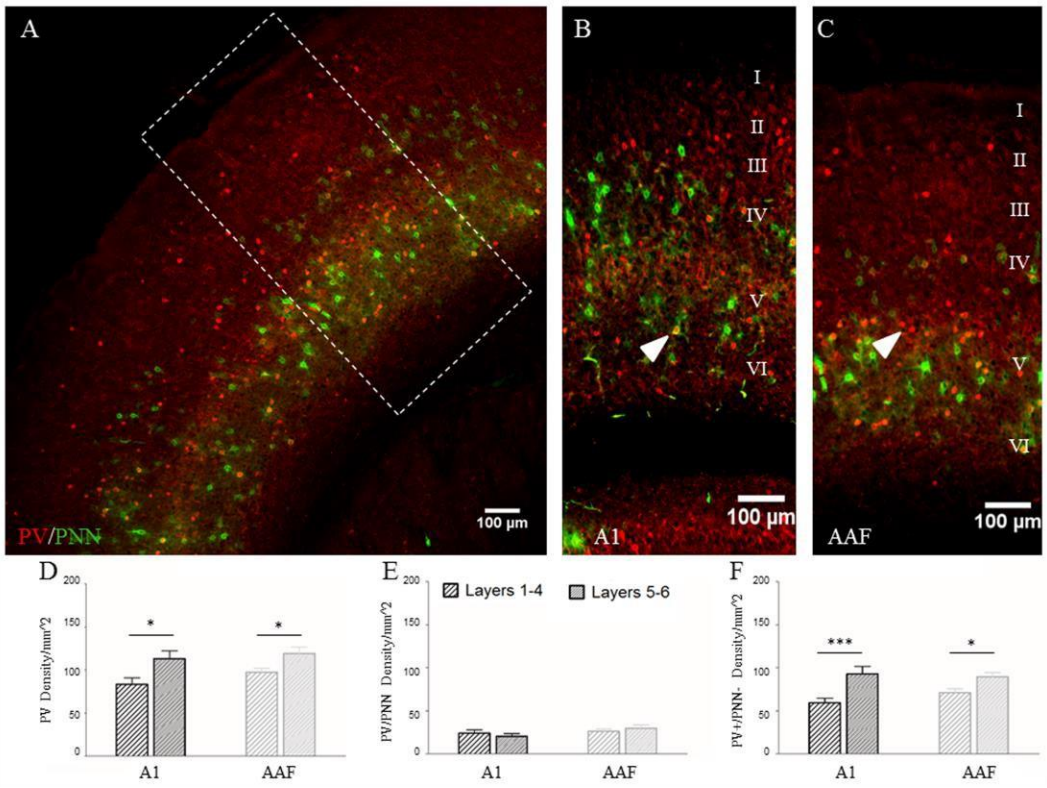

Figure 4.2. Adult mice have more PV expressing cells in deep layers of the cortex. A) Example image of a coronal AAF section taken from a P60 mouse stained with PV (red) and WFA (green). Box insert represents area used for analysis. B) Cropped example of A1 and (C) AAF taken from the same mouse. D) PV density is greater in deep layers of the cortex, in both A1 and AAF. E) While the density of PV cells surrounded with PNNs (white arrow in B) is the same across layers, (F) the density of PV-expressing cells without PNNs (white arrow in C) is greater in the deeper layers of cortex. N = 5 mice; N # Images = A1: 22, AAF: 33. Legend: # : between brain region, * : paired comparison between layers; * = 0.05, ** = 0.01, *** = 0.001.

F(1) = 0.00001, p = 0.996) and in both A1 (22.254 ± 2.9) and AAF (27.958 ± 3.2; effect of brain region: F(1) = 2.519, p = 0.115) and therefore, did not account for differences seen in the total PV population. On the other hand, more PV cells without PNNs were found in deep layers of A1 (Layers 1-4 = 59.4 ± 5.3, Layers 5-6 = 92.778 ± 8.9) and AAF (Layers 1-4 = 71.183 ± 4.4, Layers 5-6 = 89.325 ± 5.2; F(1) = 18.74 p = 0.0001), likely accounting for the difference in total PV density between superficial and deep layers.

The distribution of PV cells without PNNs was the same in both A1 and AAF ($F(1) = 0.489$, $p = 0.485$; Fig. 4.2F). Together, these data show that PV cells are more abundant in the deeper layers of both A1 and AAF, and that PV cells without PNN may carry this difference.

3.3 There are more SOM cells in deep layers compared to superficial layers of both A1 and AAF in adult mice

Figure 4.3 shows staining for somatostatin and PNN in A1 (Fig. 4.3A, 4.3B) and AAF (Fig. 4.3C). Somatostatin expressing cells are known to be a heterogeneous group of inhibitory cells, some having morphology consistent with Martinotti cells while others are bi-tufted or multipolar cells (reviewed in Yavorska and Wehr, 2016). SOM cells comprise the second largest percentage of inhibitory cells after PV (reviewed in Yavorska and Wehr, 2016). Figure 4.3 shows SOM and PNN cells in A1 (Fig. 4.3A, 4.3B) and AAF (Fig. 4.3C). SOM staining is sparse or absent from layers 1 and 2 and increases in layers 3-6. Differences in morphology between SOM cells is clear even at this magnification, where SOM cells in layers 2 and 3 are smaller with less intense staining compared to layer 6 cells, which tend to be larger and brighter. Similar to what was observed with PV cell density, SOM cells were more abundant in the deep layers of core auditory cortex (Fig. 4.3D). This was true both in A1 (Layer 1-4 = 127.983 ± 5.5, Layers 5-6 = 214.241 ± 8.5) and in AAF (Layers 1-4 = 129.665 ± 8, Layers 5-6 = 218.895 ± 10.8; $F(1) = 107.8$, $p < 0.0001$). Expression of SOM between A1 and AAF was similar (effect of brain region: $F(1) = 0.1406$, $p = 0.708$; Fig. 4.2E). It was also observed that

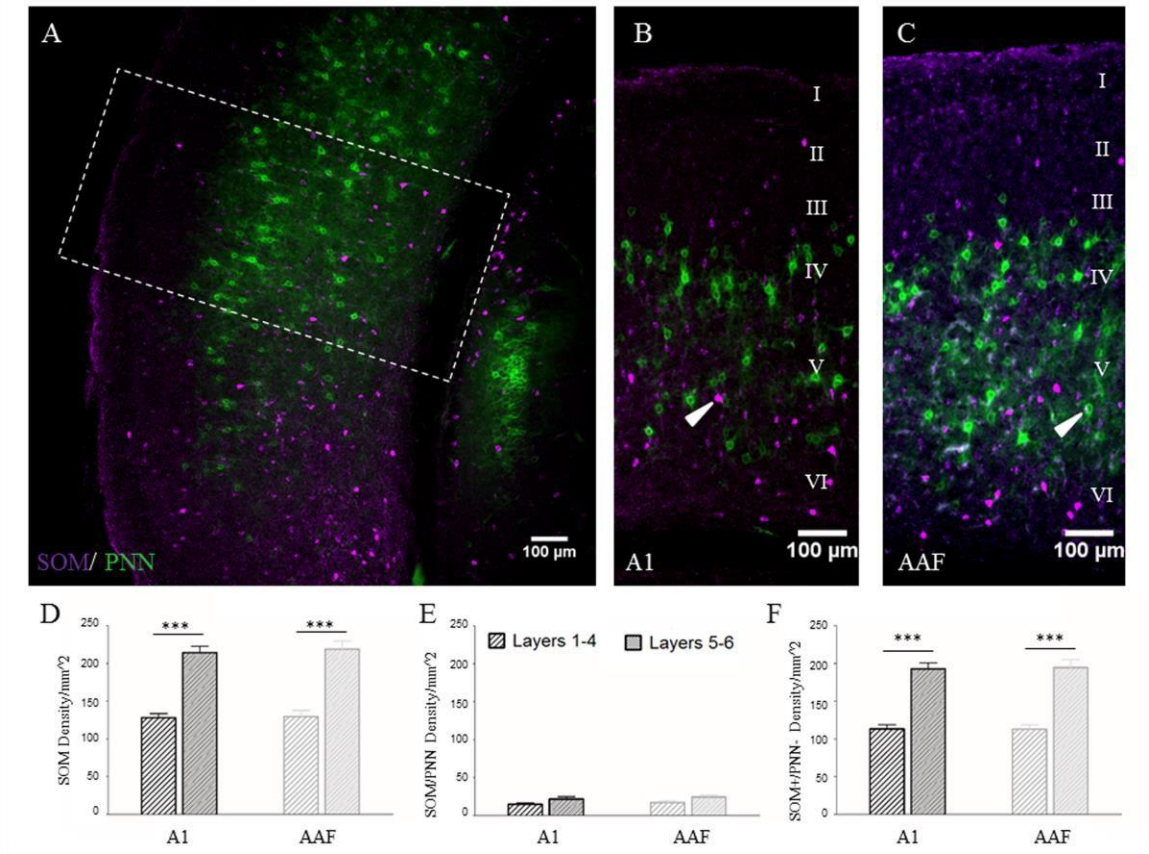

Figure 4.3. Adult mice have more SOM expressing cells in deep layers of the cortex. A) Example image of a coronal A1 section taken from a P60 mouse stained with SOM (magenta) and WFA (green). Box insert represents area used for analysis. B) Cropped example of A1 and (C) AAF taken from the same mouse. D) SOM density is greater in deep layers of the cortex, in both A1 and AAF. E) While the density of SOM cells surrounded with PNNs (white arrow in C) is the same across layers, (F) the density of SOM-expressing cells without PNNs (white arrow in B) is greater in the deeper layers of cortex. N = 5 mice; N # Images = A1: 19, AAF: 19. Legend: # : between brain region, * : paired comparison between layers; * = 0.05, ** = 0.01, *** = 0.001.

some SOM cells had PNNs (% SOM cells with PNN across all layers: 10.5% in A1 and 11.8% in AAF). Such SOM/PNN co-localized cells were denser in deep layers in both A1 (Fig. 4.3E; Layers 1-4 = 14.678 ± 1.66, Layers 5-6 =21.543 ± 3.1) and AAF (Layers 1-4 = 16.771 ± 2.7, Layers 5-6 = 24.277 ± 2.6; effect of layers: $F(1) = 7.619$, $p = 0.0073$),

but paired comparisons in each region alone were not significant. SOM/PNN expression was the same in both A1 (18.12 ± 1.99) and AAF (20.758 ± 1.88; $F(1) = 0.859$, $p = 0.357$). SOM cells without PNNs accounted for a greater proportion of the difference seen among total SOM population (Fig. 4.2F). Density of SOM cells without PNN was higher in deep layers of A1 (Layers 1-4 = 113.3 ± 5.4, Layers 5-6 = 192.698 ± 7.8) and AAF (Layers 1-4 = 112.894 ± 6, Layers 5-6 = 194.618 ± 10.1; $F(1) = 112.7$ $p = 0.0001$), with no overall difference between A1 and AAF ($F(1) = 0.0098$, $p = 0.921$; Fig. 4.3F). Together, these data show that SOM cells are more abundant in the deeper layers of both A1 and AAF. Although the majority of SOM cells were without PNN, ~10-12% of SOM cells in both A1 and AAF were co-localized with PNN.

3.4 Developmental noise exposure leads to decreased PNN density in A1, but not AAF

Figure 4.4 shows example images of control (top panel) and noise exposed mice (bottom panel) stained for GABA, PV, SOM and PNN in the A1. The PNN channel and inhibitory cell channels are shown overlaid as well as individually, to illustrate the effect on individual cell types more clearly. Exposure to a broadband noise (noise exposed, NE) from P9 to P30 led to a reduction in PNN density in A1, but not in AAF (Fig. 4.4S; effect of NE: $F(2) = 4.226$, $p = 0.0151$). This effect was carried by a reduction of PNN density between controls (C) and the noise exposed mice (NE), while there was no difference between mice raised in the sound attenuated chamber (naïve, N) and NE mice (A1: C = 97.92 ± 0.39, N = 91.44 ± 0.45, NE = 84.92 ± 0.317). While AAF showed a

similar trend, paired comparisons showed no difference (AAF: C = 94.02 ± 2.9, N = 86.37 ± 3.4, NE = 87.43 ± 6). Although A1 and AAF showed differential modulation,

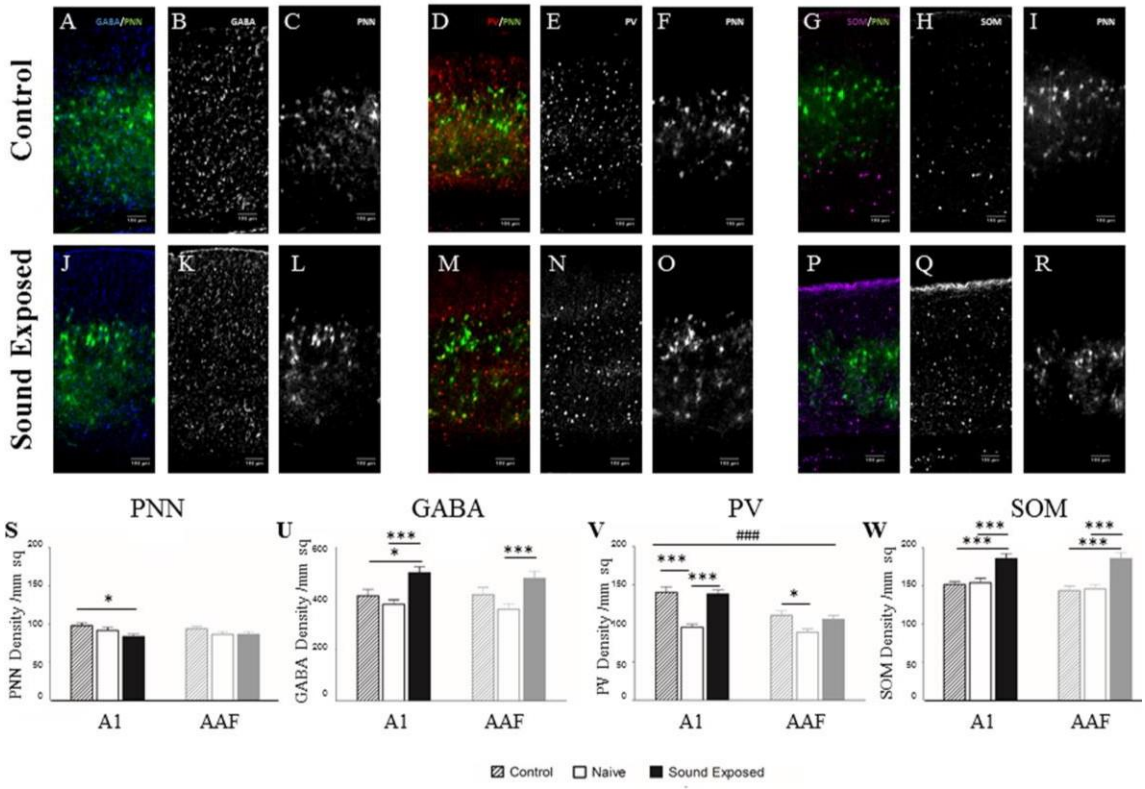

Figure 4.4. Exposing mice to broadband noise increases inhibitory cell density and decreases PNN density. All example images shown here are taken from A1 sections. A) Example of a P30 control mouse stained for GABA (B) and WFA (C) and below that an example of a P30 sound exposed mouse (J) stained for GABA (K) and WFA (L). Images D-F and M-O depict PV/WFA staining, and images G-I and P-R depict SOM/WFA staining. S) Exposure to noise led to a decrease in PNN density in A1 but no change in AAF. U) GABA density and SOM density (W) increased in noise exposed mice both in A1 and in AAF. V) PV density decreased in the A1 region of mice raised in a sound attenuating chamber when compared to control mice raised in a vivarium; after exposure to noise the PV density increased to control levels. PV density in the AAF region did not change in naïve mice, but did increase after noise exposure. N mice **(#images)** = GABA: C = 5 **(A1: 20, AAF: 19)**, N = 6 **(A1: 24, AAF: 27)**, SE = 5 mice **(A1: 20, AAF: 17)**; SOM: C = 5 **(A1: 19, AAF: 19)**, N = 6 **(A1: 21, AAF: 28)**, SE = 5 mice **(A1: 19, AAF: 20)**; PV: C = 5 **(A1: 51, AAF: 50)**, N = 5**(A1: 44, AAF: 42)**, SE = 6 **(A1: 52, AAF: 52)**; PNN: C = 10 **(A1: 90, AAF: 98)**, N = 11 **(A1: 89, AAF: 97)**, SE = 11 **(A1: 94, AAF: 96)**. Legend: # : between brain region, * : paired comparison between conditions; * = 0.05, ** = 0.01, *** = 0.001.

the overall density of PNNs was not different between the two fields (effect of brain region: $F(1) = 0.576$, $p = 0.448$) in these mice. This is not the same trend found in P60 adult mice (data presented in Figure 4.1), which had increased PNN density in AAF compared to A1. Comparison of the P30 control mice to the P60 control mice reveals that the increased PNN density observed in adult AAF develops between P30 and P60 (total PNN density across all layers: P30: A1 = 97.93, AAF = 94.02; P60: A1 = 113, AAF = 128.4; effect of age: $F(1) = 38.03$, $p < 0.0001$; paired comparison between A1 and AAF at P60 $p < 0.05$, at P30 *ns*; paired comparison between P30 and P60 AAF $p < 0.001$, A1 < 0.05; data not shown but compare Fig. 4.1F and Fig. 4.4S). Together, these data show that PNNs increase in density in both A1 and AAF between P30 and P60 with perhaps a faster rate of increase in the AAF. When exposed to noise during development and examined at P30, PNN density is significantly reduced in A1, but not AAF, indicating differential plasticity in the two core auditory fields.

3.5 Developmental noise exposure leads to altered inhibitory cell density in A1 and AAF

Noise exposed mice showed an increase in GABA cell density (effect of NE: $F(2) = 13.98$, $p < 0.0001$). This was true both in A1 (C = 411.182 ± 25.34, N = 378.545 ± 16.9, NE = 502.33 ± 22.8) and in AAF (C = 416.344 ± 28.1, N = 358.25 ± 21, NE = 479.508 ± 27.5). Overall GABA cell densities were similar in A1 and AAF ($F(1) = 0.4321$, $p = 0.512$; Fig. 4.4U).

PV cell density was reduced when mice were raised in the sound attenuating chamber compared to control mice, while NE mice were not different than control (Fig. 4.4V; effect of NE: $F(1) = 21.27$, $p < 0.0001$). This effect was more pronounced in A1

(C = 140.159 ± 6.9, N = 94.764 ± 3.9, NE = 138.05 ± 5.4), than in AAF (C = 110.551 ± 5.7, N = 88.084 ± 4.5, NE = 105.106 ± 5.2). AAF also had overall less PV density than A1 ($F(1) = 26.05$, $p < 0.0001$). This differential PV expression between A1 and AAF was not present in adult P60 mice (data presented in Figure 4.2). When directly comparing P30 controls to P60 control, it was observed that PV density decreases in A1 from P30 to P60, but this change does not take place in AAF (total PV density across all layers: P30 A1 = 141.6, AAF = 108.2; P60 A1 = 98.36, AAF = 110.6; effect of age: $F(1) = 11.39$, $p = 0.0009$; paired comparison between A1 and AAF at P30 $p < 0.001$, at P60 *ns;* paired comparison between P30 and P60 in A1 $p < 0.001$, in AAF *ns*).

In contrast to changes observed with PV cells, SOM cell density modifications were similar to changes observed with GABA after noise exposure. SOM cell density increased after NE (Fig. 4.4W; effect of NE: $F(2) = 25.26$, $p < 0.0001$). Again this increase was found in both A1 (C = 151.658 ± 3.7, N = 154.255 ± 5.5, NE = 185.793 ± 5.9) and AAF (C = 143.857 ± 5.8, N = 145.717 ± 5.6, NE = 185.692 ± 7.4). A1 and AAF had similar levels of SOM overall ($F(1) = 1.291$, $p = 0.258$). Taken together, these data show that PV and SOM cell density show different changes with developmental noise exposure, with PV expression more responsive to the reduced noise environment, while SOM expression was modulated in response to noise exposure. Overall GABA density increases in NE mice, and at least part of this is carried by SOM cell density. A1 and AAF did not show differential plasticity in inhibitory cell type density.

3.6 Inhibitory cells without PNNs are more susceptible to modification after noise exposure

PNNs are thought to have a synaptic stabilization role for the cells that they surround, protecting perisomal synaptic contacts from modification (Favuzzi et al., 2017). We determined if inhibitory cells with and without PNNs are equally susceptible to modification after noise exposure. The density of GABA neurons with PNN showed no change after noise exposure (Fig. 4.5B; $F(2) = 0.05791$, $p = 0.943$) and were expressed similarly in both A1 and AAF ($F(1) = 0.9799$, $p = 0.324$). However, GABA cells without PNNs increased in density after noise exposure (Fig. 4.5C; $F(2) = 15.37$, $p < 0.0001$). This was true both in A1 (C = 380.554 ± 24.6, N =346.665 ± 15.7, NE = 471.403 ± 21.2) and AAF (C = 386.21 ± 26.8, C = 329.57 ± 20.3, NE = 451.405 ± 27.5), with no overall difference in GABA density between the two regions ($F(1) = 0.3217$, $p = 0.571$).

Unlike GABA, PV cells with PNNs decreased in naïve compared to control mice (Fig. 4.5E; effect of NE: $F(2) = 13.94$, $p < 0.0001$) and increased in NE mice in both A1 (C = 35.9 ± 4.5, N =18.06 ± 1.6, NE = 26.987 ± 1.6) and AAF (C = 25.942 ± 2.3, N = 16.05 ± 1.7, NE = 22.956 ± 1.8). AAF also had fewer PV cells with PNNs than A1 ($F(1) = 6.406$, $p = 0.0119$). Among those PV cells without PNNs, changes were observed only in A1 following noise exposure (Fig. 4.5F), where PV cells without PNN decreased in mice compared to controls, but noise exposed mice were the same as controls (effect of NE: $F(2) = 10.76$, $p < 0.0001$; A1: C = 104.254 ± 7.4, N = 76.704 ± 3.3, NE = 111.062 ± 5.2; AAF: C = 84.61 ± 4.3, N = 72.034 ± 3.6, NE = 82.15 ± 4.5). PV without PNNs were also expressed at lower levels in AAF ($F(1) = 17.87$, $p < 0.0001$).

Density of SOM cells with PNNs showed no effect of noise exposure (Fig. 4.5I; $F(2) = 2.570$, $p = 0.08$) and were expressed at similar levels in both A1 and AAF ($F(1) = 0.04230$, $p = 0.837$). But density of SOM cells without PNNs changed with noise exposure (Fig. 4.5J; $F(2) = 23.08$, $p < 0.0001$). Specifically, SOM cell density without PNNs increased in NE mice in both A1 (C = 138.42 ± 3.7, N = 140.477 ± 5.1, NE = 170.407 ± 4.8) and in AAF (C = 130.848 ± 6.1, N = 133.405 ± 5.6, NE = 169.32 ± 7.2), but had similar overall expression in A1 and AAF ($F(1) = 1.265$, $p = 0.263$).

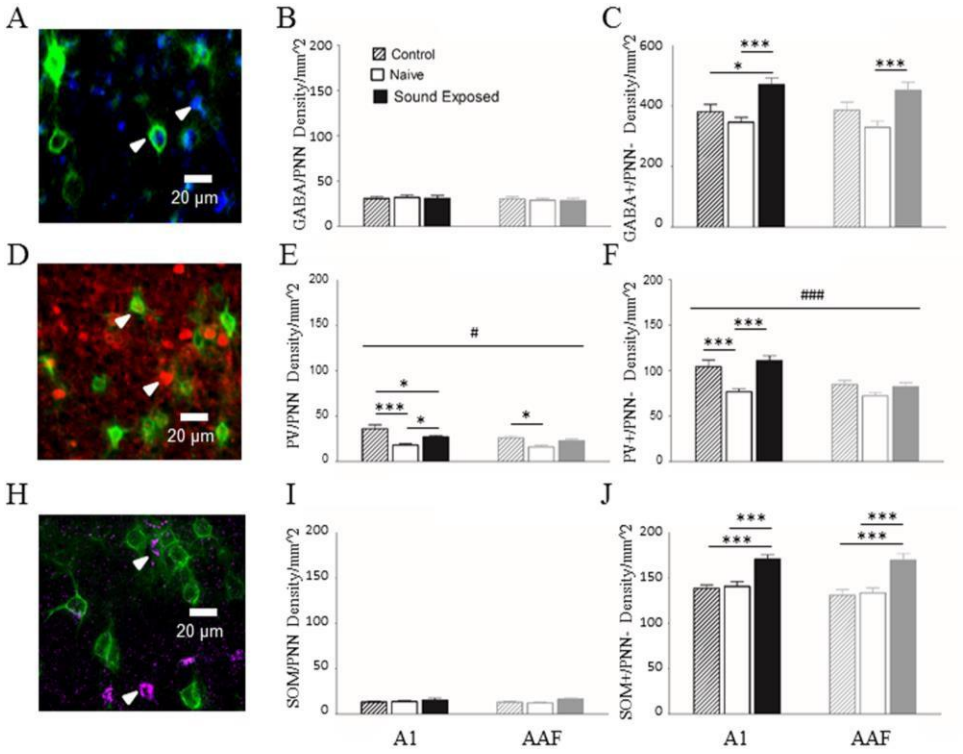

Figure 4.5. Increased inhibitory cell density is occurring in those inhibitory cells without PNN enwrappings. Example images of GABA (A), PV (B) and SOM (H) staining, showing cells both with and without PNNs (white arrows). B) GABA cells enwrapped with PNNs did not show a change after noise exposure, but (C) the density of GABA cells without PNNs increased after noise exposure. This same trend is seen in SOM expressing cells (I and J). PV expressing cells showed modifications of those cells both with (E) and without PNNs (F). N mice **(#images)** = GABA: C = 5 **(A1: 20, AAF: 19)**, N = 6 **(A1: 24, AAF: 27)**, SE = 5 mice **(A1: 20, AAF: 17)**; SOM: C = 5 **(A1: 19, AAF: 19)**, N = 6 **(A1: 21, AAF: 28)**, SE = 5 mice **(A1: 19, AAF: 20)**; PV: C = 5 **(A1: 51, AAF: 50)**, N = 5**(A1: 44, AAF: 42)**, SE = 6 **(A1: 52, AAF: 52)**. Legend: # : between brain region, * : paired comparison between conditions; * = 0.05, ** = 0.01, *** = 0.001.

3.7 Larger decrease in PNN density following noise exposure in deep layers of A1.

We previously observed decreased PNN density in A1 but not in AAF after noise exposure (Fig. 4.4). When superficial (Layers 1-4) and deep layers (Layers 5-6; Fig. 4.6A) were considered separately, it became apparent that the decreased PNN density was due to modification in deep layers (Layers 5-6: C = 98.31 ± 0.4, N = 86.042 ± 0.4, NE = 77.751 ± 0.4) whereas superficial layers showed no significant difference after noise exposure (Layers 1-4: C = 97.534 ± 0.4, N = 96.851 ± 0.5, NE = 95.884 ± 0.5; effect of layers: F(1) = 6.613, p = 0.0104; effect of NE: F(2) = 3.111, p = 0.045). AAF showed no changes due to noise exposure (Fig. 4.6B; F(2) = 2.212, p = 0.11) or differences between layers (F(1) = 0.1075, p = 0.743).

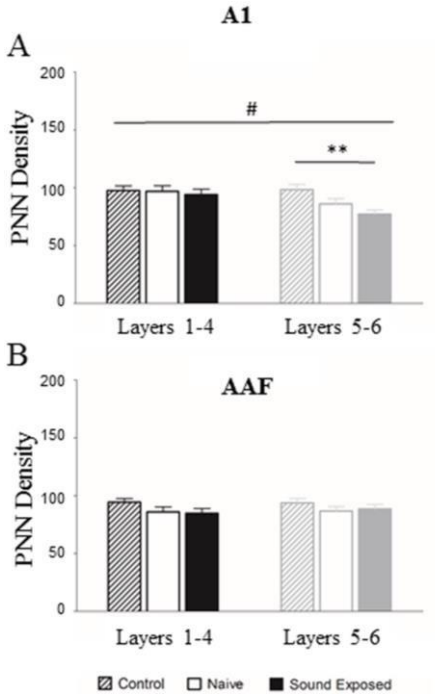

Figure 4.6. The observed reduction of PNNs in A1 after sound exposure is taking place in the deep layers of the cortex. A) PNN density in A1 decreases after noise exposure, specifically in the deep layers of the cortex. B) AAF did not show a similar reduction of PNNs. N mice **(#images)** = PNN: C = 10 **(A1: 90, AAF: 98)**, N = 11 **(A1: 89, AAF: 97)**, SE = 11 **(A1: 94, AAF: 96)**. Legend: # : between layers, * : paired comparison between conditions; * = 0.05, ** = 0.01, *** = 0.001.

3.8 Inhibitory cell density in A1 is modified in both superficial and deep layers.

To look at layer-specific effects of noise exposure on inhibitory cell density we analyzed A1 and AAF separately. In A1, we have shown evidence for an increase in GABA cell density after noise exposure (Fig. 4.4), specifically in GABA cells without PNNs (Fig. 4.5). This upregulation occurs in both superficial and deep layers in A1 (Fig. 4.7A; effect of layer: $F(1) = 0.022$, $p = 0.881$; effect of NE: $F(2) = 12.66$, $p < 0.0001$; Layers 1-4: C = 408.877 ± 23.6, N = 378.04 ± 20.1, NE = 509.944 ± 29.9; Layers 5-6: C = 413.546 ± 28.7, N = 379.272 ± 20.9, NE = 494.694 ± 30.2). The increase in GABA cell density is specific to those GABA cells without PNNs (Fig. 4.7D; effect of NE: $F(2) = 14.21$, $p < 0.0001$; Layers 1-4: C =374.812 ± 22.5, N = 342.031 ± 17.6, NE = 469.935 ± 28; Layers 5-6: C = 386.351 ± 28.4, N = 351.522 ± 20.7, NE = 472.865 ± 28.5). Noise exposure did not affect the density of GABA cells with PNN (Fig. 4.7G; $F(2) = 0.07680$, $p = 0.926$).

Modulation of PV cell density in A1 also occurred across both superficial and deep layers (Fig. 4.7B; effect of NE: $F(2) = 27.50$, $p < 0.0001$; Layers 1-4: C = 117.927 ± 7.4, N = 78.446 ± 4.3, NE = 121.481 ± 6.2; Layers 5-6: C = 162.39 ± 8.1, N = 110.99 ± 5.5, NE = 157.097 ± 7.3). PV cells without PNNs (Fig. 4.7E; effect of NE: $F(2) = 19.66$, $p < 0.0001$; Layers 1-4: C = 88.683 ± 5.6, N = 62.03 ± .8, NE = 93.59 ± 5.1; Layers 5-6: C = 129.6 ± 7.7, N = 91.272 ± 4.8, NE = 130.76 ± 7.6) as well as PV cells with PNNs

were affected (Fig. 4.7H; effect of NE: $F(2) = 14.97$, $p < 0.0001$; Layers 1-4: C = 30.938 ± 3.1, N = 16.416 ± 1.8, NE = 27.891 ± 2.4; Layers 5-6: C = 34.045 ± 3.6, N = 19.716 ± 1.9, NE = 26.338 ± 1.8).

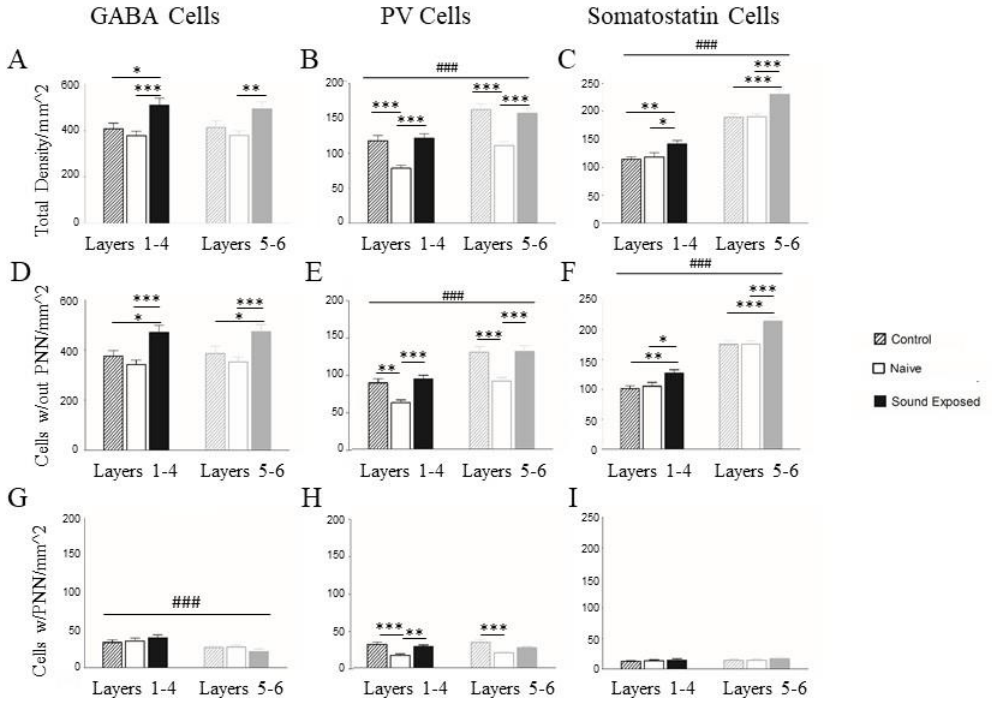

Figure 4.7. The increased inhibitory cell density is occurring across all layers in A1. A) The increased density of GABA expressing cells occurred both in superficial and deep layers of the cortex, among those GABA cells without PNNs (D). G) We also observed fewer colocalized GABA/PNN cells in deep layers of the cortex. B) PV-expressing cells showed a similar modification of density in superficial and deep layers. This modification of PV occurred in both PV cells enwrapped in PNNs (H) and in those without PNNs (E). C) Noise exposure also caused an increase in SOM cell density across all layers, and this increased occurred in SOM-cells without PNNs (F), while no change occurred in SOM cells enwrapped in PNNs (I). N mice **(#images)** = GABA: C = 5 **(A1: 20)**, N = 6 **(A1: 24)**, SE = 5 mice **(A1: 20)**; SOM: C = 5 **(A1: 19)**, N = 6 **(A1: 21)**, SE = 5 mice **(A1: 19)**; PV: C = 5 **(A1: 51)**, N = 5**(A1: 44)**, SE = 6 **(A1: 52)**. Legend: # : between layers, * : paired comparison between conditions; * = 0.05, ** = 0.01, *** = 0.001.

Density of SOM cells were also modified across both deep and superficial layer, with increased SOM density after noise exposure (Fig. 4.7C; effect of NE: $F(2) = 16.18$, $p < 0.0001$; Layers 1-4: C = 114.035 ± 4.7, N = 118.536 ± 7.3, NE = 141.237 ± 6.6; Layers

5-6: C = 189.362 ± 6.3, N = 189.954 ± 5.5, NE = 230.28 ± 8.3). Similar to GABA expressing cells, the SOM cell density increase was carried by changes in SOM cells without PNNs (Fig. 4.7F; effect of NE: $F(2) = 17.40$, $p < 0.0001$; Layers 1-4: C = 101.64 ± 4.5, N = 105.263 ± 6.5, NE = 127.026 ± 5.5; Layers 5-6: C = 175.293 ± 6.2, N = 175.68 ± 5.7, NE = 213.71 ± 6.9), whereas SOM cells with PNNs showed no difference in density after noise exposure (Fig. 4.7I; $F(2) = 0.6484$, $p = 0.524$).

3.9 In AAF, noise exposure causes modification of GABA and SOM across all layers, but modification of PV in superficial layers only.

In AAF, so far we have shown an increase in GABA cell density after noise exposure (Fig. 4.4), specifically in GABA cells without PNNs (Fig. 4.5). This increase in density occurs in both superficial and deep layers (Fig. 4.8A; effect of layer: $F(1) = 3.582$, $p = 0.06$; effect of NE: $F(2) = 9.967$, $p < 0.0001$; Layers 1-4: C = 399.167 ± 26.7, N = 333.527 ± 24.4 NE = 456.91 ± 31.8; Layers 5-6: C = 433.62 ± 33.7, N = 382.685 ± 19.9, NE = 502.1 ± 31.3).

Although the overall density of PV cells in AAF was modulated by noise exposure, (Fig. 4.8B; effect of NE: $F(2) = 6.606$, $p = 0.0016$) paired comparisons revealed PV density was only significantly modulated in the superficial layers (Layers 1- 4: C = 94.98 ± 6.4, N = 66.988 ± 5.2, NE = 87.225 ± 5.7) but not in deep layers of AAF (Layers 5-6: C = 126.124 ± 7, N = 109.148 ± 6.2, NE = 122.979 ± 6). This occurred in both PV cells with PNN (Fig. 4.8H; effect of NE: $F(2) = 8.887$, $p = 0.0002$;

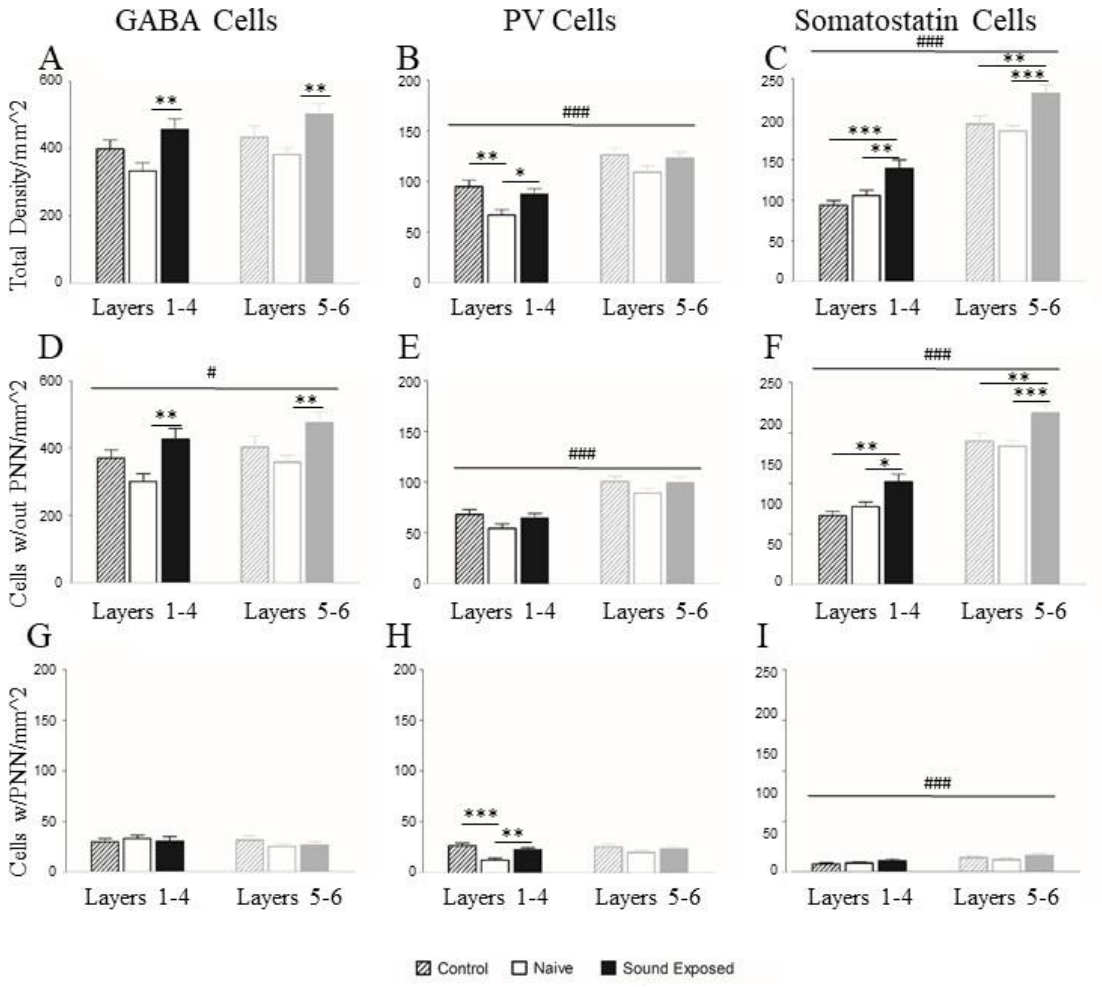

Figure 4.8. The increased inhibitory cell density is occurring across all layers in AAF. A) The density of GABA-expressing cells increased in both superficial and deep layers of AAF after noise exposure, specifically among those GABA cells without PNNs (D). G) No change was observed in GABA cells enwrapped in PNN.
B) PV-expressing cells in AAF had only a small modification of PV density after noise exposure which only took place in superficial layers. Unlike GABA, this change took place in PV cells enwrapped in PNNs (H), while no exposure-induced modification was observed among PV cells without PNNs (E). C) Noise exposure also caused an increase in SOM cell density across all layers, and this increase occurred in SOM-cells without PNNs (F), while no exposure-induced change occurred in SOM cells enwrapped in PNNs (I). Across all inhibitory cell markers, we observed more inhibitory cells in the deep layers compared to superficial layers, especially among cells without PNNs. N mice **(#images)** = GABA: C = 5 **(AAF: 19)**, N = 6 **(AAF: 27)**, SE = 5 mice **(AAF: 17)**; SOM: C = 5 **(AAF: 19)**, N = 6 **(AAF: 28)**, SE = 5 mice **(AAF: 20)**; PV: C = 5 **(AAF: 50)**, N = 5**(AAF: 42)**, SE = 6 **(AAF: 52)**. Legend: # : between layers, * : paired comparison between conditions; * = 0.05, ** = 0.01, *** = 0.001.

Layers 1-4: C = 26.599 ± 2.6, N = 12.3 ± 1.8, NE = 22.458 ± 52.1; Layers 5-6: C = 25.286 ± 2.6, N = 19.792 ± 2.2, NE = 23.452 ± 2.2) and in PV cells without PNN (Fig. 4.8E; effect of NE: F(2) = 3.208, p = 0.042; Layers 1-4: C = 68.38 ± 4.8, N = 54.68 ± 4.4, NE = 64.767 ± 4.6; Layers 5-6: C = 100.838 ± 5.4, N = 89.355 ± 4.9, NE = 99.527 ± 5.6).

SOM cell density in AAF was increased in both deep and superficial layers after noise exposure (Fig. 4.8C; F(2) = 15.44, P < 0.0001; Layers 1-4: C = 93.761 ± 5.9, N = 105.871 ± 6.5, NE = 139.472 ± 10.3; Layers 5-6: C = 194.055 ± 10.1, N = 185.289 ± 6.6, NE = 231.973 ± 10.2). SOM cells without PNNs increased in density (Fig. 4.8F; F(2) = 13.83, p < 0.0001; Layers 1-4: C = 84.708 ± 5.2, N = 95.662 ± 6, NE = 126.505 ± 9.6; Layers 5-6: C = 177 ± 10.1, N = 170.908 ± 6.7, NE = 212.191 ± 9.8), whereas density of SOM cells with PNNs was not different after noise exposure (Fig. 4.7I; F(2) = 2.708, p = 0.0705).

4. Discussion

PNNs are more densely expressed in the AAF compared to A1 in the P60 mouse auditory cortex. GABA, PV and SOM cell densities are not different between the two fields; however, PV and SOM are denser in deeper layers across fields. Moderate level noise exposure during early auditory development leads to: 1) increased GABA+ and SOM+ cell density in both A1 and AAF, 2) modification of PV density in A1, that was attenuated in AAF, and 3) decreased PNN cell density in A1, but not AAF (summarized in Figure 4.9). Additionally, PV expression was potentially more sensitive to a reduced noise environment than to noise exposure. Together these data show differential

expression of extracellular assemblies in A1 and AAF, and differential sensitivity of inhibitory cell marker density to developmental experience in these two core cortical fields.

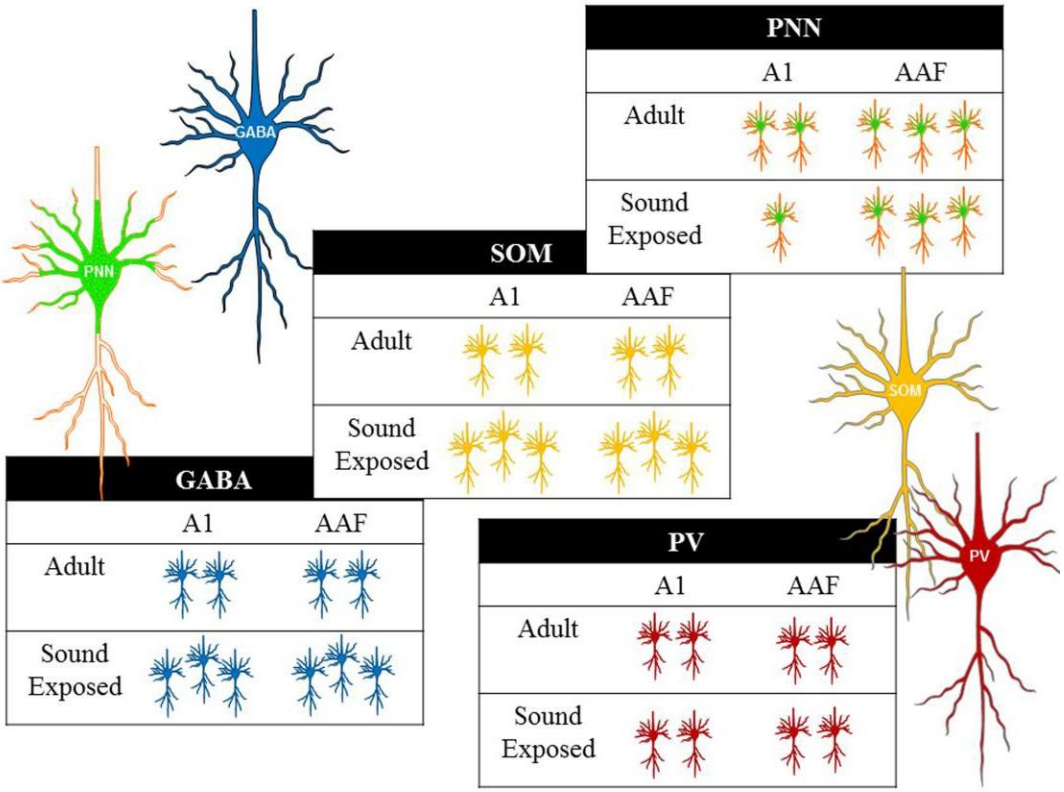

Figure 4.9. Summary of the effects of noise exposure on inhibitory cells and PNN density in A1 and AAF. PNNs were enriched in adult AAF cortex compared to A1. Noise exposure caused a decrease in PNNs in A1, but no change in AAF. Inhibitory cells were expressed similarly in both A1 and AAF of adult mice, including PV, SOM and GABA. Sound exposure caused an increase in SOM and GABA cells but no change in PV cell density (compared to controls).

This study revealed that AAF has a higher density of PNNs compared to A1 in adult (P60) mice. Under standard vivarium conditions, both A1 and AAF showed an increase in PNN density from P30 to P60, however the increase was more pronounced in AAF leading to significantly more PNNs at P60, but not at P30. Increased PNN density observed here is consistent with reports of increased PNNs in A1 from P14 to P30 (Wen

et al., 2018a) and from 2 months to 6 months (Ueno et al., 2018), and is similar to observations in visual and somatosensory cortices (Ueno et al., 2018; Ye and Miao, 2013). The P30 to P60 developmental window overlaps with periods of functional development in the core auditory cortex, where neurons become more selective for fast frequency modulated sounds and develop narrow frequency tuning (Carrasco et al., 2013) and are particularly sensitive to plasticity for FM direction selectively (Insanely et al., 2009). These are all processes which are thought to require fast and temporally precise inhibition. Interestingly, PNNs shape the fast spiking properties of PV cells (Balmer, 2016; Favuzzi et al., 2017), and may in fact maintain and/or help to mature excitatory synaptic contacts onto PV cells (Favuzzi et al., 2017). They also aid in the maturation of intrinsic PV cell properties through binding and uptake of Oxt2 into PV cells (reviewed in Wen et al., 2018b). Therefore, the increased PNN density from P30 to P60 corresponds to maturation of inhibitory circuits, leading to more precise temporal processing and sharper tuning. Increased PNN density in adult AAF and its implications for PV cell function may correspond to the faster spectrotemporal and amplitude modulated response properties (Phillips and Irvine, 1982; Schreiner and Urbas, 1988; Tian and Rauschecker, 1994; Trujillo et al., 2011). To more directly test this relationship, PNN structures could be reduced (Brakebusch et al., 2002; Zhou et al., 2001) or digested at specific time points in auditory development and functional properties tested.

Of note, most studies on the role of PNN in shaping cellular properties have focused on PV cells. However, this study and others have demonstrated that PV cells are

not the only type of cell with PNN. PNNs did not overlap with GABA expressing cells 100% of the time, indicating that excitatory cells may also be surrounded with PNNs (Lensjo et al., 2017; Morikawa et al., 2017; reviewed in van 't Spijker and Kwok, 2017). In fact, the greater density of PNNs in adult AAF was not accompanied by a greater density of co-localized PV, SOM or GABA with PNN, indicating PNNs may be forming around excitatory cells in AAF. How PNNs shape the properties of excitatory cells is not clear.

To our knowledge this is the first study to investigate changes in PNN density after developmental noise exposure in A1 and AAF of the auditory cortex. Previous studies showed reduced PNN density in the visual cortex after dark rearing (Ye and Miao, 2013) and a reduction of a specific sub-type of PNN after whisker trimming in the barrel cortex (McRae et al., 2007). Although these manipulations induce sensory deprivation while noise exposure increases sensory input, evidence suggests that developmental noise exposure does induce an immature cortical network, similar to the effects of dark rearing (de Villers-Sidani et al., 2008; Speechley et al., 2007; Sun et al., 2011; Xu et al., 2010). Prolonged noise exposure in adult rats is even suggested to restore a juvenile-like plasticity in auditory cortex (Zhou et al., 2011). The reduced PNN density observed here specifically in A1 is similar to the effects of dark rearing/whisker trimming. The fact that peripheral deprivation (visual/barrel cortex) has effects similar to overexposure to a stimulus (continuous 70 dB noise) suggests that cortical PNN maturation is sensitive to specific characteristics of the stimulus, such as the level or temporal modulation of the sensory input. PNN development is also affected by deletion

of specific cell types in developing cortex (Takada et al., 2014). Moreover, McRae et al., 2007 showed that mice deprived of sensory input across the CP did not recover normal PNN expression after 30 days of re-exposure to sensory input in adulthood, indicating that timing of sensory input is important. Altogether this suggests that PNN maturation can be altered, sometimes irreversibly, by abnormal sensory input. Additional studies are necessary in the auditory system to evaluate this hypothesis.

Although PNN reduction is consistent across different sensory cortices, the layer-specificity of PNN plasticity was different in each study (McRae et al., 2007; Ye and Miao, 2013). Here, we found that the density of PNN was reduced more in deeper layers of A1, compared to the superficial layers. Though the specific mechanism behind this reduction is not clear, deep layers of auditory cortex are particularly affected in congenitally deaf cats functionally (Kral et al., 2000) and morphologically (Berger et al., 2017), suggesting deep layers of A1 may be more susceptible to disrupted sensory input.

This study indicates that A1 is more susceptible to modification after noise exposure, especially with PNN density. There is a large body of literature focusing on A1 as a locus of auditory map plasticity (reviewed in Schreiner and Polley, 2014), but relatively less is known about AAF plasticity. The more pronounced plasticity of PNN and PV density in A1 is consistent with functional studies suggesting differential modulation in A1 and AAF after noise exposure (Takahashi et al., 2006). It is not clear why A1 and AAF should respond differently to auditory manipulation, as both have been classified as 'primary' like cortex (Kanold et al., 2014), receive input from similar regions of the auditory thalamus (Anderson et al., 1980; Llano and Sherman, 2008), and

send a large portion of corticocortical connections to one another (Carrasco and Lomber, 2009). Output from A1 and AAF to secondary cortical regions is also overlapping (Llano and Sherman, 2008). It may be possible that the molecular construction of PNNs is different in A1 vs. AAF. Studies comparing different antibodies for PNN components, including aggrecan, WFA, hyaluronic acid and brevican, have demonstrated that there are distinct populations of PNNs which can be more or less susceptible to modification (Ajmo et al., 2008; Costa et al., 2007; Matthews et al., 2002; McRae et al., 2007; Kochlamazashvili et al., 2012). Additionally, it has been demonstrated that the type of sulfation of a PNN structure, by chondroitin 6-sulfotransferase-1 or by chondroitin 4-sulfotransferase-1, effects whether a PNN structure maintains a juvenile-like plasticity or is less permissive to plasticity (Miyata et al., 2012; Miyata and Kitagawa, 2017; Reviewed in Sorg et al., 2016). Differences in the molecular structure or in the sulfation patterns of PNNs in the auditory cortex could explain the differential susceptibility to noise-induced modification in A1.

In addition to changes in PNN density, noise exposure from P9-P30 causes an increase in inhibitory cell markers across both A1 and AAF, in particular, increases in GABA and SOM cell density. Interestingly, PV expressing cells in this study had a somewhat different pattern of regulation after noise exposure than that of GABA and SOM. When mice were raised in a sound attenuating chamber, where the ambient background noise was ~35 dB SPL, the PV levels decreased compared to mice raised in the vivarium, with an ambient background noise of ~50 dB SPL. After exposure to a 70 dB continuous white noise, PV cell density was similar to control levels, whereas both

GABA and SOM cell densities increased after noise exposure. This result is somewhat surprising based on the previous literature (see Table 4.1).

Table 4.1. Summary of literature on altered inhibition after noise exposure

Exposure	Reference	Exp. Age	Inhibitory Cell	Effect
Moderate (≤ 70 dB)	de Villers – Sidani et al., 2008	P7 – P20 (r.)	PV density	↓
Development	Xu et al., 2010	P7 – P56 (r.)	GAD65 protein	↓
			GABA-A α1 protein	↓
			GABA-A α3 protein	↑
Moderate (≤ 70 dB)	Zhou et al., 2011	P60 – P104 (r.)	GABA-A α1 protein	↓
			GABA-A β2/3 protein	↓
			BDNF protein	↓
Adult	Zhou and Merzenich, 2012	P90 – P150 (r.)	PV density	↓
			BDNF density	↑
	Turner et al., 2013	~ P660 –P704 (m.)	GAD67 inferior colliculus	↑
			GAD67 AC	F ↑ M ↓
Traumatic (≥105 dB)	Kumar et al., 2014	15 min/ 6 x's (chicks)	Gephyrin	↓
Development			GABA-A γ2	↓
Traumatic (≥105 dB)	Nguyen et al., 2017	8 hours (m.)	PV density	X
Adult				

The difference observed between the pattern of PV regulation and that of GABA and SOM may be due in some part to the functional role that these proteins, used as cell markers, actually have within neural networks. GABA and somatostatin act as neurotransmitter and neuropeptide respectively (reviewed in Yavorska and Wehr, 2016) but parvalbumin acts as a mobile calcium buffer within the cell (Schwaller, 2018). Therefore, the regulation of PV protein within a cell may be particularly responsive to increases or decreases in activity levels within a cellular network in order to properly sequester free calcium within the cell. Increases in GABA/SOM may instead reflect a homeostatic upregulation of inhibition. Many studies have focused on alterations in PV cell populations after experimental manipulation and found PV levels are modulated in response to learning and memory 24 hours post training (Donato et al., 2013), after developmental plasticity manipulations (de Villers Sadini et al., 2008; Tropea e al., 2006) and seizure activity (Kuruba et al., 2011; Wolf et al., 2016), indicating levels of PV expression commonly fluctuate even within hours of an event (Kuruba et al., 2011). Indeed, simple exposure to a sound for 20 min activates intracellular signaling pathways within PV cells (Cohen et al., 2016).

Differences between PV and SOM cells may also be due to their separable roles within local circuits. In the somatosensory cortex, PV neurons inhibit mainly other PV cells and pyramidal cells whereas SOM cells instead target a large range of inhibitory cells as well as pyramidal cells, and are only inhibited themselves weakly by VIP neurons (Pfeffer et al., 2013). This suggests that SOM cells have a larger role in the control of intracortical inhibitory networks than PV cells and, in response to increased auditory

excitation, might be the main locus of inhibitory compensation. Studies in the visual cortex have also demonstrated differential regulation of PV and SOM genes after monocular deprivation (Tropea et al., 2006), while in the auditory cortex, acoustic trauma causes increased spontaneous and evoked spikes in SOM but not PV cells (Novak et al., 2016). Results presented here suggest that the auditory cortex is engaging in a 'gain control' response after developmental noise exposure, specifically by engaging SOM cells which may then control the larger inhibitory cell network. This is consistent with functional changes in SOM cells after acoustic trauma in adulthood (Novak et al., 2016), however it is not completely consistent with the developmental noise exposure literature (Table 1).

5. Conclusions

Here we have demonstrated differential regulation of PNNs in A1 and AAF after developmental noise exposure. This leads to interesting questions about potential differences in the molecular structure of PNNs in A1 and AAF, and their activity-dependent modifications. Determining the answer to these questions will expand our knowledge on differential plasticity in A1 AAF. SOM and PV cells also showed differential modification after noise exposure, suggesting a role for SOM in control of intracortical inhibitory networks. Functionally targeting SOM cells in future noise exposure studies could confirm this hypothesis.

References

Ajmo, J.M., Eakin, A.K., Hamel, M.G., Gottschall, P.E., (2008). Discordant localization of WFA reactivity and brevican/ADAMTS-derived fragment in rodent brain. BMC *Neuroscience*, **9**, 14. https://doi.org/10.1186/1471-2202-9-14

Anderson, L.A., Christianson, G.B., Linden, J.F., (2009). Mouse auditory cortex differs from visual and somatosensory cortices in the laminar distribution of cytochrome oxidase and acetylcholinesterase. *Brain Research,* **1252**, 130–142. https://doi.org/10.1016/j.brainres.2008.11.037

Atencio, C.A., Schreiner, C.E., (2008). Spectrotemporal processing differences between auditory cortical fast-spiking and regular-spiking neurons. *Journal of Neuroscience,* **28**, 3897–3910. https://doi.org/10.1523/JNEUROSCI.5366-07.2008

Balmer, T.S., (2016). Perineuronal nets enhance the excitability of fast-spiking neurons. *eNeuro*, **3**, 1-13. https://doi.org/10.1523/ENEURO.0112-16.2016

Berger, C., Kühne, D., Scheper, V., Kral, A., (2017). Congenital deafness affects deep layers in primary and secondary auditory cortex: BERGER et al. *Journal of Comparative Neurology,* **525**, 3110–3125. https://doi.org/10.1002/cne.24267

Brakebusch, C., Seidenbecher, C.I., Asztely, F., Rauch, U., Matthies, H., Meyer, H., Krug, M., Bockers, T.M., Zhou, X., Kreutz, M.R., Montag, D., Gundelfinger, E.D., Fassler, R., (2002). Brevican-deficient mice display impaired hippocampal CA1 long-term potentiation but show no obvious deficits in learning and memory. *Molecular and Cellular Biology,* **22**, 7417–7427. https://doi.org/10.1128/MCB.22.21.7417-7427.2002

Cabungcal, J.-H., Steullet, P., Morishita, H., Kraftsik, R., Cuenod, M., Hensch, T.K., Do, K.Q., (2013). Perineuronal nets protect fast-spiking interneurons against oxidative stress. *Proceedings of the National Academy of Sciences,* **110**, 9130–9135. https://doi.org/10.1073/pnas.1300454110

Carrasco, A., Lomber, S.G., (2009). Differential modulatory influences between primary auditory cortex and the anterior auditory field. *Journal of Neuroscience,* **29**, 8350–8362. https://doi.org/10.1523/JNEUROSCI.6001-08.2009

Carrasco, M.M., Trujillo, M., Razak, K., (2013). Development of response selectivity in the mouse auditory cortex. *Hearing Research,* **296**, 107–120. https://doi.org/10.1016/j.heares.2012.11.020

Cohen, S.M., Ma, H., Kuchibhotla, K.V., Watson, B.O., Buzsáki, G., Froemke, R.C., Tsien, R.W., (2016). Excitation-transcription coupling in parvalbumin-positive interneurons employs a novel CaM Kinase-dependent pathway distinct from excitatory neurons. *Neuron,* **90**, 292–307. https://doi.org/10.1016/j.neuron.2016.03.001

Costa, C., Tortosa, R., Domènech, A., Vidal, E., Pumarola, M., Bassols, A., (2007). Mapping of aggrecan, hyaluronic acid, heparan sulphate proteoglycans and aquaporin 4 in the central nervous system of the mouse. *Journal of Chemical Neuroanatomy,* **33**, 111–123. https://doi.org/10.1016/j.jchemneu.2007.01.006

de Villers-Sidani, E., Simpson, K.L., Lu, Y.-F., Lin, R.C.S., Merzenich, M.M., (2008). Manipulating critical period closure across different sectors of the primary auditory cortex. *Nature Neuroscience,* **11**, 957–965. https://doi.org/10.1038/nn.2144

Donato, F., Rompani, S.B., Caroni, P., (2013). Parvalbumin-expressing basket-cell network plasticity induced by experience regulates adult learning. *Nature*, **504**, 272–276. https://doi.org/10.1038/nature12866

Eggermont, J.J., (2017). Effects of long-term non-traumatic noise exposure on the adult central auditory system. Hearing problems without hearing loss. *Hearing Research,* **352**, 12–22. https://doi.org/10.1016/j.heares.2016.10.015

Favuzzi, E., Marques-Smith, A., Deogracias, R., Winterflood, C.M., Sánchez-Aguilera, A., Mantoan, L., Maeso, P., Fernandes, C., Ewers, H., Rico, B., (2017). Activity-dependent gating of parvalbumin interneuron function by the perineuronal net protein brevican. *Neuron*, **95**, 639-655.e10. https://doi.org/10.1016/j.neuron.2017.06.028

Hackett, T.A., Rinaldi Barkat, T., O'Brien, B.M.J., Hensch, T.K., Polley, D.B., (2011). Linking topography to tonotopy in the mouse auditory thalamocortical circuit. *Journal of Neuroscience*, **31**, 2983–2995. https://doi.org/10.1523/JNEUROSCI.5333-10.2011

Happel, M.F.K., Niekisch, H., Castiblanco Rivera, L.L., Ohl, F.W., Deliano, M., Frischknecht, R., (2014). Enhanced cognitive flexibility in reversal learning induced by removal of the extracellular matrix in auditory cortex. *Proceedings of the National Academy of Sciences,* **111**, 2800–2805. https://doi.org/10.1073/pnas.1310272111

Hensch, T.K., (2005). Critical period plasticity in local cortical circuits. *Nature Reviews Neuroscience*, **6**, 877–888. https://doi.org/10.1038/nrn1787

Insanally, M.N., Kover, H., Kim, H., Bao, S., (2009). Feature-dependent sensitive periods in the development of complex sound representation. *Journal of Neuroscience,* **29**, 5456– 5462. https://doi.org/10.1523/JNEUROSCI.5311-08.2009

Kaas, J.H., (2011). The evolution of auditory cortex: The core areas, in: Winer, J.A., Schreiner, C.E. (Eds.), *The Auditory Cortex*. Springer US, Boston, MA, pp. 407–427.

Kanold, P.O., Nelken, I., Polley, D.B., (2014). Local versus global scales of organization in auditory cortex. *Trends in Neurosciences,* **37**, 502–510. https://doi.org/10.1016/j.tins.2014.06.003

Kochlamazashvili, G., Henneberger, C., Bukalo, O., Dvoretskova, E., Senkov, O., Lievens, P.M.-J., Westenbroek, R., Engel, A.K., Catterall, W.A., Rusakov, D.A., Schachner, M., Dityatev, A., (2010). The extracellular matrix molecule hyaluronic acid regulates hippocampal synaptic plasticity by modulating postsynaptic L-type Ca2+ channels. *Neuron*, **67**, 116–128. https://doi.org/10.1016/j.neuron.2010.05.030

Kral, A., Hartmann, R., Tillein, J., Heid, S., Klinke, R., (2000). Congenital auditory deprivation reduces synaptic activity within the auditory cortex in a layer-specific manner. *Cerebral Cortex,* **10**, 714–726. https://doi.org/10.1093/cercor/10.7.714

Kuruba, R., Hattiangady, B., Parihar, V.K., Shuai, B., Shetty, A.K., (2011). Differential susceptibility of interneurons expressing neuropeptide Y or parvalbumin in the aged hippocampus to acute seizure activity. *PLoS ONE,* **6**, e24493. https://doi.org/10.1371/journal.pone.0024493

Lensjø, K.K., Christensen, A.C., Tennøe, S., Fyhn, M., Hafting, T., (2017). Differential expression and cell-type specificity of perineuronal nets in hippocampus, medial entorhinal cortex, and visual cortex examined in the rat and mouse. *eneuro*, **4**, ENEURO.0379-16.2017. https://doi.org/10.1523/ENEURO.0379-16.2017

Llano, D.A., Sherman, S.M., (2008). Evidence for nonreciprocal organization of the mouse auditory thalamocortical-corticothalamic projection systems. *The Journal of Comparative Neurology*, **507**, 1209–1227. https://doi.org/10.1002/cne.21602

Matthews, R.T., Kelly, G.M., Zerillo, C.A., Gray, G., Tiemeyer, M., Hockfield, S., (2002). Aggrecan glycoforms contribute to the molecular heterogeneity of perineuronal nets. *Journal of Neuroscience,* **22**, 7536–7547.

Meredith, M.A., Lomber, S.G., (2011). Somatosensory and visual crossmodal plasticity in the anterior auditory field of early-deaf cats. *Hearing Research,* **280**, 38–47. https://doi.org/10.1016/j.heares.2011.02.004

Miyata, S., Komatsu, Y., Yoshimura, Y., Taya, C., Kitagawa, H., (2012). Persistent cortical plasticity by upregulation of chondroitin 6-sulfation. *Nature Neuroscience,* **15**, 414–422. https://doi.org/10.1038/nn.3023

Miyata, S., Kitagawa, H., (2017). Formation and remodeling of the brain extracellular matrix in neural plasticity: Roles of chondroitin sulfate and hyaluronan. *Biochimica et Biophysica Acta (BBA) - General Subjects,* **1861**, 2420–2434. https://doi.org/10.1016/j.bbagen.2017.06.010

Morikawa, S., Ikegaya, Y., Narita, M., Tamura, H., (2017). Activation of perineuronal net- expressing excitatory neurons during associative memory encoding and retrieval. *Scientific Reports,* **7**. https://doi.org/10.1038/srep46024

Novák, O., Zelenka, O., Hromádka, T., Syka, J., (2016). Immediate manifestation of acoustic trauma in the auditory cortex is layer specific and cell type dependent. *Journal of Neurophysiology*, **115**, 1860–1874. https://doi.org/10.1152/jn.00810.2015

Nowicka, D., Soulsby, S., Skangiel-Kramska, J., Glazewski, S., (2009). Parvalbumin-containing neurons, perineuronal nets and experience-dependent plasticity in murine barrel cortex. *European Journal of Neuroscience,* **30**, 2053–2063. https://doi.org/10.1111/j.1460-9568.2009.06996.x

Oswald, A.-M.M., Reyes, A.D., (2011). Development of inhibitory timescales in auditory cortex. *Cerebral Cortex*, **21**, 1351–1361. https://doi.org/10.1093/cercor/bhq214

Pfeffer, C.K., Xue, M., He, M., Huang, Z.J., Scanziani, M., (2013). Inhibition of inhibition in visual cortex: the logic of connections between molecularly distinct interneurons. *Nature Neuroscience*, **16**, 1068–1076. https://doi.org/10.1038/nn.3446

Phillips, D.P., Irvine, D.R.F., (1982). Properties of single neurons in the anterior auditory field (AAF) of cat cerebral cortex. *Brain research,* **248**, 237–244.

Pienkowski, M., Munguia, R., Eggermont, J.J., (2011). Passive exposure of adult cats to bandlimited tone pip ensembles or noise leads to long-term response suppression in auditory cortex. *Hearing Research,* **277**, 117–126. https://doi.org/10.1016/j.heares.2011.02.002

Pienkowski, M., Munguia, R., Eggermont, J.J., (2013). Effects of passive, moderate-level sound exposure on the mature auditory cortex: Spectral edges, spectrotemporal density, and real-world noise. *Hearing Research*, **296**, 121–130. https://doi.org/10.1016/j.heares.2012.11.006

Pizzorusso, T., Medini, P., Berardi, N., Chierzi, S., Fawcett, J.W., Maffei, L., (2002). Reactivation of ocular dominance plasticity in the adult visual cortex. *Science*, **298** 1248–1251.

Polley, D.B., Read, H.L., Storace, D.A., Merzenich, M.M., (2007). Multiparametric auditory receptive field organization across five cortical fields in the albino rat. *Journal of Neurophysiology*, **97**, 3621–3638. https://doi.org/10.1152/jn.01298.2006

Ranasinghe, K.G., Carraway, R.S., Borland, M.S., Moreno, N.A., Hanacik, E.A., Miller, R.S., Kilgard, M.P., (2012). Speech discrimination after early exposure to pulsed-noise or speech. *Hearing Research*, **289**, 1–12. https://doi.org/10.1016/j.heares.2012.04.020

Sanes, D.H., Bao, S., (2009). Tuning up the developing auditory CNS. *Current Opinion in Neurobiology*, **19**, 188–199. https://doi.org/10.1016/j.conb.2009.05.014

Schreiner, C.E., Urbas, J.V., (1988). Representation of amplitude modulation in the auditory cortex of the cat. II. Comparison between cortical fields. *Hearing research,* **32**, 49–63.

Schreiner, C.E., Polley, D.B., (2014). Auditory map plasticity: diversity in causes and consequences. *Current Opinion in Neurobiology*, **24**, 143–156. https://doi.org/10.1016/j.conb.2013.11.009

Schwaller, B., (2010). Cytosolic Ca2+ buffers. *Cold Spring Harbor Perspectives in Biology*, **2**, a004051–a004051. https://doi.org/10.1101/cshperspect.a004051

Sorg, B.A., Berretta, S., Blacktop, J.M., Fawcett, J.W., Kitagawa, H., Kwok, J.C.F., Miquel, M., (2016). Casting a wide net: Role of perineuronal nets in neural plasticity. *The Journal of Neuroscience*, **36**, 11459–11468. https://doi.org/10.1523/JNEUROSCI.2351-16.2016

Speechley, W.J., Hogsden, J.L., Dringenberg, H.C., (2007). Continuous white noise exposure during and after auditory critical period differentially alters bidirectional thalamocortical plasticity in rat auditory cortex in vivo: Auditory development, white noise and LTP/LTD. *European Journal of Neuroscience*, **26**, 2576–2584. https://doi.org/10.1111/j.1460-9568.2007.05857.x

Stiebler, I., Neulist, R., Fichtel, I., Ehret, G., (1997). The auditory cortex of the house mouse: left-right differences, tonotopic organization and quantitative analysis of frequency representation. *Journal of Comparative Physiology A*, **181**, 559–571.

Sun, W., Tang, L., Allman, B.L., (2011). Environmental noise affects auditory temporal processing development and NMDA-2B receptor expression in auditory cortex. *Behavioural Brain Research*, **218**, 15–20. https://doi.org/10.1016/j.bbr.2010.11.028

Takada, N., Pi, H.J., Sousa, V.H., Waters, J., Fishell, G., Kepecs, A., Osten, P., (2014). A developmental cell-type switch in cortical interneurons leads to a selective defect in cortical oscillations. *Nature Communications*, **5**. https://doi.org/10.1038/ncomms6333

Takahashi, K., Hishida, R., Kubota, Y., Kudoh, M., Takahashi, S., Shibuki, K., (2006). Transcranial fluorescence imaging of auditory cortical plasticity regulated by acoustic environments in mice. *European Journal of Neuroscience*, **23**, 1365–1376. https://doi.org/10.1111/j.1460-9568.2006.04662.x

Tian, B., Rauschecker, J.P., (1994). Processing of frequency-modulated sounds in the cat's anterior auditory field. *Journal of Neurophysiology*, **71**, 1959–1975.

Tropea, D., Kreiman, G., Lyckman, A., Mukherjee, S., Yu, H., Horng, S., Sur, M., (2006). Gene expression changes and molecular pathways mediating activity-dependent plasticity in visual cortex. *Nature Neuroscience*, **9**, 660–668. https://doi.org/10.1038/nn1689

Trujillo, M., Measor, K., Carrasco, M.M., Razak, K.A., (2011). Selectivity for the rate of frequency-modulated sweeps in the mouse auditory cortex. *Journal of Neurophysiology*, **106**, 2825–2837. https://doi.org/10.1152/jn.00480.2011

Ueno, H., Takao, K., Suemitsu, S., Murakami, S., Kitamura, N., Wani, K., Okamoto, M., Aoki, S., Ishihara, T., (2018). Age-dependent and region-specific alteration of parvalbumin neurons and perineuronal nets in the mouse cerebral cortex. *Neurochemistry International*, **112**, 59–70. https://doi.org/10.1016/j.neuint.2017.11.001

van 't Spijker, H.M., Kwok, J.C.F., (2017). A sweet talk: The molecular systems of perineuronal nets in controlling neuronal communication. *Frontiers in Integrative Neuroscience*, **11**. https://doi.org/10.3389/fnint.2017.00033

Wen, T.H., Afroz, S., Reinhard, S.M., Palacios, A.R., Tapia, K., Binder, D.K., Razak, K.A., Ethell, I.M., (2018a). Genetic reduction of matrix metalloproteinase-9 promotes formation of perineuronal nets around parvalbumin-expressing interneurons and normalizes auditory cortex responses in developing Fmr1 knock-out mice. *Cerebral Cortex*, **28**, 3951–3964. https://doi.org/10.1093/cercor/bhx258

Wen, T.H., Binder, D.K., Ethell, I.M., Razak, K.A., (2018b). The perineuronal 'safety' net? Perineuronal net abnormalities in neurological disorders. *Frontiers in Molecular Neuroscience*, **11**. https://doi.org/10.3389/fnmol.2018.00270

Wolf, D.C., Bueno-Júnior, L.S., Lopes-Aguiar, C., Do Val Da Silva, R.A., Kandratavicius, L., Leite, J.P., (2016). The frequency of spontaneous seizures in rats correlates with alterations in sensorimotor gating, spatial working memory, and parvalbumin expression throughout limbic regions. *Neuroscience*, **312**, 86–98. https://doi.org/10.1016/j.neuroscience.2015.11.008

Wong, C., Chabot, N., Kok, M.A., Lomber, S.G., (2015). Amplified somatosensory and visual cortical projections to a core auditory area, the anterior auditory field, following early- and late-onset deafness: Modified projections to AAF following deafness. *Journal of Comparative Neurology*, **523**, 1925–1947. https://doi.org/10.1002/cne.23771

Xu, J., Yu, L., Cai, R., Zhang, J., Sun, X., (2010). Early continuous white noise exposure alters auditory spatial sensitivity and expression of GAD65 and GABAA receptor subunits in rat auditory cortex. *Cerebral Cortex*, **20**, 804–812. https://doi.org/10.1093/cercor/bhp143

Yanagawa, Y., Takasu, K., Osanai, H., Tateno, T., (2017). Salicylate-induced frequency-map reorganization in four subfields of the mouse auditory cortex. *Hearing Research,* **351**, 98–115. https://doi.org/10.1016/j.heares.2017.06.003

Yavorska, I., Wehr, M., (2016). Somatostatin-expressing inhibitory interneurons in cortical circuits. *Frontiers in Neural Circuits*, **10**. https://doi.org/10.3389/fncir.2016.00076

Ye, Q., Miao, Q., (2013). Experience-dependent development of perineuronal nets and chondroitin sulfate proteoglycan receptors in mouse visual cortex. *Matrix Biology*, **32**, 352–363. https://doi.org/10.1016/j.matbio.2013.04.001

Zhou, X.-H., Brakebusch, C., Matthies, H., Oohashi, T., Hirsch, E., Moser, M., Krug, M., Seidenbecher, C.I., Boeckers, T.M., Rauch, U., Buettner, R., Gundelfinger, E.D., Fassler, R., (2001). Neurocan is dispensable for brain development. *Molecular and Cellular Biology*, **21**, 5970–5978. https://doi.org/10.1128/MCB.21.17.5970-5978.2001

Zhou, X., Panizzutti, R., de Villers-Sidani, E., Madeira, C., Merzenich, M.M., (2011). Natural restoration of critical period plasticity in thejuvenile and adult primary auditory cortex. *Journal of Neuroscience*, **31**, 5625–5634. https://doi.org/10.1523/JNEUROSCI.6470-10.2011

Chapter 5:

Developmental noise exposure causes comparable plasticity in A1 and AAF in the mouse auditory cortex

Abstract

A lingering question in the field of auditory neuroscience lies in the precise roles of the primary (A1) and the anterior auditory fields (AAF) of the auditory cortex. Both regions receive lemniscal input from thalamus and share similar response properties to sounds. Although a large body of evidence supports a role for A1 in developmental plasticity in response to passive sound exposure, it is not clear whether AAF undergoes a similar type of developmental plasticity. Here we investigated critical period plasticity in the A1 and AAF of mouse auditory cortex. Mice were raised in a sound attenuating chamber and exposed to 14 kHz pure tone pips from P9-P20. From P30-P40, the A1 and AAF of sound exposed mice were mapped using multiunit recordings under anesthesia, to determine the response characteristics of neurons. We found that both A1 and AAF show 1) decreased response magnitude to 14 kHz across all responses, and 2) a specific reduction of response to 14 kHz tones in neurons that do not prefer 14-16 kHz. A1 and AAF both show changes in the latency of response to the characteristic frequency (CF), but this effect is differential; sound exposure caused faster response latencies in A1, but in AAF the response to the CF shifted to a slower response window (>50 ms). Although we did not observe an increased representation of our exposure-tone (14 kHz) in either A1 or AAF, we did see an increased percent of neurons in A1 with a CF of 19 kHz, and with a best frequency (BF) of 18 kHz. This change did not take place in AAF. Together this provides evidence for developmental plasticity in both A1 and AAF, however tonotopic re-organization of CF and/or BF may be specific to A1.

Abbreviations

Anterior auditory field (AAF), Best frequency (BF), Characteristic frequency (CF), Primary auditory cortex (A1)

1. Introduction

Critical periods (CP) pose unique, defined windows during which neuronal plasticity is particularly malleable relative to adulthood (Hensch, 2004). What is distinctive to this period of development is the convergence of intrinsic developmental changes, together with extrinsic (sensory-driven) modifications to the network. Intrinsic changes such as shifts in receptor sub-composition (Ben-Ari, 2002; Nase et al., 1999), voltage-gated ion channel expression (Spitzer et al., 2002), and developmental shifts in protein expression (Sanes et al., 2005) together affect the morphologic shape of a synapse, the motility of receptors at the synapse and the overall excitability of a cell. These processes are further modified by extrinsic sensory input that influences protein expression, receptor composition at the synapse, maturation of synapses and stabilization of synaptic contacts (Kuczewski et al., 2011; Liu eta al., 2013; Lu eta al., 2016; Nase et al., 1999; Reinhard et al., 2015). Altogether these changes affect the physiologic response properties of neurons, which then reflect the sensory input received. Because alterations in neuronal networks during this time set up the mature response properties of neurons, and sensory processing is a foundation for perception and cognition, understanding CP development is an important step for potential treatment of neurodevelopmental and other psychiatric disorders.

A large body of research has focused on the primary auditory cortex (A1) and its role in CP plasticity in the auditory system (Anomal et al., 2013; Barkat et al., 2011; Chang et al., 2005; de Villers-Sidani et al., 2007; dev Villers-Sidani et al., 2008; Insanally et al., 2009 Kim and Bao, 2009; Yang et al., 2014). However, whether other regions within the

auditory cortex also respond to critical period manipulations is less clear. The anterior auditory field (AAF) is considered to be a 'primary-like' core auditory field (Kanold et al., 2014), is well conserved across species (Kass, 2011) and demonstrates developmental plasticity after either permanent or temporary loss of peripheral input (Meredith and Lomber, 2011; Wong et al., 2015; Yanagawa et al., 2017). Few studies have considered CP plasticity in AAF.

Peripheral-driven development of the auditory system in rodents begins at hearing onset and extends until about P30 - P40 (Barkat et al., 2011; Carrasco et al., 2013; Insanally et al., 2009). Spanning this time, there are several 'sensitive periods' during which different neuronal response properties undergo change (Carrasco et al., 2013; Insanally et al., 2009). The first window involves re-organization of a property called tonotopy, which is considered to be the most fundamental organizing property in the auditory system (Lee, 2005). In A1, neurons will respond preferably or most strongly to a given tone. Neurons in close proximity to each other tend to prefer similar tones (frequencies; Wu et al., 2008), allowing for a structured frequency gradient from low to high frequencies represented across the extent of A1 (caudal to rostral) – this is what is referred to as tonotopy. AAF is likewise tonotopically organized, located immediately rostral to A1 with a mirror frequency gradient (high to low; caudal to rostral).

The window for tonotopic re-organization in A1 occurs in as little as 4 days after hearing onset from P12 - P15 (Barkat et al., 2011), during which if a particular tone is played throughout those 4 days, a larger percentage of neurons will respond preferably to that tone. This can be measured by finding the characteristic frequency (CF) of a neuron,

which is the frequency that a neuron responds to selectively when the sound is played at a low intensity. This sound-induced shift in tonotopic organization remains stable into adulthood. While tonotopic plasticity has been thoroughly studied in A1 of the rat, the effect of passive developmental sound exposure on AAF is less clear.

Therefore, this study focuses on the effect of passive sound exposure from P9 – P20 on both A1 and AAF of the auditory cortex. Multiunit recordings will be used to determine whether tonotopic plasticity is observed in mature (P30-P40) A1 and AAF of the mouse. Results will elucidate the basic regionalization and function of the auditory cortical system, and improve our understanding on the effects that developmental intervention may have in specific auditory fields.

2. Methods

2.1 Mice

FVB.129P2-Pde6b^{+} Tyr$^{c\text{-}ch}$/AntJ mice ('sighted' FVB mice) were obtained from Jackson laboratories and housed in an accredited vivarium on a 12h light/dark cycle. Food and water were provided *ad libitum*. All procedures were approved by the Institutional Animal Care and Use Committee at the University of California, Riverside. The total number of mice used in this study was: A1: Naïve = 9, Sound Exposed = 11; AAF: Naïve = 6, Sound Exposed = 9.

2.2 Noise Exposure

'Naïve' and 'noise exposed' mice were raised in a sound-attenuating chamber (ambient noise ~35 dB SPL; dimensions 4'L x 4'W x 3'H) from P5 until the time of recording (P30-P40). The room where the chamber was housed was accessed only for

daily animal inspection and weekly cleaning, with a background room noise of ~55dB. Mice within the chamber were on a 12-hour light/dark cycle and were inspected daily for visible signs of health. Mice in the chamber were raised either with no additional sounds played (naïve) or were exposed to a 14 kHz tone (30 ms with 5 ms rise/fall, 6 tone pips at 5 Hz repetition rate) played ~65 dB SPL. The tone was played from P9 to P20, and mice remained in the sound attenuating chamber until the day of recording (P30 – P40). The tone was generated (Avisoft Bioacoustics) and played using a speaker (UltraSoundGate Player BL Light; RECORDER USGH software; Avisoft Bioacoustics) mounted to the center of the chamber. The intensity level of the noise was measured (spectra PLUS) within a standard mouse cage using a speaker (Sokolich Ultrasonic Probe Microphone System) placed inside the cage within the chamber.

2.3 Mapping

The auditory cortex was mapped using multi-unit recordings. For surgery and mapping of the auditory cortex, mice were anesthetized with a ketamine (10mg/mL) and xylazine mixture (1.35 mg/mL), supplemented with isoflurane (0.1 – 0.9%) or a half dose of Ketamine/Xylazine mix as needed. The right auditory cortex, identified based on coordinates from bregma and vascular landmarks, was exposed using a dental drill. Experiments were conducted in a sound-attenuating room (Gretch-Ken Industries Inc.) lined with anechoic foam. Acoustic stimulation and data acquisition were driven by custom software and Microstar digital signal processing system. Sounds were delivered with a calibrated free-field speaker (UltraSoundGate Player BL Light) located 6” and 45° from the left ear, contralateral to recording sites. Glass electrodes (1 M NaCl, 2-10 MΩ

impedance) were advanced (Kopf 2660) to cortical depths between 300-500 μm from pia (layers III-IV) to record sound-driven responses, with 100 μm spacing between penetrations. Multi-unit recordings were used to identify the characteristic frequency (CF; the frequency at which a neuron is excited at the lowest intensity tested) of a given neuron. A1 and AAF responses were determined based on the characteristic shift in tonotopy from A1 to AAF (A1: low to high CF; AAF: high to low CF; caudal to rostral) as well as short latency responses to tones and broadband noises.

CF and the threshold of response were determined by hand. Recordings were taken 15 dB above threshold at the CF to determine response magnitude and latency of response within a 200 ms window. To determine the best frequency (BF; the frequency a neuron responds to the most across all intensities), auto tuning curves were recorded on a subset of mice with a 2 kHz (4 to 36 kHz) resolution in 10 dB steps, averaging 5 repetitions at 1 Hz, each within a 200 ms response window. Spontaneous responses were recorded after each sound presentation and subtracted from sound evoked responses. Spikes occurring within 75 ms of the tone were included in the tuning curve, and a running average was used for smoothing. From this was calculated the BF for each neuron, the response magnitude across all frequencies (normalized to avg. response magnitude), and response magnitude at 14 kHz (normalized to avg. response magnitude). Because 14 kHz was our exposure frequency, we recorded a larger range of intensities (15-75 dB SPL) than for all other frequencies (15-55 dB SPL; Figures 5.1 and 5.5). Additionally, we calculated the percent of 14 kHz normalized responses that were 1 and above (i.e. the % of 14 kHz responses ≥ average response magnitude) for each BF.

To calculate changes in the tonotopic organization of the cortex, the position of the electrode relative to bregma was recorded and converted the rostral-caudal coordinates to a scale ranging from 1-2. With this, Voronoi tessellation maps were generated (Matlab) for each mouse. The scaled coordinates were used to calculate the regression curve of CF distribution along the rostral-caudal axis. In addition, to determine whether neighboring neurons shared similar response characteristics, a Pearson distance correlation and the topological correlation (methods described in Yarrow et al., 2014) were calculated. For each correlation analysis, one value was determined for each mouse, and naïve and sound exposed groups were compared using a student's t-test.

3. Results

3.1 Primary auditory cortex

3.1.1 Sound exposure causes reduced response to 14 kHz, but no overall change in response magnitude across the frequency spectrum

Previous studies in adult cats have shown that sound exposure causes a decrease in the response magnitude to the exposure sound(s) (Pienkowski et al., 2011; Pienkowski et al., 2013). Therefore, the response magnitude of neurons across the frequency spectrum (4 – 36 kHz) was compared in naïve and sound exposed mice. Responses to a given frequency were averaged across all intensities (15 – 55 dB SPL). For comparison purposes, each neuron was normalized to its own average response across all frequency-intensity combinations. Comparison of the distribution curves revealed no difference in the response magnitude between naive and sound exposed mice across the frequency spectrum (two-way Kolmogorov-Smirnov: $D = 0.2941$, $p = 0.387$; Figure 5.1).

Repose magnitude to 14 kHz alone was also computed, using a larger range of intensities (15 – 77 dB) than for the total frequency distribution. This revealed that response to a 14 kHz tone was actually reduced in sound exposed mice (Naïve = 1.36 ± 0.055, N=225, SE = 1.04 ± 0.057, N=78; $t(220) = 4.057$, $p < 0.0001$, with Welch's correction). Together this indicates that the reduced response to 14 kHz is occurring at louder intensities, suggesting non-monotonic response to 14 kHz in sound exposed mice.

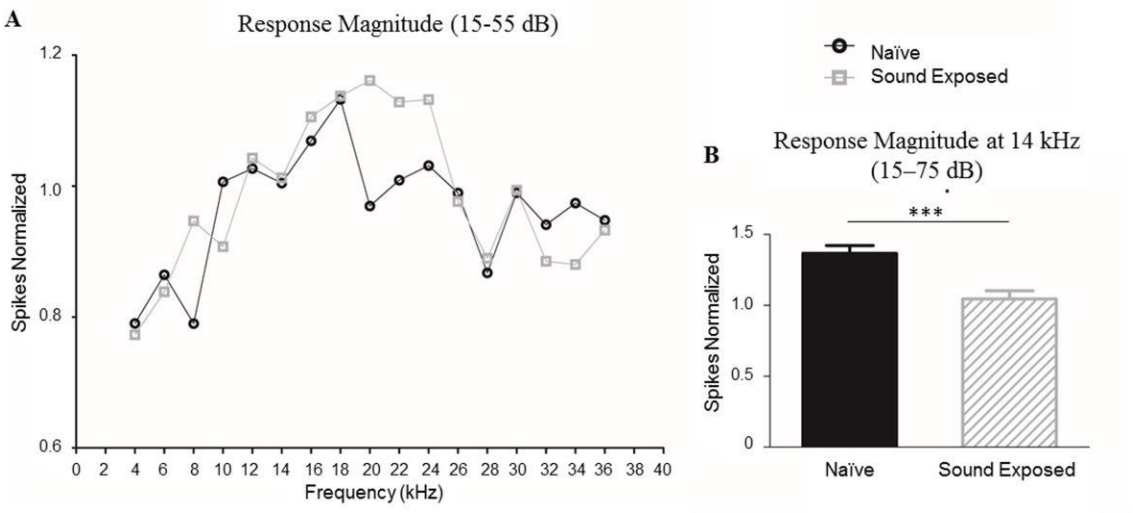

Figure 5.1. Developmental exposure to a 14 kHz tone causes a reduction in response magnitude to 14 kHz in A1. A) The normalized response magnitude of neurons across the frequency spectrum was similar in both naïve and sound exposed mice (averaging all responses from 15-55 dB SPL). B) However the overall response magnitude to a 14 kHz tone was reduced (averaging responses from 15-75 dB SPL). * = 0.05, ** = 0.01, *** = 0.001. N (neurons): 14 kHz alone: Naïve = 225, SE = 78; across frequencies: Naïve = 193-222, SE = 71-77.

3.1.2 Sound exposure did not change the tonotopic representation of 14 kHz characteristic frequency

One of the most consistent effects of developmental sound exposure is an increased area within A1 that is responsive to the exposure tone (Kim et al., 2013; Barkat et al., 2011). As our spacing was held consistent between mice, we calculated the total percent of neurons within A1 of a given mouse with a CF of 14 kHz, reflective of the total area of cortex. Figure 5.2 shows Voronoi tessellation maps depicting the distribution of CFs across A1 in naïve and sound exposed mice. A large percent of neurons (~25 – 35%) were selectively responsive to 18 -21 kHz at threshold (CF), with 10 -20% of neurons selective for 14 – 17 kHz. The distribution of CFs however was not altered after sound exposure (frequencies grouped into 4; Two-way ANOVA: effect of fq: $F(5) = 11.97$, $p < 0.0001$; effect of SE: $F(1) = 0.26$, $p = 0.61$). When frequencies were not grouped, Bonferroni corrected paired comparisons revealed a significant increase in the percent of neurons with a CF of 19 kHz ($p < 0.05$; data not shown) but no difference in the percent of neurons with a CF of 14 kHz (Naïve = 2.48 ± 1.36, N=9; SE = 2.35 ± 1.13, N=11; $p = 0.943$).

It has been shown that the tonotopic gradient of CFs along the rostral-caudal axis is maintained by different mechanisms than those involved in expansion of CF representation (Anomal et al., 2013; Yang et al., 2014). Therefore, the strength of the topographic gradient of CFs across the caudal-rostral axis was calculated in A1, using 3 correlational measures. Sound exposure did not cause a significant change in the correlation between CF and the caudal-rostral axis, however there was small trend,

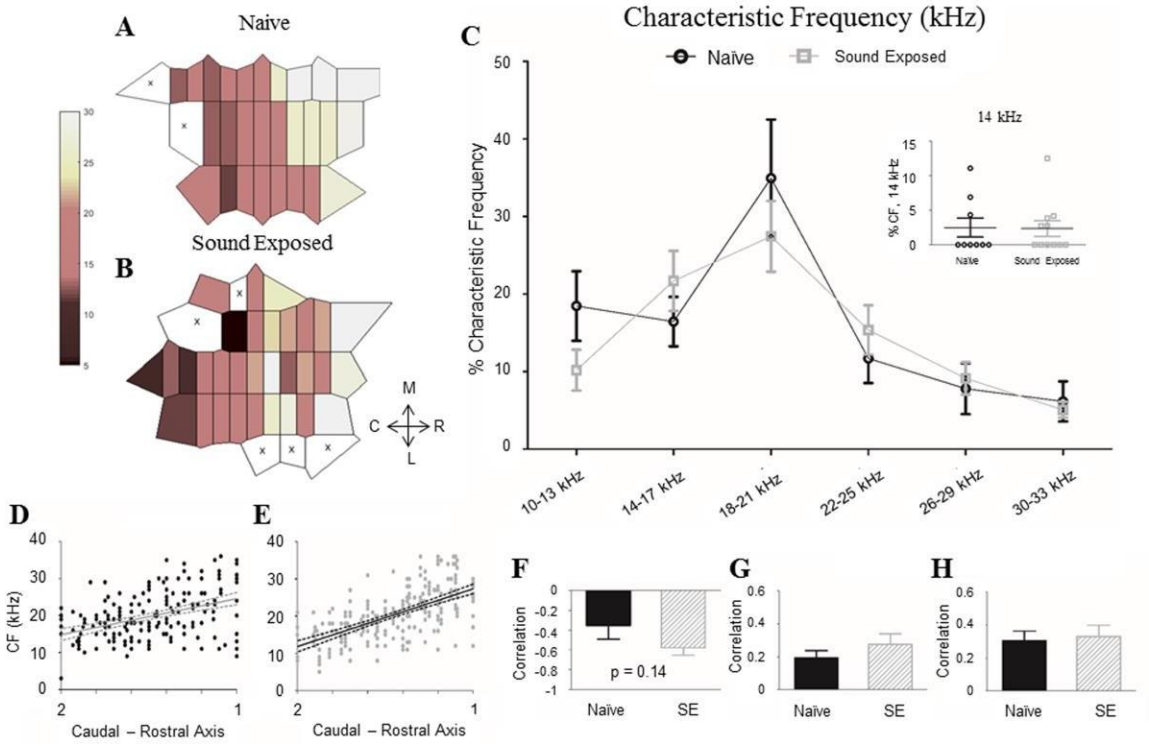

Figure 5.2. Developmental exposure to 14 kHz did not induce detectable changes in tonotopic map plasticity in A1. A) Representative maps of a naïve and sound exposed (B) mouse are presented, showing a shift in CF distribution from low (caudal) to high (rostral) frequencies. C) The percent of neurons with a CF of a given frequency was not different between naïve and sound exposed mice, nor was the percent of neurons with a CF of 14 kHz (insert). D) The CF of a neuron is plotted against its location along the caudal-rostral axis in naïve mice (E) and in sound exposed mice. F) Sound exposed mice has a slightly higher (*ns*) correlation between CF and caudal-rostral location. However, correlation between neighboring pairs of neurons was not different after sound exposure using either the Pearson distance correlation (G) or the topological correlation (H). N (mice): Naïve = 9, SE = 11.

indicating sound exposure may improve the tonotopic organization of neurons in A1 (Naïve = -0.35 ± 0.14 N=9; SE = -0.58 ± 0.07 N=11, t(18) = 1.518, p = 0.14). Two measures were used which compare how tightly correlated neighboring neurons are compared to distant neurons, the Pearson distance correlation (PC) and the topological

correlation (TC). Both measures revealed a moderate correlation between neighboring neurons which was not altered by sound exposure (PC: Naïve = 0.19 ± 0.04, N=9; SE = 0.27 ± 0.06, N=11; $t(18) = 1.0$, $p = 0.328$; TC: Naïve = 0.30 ± 0.05, N=9; SE = 0.33 ± 0.06, N=11; $t(18) = 0.28$, $p = 0.779$).

3.1.3 Sound exposure causes faster response latencies to the CF at 15 dB above threshold

We next characterized the response properties of a neuron at its preferred CF, including latency and response magnitude. Sound exposure did not change the overall response magnitude of a neuron to its preferred CF (Naïve = 3.64 ± 0.51, N=34; SE = 2.98 ± 0.25, N=36; $t(48) = 1.128$, $p = 0.264$; Figure 5.3), however sound exposure specifically decreased the magnitude of responses occurring after 50 ms (two-way ANOVA: Naïve: <50 ms = 2.26, >50 ms = 3.61; SE: <50ms = 2.6, >50ms = 2.46; effect of time $F(1) = 4.514$, $p = 0.035$; effect of SE: $F(1) = 2.02$, $p = 0.157$; interaction: $F(1) = 6.86$, $p = 0.0098$; Bonferroni corrected paired comparisons N vs SE >50ms: $p < 0.05$).

Sound exposure also caused neurons to respond to their preferred CF with a faster latency (Naïve = 33 ± 3.0, N=34; SE = 22.4 ± 1.8, N=36; $t(55) = 2.999$, $p = 0.0041$, Welch's correction). This was reflected in a reduced proportion of responses after 50 ms in sound exposed mice (Bonferroni corrected paired comparison between SE mice: <50ms vs >50 ms: $p < 0.001$).

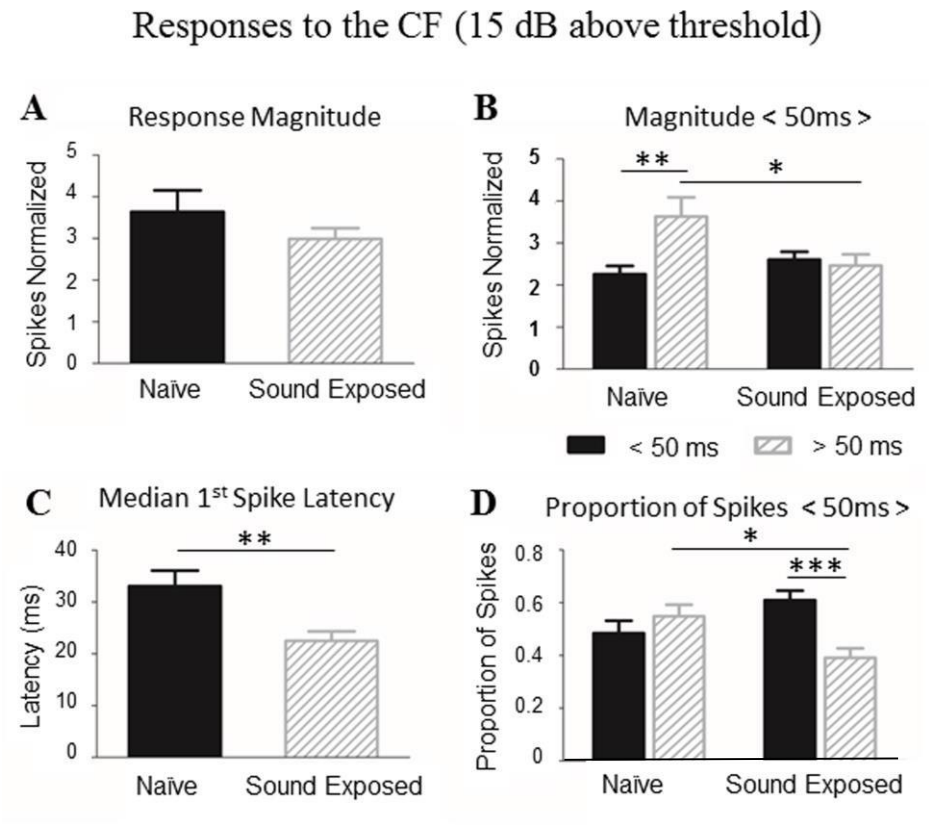

Figure 5.3. Developmental exposure causes neurons in A1 to responds with faster latencies to their preferred CF (15 dB SPL above threshold). A) The response magnitude of a neuron to its preferred CF was not affected by sound exposure, however (B) sound exposure did reduce the magnitude of those responses occurring after 50 ms. C) Sound exposure also decreased the latency of response to the CF, (D) specifically decreasing those responses occurring after 50 ms. * p = 0.05, ** p = 0.01, *** p = 0.001. N (neurons): Naïve = 34, SE = 36.

3.1.4 Sound exposure does not increase BF preference for14 kHz, but instead reduces responsiveness of neurons to 14 kHz.

Studies on auditory critical period plasticity have often used measures of BF instead of CF because there is some inherent subjectivity in the calculation of CF. As BF is a more objective measure (Barkat et al., 2011; Hackett et al., 2011), a BF for each neuron was calculated and plotted the total percent of neurons with a given BF. Sound

exposure did cause a significant increase in the percent of neurons with a BF of 18-21 kHz (Bonferroni corrected paired comparison: $p < 0.01$, BF grouped into 4; effect of frequency: $F(5) = 3.912$, $p = 0.0036$; effect of SE: $F(1) = 0.2833$; interaction: $F(5) = 3.997$, $p = 0.0031$; Figure 5.4). Analysis of the individual BF distribution (not grouped) revealed this increase was specific to 18 kHz (Bonferroni corrected paired comparisons: $p < 0.01$). However, there was no difference in the % of neurons with a BF of 14 kHz (Naïve = 3.94 ± 1.93, N=9; SE = 2.74 ± 1.72, N=4; $t(11) = 0.37$, $p = 0.71$). Increased 18 kHz representation observed using the more objective BF measurement is a similar change as that observed using CF measurements, in which there was increased representation of 19 kHz. These similar changes across measures validate an increased representation of 18-19 kHz after sound exposure.

To further understand why sound exposure did not cause altered representation of 14 kHz using measures of CF or BF, the distribution of response to 14 kHz across all neurons was plotted this against each neuron's BF. For each BF, the percent of neurons that responded to 14 kHz at ≥ 1 was determined. In naïve mice, 50 -100% of neurons across all BFs responded to 14 kHz at ≥ 1. However, in sound exposed mice, 0 -50% of neurons across all BFs responded to 14 kHz at ≥ 1, with the exception of 14, 16 and 18 kHz. This suggests that response to 14 kHz is selectively decreased in neurons which do not preferentially respond to 14 kHz and its surrounding frequencies. Statistical comparison of the distribution of this data confirms that sound exposure alters the relationship between 14 kHz response magnitude and BF (two-way Kolmogorov-Smirnov: $D = 0.875$, $p < 0.0001$).

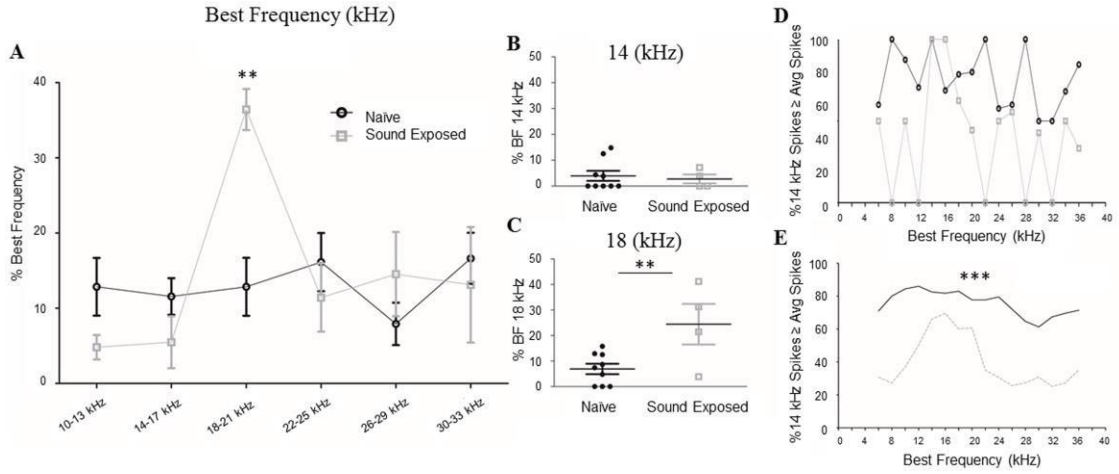

Figure 5.4. Developmental exposure to a 14 kHz tone does not increase BF preference for14 kHz, but instead reduces responsiveness of neurons to 14 kHz. A) The percentage of neurons with a BF of a given frequency was altered by sound exposure. B) Specifically, the % of neurons with a BF of 14 kHz did not change, but (C) there was an increased % of neurons with a BF of 18 kHz. D) In naïve mice, 1/2-all neurons with BFs across the frequency spectrum respond to 14 kHz at a spike rate equal to or greater than the average spike rate of that neuron. However in sound exposed mice, neurons which do not prefer 14 or 16 kHz reduce their response to 14 kHz to less than the average spike rate. E) The smoothed curve (data from D) of sound exposed mice is significantly different from that of naïve mice. * p = 0.05, ** p = 0.01, *** p = 0.001. N (mice; graph A, B, C): Naïve = 9, SE = 4. Proportion in D and E based off of N (neurons): Naive = 199, SE = 69.

3.2 Anterior auditory field

3.2.1 Sound exposure causes reduced response to 14 kHz, but no overall change in response magnitude across the frequency spectrum

As was observed in A1, comparison of the distribution curves revealed no difference in the response magnitude between naive and sound exposed mice across the frequency spectrum (two-way Kolmogorov-Smirnov: D = 0.2941, p = 0.387; Figure 5.5). However, response magnitude to 14 kHz was reduced in sound exposed mice (Naïve = 1.31 ± 0.05, N=173; SE = 1.12 ± 0.03, N=167; t(304) = 2.84, p = 0.0048, with Welch's

correction). Therefore, AAF is undergoing plasticity in response to developmental sound exposure in manner similar to A1, by reducing 14 kHz response magnitude.

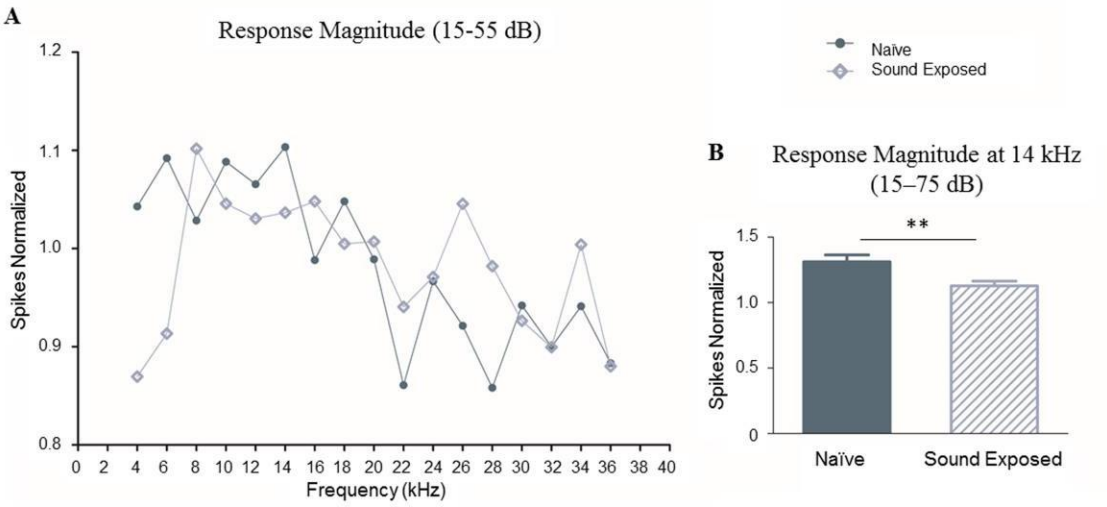

Figure 5.5. Developmental exposure to a 14 kHz tone causes a reduction in response magnitude to 14 kHz in AAF. A) The normalized response magnitude of neurons across the frequency spectrum was similar in both naïve and sound exposed mice (averaging all responses from 15-55 dB SPL). B) However the overall response magnitude to a 14 kHz tone was reduced (averaging responses from 15-75 dB SPL). * = 0.05, ** = 0.01, *** = 0.001. N (neurons): 14 kHz alone: Naïve = 173, SE = 164; across frequencies: Naïve = 152-167, SE = 155-164.

3.2.2 Sound exposure did not change the tonotopic representation of 14 kHz characteristic frequency

Figure 5.6 shows Voronoi tessellation maps depicting the distribution of CFs across AAF in naïve and sound exposed mice. A large percent of neurons (~27– 40%) were selectively responsive to 10-13 kHz at threshold (CF), with ~ 15% of neurons selective for 14 – 17 kHz. The distribution of CFs however was not altered after sound exposure (frequencies grouped into 4; Two-way ANOVA: effect of fq: $F(5) = 28.51$, $p < 0.0001$; effect of SE: $F(1) = 0.23$, $p = 0.62$). There was also no difference in the percent

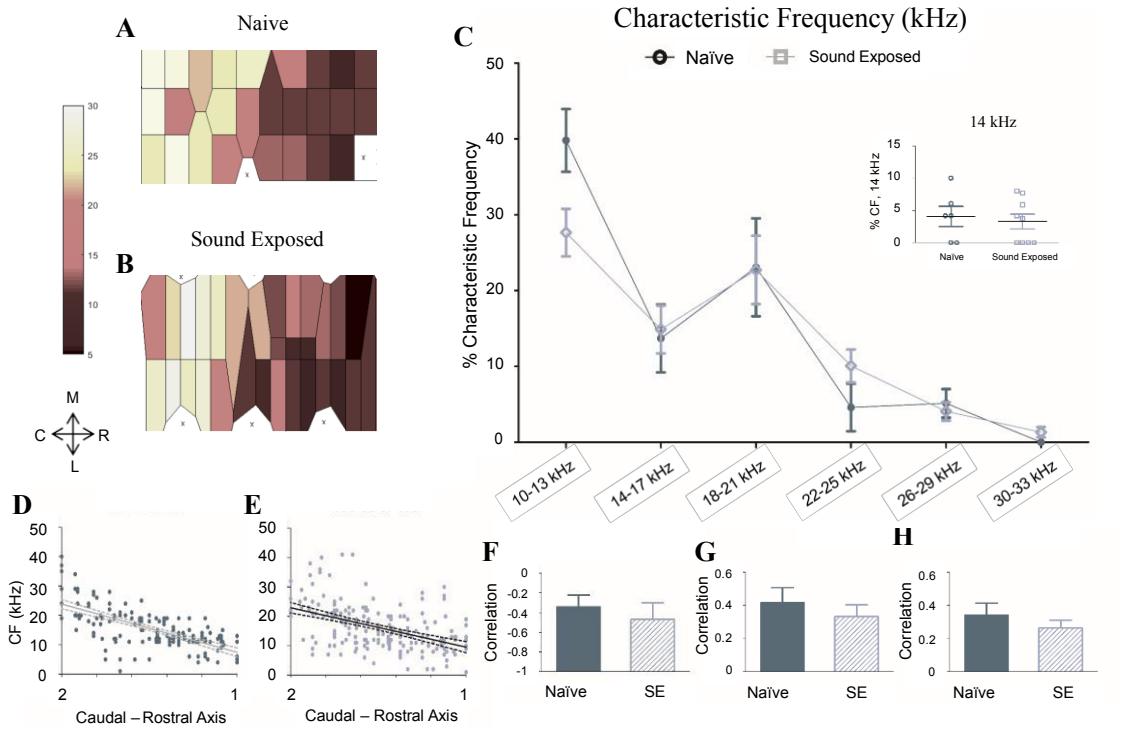

Figure 5.6. Developmental exposure to 14 kHz did not induce detectable changes in tonotopic map plasticity in AAF. A) Representative maps of a naïve and sound exposed (B) mouse are presented, showing a shift in CF distribution from high (caudal) to low (rostral) frequencies. C) The percent of neurons with a CF of a given frequency was not different between naïve and sound exposed mice, nor was the percent of neurons with a CF of 14 kHz (insert). D) The CF of a neuron is plotted against its location along the caudal-rostral axis in naïve mice (E) and in sound exposed mice. F) Sound exposed mice showed no difference in correlation between CF and caudal-rostral location. Correlation between neighboring pairs of neurons was also not different after sound exposure, using either the Pearson distance correlation (G) or the topological correlation (H). N (mice): Naïve = 6, SE = 9.

of neurons with a CF specifically of 14 kHz (Naïve = 4.06 ± 1.55, N=6; SE = 3.27 ± 1.13, N=9; p = 0.679). Unlike A1, there was no increase in the % of neurons selective for 18 kHz or 19 kHz. Just as in A1, sound exposure did not cause a significant change in the correlation between CF and the caudal-rostral axis (Naïve = 0.65 ± 0.11 N=6; SE = - 0.53 ± 0.16 N=10; t(14) = 0.53, p = 0.6). This correlation was much stronger than that

observed in A1. The Pearson distance correlation (PC) and the topological correlation (TC) both revealed a correlation between neighboring neurons which was not altered by sound exposure (PC: Naïve = 0.41 ± 0.09, N=6; SE = 0.33 ± 0.07, N=10; $t(14) = 0.73$, $p = 0.47$; TC: Naïve = 0.34 ± 0.07, N=6; SE = 0.26 ± 0.04, N=10; $t(14) = 0.96$, $p = 0.35$).

3.2.3 Sound exposure causes neurons in AAF to shift their window of response time to the CF (15 dB above threshold)

We next characterized the response properties of a neuron at its preferred CF in AAF. Sound exposure did not change the overall response magnitude of a neuron to its preferred CF (Naïve = 2.965 ± 0.2554, N=40; SE = 3.293 ± 0.1718, N=155; $t(193) = 0.905$, $p = 0.36$; Figure 5.7), however sound exposure caused an increase in the magnitude of responses occurring after 50 ms (two-way ANOVA: Naïve: <50 ms = 2.5, >50 ms = 2.3; SE: <50ms = 2.4, >50ms = 3.1; effect of time $F(1) = 1.726$, $p = 0.189$; effect of SE: $F(1) = 3.33$, $p = 0.068$; interaction: $F(1) = 4.87$, $p = 0.027$; Bonferroni corrected paired comparisons N vs SE >50ms: $p < 0.05$). Although median first spike latency was not overall affected in AAF (Naïve = 26.2 ± 2.7 N=40; SE = 26.3 ± 0.8 N=155; $t(47) = 0.028$, $p = 0.977$, Welch's correction), still the proportion of responses that occurred before 50 ms was reduced in sound exposed compared to naïve mice (Bonferroni corrected paired comparison between <50ms response: N vs SE: $p < 0.01$). So while A1 is developing faster latencies to the CF after developmental sound exposure, AAF data indicates it is instead shifting towards longer latencies. This latency shift is not as pronounced as that found in A1.

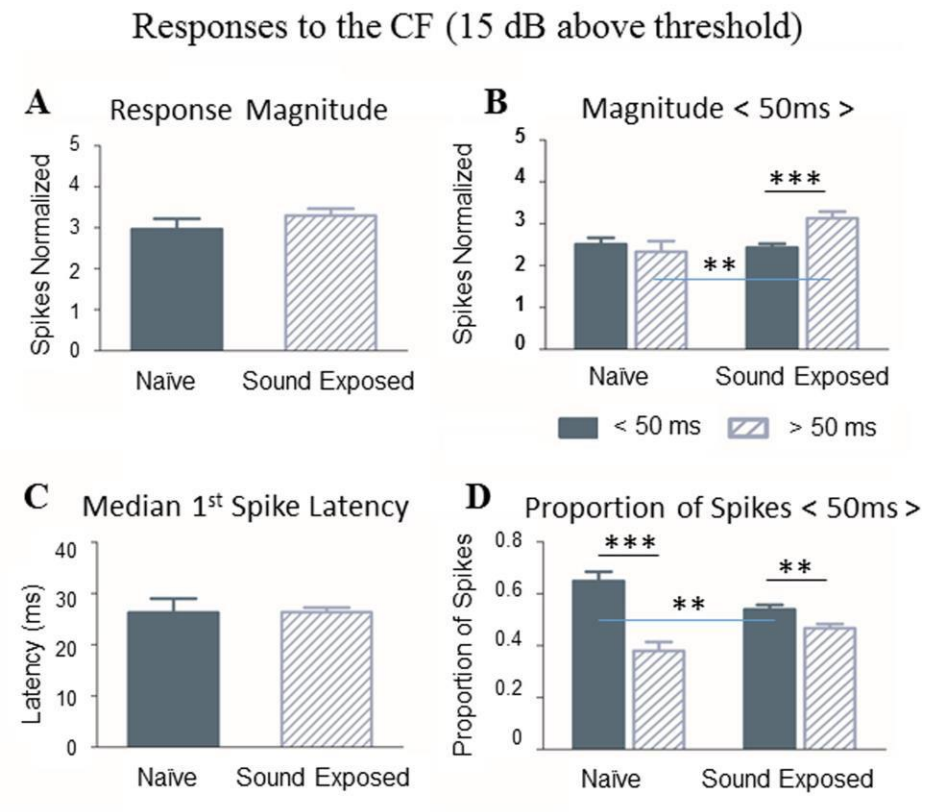

Figure 5.7. Neurons in AAF shift their window of response time to the preferred CF (15 dB SPL above threshold) after developmental exposure. A) The response magnitude of a neuron to its preferred CF was not affected by sound exposure, however (B) sound exposure did increased the magnitude of responses occurring after 50 ms. C) Although sound exposure did not effect the overall latency of response to the CF, (D) if did decrease the proportion of responses that occurred before 50 ms. * p = 0.05, ** p = 0.01, *** p = 0.001. N (neurons): Naïve = 40, SE = 155.

3.2.4 Sound exposure does not increase BF preference for14 kHz, but instead reduces responsiveness of neurons to 14 kHz.

The distribution of BF in the AAF region of cortex was also explored (Figure 8). Sound exposure did not affect the % of neurons with a given BF in the AAF (grouped into 4; effect of frequency: $F(5) = 2.9$, $p = 0.019$; effect of SE: $F(1) = 0.205$, $p = 0.651$; interaction: $F(5) = 0.45$, $p = 0.81$). There was a non-significant trend towards decreased

% of 18 kHz BF (Naïve = 12.63 ± 4.6, N=6, SE = 4.2 ± 1.38, N=8; t(5) = 1.74, p = 0.14) and no difference in the % of neurons with a BF of 14 kHz (Naïve = 13.36 ± 4.6, N=6; SE = 9.0 ± 3.36, N=8; t(12) = 0.77, p = 0.45). Although increased representation of 18 kHz or 19 kHz was not observed in AAF, still the response to 14 kHz in sound exposed mice was reduced in populations of neurons whose BF was not 14 or 16 kHz. This same pattern was not observed in naïve mice (comparison of distributions: two-way Kolmogorov-Smirnov: D = 0.5882, p < 0.003), and confirms results found in A1 of the auditory cortex.

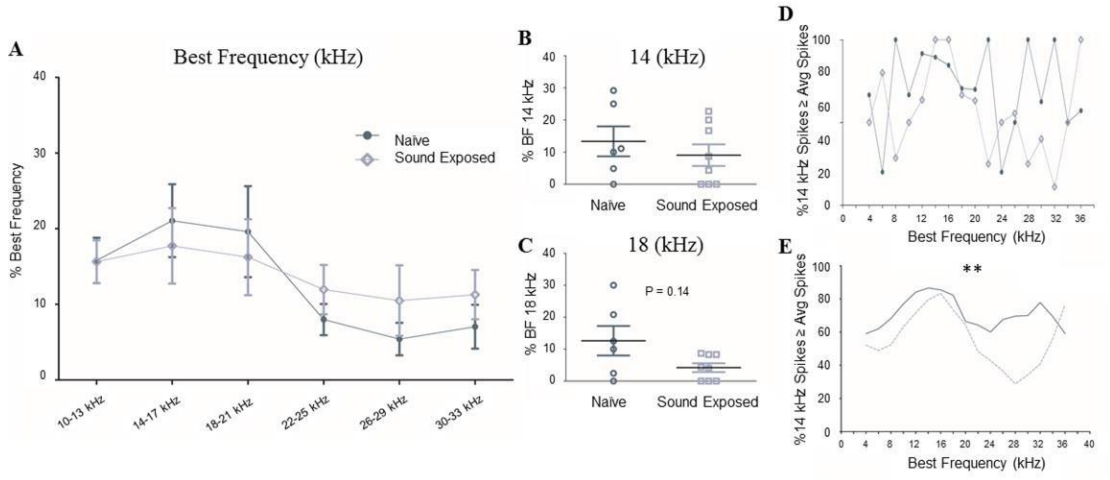

Figure 5.8. Developmental exposure to a 14 kHz tone does not increase BF preference for14 kHz in AAF, but instead reduces responsiveness of neurons to 14 kHz. A) The percentage of neurons with a BF of a given frequency was not altered by sound exposure. B) Neither14 kHz (C) nor 18 kHz showed an increased percentage of BF in AAF, although there was a trend toward increased 18 kHz. D) In naïve mice, 1/2-all neurons with BFs across the frequency spectrum respond to 14 kHz at a spike rate equal to or greater than the average spike rate of that neuron. However in sound exposed mice, neurons which do not prefer 14 or 16 kHz reduce their response to 14 kHz to less than the average spike rate. E) The smoothed curve (data from D) of sound exposed mice is significantly different from that of naïve mice. * p = 0.05, ** p = 0.01, *** p = 0.001. N (mice; graph A, B, C): Naïve = 6, SE = 8. Proportion in D and E based off of N (neurons):

4. Discussion

In this study we have determined that passive exposure to a tone during the auditory critical period does induce plasticity in the AAF, but this change was less pronounced than that measured in A1. Both A1 and AAF show: 1) decreased response magnitude to 14 kHz overall, and 2) a specific reduction of response to 14 kHz tones in neurons with a BF other than 14-18 kHz. A1 and AAF both show changes in the latency of response to the CF, but this effect is differential. In particular, sound exposure caused faster response latencies in A1, but AAF responses shifted to a later response window (>50 ms). Finally, although an increase in the exposure-tone (14 kHz) was not observed, data did reveal an increased percent of neurons with a CF of 19 kHz, and with a BF of 18 kHz, in A1 but not in AAF. Together this provides evidence for developmental plasticity in both A1 and AAF, however re-organization of the tonotopic arrangement of CF and/or BF may be specific to A1.

Here we did not find an increased representation of the exposure-sound, as has been much reported in rat models (Anomal et al., 2013; Chang et al., 2005; de Villers-Sidani et al., 2007; dev Villers-Sidani et al., 2008; Insanally et al., 2009) and more recently in mice (Barkat et al., 2011; Kim and Bao, 2009; Yang et al., 2014). There was also no increase in response magnitude to the exposure-tone (Takahashi et al., 2006). Potential differences in experimental setup such as the anesthetic used, the spacing between electrode penetrations, the intensity of the exposure sound and the repetition rate of the tone pips during sound exposure have all been specifically tested (data not shown), but still did not replicate. One remaining possibility is that the region which we consider

to be A1 may not be the exact area of cortex considered to be A1 in other labs. In the mouse specifically there a lack of consensus about the exact location of A1 in the cortex, especially when comparing single unit studies to population based methods (see figure 5.9). In studies presented here, A1 and AAF were defined according to traditional methods from single unit studies (Linden et al., 2003; Stiebler et al., 1997; Trujillo et al., 2011), such as the rostral-caudal shift in the tonotopic gradient, strong response to tone and broadband sounds, single peaked tuning curves and short latency responses. Future studies would greatly benefit from a multi-array electrode setup, with 50-100 µm spacing

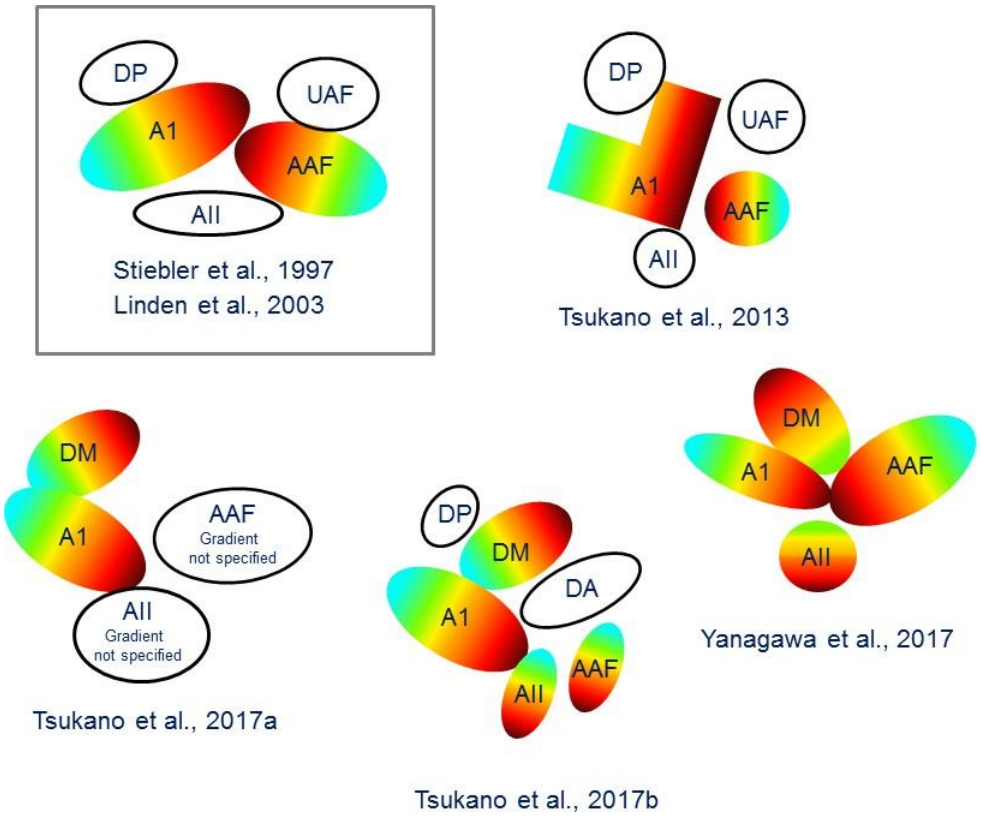

Figure 5.9. Summary of mouse auditory cortex regionalization literature. Each cartoon is representative of results from studies on the auditory cortex of the mouse. A1(primary auditory cortex), AAF (anterior auditory field), UAF (ultrasonic field), AII (secondary auditory cortex), DP (dorsal posterior), DM (dorsomedial field), DA (dorsoanterior field). Red = high freqencies, blue = low frequencies.

spanning the entire length of auditory cortex. This would provide the resolution necessary to test plasticity across each region of cortex simultaneously, at the level of small populations of neurons, yielding a more precise and clearly delineated auditory map.

Instead of increased representation, sound exposure in this study caused an overall decreased response to the exposure sound and an increased response to 18 kHz, outside of the exposure band. This data supports studies in adult cats, where neurons show reduced response to the exposure sound(s) when exposed in adulthood (Pienkowski et al., 2011; Pienkowski et al., 2013) and an increased response to frequencies outside of the exposure band (Pienkowski et al., 2013). Data here demonstrate that the response of neurons to 14 kHz was selectively reduced in all neurons which did not preferentially respond to 14 – 16 kHz (BF). This was accompanied by a slightly higher correlation of CF along the tonotopic axis and faster latency of responses to the CF after sound exposure. Together this suggests that, under our experimental conditions, passive developmental sound exposure results in increased selectivity of neurons. Interestingly, the decreased response to 14 kHz was only detected when responses to louder intensity sounds were included in the analysis (75-15 dB vs 55-14 dB) indicating sound exposure induces the development of more non-monotonic responses to the exposure-sound, potentially due to increased inhibition at the exposure sound.

Although AAF did show decreased response to the 14 kHz exposure-sound, it did not show changes in response latency or CF/BF representation along the rostral caudal axis. This ‘attenuated’ AAF plasticity is consistent with previous studies using

endogenous florescent imaging, in which AAF required a longer exposure period for induction of plasticity after developmental sound exposure (Takahashi et al., 2006). It also supports studies from our lab indicating that noise exposure during development causes reduced expression of perineuronal nets in A1 but not AAF (data not published). Studies in adult cats have likewise found attenuated sound-induced plasticity in the AII of cat cortex compared to A1 (Pienkowski and Eggermont, 2010). This supports the idea that sound-induced plasticity is most prevalent in A1 of the auditory cortex.

5. Conclusions

Data presented here suggest that passive exposure to a tone during auditory critical period development induces cortical reorganization in both A1 and AAF of the auditory cortex. Reorganization seems to reflect and increased overall inhibitory tone, especially at the exposure frequency. However, plasticity is more pronounced in A1 than in AAF. This together with previous studies suggest that A1 may be the primary locus of sound-induced plasticity in the auditory cortex, and therefore may be an important target for future studies on auditory processing deficits in developmental and psychiatric disorders.

References

Anomal, R., de Villers-Sidani, E., Merzenich, M.M., and Panizzutti, R. (2013). Manipulation of BDNF signaling modifies the experience-dependent plasticity induced by pure tone exposure during the critical period in the primary auditory cortex. *PLoS ONE*, **8**, e64208.

Barkat, T.R., Polley, D.B., and Hensch, T.K. (2011). A critical period for auditory thalamocortical connectivity. *Nature Neuroscience ,***14**, 1189–1194.

Ben-Ari, Y. (2002). Excitatory actions of gaba during development: the nature of the nurture. *Nature Reviews Neuroscience*, **3**, 728–739.

Carrasco, M.M., Trujillo, M., and Razak, K. (2013). Development of response selectivity in the mouse auditory cortex. *Hearing Research*, **296**, 107–120.

Chang, E.F., Bao, S., Imaizumi, K., Schreiner, C.E., and Merzenich, M.M. (2005). Development of spectral and temporal response selectivity in the auditory cortex. *Proceedings of the National Academy of Sciences of the United States of America*, **102**, 16460–16465.

de Villers-Sidani, E., Chang, E.F., Bao, S., Merzenich, M.M., 2007. Critical period window for spectral tuning defined in the primary auditory cortex (A1) in the rat. *Journal of Neuroscience*, **27**, 180–189. https://doi.org/10.1523/JNEUROSCI.3227-06.2007

de Villers-Sidani, E., Simpson, K.L., Lu, Y.-F., Lin, R.C.S., Merzenich, M.M., (2008). Manipulating critical period closure across different sectors of the primary auditory cortex. *Nature Neuroscience*, **11**, 957–965. https://doi.org/10.1038/nn.2144

Hackett, T.A., Rinaldi Barkat, T., O'Brien, B.M.J., Hensch, T.K., Polley, D.B., (2011). Linking topography to tonotopy in the mouse auditory thalamocortical circuit. *Journal of Neuroscience*, **31**, 2983–2995. https://doi.org/10.1523/JNEUROSCI.5333-10.2011

Hensch, T.K. (2004). Critical period regulation. *Annual Review of Neuroscience*, ***27***, 549–579.

Hensch, T.K. (2005). Critical period plasticity in local cortical circuits. *Nature Reviews Neuroscience*, **6**, 877–888.

Insanally, M.N., Kover, H., Kim, H., and Bao, S. (2009). Feature-dependent sensitive periods in the development of complex sound representation. *Journal of Neuroscience*, **29**, 5456–5462.

Kaas, J.H., 2011. The evolution of auditory cortex: The core areas, in: Winer, J.A., Schreiner, C.E. (Eds.), *The Auditory Cortex*. Springer US, Boston, MA, pp. 407–427.

Kanold, P.O., Nelken, I., Polley, D.B., (2014). Local versus global scales of organization in auditory cortex. *Trends in Neurosciences*, **37**, 502–510. https://doi.org/10.1016/j.tins.2014.06.003

Kim, H., and Bao, S. (2009). Selective increase in representations of sounds repeated at an ethological rate. *Journal of Neuroscience*, ***29***, 5163–5169.

Kim, H., Gibboni, R., Kirkhart, C., and Bao, S. (2013). Impaired critical period plasticity in primary auditory cortex of fragile X model mice. *Journal of Neuroscience*, **33**, 15686–15692.

Kuczewski, N., Fuchs, C., Ferrand, N., Jovanovic, J.N., Gaiarsa, J.-L., and Porcher, C. (2011). Mechanism of GABAB receptor-induced BDNF secretion and promotion of GABAA receptor membrane expression: GABAB receptor- mediated BDNF secretion. *Journal of Neurochemistry*, **118**, 533–545.

Lee, C.C. (2005). Principles governing auditory cortex connections. *Cerebral Cortex*, **15**, 1804–1814.

Linden, J.F., Liu, R.C., Sahani, M., Schreiner, C.E., Merzenich, M.M., (2003). Spectrotemporal structure of receptive fields in areas AI and AAF of mouse auditory cortex. *Journal of Neurophysiology*, **90**, 2660–2675. https://doi.org/10.1152/jn.00751.2002

Liu, H., Gao, P.-F., Xu, H.-W., Liu, M.-M., Yu, T., Yao, J.-P., and Yin, Z.-Q. (2013). Perineuronal nets increase inhibitory GABAergic currents during the critical period in rats. *International Journal of Ophthalmology*, **6,** 120.

Lu, W., Bromley-Coolidge, S., and Li, J. (2016). Regulation of GABAergic synapse development by postsynaptic membrane proteins. *Brain Research Bulletin*. (in press)

Meredith, M.A., Lomber, S.G., (2011). Somatosensory and visual crossmodal plasticity in the anterior auditory field of early-deaf cats. *Hearing Research*, **280**, 38–47. https://doi.org/10.1016/j.heares.2011.02.004

Nase, G., Weishaupt, J., Stern, P., Singer, W., and Monyer, H. (1999). Genetic and epigenetic regulation of NMDA receptor expression in the rat visual cortex. *European Journal of Neuroscience*, **11**, 4320–4326.

Pienkowski, M., Eggermont, J.J., (2010). Passive exposure of adult cats to moderate-level tone pip ensembles differentially decreases AI and AII responsiveness in the exposure frequency range. *Hearing Research*, **268**, 151–162. https://doi.org/10.1016/j.heares.2010.05.016

Pienkowski, M., Munguia, R., Eggermont, J.J., (2011). Passive exposure of adult cats to bandlimited tone pip ensembles or noise leads to long-term response suppression in auditory cortex. *Hearing Research*, **277**, 117–126. https://doi.org/10.1016/j.heares.2011.02.002

Pienkowski, M., Munguia, R., Eggermont, J.J., (2013). Effects of passive, moderate-level sound exposure on the mature auditory cortex: Spectral edges, spectrotemporal density, and real-world noise. *Hearing Research,* **296**, 121– 130. https://doi.org/10.1016/j.heares.2012.11.006

Reinhard, S.M., Razak, K., and Ethell, I.M. (2015). A delicate balance: role of MMP- 9 in brain development and pathophysiology of neurodevelopmental disorders. *Frontiers in Cellular Neuroscience*, **9**.

Sanes, D.H., Reh, T.A., and Harris, W.A. (2005). Development of the nervous system (Academic Press).

Spitzer, N.C., Kingston, P.A., Manning, T.J.J., and Conklin, M.W. (2002). Outside and in: Development of neuronal excitability. *Current Opinion in Neurobiology*, **12**, 315–323.

Stiebler, I., Neulist, R., Fichtel, I., Ehret, G., (1997). The auditory cortex of the house mouse: left-right differences, tonotopic organization and quantitative analysis of frequency representation. *Journal of Comparative Physiology A*, **181**, 559–571.

Takahashi, K., Hishida, R., Kubota, Y., Kudoh, M., Takahashi, S., Shibuki, K., (2006). Transcranial fluorescence imaging of auditory cortical plasticity regulated by acoustic environments in mice. *European Journal of Neuroscience,* **23**, 1365–1376. https://doi.org/10.1111/j.1460-9568.2006.04662.x

Trujillo, M., Measor, K., Carrasco, M.M., Razak, K.A., (2011). Selectivity for the rate of frequency-modulated sweeps in the mouse auditory cortex. *Journal of Neurophysiology*, **106**, 2825–2837. https://doi.org/10.1152/jn.00480.2011

Tsukano, H., Horie, M., Honma, Y., Ohga, S., Hishida, R., Takebayashi, H., Takahashi, S., Shibuki, K., (2013). Age-related deterioration of cortical responses to slow FM sounds in the auditory belt region of adult C57BL/6 mice. *Neuroscience Letters*, **556**, 204–209. https://doi.org/10.1016/j.neulet.2013.10.015

Tsukano, H., Horie, M., Takahashi, K., Hishida, R., Takebayashi, H., Shibuki, K., (2017a). Independent tonotopy and thalamocortical projection patterns in two adjacent parts of the classical primary auditory cortex in mice. *Neuroscience Letters*, **637**, 26–30. https://doi.org/10.1016/j.neulet.2016.11.062

Tsukano, H., Horie, M., Ohga, S., Takahashi, K., Kubota, Y., Hishida, R., Takebayashi, H., Shibuki, K., (2017b). Reconsidering tonotopic maps in the auditory cortex and lemniscal auditory thalamus in mice. *Frontiers in Neural Circuits*, **11**. https://doi.org/10.3389/fncir.2017.00014

Wong, C., Chabot, N., Kok, M.A., Lomber, S.G., (2015). Amplified somatosensory and visual cortical projections to a core auditory area, the anterior auditory field, following early- and late-onset deafness: Modified projections to AAF following deafness. *Journal of Comparative Neurology*, **523**, 1925–1947. https://doi.org/10.1002/cne.23771

Wu, G.K., Arbuckle, R., Liu, B., Tao, H.W., and Zhang, L.I. (2008). Lateral sharpening of cortical frequency tuning by approximately balanced inhibition. *Neuron*, **58**, 132–143.

Yanagawa, Y., Takasu, K., Osanai, H., Tateno, T., (2017). Salicylate-induced frequency-map reorganization in four subfields of the mouse auditory cortex. *Hearing Research*, **351**, 98–115. https://doi.org/10.1016/j.heares.2017.06.003

Yang, S., Zhang, L.S., Gibboni, R., Weiner, B., and Bao, S. (2014). Impaired development and competitive refinement of the cortical frequency map in tumor necrosis factor-deficient mice. *Cerebral Cortex*, **24**, 1956–1965.

Yarrow, S., Razak, K.A., Seitz, A.R., Seriès, P., (2014). Detecting and quantifying topography in neural maps. *PLoS ONE*, **9**, e87178. https://doi.org/10.1371/journal.pone.0087178

Conclusions

In this series of studies, I have addressed several open questions in the field of FXS and more generally, in auditory neuroscience. Within the developing auditory cortex, I have determined that, 1) FMRP and MMP-9 levels peak just before the onset of the auditory critical period and are reduced into adulthood, 2) MMP-9 is elevated in developing auditory cortex (AC) of *fmr1* KO mice but not in the inferior colliculus, 2) Minocycline treatment causes a moderate reduction in MMP-9 levels, but this effect was not robust. Elevated MMP-9 levels in *fmr1* KO mice during auditory development are implicated in impaired development of PNNs in *fmr1* KO mice (Wen et al., 2018a) and increased excitability, which was rescued by genetic reduction of MMP-9.

In adult *fmr1* KO mice, I determined that the reduced PNN density in developing auditory cortex is maintained into adulthood. PNNs were also reduced in the amygdala and CA2 hippocampus, likely contributing to impaired fear memory formation in *fmr1* KO mice. These results contribute to a growing body of research in FXS literature suggesting that dysregulated MMP-9 in FXS leads to impaired formation of PNNs. Because PNNs affect the firing properties of cells, particularly of parvalbumin positive interneurons (PV), as well as maintain synaptic contacts around the cells, impaired PNN formation likely alters the response properties of neurons within a circuit, leading to increased excitability and impaired inhibition and ultimately, impaired memory formation.

Here I have determined the time course of MMP-9 expression in the AC, suggesting that treatment of MMP-9 may be most critical during very early development

to ensure proper circuit maturation. Although MMP-9 levels were not elevated in all brain regions of *fmr1* KO mice (inferior colliculus), and PNNs under basal conditions were not always affected (DG, CA3, CA1), still multiple brain regions show impaired PNN formation. It is not clear why some regions may be more susceptible to PNN impairments. Certainly more studies are needed on the role of PNNs in FXS, including system-wide expression, the most appropriate treatment windows and their specific role in behavioral phenotypes.

Within this body of work, I have also studied regionalization in the auditory cortex and its implications for developmental plasticity. In particular, I have determined that 1) A1 and AAF have similar expression of inhibitory cells, and both regulate inhibitory cell expression after developmental noise exposure, 2) A1 and AAF show differential expression of PNNs in adulthood, and differential regulation of PNNs after developmental noise exposure, and 3) both A1 and AAF respond to developmental exposure to a pure tone by decreasing their response to the pure-tone, however this effect was more pronounced in A1. This adds to the body of research on developmental plasticity in the auditory cortex, and supports previous findings of attenuated plasticity in AAF to passive sounds. As might be expected based on their morphologic and functional properties, these results lend support to the idea that A1 and AAF have some overlapping roles in auditory processing, and some separable roles. It is not clear why such overlap exists in the auditory system, and so there remains much to explore in the future.